

Department of Geosciences, Geography
University of Fribourg (Switzerland)

**The evolution of mountain permafrost in the context of
climate change – towards a comprehensive analysis of
permafrost monitoring data from the Swiss Alps**

THESIS

Presented to the Faculty of Science of the University of Fribourg (Switzerland)
in consideration for the award of the academic grade of *Doctor rerum naturalium*

by

Benno Staub

from

Wohlen BE, Switzerland

Thesis No: 1949

UNIprint

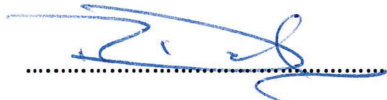
2015

Accepted by the Faculty of Science of the University of Fribourg (Switzerland) upon the recommendation of

Prof. Dr. Reynald Delaloye	(Supervisor)
Dr. Marcia Phillips	(Expert)
Dr. Xavier Bodin	(Expert)
Prof. Dr. Antoni Lewkowicz	(Expert)
Prof. Dr. Bernard Grobéty	(President of the jury)

Fribourg, 17th of December 2015

Thesis supervisor



(Prof. Dr. Reynald Delaloye)

Dean



(Prof. Dr. Fritz Müller)

Summary

In the Swiss Alps, permafrost occurs discontinuously and commonly has a temperature close to 0 °C. A reduction of Alpine permafrost area and volume is expected in the course of atmospheric warming, but to date, limited evidence is available for Alpine permafrost degradation. Permafrost warming or thaw is accompanied by structural changes in the subsurface, which endanger infrastructure by increasing kinematic activity or slope instability. Changes in the permafrost impact sediment transport to the valley bottom as well as gravitational natural hazards such as rock falls, landslides or debris flows. For these reasons, the quantitative analysis of past and potential future changes in the Alpine permafrost is of great interest and importance.

The objective of this PhD project was to investigate observational data from the Swiss Permafrost Monitoring Network PERMOS using an interdisciplinary approach and to develop new methods for the homogenisation and quantitative analysis of long-term monitoring data. The main focus was on assessing changes in the energy fluxes at the ground surface as a function of the snow cover, as well as on evaluating permafrost response to different meteorological conditions and events. This PhD project was part of the research project *The Evolution of Mountain Permafrost in Switzerland* (TEMPS, 2011-2015), which used combined observational and model-based approaches and aimed at improving the consistency and completeness of permafrost monitoring data. One achievement of this PhD thesis consists of the development of data processing algorithms for filling data gaps in temperature time series and the quantification of resulting uncertainties. Moreover, algorithms for the approximation of the thermal insulation effect of the snow cover based on ground surface temperature (GST) data were developed. This was of particular importance because snow information is usually not available for the points of interest. Furthermore, possibilities for estimating temperature variations at depth based on GST data were evaluated. The information obtained about the propagation of the thermal signal into the ground led to new insights into the temperature dependency of rock glacier creep, which were supported by observational data.

Data from more than 20 study sites were made comparable in order to quantify differences at the site- and the regional scale. The GST variability proved to be almost as high at the site scale as at the regional scale. This was explained by heterogeneous topo-climatic conditions as well as by the variable snow cover in the geographic context of the Swiss Alps. The roughness of the terrain played a key role, since it modifies the thermal insulation effect of the snow. Coarse-blocky terrains require more snow to be thermally insulated from the atmosphere and freeze more rapidly compared to smooth ground surfaces. The seasonal GST pattern showed that differences among sites and years were large in early winter, whereas GST were less variable in the summer season. Many locations showed similar snow conditions and therefore similar seasonal and inter-annual GST variations, which could not be explained by variations in air temperature. Although no overall increase in GST was found, the data indicate persistent warm conditions at the ground surface since 2009.

Ground temperatures (GT) experienced an overall warming trend down to several tens of m depth over the past 10-25 years. This warming was most distinct in relatively cold permafrost with temperatures below -1 °C. Since the GT at depths between 10-30 m influences the kinematic activity of rock glaciers, the surface deformation rates of the majority of the observed rock glaciers reached maxima between 2013 and 2015. Surface deformation rates quantified by photogrammetry for selected rock glaciers showed an increase in the order of 200-600 % compared to 1990-1995 and 400-800 % compared to 1960-1980.

Long-lasting warm conditions at the ground surface were identified to be the cause of the rise in ground temperature and the increased kinematic activity of rock glaciers. Compared with air temperature, where direct effect on the ground is limited to the snow-free period, the snow cover and its onset in early winter had a much greater influence on the heat and energy exchange at the ground surface. After one or two snow-poor winters, permafrost was able to regenerate thermally. Strong ground cooling occurred between 2005 and 2007, which caused a temporary trend reversal in the warming ground temperatures, limiting the effect of the particularly warm air temperatures between June 2006 and May 2007. Since Alpine permafrost is not in equilibrium with the current climatic conditions, recovery periods of efficient winter cooling will probably play a key role for its future evolution and preservation.

Overall, the results of this PhD project contribute to an improved process understanding and put observed ground thermal and kinematic phenomena in the context of past and potential future changes of permafrost in the Swiss Alps.

Zusammenfassung

Im Schweizer Alpenraum kommt Permafrost nur diskontinuierlich vor und ist mehrheitlich nahe an 0 °C. Im Zuge der bisherigen und noch bevorstehenden Klimaerwärmung ist sowohl eine flächenmässige als auch volumetrische Abnahme des alpinen Permafrost wahrscheinlich, was jedoch nur punktuell mit Messdaten belegt ist. Mit der Erwärmung und dem Auftauen von Permafrost gehen auch Strukturänderungen im Untergrund einher, welche durch zunehmende Bewegungsaktivität oder Instabilitäten Infrastruktur gefährden können. Veränderungen im Permafrost können sich auch auf den Sedimenttransport bis zum Talgrund sowie auf gravitative Naturgefahrenprozesse wie Felsstürze, Rutschungen oder Murgänge auswirken. Aus all diesen Gründen besteht ein grosses Interesse an einer quantitativen Analyse bisheriger sowie möglicher zukünftiger Veränderungen im alpinen Permafrost.

Das Hauptziel dieses Dissertationsprojekts war die gesamtheitliche und interdisziplinäre Analyse von Permafrost-Messdaten, welche im Rahmen des Schweizer Permafrost Monitoring Netzwerks PERMOS zusammengetragen wurden. Im Zentrum stand die Erforschung von Veränderungen der Energieflüsse an der Bodenoberfläche in Abhängigkeit von der Schneedecke sowie der Reaktion des Permafrost auf verschiedene Witterungsbedingungen. Das Forschungsprojekt *The Evolution of Mountain Permafrost in Switzerland* (TEMPS, 2011-2015), in wessen Rahmen diese Dissertation entstand, wandte einen kombinierten, sowohl auf Beobachtungen als auch Modell-basierten Forschungsansatz an zur Verbesserung der Konsistenz und Vollständigkeit von Permafrost-Messdaten. Hierzu hat diese Dissertation neue Algorithmen entwickelt um Datenlücken in Temperaturmessreihen zu füllen und daraus resultierende Unsicherheiten zu quantifizieren. Auch die thermische Isolationswirkung der Schneedecke wurde basierend auf Bodenoberflächentemperaturen (engl. Abk. „GST“) approximiert und in der Form von Zeitreihen nutzbar gemacht. Dies war von besonderer Bedeutung, weil Schneedaten für die Permafrost Messstandorte zumeist nicht verfügbar sind. Zudem wurden Möglichkeiten erprobt, um Temperaturänderungen in der Tiefe basierend auf GST-Daten zu simulieren. Mit den dabei gewonnen Erkenntnissen konnte die Temperaturabhängigkeit von Blockgletscherbewegungen mit Messdaten belegt werden.

Um lokale und regionale Unterschiede verschiedener Permafrost-Messgrössen zu quantifizieren, wurden Daten von über 20 Standorten miteinander vergleichbar gemacht. Dabei stellte sich heraus, dass thermische Charakteristika der Bodenoberfläche kleinräumig fast ebenso variabel sind wie im regionalen Vergleich. Im geographischen Kontext des Schweizer Alpenraums lässt sich dies primär durch heterogene topo-klimatische Bedingungen sowie die hohe räumlich-zeitliche Dynamik der Schneedecke erklären. Dabei spielt die Rauigkeit der Geländeoberfläche eine entscheidende Rolle, weil sie den thermischen Isolationseffekt der Schneedecke modifiziert. Insbesondere grob-blockige Oberflächen bedürfen grösserer Schneemengen zur thermischen Isolation gegenüber der Atmosphäre und kühlen deshalb im Frühwinter wesentlich besser aus als feinkörnige oder glatte Oberflächen. Der saisonale Verlauf der GST zeigt, dass im Frühwinter die Unterschiede der GST sowohl zwischen verschiedenen Standorten als auch im Vergleich verschiedener Jahre wesentlich

grösser sind als während der Auftauphase im Sommer. Viele Standorte mit vergleichbaren Schneeeigenschaften zeigen sehr ähnliche saisonale und jährliche Veränderungen der GST, welche sich nicht mit Veränderungen der Lufttemperatur erklären lassen. Obwohl die GST keinen langfristigen Temperaturanstieg zeigen, herrschen an der Bodenoberfläche seit 2009 anhaltend warme Bedingungen.

Messungen von Bodentemperaturen (engl. Abk. „GT“) zeigten für die vergangenen 10-25 Jahre insgesamt eine Erwärmung bis in grössere Tiefen. Am deutlichsten war diese Erwärmung an kühlen Standorten mit Temperaturen < -1 °C. Die Erwärmung im Untergrund in 10-30 m Tiefe beeinflusst zudem die Bewegungsaktivität von Blockgletschern. Die Mehrheit der beobachteten Blockgletscher erreichte zwischen 2013 und 2015 ein neues Maximum der dokumentierten Bewegungsaktivität. Photogrammetrische Analysen für ausgewählte Blockgletscher zeigen eine Zunahme der Oberflächenbewegungen in der Grössenordnung von 200-600 % gegenüber 1990-1995, resp. 400-800 % gegenüber 1960-1980.

Die Ursache ansteigender Bodentemperaturen in der Tiefe sowie der erhöhten Bewegungsaktivität von Blockgletschern sind langandauernd warme Bedingungen an der Bodenoberfläche. Im Vergleich zur Lufttemperatur, wessen direkter Einfluss sich auf die schneefreien Sommermonate begrenzt, hat die Schneedecke und insbesondere deren Aufbau im Frühwinter den grösseren Effekt auf den Energieaustausch zwischen Boden und Atmosphäre. Thermisch kann sich Permafrost nach einem oder mehreren kalten Wintern mit wenig Schnee rasch regenerieren, v.a. solange der Wassergehalt des Untergrunds gering ist. Dies haben die kühlen Winter zwischen 2005 und 2007 eindrücklich gezeigt, welche z.B. den Einfluss der ausserordentlich warmen Lufttemperaturen zwischen Juni 2006 und May 2007 auf den Permafrost begrenzt haben. Gerade weil der alpine Permafrost mit dem heutigen Klima im Ungleichgewicht steht, dürften solche Regenerationsphasen für dessen langfristigen Erhalt eine zentrale Rolle spielen.

Insgesamt trägt diese Dissertation zu einem verbesserten Prozessverständnis bei und stellt beobachtete thermische und kinematische Phänomene in einen grösseren Zusammenhang zu früheren sowie gegenüber möglichen zukünftigen Veränderungen des alpinen Permafrosts.

Acknowledgements

This thesis would not have been possible without the priceless work of many contributors to PERMOS, who probably spent thousands of hours in the field and in front of computers to provide the collected and partly pre-processed data and meta data. This engagement for the long-term observation of permafrost is driven by passion for the high-mountain areas, the interest in visible and measurable environmental changes and it involves a lot of personal investigation – a precious commitment to the challenging task of maintaining systematic and long-term observations in the harsh high-alpine terrain. In this connection I am very grateful for the immense support and confidence I received from my present and former supervisors and colleagues at the Universities of Fribourg and Berne.

Hans Kienholz, Bernhard Krummenacher and Dragan Vogel provided the perfect framework for innovative permafrost research at the Gemmi site and they supported and encouraged me to become part of the Swiss permafrost monitoring community already as an under-graduate student. Especially I would like to thank to Anina Chiapolini, the members of the Förderverein ProGemmi and the numerous volunteers who assisted in doing the field work in the “Furggentälti”. Without the possibility of being part of the PERMOS network since more than 10 years, I would probably not have focussed on graduating in this domain of research.

Furthermore I would like to thank to all the collaborators within the TEMPS project for their engagement in joint research work and advice on this fascinating but challenging PhD topic. First of all my gratitude goes to Reynald Delaloye for sharing his vast experience in the domain of observational permafrost research and mountain geomorphology and for trusting and encouraging me in the course of the TEMPS project. I was always impressed by his powers of recall regarding the meteorological conditions in the high-mountain areas of Switzerland for the past two decades (at daily to weekly precision!). Reynald clearly sparked my enthusiasm for exploring these large sets of data for thermal and kinematic phenomena.

As each PhD thesis has its ups and downs, I am particularly grateful for all the scientific but also the technical and moral support I received from my colleagues in Fribourg. I appreciated the enjoyable working atmosphere at the University of Fribourg and would like to thank the entire Geography unit, too numerous to mention everyone, for sharing the office and coffee breaks or doing joint field work. I am really looking forward keeping a foot in the door of this friendly, interdisciplinary and multi-cultural research institute also in future.

Moreover I would like to thank Jeannette Noetzi, Christin Hilbich, Andreas Hasler, Antoine Marmy, Christian Hauck, Martin Hoelzle, Ingo Völksch and Christophe Lambiel for their great support in case of any question arose regarding measurements, data processing or metadata. The close connection to the PERMOS project motivated me to put effort in research work which hopefully will find some application also after the TEMPS project will be finished. In this context I would like to specially thank to all TEMPS subprojects for providing data, shearing ideas and for the scientific and personal

exchange at conferences and meetings. The research work done in the frame of this thesis significantly benefited from large sets of snow data provided by SLF, reconstructed meteorological data provided by ETH as well as meteorological data from MeteoSwiss.

Special thanks go to Antoni Lewkowicz, Marcia Phillips and Xavier Bodin for having examined this PhD thesis as experts. I appreciate the fruitful discussions and your very constructive and detailed comments on my research work.

Last but certainly not least I would like to thank to my family and to Sabine for always supporting and encouraging me when needed.

This dissertation was financed by a grant from the Swiss National Science Foundation (project CRSII2_136279, 2011-2015) entitled «The Evolution of Mountain Permafrost in Switzerland» (TEMPS).

Table of contents

Summary	i
Zusammenfassung.....	iii
Acknowledgements	v
Table of contents.....	vii
Figures and tables	xi
List of abbreviations	xv
PART I: OVERVIEW.....	1
1 Mountain permafrost in the context of climate change.....	3
1.1 Permafrost definition and relevance of mountain permafrost.....	3
1.2 The evolution of Alpine permafrost with regard to climate change.....	3
1.3 Open questions in mountain permafrost research and monitoring.....	6
1.4 Research objectives and questions	6
1.5 Outline of the thesis	8
2 Scientific background on mountain permafrost	9
2.1 Mountain permafrost in the Swiss Alps	9
2.1.1 Spatial permafrost distribution and direct permafrost observations	9
2.1.2 Heterogeneity of the mountainous terrain and snow cover	12
2.1.3 Characteristics of periglacial landforms	13
2.2 Properties and processes influencing the ground thermal regime.....	16
2.2.1 Heat and energy exchange at the ground surface	16
2.2.2 Influence of the snow cover on the surface energy balance	17
2.2.3 Heat and energy exchange as a function of subsurface characteristics	21
2.2.4 Characteristics of coarse-blocky and ice-rich substrates	23
2.3 Mechanics of frozen ground materials and ice	24
PART II: DATA AND METHODS.....	27
3 Permafrost monitoring data.....	29
3.1 Permafrost monitoring sites.....	29
3.2 Temperature measurements	31

Table of contents

3.2.1	Ground surface temperatures (GST)	31
3.2.2	Ground temperatures (GT).....	33
3.3	Micrometeorological measurements	34
3.4	Kinematic measurements.....	36
3.5	Geophysical measurements	37
4	Processing of observational mountain permafrost data.....	41
4.1	Processing and homogenization of raw data	41
4.1.1	Ground temperature (GT) and ground surface temperature (GST) data.....	41
4.1.2	Meteorological data	45
4.1.3	Kinematic data.....	45
4.1.4	Geophysical data	47
4.2	Reconstruction of missing data and quantification of uncertainties	48
4.2.1	Comparison of approaches	48
4.2.2	Uncertainty assessment and error propagation	49
4.2.3	Procedures for filling gaps in thermal data	49
4.2.4	Procedures for meteorological data.....	52
4.2.5	Procedures for kinematic data	56
5	Integrative analysis of permafrost monitoring data	59
5.1	Addressing different scales in time and space with aggregates and indices	59
5.2	Deriving snow information based on GST data.....	62
5.2.1	Generalities and GST-derived snow information	62
5.2.2	Use and limitations of the methods.....	64
5.2.3	Potential improvements of the melt-index by considering global radiation	65
5.3	Quantification of the time lag between GST and GT at depth.....	65
5.4	Visualization of the degree of conductivity with thermal orbits.....	67
5.5	Approximation of GT variations from GST data for analysing rock glacier kinematics.....	69
5.6	Image correlation methods for the analysis of rock glacier kinematics	71

PART III: RESULTS.....	73
6 Evolution and variability of mountain permafrost parameters	75
6.1 Meteorological and snow data.....	75
6.2 Temporal evolution and variations observed in ground temperature data	77
6.3 Evolution of rock glacier creep activity	81
6.4 Temporal and spatial variability of electrical resistivity.....	82
6.5 Spatial variability of permafrost-relevant topo-climatic parameters	84
6.6 Concluding remarks.....	85
7 Thermal and kinematic response to meteorological events.....	87
7.1 Important meteorological events between 2000 and 2015	87
7.2 Thermal response.....	90
7.2.1 Response time and persistence of meteorological events	90
7.2.2 Relative importance of air temperature and snow on the surface energy balance	94
7.2.3 Reversibility of GST and GT in function of the snow thermal insulation	95
7.3 Kinematic response	97
7.3.1 Inter-annual variations of rock glacier velocities in reaction to GT variations.....	97
7.3.2 Relative importance of ground temperature and melt water infiltration	101
7.4 Concluding remarks.....	103
PART IV: SYNTHESIS.....	105
8 General discussion.....	107
8.1 Techniques for data homogenization, gap filling and integrative analysis.....	107
8.1.1 Gap filling of thermal, meteorological and kinematic data.....	107
8.1.2 Indices describing the snow thermal insulation and snow melt rate	109
8.1.3 Temperature time lags between the surface and different depths.....	110
8.1.4 Approximation of temperature variations at depth based on GST time series	111
8.2 Influence of meteorological events and snow conditions on ground temperatures.....	111
8.3 Permafrost creep in response to ground temperature variations.....	114
8.4 Evaluation of the permafrost monitoring strategy of PERMOS	117
9 Conclusions and perspectives	119
9.1 Main findings.....	119
9.1.1 Procedures for data homogenization and integrative data analysis	119

Table of contents

9.1.2	The evolution of mountain permafrost in Switzerland since 2000	120
9.1.3	Recommendations for the mountain permafrost monitoring in the Swiss Alps	122
9.2	Perspectives and future research needs	123
	References	125
	PART V: JOURNAL PUBLICATIONS	139
	Publication I	141
	Publication II	161
	Publication III	179
	APPENDIX	199
	Curriculum Vitae	205

Figures and tables

Fig. 1.1: Evolution of air temperatures in the Swiss Alps between 1864 and 2014	4
Fig. 1.2: Evolution of air and ground temperature at Murtèl-Corvatsch	5
Fig. 2.1: The potential permafrost occurrence in the Swiss Alps based on the APIM index	10
Fig. 2.2: Examples of direct observation of ground ice and permafrost	11
Fig. 2.3: The heterogeneity of terrain roughness and snow coverage in mountainous terrain	12
Fig. 2.4: Temporal evolution and spatial variability of snow depth on a rock glacier	13
Fig. 2.5: Overview of periglacial landforms typical for the mountain permafrost domain	15
Fig. 2.6: Heat and energy exchange at the ground surface over permafrost	17
Fig. 2.7: Influence of snow on GST at the example of the Gemmi rock glacier	18
Fig. 2.8: Convective air circulation within coarse-blocky material	23
Fig. 3.1: Permafrost monitoring sites in the Swiss Alps	30
Fig. 3.2: Miniature data loggers for measuring GST continuously	31
Fig. 3.3: Completeness and gap characteristics of the PERMOS & TEMPS GST monitoring data	32
Fig. 3.4: Field impressions from borehole drilling and thermistor calibration	33
Fig. 3.5: Overview of the PERMOS ground temperature data	34
Fig. 3.6: Weather stations at the monitoring site Gemmi/Furggental	35
Fig. 3.7: Measuring displacement rates and surface changes on rock glaciers	37
Fig. 3.8: Application of geophysical methods for mountain permafrost monitoring	38
Fig. 3.9: Field impressions from ERT monitoring at the Réchy site	39
Fig. 4.1: Theoretical aspects on the accuracy and precision of data	41
Fig. 4.2: Zero curtain correction of GST time series	42
Fig. 4.3: Correction of GT data measured in the LAP_0198 borehole	43
Fig. 4.4: Influence of the precision of UTL-1 thermistors on the measured time series	44
Fig. 4.5: Correction of coordinates measured by DGPS from two surveying campaigns	46
Fig. 4.6: GST gap filling by linear interpolation	50
Fig. 4.7: GST gap filling using the quantile mapping (QM) approach	52

Figures and tables

Fig. 4.8: Two-step bias correction approach for meteorological parameters	53
Fig. 4.9: Seasonal pattern of air temperature lapse rates in high-alpine terrain	54
Fig. 4.10: Comparison of grid-derived air temperature with station observations	54
Fig. 4.11: Approximation of the incoming shortwave solar radiation	55
Fig. 4.12: Gap filling of kinematic data and estimation of uncertainties	57
Fig. 5.1: GST aggregates and indices for the integrative analysis of the surface energy balance	60
Fig. 5.2: BTS, WeQT and LWST values derived from daily mean GST data	61
Fig. 5.3: Seasonal patterns of AirT and GST measured on a rock glacier at “Alpage de Mille”	63
Fig. 5.4: Comparison of GST and snow indices for selected GST time series	64
Fig. 5.5: Time lag of the GST signal at different depths in borehole COR_0278	66
Fig. 5.6: Thermal orbits for the visualization of heat conduction between GT time series	68
Fig. 5.7: Approximation of GT variations at depth using GST data	70
Fig. 5.8: Image correlation for the extraction of displacement vectors from orthophotos	72
Fig. 6.1: Evolution of air temperature and snow depth at permafrost monitoring sites	76
Fig. 6.2: Evolution of GST aggregates and indices between 1998 and 2014	77
Fig. 6.3: Spatial variability of permafrost-relevant indices and aggregates	78
Fig. 6.4: Evolution of GT at selected PERMOS boreholes	80
Fig. 6.5: Evolution of GT around the zero annual amplitude (ZAA)	80
Fig. 6.6: Photogrammetric reconstruction of horizontal rock glacier creep velocities since 1960	81
Fig. 6.7: Evolution of horizontal surface velocities on selected rock glaciers	82
Fig. 6.8: The seasonal pattern of mean apparent electrical resistivity measured at the Schilthorn	83
Fig. 6.9: Evolution of apparent electrical resistivities compared with ground temperatures	84
Fig. 6.10: Representativeness of GST and GT observations regarding topo-climatic characteristics	85
Fig. 7.1: Influence of meteorological events on the ground thermal regime	88
Fig. 7.2: Comparison of MAGST and MAGST changes compared with other GST indices	90
Fig. 7.3: The ground thermal response on early and late onset of the insulating snow cover	91
Fig. 7.4: Ground thermal effect of the snow melt illustrated with data from the Schilthorn	92
Fig. 7.5: Time lags of the GST signal at depth, analysed for all PERMOS/TEMPS boreholes	93

Fig. 7.6: Influence of the snow onset on ground freezing	94
Fig. 7.7: Influence of snow disappearance, AirT and ISR on the ground thawing	95
Fig. 7.8: Cumulative GST degree days (CDD) compared for different years and loggers	96
Fig. 7.9: Relationship between variations in GST and horizontal surface velocities of rock glaciers	98
Fig. 7.10: Density distribution of filter windows and time lags for GT_{synt} at five rock glaciers	99
Fig. 7.11: The thermo-mechanical movement behaviour of rock glaciers: obtained parameters	100
Fig. 7.12: Comparison of the temperature-velocity relationship of selected rock glaciers	101
Fig. 7.13: Inter-annual variations of rock glacier creep velocity residuals	102
Fig. 7.14: Seasonal variations of rock glacier creep velocities compared with snow melt rates	103
Table 3.1: Parameters measured at permafrost monitoring sites from PERMOS & TEMPS	30

List of abbreviations

AirT	Air temperature (°C), usually recorded ~2 m above ground
ALT	Thickness of the active layer (m), surface layer in which water thaws and freezes annually
DEM	Digital elevation model
BTS	Basal temperature of the Snow cover (°C)
CCD	Cumulative degree days (e.g. sum of daily mean temperatures)
ERT	Electrical resistivity tomography (geophysical method)
FDD	Freezing degree days, temperature-index summarizing negative daily mean values
GST	Ground surface temperature (°C), usually measured ~5-20 cm below the surface
GT	Ground temperature (°C) measured in the substrate, e.g. in boreholes
GT _{synt}	Synthetic GT variations approximated by GST time series (Sect. 5.5)
HTIstart	Start of the period of high thermal insulation by snow (date or day of the year)
Hyear	Hydrological year (October 1 to September 30), e.g. 2014 for the period 2013/2014
ISR	Incoming shortwave radiation (Wm ⁻²)
LI	Linear interpolation
LR	Linear regression
LWST	Late winter surface temperature (°C, Sect. 5.1)
MAAR	Mean annual apparent electrical resistivity (Ωm)
MAAT	Mean annual air temperature (°C)
MAGST	Mean annual ground surface temperature (°C)
MAGT	Mean annual ground temperature (°C)
PERMOS	Swiss Permafrost Monitoring Network
PISR	Potential ISR (Wm ⁻²) for clear sky conditions, computed using GIS software
QM	Quantile mapping (method used for bias correction and spatial transfer of data)
RD	Basal ripening date of the snow cover, start of the snow melt (date or day of the year)
RMSE	Root mean square error
RST	Refraction seismic tomography (geophysical method)
SD	Standard deviation
SDD	Snow disappearance date (date or day of the year)
SOD	Snow onset date (date or day of the year)
SO	Surface offset, namely GST-AirT (K)
SWE	Snow water equivalent (mm)
TEMPS	SNSF project (2011-2015) on “The evolution of mountain permafrost in Switzerland”
TDD	Thawing degree days, temperature-index summarizing positive daily mean values
TO	Thermal offset, namely GT-GST (K)
ZAA	Zero annual amplitude, depth below the ground surface (m)
ZC	Zero curtain (period of phase changes, detected in GST or GT data)
WEqT	Winter equilibrium temperature (°C)
ρ _a	Apparent electrical resistivity (Ωm)

PART I: OVERVIEW

1 Mountain permafrost in the context of climate change

1.1 Permafrost definition and relevance of mountain permafrost

Permafrost is a **subsurface phenomenon** usually not visible from the surface. It is defined as ground material remaining at **temperatures below or at 0 °C** for two or more consecutive years (Williams and Smith, 1989). The respective ground material may – but does not necessarily need to – contain ice. Since hydro-thermo-mechanical processes as well as the energy and heat-exchange towards the atmosphere substantially differ from unfrozen substrate and from glacier ice, permafrost has its own research discipline within the cryospheric sciences.

In periods of **transition to a warmer climate**, changes in permafrost temperatures as well as other ground properties, such as the content of organic matter, the portion of ground ice and water or its kinematic behaviour, become particularly important (Lawrence and Slater, 2005). Permafrost thaw endangers entire ecosystems and the global climate by potentially significant emissions of carbon dioxide and methane (Anisimov, 2007; Anthony et al., 2012; Schuur et al., 2008). At **high-latitudes**, major concerns are related to the construction and maintenance of infrastructure as well as severe modifications of the morphology and hydrology (e.g. by costal erosion or the collapse of thermocarst). In arid and semi-arid areas such as the central Asian mountains or the Andes, permafrost landforms (e.g. rock glaciers, push moraines or talus slopes) may be or become relevant for the water supply of entire river systems (Rangecroft et al., 2013). Changes in **high-mountain permafrost** in steep terrains can influence the frequency and magnitude of gravitational natural hazards with consequences at the local and regional scale (Deline et al., 2015).

In Switzerland the **permafrost occurrence** is discontinuous and confined to the highest elevation bands of the Alps (Sect. 2.1.1). In the light of permafrost degradation, stability issues in steep terrain and mass movements of rock and debris are directly or indirectly affecting infrastructure. The bonding of fractured hillslope materials by interstitial ice and the creep of ice-saturated sediments are known to be temperature-dependant and prone to changes with proceeding permafrost warming or thaw (Davies et al., 2001; Gruber and Haeberli, 2007; Rist and Phillips, 2005). Yet, these processes are still not fully understood (Krautblatter et al., 2012). In this context, the comprehensive analysis of observational data from high-mountain permafrost environments is very promising to improve the process-understanding. The development of new approaches towards a **quantitative and integrative analysis of long-term permafrost monitoring data** as well as maximizing the scientific outcome from existing data are the major scientific aims of this PhD thesis.

1.2 The evolution of Alpine permafrost with regard to climate change

At the global scale air temperature has risen about +0.8 °C during the past 100 years and is still increasing (IPCC, 2013). In the European Alps, the **atmospheric warming** was even more distinct with a first peak in the late 1940^{ties} and a second, very strong air temperature increase of +1.3 °C between 1975 and 2000 (Auer et al., 2007; Begert et al., 2005). For Switzerland during the period 1961-2013,

air temperatures rose $+0.37\text{ }^{\circ}\text{C}/\text{decade}$ on an annual basis and $+0.5\text{ }^{\circ}\text{C}/\text{decade}$ in the summer months June-August, causing an average increase of the zero degree level of about $+60\text{ m}/\text{decade}$ (MeteoSwiss, 2014). The strong warming around the 1980^{ties} and the ongoing warm conditions are also shown in Fig. 1.1. In spite of large inter-annual variations, 17 of the warmest 20 years since the beginning of the observations in 1864 occurred since 1990 (MeteoSwiss, 2014).

Scenarios for future climate evolution in Europe predict an additional air temperature increase of 2-5 $^{\circ}\text{C}$ (IPCC, 2013) until the end of the 21st century (Fig. 1.2a), with a maximum at high elevations (Kotlarski et al., 2015). This warming will very probably be accompanied by changes in the seasonal cycle of precipitation, snow coverage and global radiation as well as a higher frequency of **weather extremes** (CH2011, 2011; Gobiet et al., 2014; Steger et al., 2012). Hot periods like the heat waves in summer 2003 are likely to occur every second year towards the end of the century (Gobiet et al., 2014). The strongest air temperature rise is expected for the summer season, which may lead to earlier and more intense snow melt as well as warmer and drier ground conditions (CH2011, 2011). Concerning precipitation, the predictions on annual and seasonal changes are less clear: similar or even slightly larger amounts of precipitation between December and May and drier conditions between June and August are most probable (CH2011, 2011). However, precipitation extremes are very likely to occur more frequently, particularly in autumn (Rajczak et al., 2013). Studies from Morán-Tejeda et al. (2013) and Schmucki et al. (2014) indicate that future **snow evolution** at high elevation might depend on the evolution of precipitation rather than on temperature. This implies that very early as well as very late thermal insulation of the ground by the snow cover may still occur in the future.

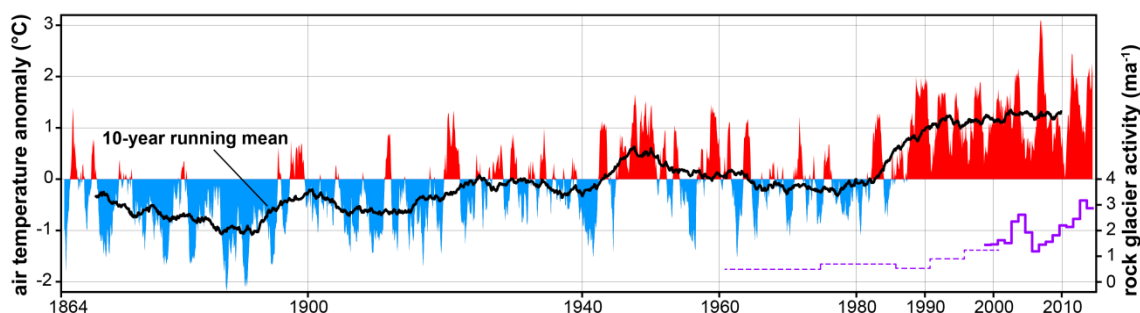


Fig. 1.1: Evolution of air temperatures in the high-alpine domain of the Swiss Alps between 1864 and 2014, measured at 2500 m asl at the Säntis mountain peak the north-east of the Swiss Alps (source: MeteoSwiss): The black curve shows the 10-year running average of homogenized air temperature anomalies relative to the mean of all observations. The outline of the coloured area represents running annual means of the same data with positive and negative temperature anomalies. For comparison, rock glacier surface displacement rates (m/year) observed at the Gemmi rock glacier in the northern Swiss Alps are illustrated with the purple lines (dotted line: photogrammetric reconstruction based on aerial images; thick line: annual terrestrial surveys). The Swiss Permafrost Monitoring Network PERMOS is operational since 2000.

Compared to 1990, about 45 % of the area and 50 % of the volume of the Alpine glaciers will be melted towards the end of the 21st century (Huss, 2012). This drastic reduction of glaciated and snow covered areas will decrease the surface albedo and act as a positive feedback mechanism increasing air and ground temperatures even more. Although permafrost is covered with sediment or rock and is thus – contrary to glaciers – not as directly influenced by air temperature, the **changing climatic conditions will certainly affect permafrost environments**, in the Swiss Alps as elsewhere.

Section 1.2: The evolution of Alpine permafrost with regard to climate change

Mountain permafrost is mainly characterized by rough terrain in complex topography with spatially variable micro-climatic conditions and ground properties (Sect. 2.1 and 2.2). The energy and heat transfer between the ground and the atmosphere is strongly modified by the timing and thickness of the snow cover and the properties of the surface and subsurface (e.g. terrain roughness, porosity, water and ice content, thermal conductivity of the material). Despite the existence of generally snow-free locations such as oversteepened rock walls, where surface temperatures are highly correlated to air temperature and radiation, **air temperature is not an adequate proxy for the evolution of the ground thermal regime** over the course of years or decades. Ground surface temperatures (so-called GST, measured ~5-20 cm below the surface) are more representative because they constitute a filtered integral of the surface energy balance (Sect. 2.2), including the effects of the snow cover (thermal insulation and modified radiation balance). With increasing depth, the temperature signal from the surface gets buffered and delayed. Therefore, ground temperatures (GT) recorded in boreholes at >10-20 m depth can be used as an indicator for variations of the surface energy balance at the decadal scale (Fig. 1.1). The **spatio-temporal variability of ground and ground surface temperatures** is a key for understanding the processes that act today and were relevant in the past, and from this, the basis to learn more about the future permafrost evolution. Observations are the link between the real world and its representation in models (Fig. 1.2b).

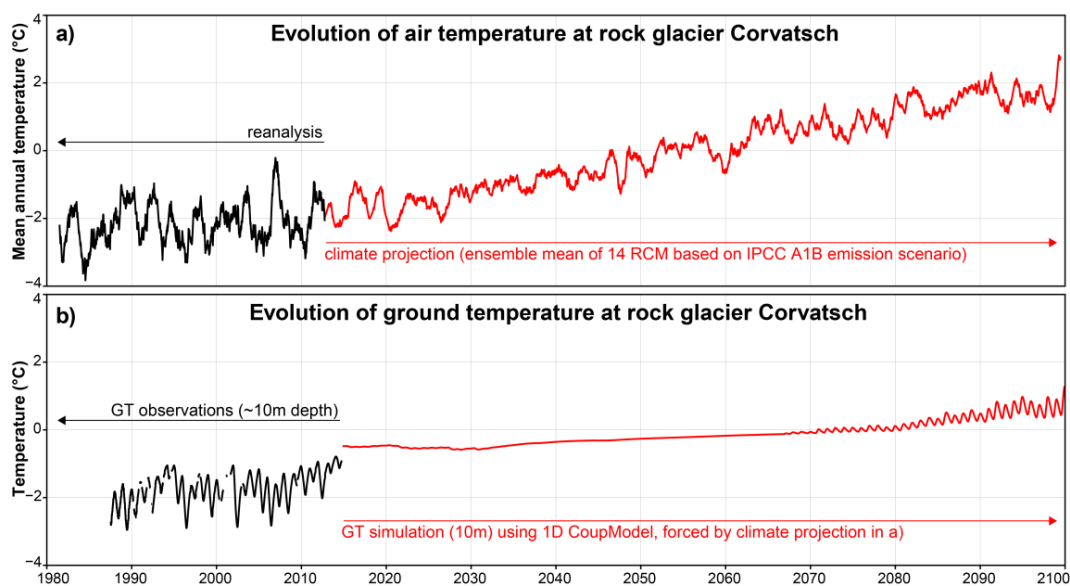


Fig. 1.2: Evolution of air and ground temperature at the Murtèl-Corvatsch rock glacier (Upper Engadine): a) shows in black the mean annual air temperature from downscaled and bias-corrected reanalysis data (Rajczak et al., 2015) and in red the corresponding climate projection for the same station (ensemble mean of 14 Regional Climate Models (RCM) and on the basis of the IPCC A1B emission scenario); b) shows ground temperatures (GT) measured at 10 m depth in borehole COR_0287 and simulation results based on the climate projections for the same depth (Marmy et al., 2015).

Because mountain permafrost research is a young discipline, the first **measurements** in the Swiss Alps started in the late 1980^{ties}. Hence, the most striking increase in air temperature is only indirectly documented in the delayed ground temperature increase (Fig. 1.2) recorded in the oldest borehole from rock glacier Murtèl-Corvatsch, drilled in 1987 (Haeberli et al., 1988). Based on ground temperature measurements from a handful of deep boreholes in the European Alps, Harris et al. (2003) have shown that permafrost has warmed in the order of +0.5-0.8 °C within the uppermost

tens of meters substrate during the 20th century. Even though ground truth data from boreholes drilled in Alpine permafrost only exists for a few points, the Swiss Permafrost Monitoring Network (**PERMOS**) nowadays comprises large sets of thermal (mainly GST), meteorological, kinematic, as well as geophysical, observations. However, very diverse topographic situations and subsurface properties as well as various technical issues and data gaps complicate a coherent analysis.

1.3 Open questions in mountain permafrost research and monitoring

Many questions still remain open in the field of mountain permafrost research, particularly regarding the processes which dominate the evolution of the ground thermal regime and their influence on terrain movements and slope stability. Distinct morphological changes and an increasing activity (Fig. 1.1) observed for a multitude of rock glaciers (Delaloye et al., 2010, 2013; Roer et al., 2008) raise questions about potential destabilization and systemic changes of creeping landforms in the context of climate change. Therefore, the influence of subsurface properties (such as the ice and water content) on the thermal and kinematic response of permafrost to meteorological events and different snow conditions are being intensively investigated at present. In summary, a particular scientific interest is devoted to the **consequences of potential permafrost warming and degradation** and which regions, substrates or landforms will most likely undergo changes in the near future. A comprehensive analysis of permafrost observations is a prerequisite for answering these questions. Also the permafrost modelling community has a great need for high-quality observational data and the assessment of the model performance during the calibration period would be an ideal point of contact for collaboration between the modellers and those who collect and study field data.

Regarding **permafrost monitoring**, the current monitoring setup deserves careful revision. Many measurements evolved historically because of the research priorities of the investigating research institutions but have not been scientifically evaluated to be representative for the high-mountain permafrost domain. In this context, the TEMPS project as well as this PhD thesis seeks at contributing to an evaluation and potential improvement of the permafrost monitoring strategy.

1.4 Research objectives and questions

To reach conclusions concerning the recent thermal evolution of different mountain permafrost landforms, a comprehensive analysis of temperature time series from many different field sites and comparison with additional data such as surface displacement rates of rock glaciers or geophysical measurements are required. In this context, this PhD thesis – which is part of the SNSF Sinergia research project “The Evolution of Mountain Permafrost in Switzerland” (TEMPS, 2011-2015, project no. CRSII2_136279) – **aims at developing adequate methods and procedures for combining and analysing a large set of observations as well as characterizing the state and recent evolution of permafrost properties in the Swiss Alps**. It specifically focuses on meteorological events that influence the thermal regime at the ground surface at the time scales of days to several years, but which are believed to be relevant for the evolution of ground temperatures also at depth and over long-term. Methodically, it ranges between a detailed geomorphological case study and the

statistical analysis of a large data set. Consciously seeking points of contact with the climate and permafrost modelling community, this PhD thesis pursues an inter-disciplinary and process-oriented approach. For reaching the overall aim, the **four main objectives** are as follows:

Objective A: *Quantification of the effects of meteorological conditions and events on **ground surface temperatures** considering differing topo-climatic situations and ground properties.*

A deep knowledge of the thermal evolution and the processes at the ground surface is essential to understand the potential future permafrost evolution. The following research questions were formulated to assess objective A:

- 1) **Meteorological events:** *Which meteorological events, terrain types and snow properties have the strongest warming or cooling effects on the ground? How can this be shown with long-term monitoring data?*
- 2) **Snow effects:** *How relevant is the snow cover relative to air temperature? How variable is the thermal insulation effect of the snow cover in time and space?*
- 3) **GST response:** *Which effects lead to a delayed or weakened response of GST to increased air temperatures? Which terrain types and landforms are particularly sensitive to meteorological events and what could this imply regarding the sensitivity of mountain permafrost to climate change?*

Objective B: *Improvement of the understanding of processes influencing the thermal evolution at depth and the seasonal and inter-annual variations of **rock glacier kinematics and permafrost creep** based on long-term observations.*

Regarding rock glacier kinematics, the ground thermal conditions at depth (i.e. at the “shear horizon”, Sect. 2.3) and the relative importance of temperature variations and melt water infiltration deserve particular attention. This is assessed by the following specific research questions:

- 1) **Ground temperatures:** *How fast does the temperature signal from the surface propagate into the ground and what are typical time lags at depth?*
- 2) **Kinematic response:** *Do short-term meteorological conditions affect the kinematic behaviour of rock glaciers and what is their relative importance?*
- 3) **Destabilisation signs:** *Are phenomena of permafrost degradation and rock glacier destabilisation detectable (and predictable) from long-term observation?*

Objective C: *Optimization of the value of scientific information of observational permafrost data, particularly regarding site-specific terrain and snow characteristics.*

To reach objectives A and B with an observational approach, considerable efforts are required for data processing and analysis. Therefore, objective C aims at the development of adequate **methods for data homogenization and integrative data analysis**. Although monitoring data from the Swiss

Alps was used here, these methods will potentially be applicable for mountain permafrost applications also in other regions. Objective C is linked to the following research questions:

- 1) **Homogenization and gap filling:** *How can data gaps in GST, GT and kinematic data be filled and the resulting uncertainties quantified?*
- 2) **Relationship between GST and GT:** *How and up to what depth can seasonal and inter-annual ground temperature variations be approximated by GST?*
- 3) **GST-derived snow characteristics:** *To what degree can the thermal insulation effect of the snow cover and the snow melt rate be quantified based on GST and air temperature data?*
- 4) **Integrative data analysis:** *Which data sets and methods are best suited to compare permafrost evolution and its influencing processes among different sites, years and monitoring parameters?*

Objective D: Recommendations for mountain permafrost monitoring and climate impact research.

Objective D evaluates needs for action in permafrost monitoring **and aims at contributing to an improved permafrost monitoring strategy**. Moreover, key messages on the **evolution of mountain permafrost in the Swiss Alps** are formulated, which may be of interest to climate impact research or related fields. The following research questions guide towards achieving objective D:

- 1) **Monitoring setup:** *Which methods and data sets are particularly important to document changes in mountain permafrost? How could the future mountain permafrost monitoring setup be improved to efficiently cover small-scale variability relating to snow cover dynamics and subsurface properties? Where is there potential for increasing efficiency?*
- 2) **Complementary data and meta data:** *Which additional data sets and meta information are most important or still missing?*
- 3) **Permafrost evolution:** *Which are the most important facts regarding permafrost evolution over the past 2 decades? What does this imply for potential future permafrost evolution?*

1.5 Outline of the thesis

This thesis is organised in five parts: following the introduction in chapter 1, chapter 2 presents the scientific background and closes the overview (**Part I**). In **Part II**, the data (chapter 3) and methodological approaches of the thesis are described, while chapters 4 and 5 focus on answering the questions in objective C. Part II further summarizes the main scientific outcome of the publications Staub and Delaloye (2016) and Staub et al. (subm.). Within **Part III**, the results on an integrative data analysis as well as key findings on the mountain permafrost evolution and selected results of publication Staub et al. (2015) are presented. As a synthesis (**Part IV**), the methodological approach and the obtained results are discussed in chapter 8, which is structured according to the main research objectives. Chapter 9 provides the conclusions and an outlook for future research needs. Journal publications which have been published or prepared for submission in the frame of this PhD project can be found in **Part V**.

2 Scientific background on mountain permafrost

2.1 Mountain permafrost in the Swiss Alps

Various periglacial landforms and a large variety of topo-climatic conditions need to be taken into account to obtain a representative view of the conditions and the evolution of permafrost in the high-mountain domain of Switzerland. The rough topography and heterogeneous terrain and snow characteristics of high-mountain environments make ground temperatures very variable in time and space. Therefore, mountain permafrost research should address also small spatial scales while considering a wide range of temporal scales (hours – several years).

2.1.1 Spatial permafrost distribution and direct permafrost observations

In the Alps, permafrost is covering approximately 5 % of the surface area of Switzerland (Boeckli et al., 2012c; Keller et al., 1998). Permafrost is found particularly in locations with a cold micro-climate at elevations above 2500 m asl that are not covered by thick glaciers (Gruber and Haeberli, 2009; Noetzli and Gruber, 2005). Fig. 2.1 illustrates with data from Boeckli et al. (2012b) that the area fraction of **potential permafrost occurrence** not covered by glaciers is largest in the elevation band from 2400 to 3000 m asl, with considerable differences as a function of aspect and slope. Due to the increasing area fraction of glaciated surfaces at high elevations, the proportion of permafrost starts to decrease from 2600-2800 m asl upwards. The rock behind hanging glaciers mainly in north-exposed rock faces at very high elevation should technically also be considered to be permafrost (Fig. 2.2a). To reach similar area fractions underlain by permafrost as on north slopes, mountain flanks oriented southwards need to be at 300-400 m higher elevation (Fig. 2.1b), due to the increased global radiation. Rock surface temperatures simulated by Gruber et al. (2004) and Noetzli et al. (2007) indicate maximal north-south differences in the order of 6-7 °C. The difference between east and west could be due to the higher probability of convective clouds in the afternoon (Gubler et al., 2011) or due to prevailing winds from the west causing more snow accumulation on east slopes. Indeed, east-exposed slopes are warmer than west-exposed slopes over the year: differences in mean annual values of 0.8 °C were measured over loose debris by Gubler et al. (2011) and simulations from Noetzli et al. (2007) for steep rock faces revealed 2.5 °C warmer surface temperatures on east slopes. If they are less influenced by snow, steep slopes may be favourable for permafrost occurrence compared to flat or gently inclined terrain (Fig. 2.1c). The differing permafrost area fraction among slopes at high elevation can be explained by the high proportion of glaciated areas in flat and gently inclined terrain. Fig. 2.1 illustrates the high spatial variability of permafrost occurrence as a subsurface phenomenon and its dependency on topo-climatic factors for the Swiss Alps.

a) potential permafrost occurrence in Switzerland

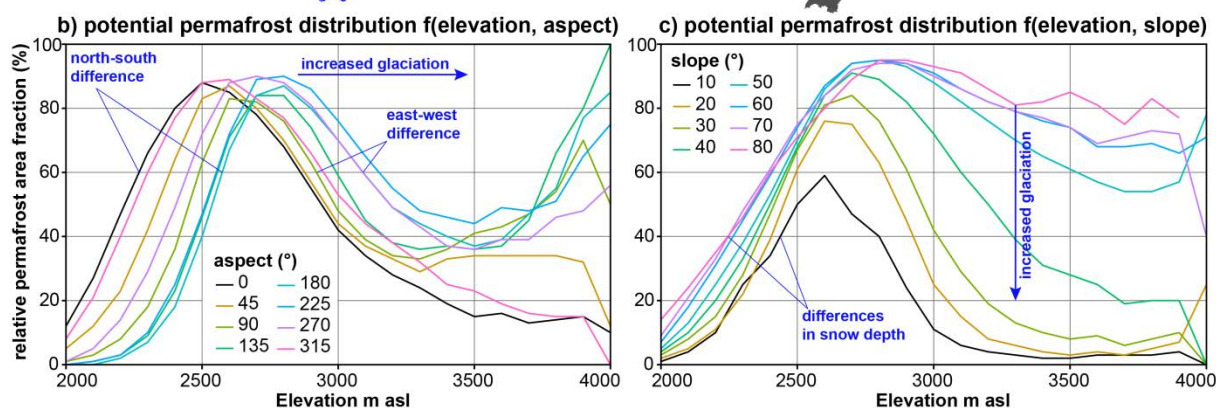
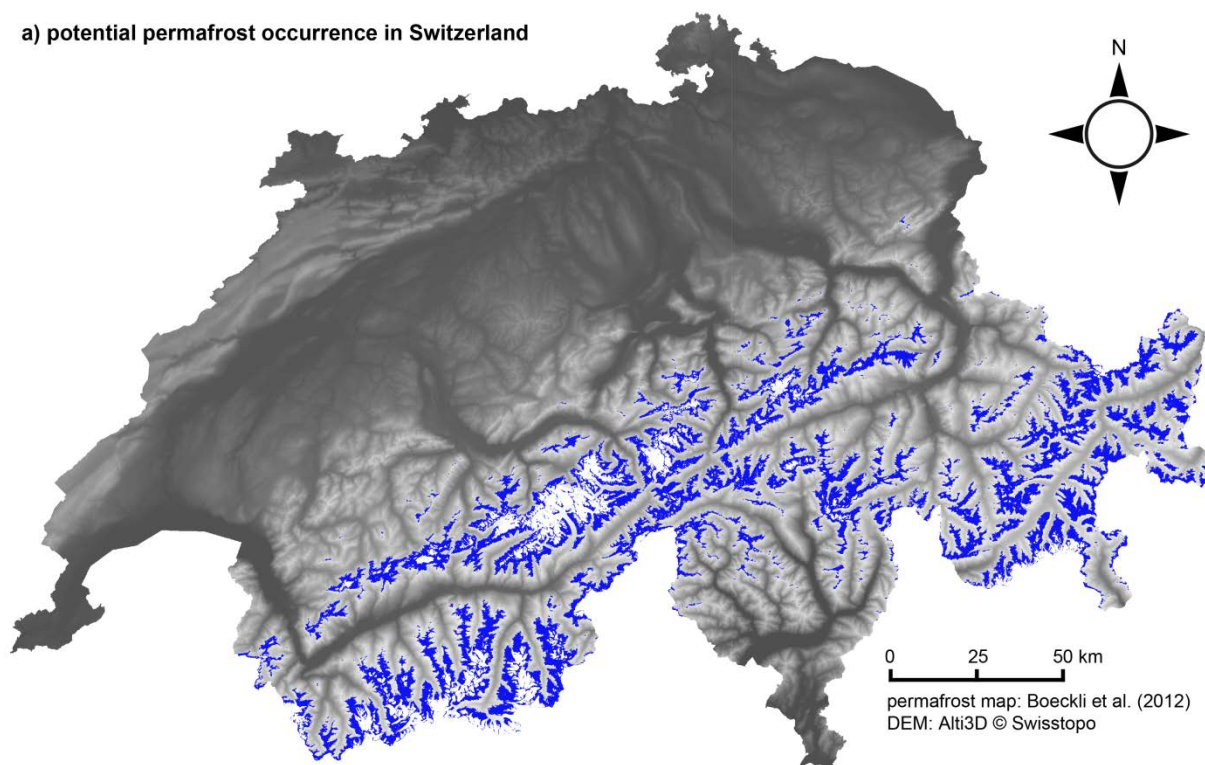


Fig. 2.1: The potential permafrost occurrence in the Swiss Alps based on the Alpine Permafrost Index Map (APIM) from Boeckli et al. (2012a, 2012c): a) in blue the maximum permafrost extent excluding glaciated areas (white) on an elevation map of Switzerland (source: Alti3D © Swisstopo); b) and c) show the relative area fractions potentially underlain by permafrost as a function of elevation (m asl), aspect (degrees north) and slope (°).

At local scales (e.g. for the planning of borehole locations for research projects or engineering), permafrost is usually **mapped by field observations** such as BTS measurements (basal temperature of the winter snow cover introduced by Haeberli (1973)), continuous ground surface temperature (GST) measurements (Hoelzle et al., 1999) or geophysical surveys (Hauck, 2013; Scapozza et al., 2010; Vonder Mühl et al., 2002). Single BTS surveys and short GST time series may not be representative due to the large inter-annual and seasonal variability of GST. Repeated observations are required to make sound conclusions about the ground thermal regime, ideally by combining the strengths of several methods (Sect. 3). Because GST may vary in the order of meters (Gubler et al., 2011) the spatial resolution of these methods needs to be adapted to the desired accuracy of the results.

Direct observations of mountain permafrost are usually limited to very small areas (mostly points) or rather qualitative information such as inventories of active rock glaciers or rock fall events (Cremonese et al., 2011). Examples of direct observations of permafrost are illustrated in Fig. 2.2. In some cases, ground ice has been directly visible after **drilling** or excavations in trenches at construction sites or in scars after rock fall events. According to the PERMOS rock fall inventory, prominent recent **rock fall events** happened in summer 2003 at the Matterhorn (CH), the Eiger (CH), the Aiguille du Midi in the Mont Blanc massif (FR) and were attributed to the exceptionally warm air temperatures at this time (Gruber, 2004). However, many rock fall events remain undocumented, e.g. because they are small or do not directly affect infrastructure. Rock volumes have been quantified only for a small number of events (Ravanel et al., 2010). Furthermore, the cause of rock fall events and the relation to permafrost is often unclear (Hasler, 2011). Yet, alternating cycles of thawing and freezing are supposed to exert mechanical stress in rock fractures (Sect. 2.3).

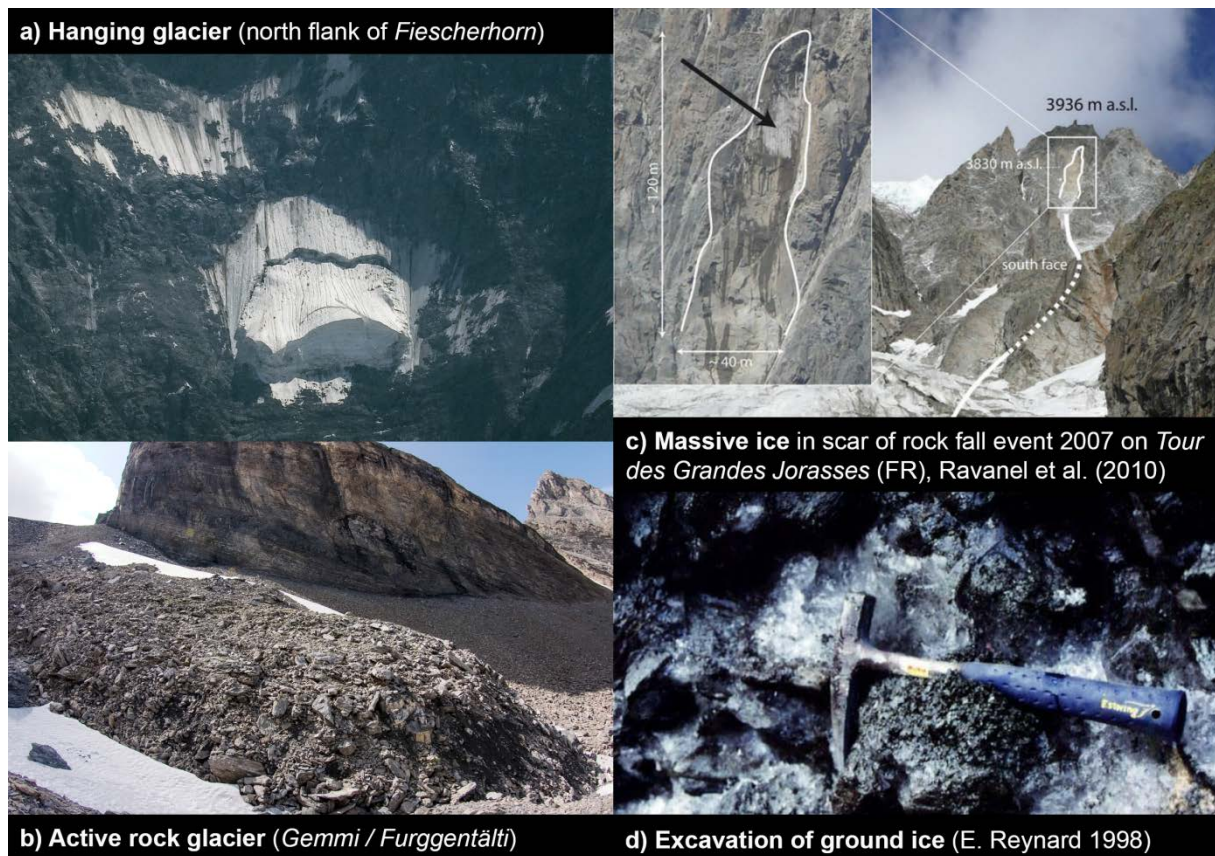


Fig. 2.2: Examples of direct observation of ground ice and/or permafrost conditions: a) Remnants of a hanging glacier on the north flank of the Fiescherhorn in the Bernese Alps indicate frozen rock; b) typical shape of an active rock glacier with a steep front as indicator of the presence of high ground ice contents; c) massive ice and seeping water in the scar on the Tour des Grandes Jorasses in the Mont Blanc area two weeks after rock fall event 2007 (Ravanel et al., 2010); d) Ground ice found during excavations in 1998 at the Lapires site (Photo: Emmanuel Reynard).

Direct observations provide valuable information about ground properties and ongoing processes. But to draw conclusions about changes and trends, **continuous or systematically repeated observations are required.**

2.1.2 Heterogeneity of the mountainous terrain and snow cover

In mountainous regions as the Swiss Alps, topography and snow greatly affect the local climate and the energy balance at the ground surface at different spatial scales. **Snow** is known to be a **key factor for the surface energy balance** of permafrost as well as for the variability of GST over short distances (Gisnås et al., 2014; Goodrich, 1982; Gubler et al., 2011; Stocker-Mittaz et al., 2002; Vonder Mühll et al., 2001a). The spatial patterns of snow accumulation, re-distribution by wind and avalanches and melt are influenced by the shape and curvature of the terrain. Therefore, **topography** and **terrain roughness** are essential for the ground thermal regime and mountain permafrost evolution at various scales. Shading by mountain ridges (100 m - 10 km) as well as unique boulders or rock spurs (~1-10 m) affect wind and radiation. These effects are illustrated in Fig. 2.3.



Fig. 2.3: Illustration of the heterogeneity of terrain roughness and snow coverage: At many different spatial scales, topography and terrain roughness influence the topo-climatic conditions, snow coverage and related processes of heat and energy exchange at the ground surface. The photograph was taken in October 2011 on Gornergrat (Zermatt, VS).

The effect of topography on the radiation balance remains constant over years, but snow cover is prone to large seasonal- and inter-annual variations in dependence on the frequency and amplitude of precipitation. The snow cover underlies changing spatial patterns depending mainly on the prevailing wind direction and avalanche activity. Fig. 2.4 illustrates that snow data from one point may not be representative for an entire landform. Moreover, the micro-roughness of the terrain greatly modifies the thermal insulation effect of the snow, so that energy fluxes through the snow cover may be higher around obstacles such as rocks or spurs compared to flat or regular terrain. Therefore, **permafrost observations like GST are mainly representative for the specific measurement location**. Hence, large amounts of data covering several years and various terrain characteristics are required to draw sound conclusions regarding permafrost evolution. For permafrost modelling this implies that an accurate description of the ground thermal regime is only possible for sites with excellent observational data and by considering a realistic snow cover for the surface energy balance. Differing ground properties and snow conditions may provoke disparate reactions of the ground thermal regime to meteorological events.

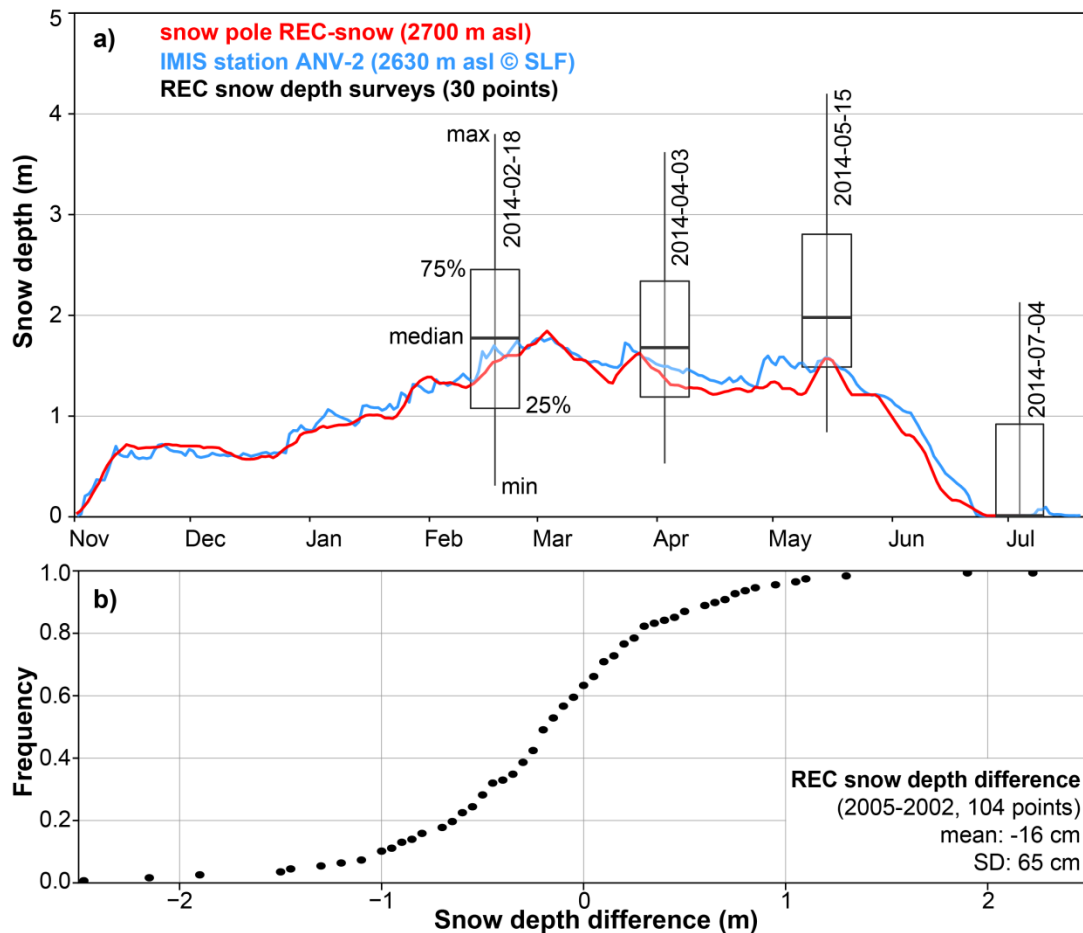


Fig. 2.4: The temporal evolution and spatial variability of snow depth at the Becs de Bosson rock glacier at the Réchy site (REC in Fig. 3.1): a) the coloured lines represent 7-day running means of continuously measured snow depths during winter 2013-2014: in red data from a snow pole on the same landform, in blue from the snow station ANV-2 at ~ 3 km distance (IMIS data © 2015, SLF). Although the snow depth evolution at these two stations is similar in this particular year, the spatial variability is very large even over short distances. This is illustrated with the boxplots representing the range of snow depth values for 30 monitoring points (~ 0.15 km²) near to the REC snow pole of roughly similar elevation, slope and aspect at four specific dates. In b) snow depths measured on the same landform in March 2002 and 2005 at 104 points reveal that the spatial snow distribution can greatly differ from year to year with local deviations of up to ± 2 m (SD: ± 65 cm).

Finally, the definition of the ground-atmosphere boundary as well as the exact snow depth is not trivial. Therefore, snow depth measurements should not be analysed at the cm-scale but for larger variations and in reference to other years. For analysing the effects of terrain and snow heterogeneity on the evolution of mountain permafrost, broad background knowledge about the measurements and the terrain characteristics is required. In the following section, specificities of typical permafrost and periglacial landforms are described.

2.1.3 Characteristics of periglacial landforms

Being a “visible expression of cumulative deformation by long-term creep of ice/debris mixtures under permafrost conditions” (Berthling, 2011: 103), kinematically **active rock glaciers** (Fig. 2.5d and g) directly indicate the presence and action of permanently frozen ground material and are therefore widely used for permafrost mapping at large scales (Boeckli et al., 2012b; Brenning, 2005; Cremonese et al., 2011). Active rock glaciers usually contain layers of very high ice content, in which relatively thin zones of minimal viscosity (so-called “shear horizons”, Arenson et al., 2002) are responsible for the largest part ($\gg 50$ %) of the internal deformation (Sect. 2.3).

As examples from Lapires, Sanetsch, Flüela, Ritord and many other sites show, **ice can also be found for various reasons in other landforms** such as talus slopes (Fig. 2.5e) or moraines (Fig. 2.5f). Particularly in the lower parts of talus slopes, cold ground temperature anomalies have been observed in comparison with the upper parts (Delaloye, 2004). This phenomenon was explained by ascending circulation of cold air throughout the landform during winter when the air outside is colder and more dense, leading to an energy transport towards the top of the talus where the air escapes to the atmosphere again. Since this process is reversible when outside air is warmer and lighter as the air within the ground, the same temperature pattern in the talus is fostered also during summer time. This so-called “**chimney effect**” was first observed at low-elevation talus slopes below the treeline, where it is dominant for the presence of permafrost (Delaloye et al., 2003; Morard et al., 2008; Wakonigg, 1996). A prominent example in the Swiss Prealps is the “Creux du Van” talus slope located at 1200 m asl. Nevertheless, the chimney effect can play a secondary but still important role also at high elevation (Delaloye and Lambiel, 2005). The chimney effect is not strictly restricted to talus slopes, but may also occur within other landforms situated on steep slopes and consisting of coarse-blocky, porous ground material (Delaloye, 2004).

For other landforms, such as ice-cored moraines and push-moraines, which often contain a higher proportion of fine material, the exposure to cold climatic conditions as well as the integration of ice through geomorphological processes are relevant. Hence, from a **geomorphological perspective**, the co-existence and interaction between glaciers and permafrost needs to be considered (Harris and Murton, 2005; Lugon et al., 2004). Glacier advances during the little ice age (LIA, 15th-19th century) were responsible for significant changes in the landscape of today, and these are visible in most regions of the Alpine arc on distinct morainic structures. During the LIA, the preservation and formation of ground ice were favoured on the front and outside of advancing glaciers (most typically on **push-moraines**), whereas areas temporally covered by the ice mass have been thermally insulated and possibly warmed up (Delaloye and Lambiel, 2008). Therefore, the central parts of most LIA glacier forefields in the Alps are nowadays permafrost-free or occupied by degrading **debris-covered glaciers** (Fig. 2.5a) or patches of buried ice (Delaloye and Lambiel, 2008). Although the permafrost definition includes debris-covered glaciers, they are usually considered as glacial features and thus not attributed to permafrost. In comparison with rock glaciers, debris-covered glaciers differ regarding the shape of the borders and the tongue. In contrast to rock glaciers, the kinematic behaviour of debris-covered glaciers is often dominated by a strong vertical component, due to rapid ice loss if the sediment coverage is not thick enough to thermally insulate the ice.

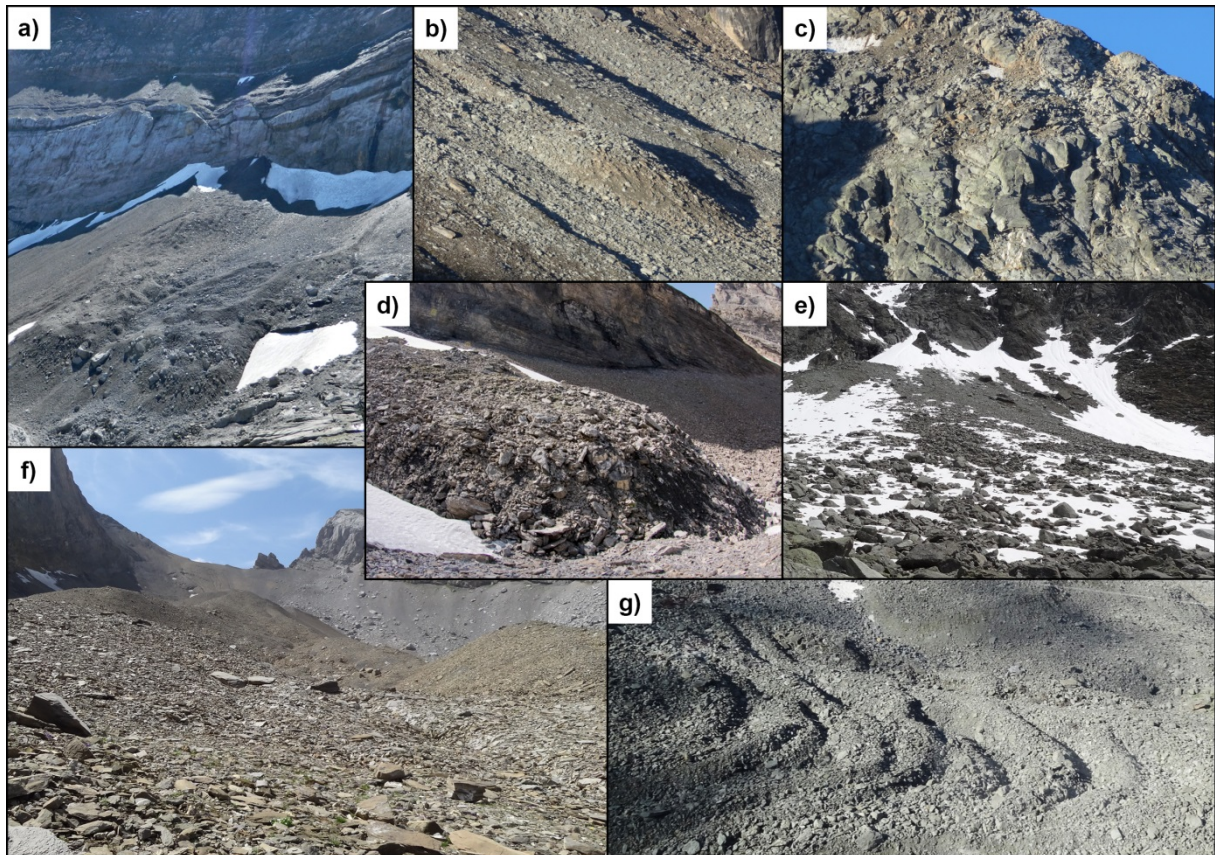


Fig. 2.5: Overview of periglacial landforms typical for the mountain permafrost domain: a) **debris covered glacier** at “Entre la Reille” (Les Diablerets, Photo kindly provided by Jean-Baptiste Bosson); b) **protalus rampart** above “Crap da las Ravulaunas” (Corvatsch, Upper Engadine); c) **fractured rock slope** of “Chastelets / Corvatsch; d) tongue of a **rock glacier** in the “Furggentälti” (Gemmi, Bernese Alps); e) talus slope below the “Blanche de Perroc” (Tsarmine, Val d’Arolla); f) **push moraines** at “Creux de la Lé” (Sanetsch) and g) characteristic **furrows and ridges** on the rock glacier Murtèl-Corvatsch.

In summary, periglacial landforms need to be discussed mainly because of their formation and evolution but they do not unambiguously describe the spatial variability of mountain permafrost. For a comprehensive view of specific permafrost landforms, the driving factors of the ground thermal evolution, namely the snow conditions and the topo-climatic and ground characteristics need to be considered. Regarding snow, two major categories can be distinguished, snow-rich (with at least 50-100 cm of snow in late winter, usually insulating the ground for several months) and snow-poor locations. The **snow-rich** comprises flat or gently inclined terrain, furrows and gullies, the lee side of crests and deposition zones of frequent avalanches, whereas the **snow-poor** category covers very steep and/or wind-exposed **locations**. At the latter, GST behaves similarly to air temperature. Both categories could be further separated into sub-categories according to the **composition and structure of the subsurface** and the **roughness of the surface**. A higher roughness decreases the thermal insulation effect of the snow. In this regard, rock glaciers as well as talus and scree slopes, which consist of very coarse-blocky material, are most likely to contain permafrost. Depending on the geomorphological history, ground ice may originate from former colder climatic conditions, the integration of ice by terrain movements or from in-situ formation due to intense ground cooling.

2.2 Properties and processes influencing the ground thermal regime

The ground thermal regime is mainly influenced by the **energy fluxes between the ground surface and the atmosphere** which are temporally and spatially highly variable (Hoelzle et al., 2001; Williams and Smith, 1989). In contrast, the geothermal heat flux Q_g (Wm^{-2}) remains constant for large time scales. For the Alps, 0.08 Wm^{-2} is a common estimate of Q_g (Medici and Rybach, 1995), but due to topographic and transient effects it is spatially variable as well (Gruber et al., 2004; Harris et al., 2003). However, since the energy fluxes at the ground surface are by factors larger than Q_g (Mittaz et al., 2000; Scherler et al., 2014), the geothermal heat flux can be neglected when focusing on the evolution and spatial variability of mountain permafrost at the time scales of years to decades.

2.2.1 Heat and energy exchange at the ground surface

The surface energy balance is the most important boundary condition for permafrost evolution. Theoretically, it can be measured at the point-scale (Mittaz et al., 2000), but to date this is not yet possible for larger areas or a high quantity of points in steep mountainous terrains. Studies based on micro-meteorological data (Sect. 3.3) have shown that the surface energy fluxes depend on point-specific properties, such as the surface albedo, the humidity of the near-surface substrate and the temperature gradient at the ground-atmosphere boundary (Hoelzle et al., 2001; Mittaz et al., 2000; Schneider, 2014). All these properties are greatly **influenced by the presence or absence and the properties of the snow cover** (Sect. 2.1.2 and 2.2.2).

The **components of the surface energy balance** are illustrated in Fig. 2.6a for different topo-climatic and snow conditions. According to Eq. 1, the sum of all energy fluxes equals 0:

$$Q_{rad} + Q_h + Q_{le} + Q_g + \Delta Q_m + Q_s = 0 \quad \text{Eq. 1}$$

$$Q_{rad} = S_{\downarrow} + S_{\uparrow} + L_{\downarrow} + L_{\uparrow} \quad \text{Eq. 2}$$

Q_{rad} (Wm^{-2}) corresponds to the net radiation; Q_h (Wm^{-2}) to the sensible heat flux, Q_{le} (Wm^{-2}) to the latent heat flux, Q_g (Wm^{-2}) to the geothermal (ground) heat flux; ΔQ_m (Wm^{-2}) to the melt energy at the snow surface and Q_s (Wm^{-2}) the heat flux through the snow cover (Scherler et al., 2014; Williams and Smith, 1989). Q_{rad} (Eq. 2) consists of shortwave incoming and outgoing radiation (S_{\downarrow} , S_{\uparrow} in Wm^{-2}) and longwave components of incoming and outgoing radiation (L_{\downarrow} , L_{\uparrow} in Wm^{-2}). More detailed descriptions of the surface energy balance can be found in Oke (1987) or Stocker-Mittaz (2002).

In most situations temperature and particularly temperature differences (Sect. 3.2) are good approximations for the integral of the surface energy balance at steady-state (Oke, 1987). Based on temperature indices or aggregates, heat and energy fluxes can only be qualitatively estimated. The latent heat of fusion (334 MJm^{-3} for liquid water) and changes of in the heat capacity ($4.18 \text{ MJm}^{-3}\text{K}$ for liquid water at 0°C ; $2.29 \text{ MJm}^{-3}\text{K}$ for ice at 0°C), e.g. due to ice loss, over time need to be considered (Williams and Smith, 1989). In addition to the terrain and snow cover, the substrate greatly influences the heat and energy transport between the surface and the permafrost (Fig. 2.6b-d). It is most complex for coarse blocky substrate because of turbulent fluxes (Sect. 2.2.3 and 2.2.4).

The permafrost is defined as the zone of GT remaining below or at the **freezing point of water** for two or more years between its base and the permafrost table; the surface layer in which water is subject to annual thawing and freezing is called **active layer** (Fig. 2.6).

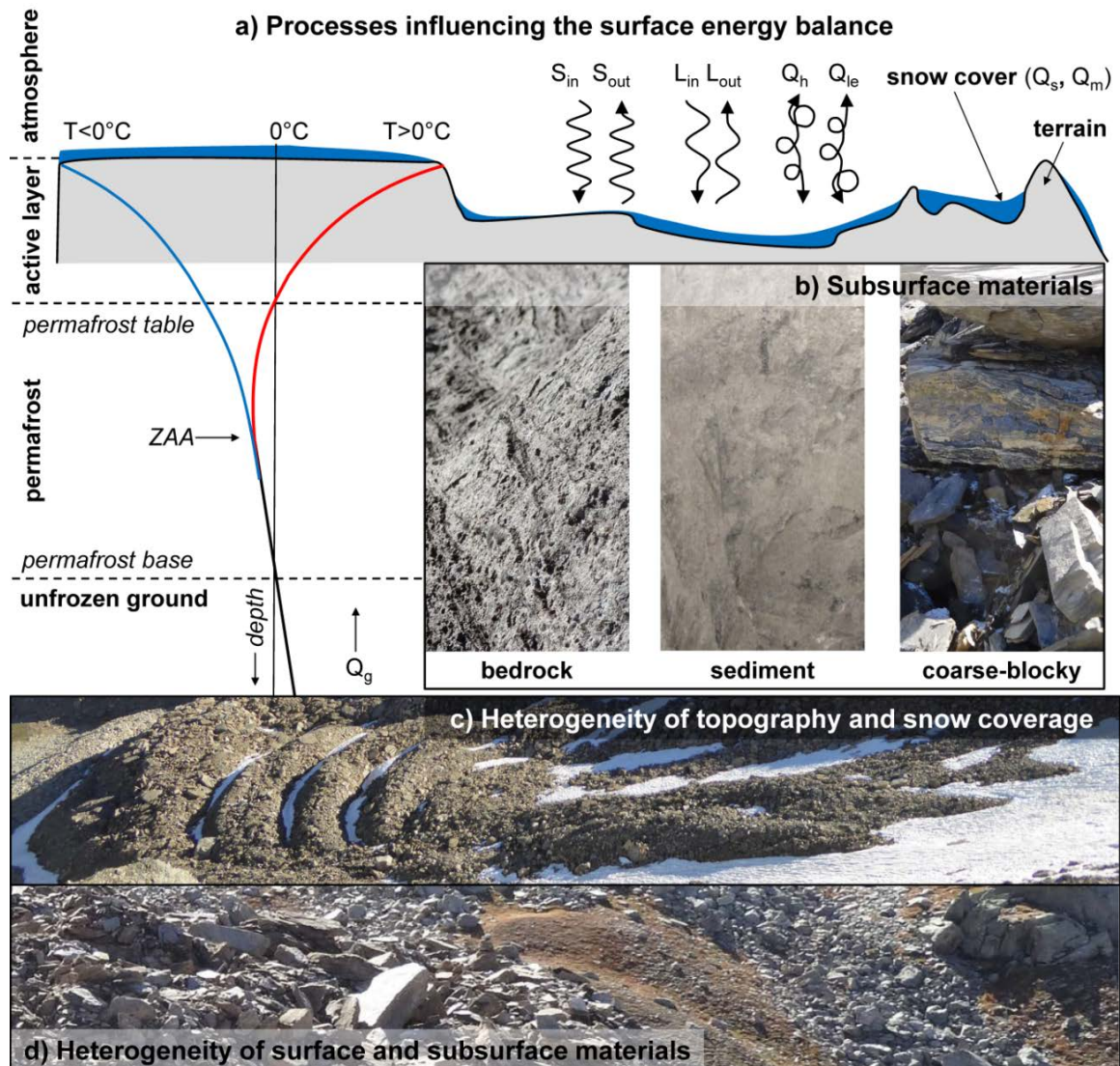


Fig. 2.6: Processes of heat and energy exchange at the ground surface and typical characteristics of mountain permafrost: a) Processes influencing the surface energy balance are illustrated on a fictional terrain with variable snow coverage. On the left, a typical temperature profile is shown, which defines the vertical extent of the permafrost. The shallowest depth at which seasonal temperature variations become nonexistent is called zero annual amplitude (ZAA). Different types of subsurface materials are shown on inset b), where the complexity of the heat transport mechanisms is highest for coarse-blocky substrate. The photographs c) and d) illustrate the heterogeneity of topography, radiation, snow coverage and near-surface substrate on small spatial scales, which make the heat transport over mountain permafrost very complex.

The following section illustrates the high importance of the snow cover for the surface energy balance by comparing snow characteristics with GST time series.

2.2.2 Influence of the snow cover on the surface energy balance

The temporal variability of the snow cover, or more precisely its thermal insulation effect and the modification of the radiation balance, are crucial for the evolution of GST (Gądek and Leszkiewicz, 2010; Goodrich, 1982; Luetsch et al., 2008; Zhang, 2005). The relationship between snow and GST is illustrated in Fig. 2.7 at the example of the Gemmi rock glacier (GFU in Fig. 3.1).

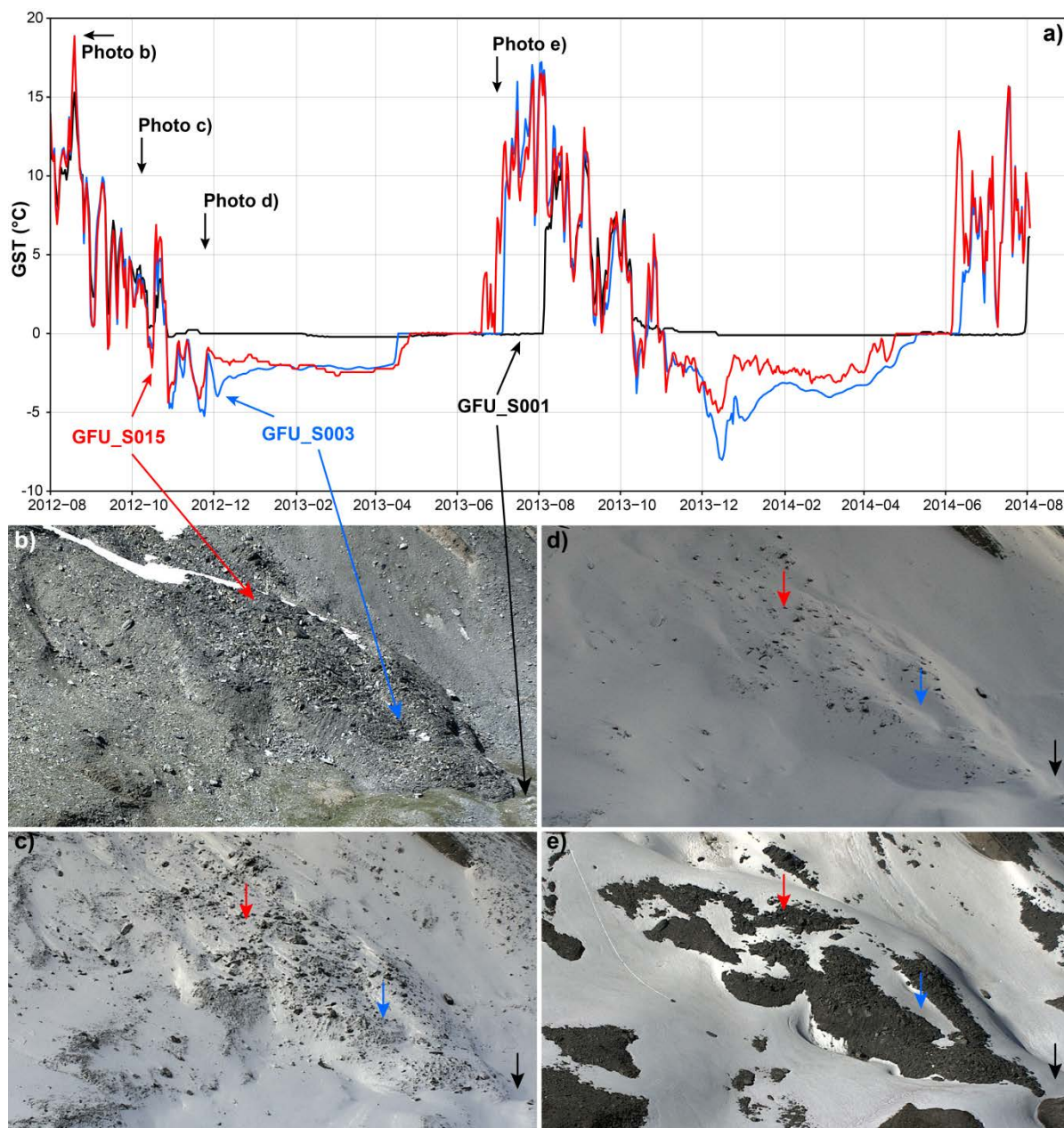


Fig. 2.7: Influence of snow on GST at the example of the Gemmi rock glacier: Panel a) shows the evolution of GST for three different GST loggers (in red, blue and black). On b-e, varying snow conditions over the season are illustrated using webcam images. The geographic position of the thermistors and the time of the four photographs are indicated by arrowheads.

During the snow-free period in summer (Fig. 2.7b), GST generally closely follow the variations of air temperature (Fig. 2.7a-b). Daily GST amplitudes may differ depending on the placement depth of the thermistors, the exposure to solar radiation, wind and the moisture content of the surrounding ground material. Logger GFU_S001, which is placed in fine-grained soil material, reacts very sensitively to snow events in autumn and remains at 0 °C for a long period. These so-called **zero curtains** (Outcalt et al. 1990) typically persist in non-permafrost areas and occur on permafrost during the snow melt and freeze-up. The signals of the other two loggers (GFU_S003 and GFU_S015) show considerable short-term variations in early winter because the surrounding subsurface material freezes very quickly and the ground remains influenced by air temperature. The thermal **insulation effect of the snow** is slightly more pronounced for logger GFU_S003 (snow accumulation in a gully)

compared with GFU_S015 (more exposed to wind). In spring, the **snow melt** starts a few days earlier at GFU_S003, because it is considerably more exposed to solar radiation than GFU_S015. But due to the higher total amount of snow, the melting period takes longer at GFU_S003 compared with GFU_S015. In early summer, the spatial heterogeneity of the snow is very great (Fig. 2.7e) and significantly affects the thawing of the ground. Because of the high position of the sun and warm air temperatures, GST may be up to 5-10 °C warmer as a daily mean where snow-free compared with a snow-covered state. Moreover, the comparison with other years reveals important inter-annual variations in the response of GST to meteorological events (Sect. 7.1). For instance the snow-rich winter and spring 2013 caused a late melt-out despite of very intense snow melt in June (Fig. 2.7a).

Due to the spatial and temporal variability of snow (Sect. 2.1.2 and Fig. 2.4), the **physical properties of snow** require special attention regarding their influence on the surface energy balance. The thermal conductivity of snow ranges from $0.1 \text{ Wm}^{-1}\text{K}^{-1}$ for fresh snow with a large fraction of air to $0.5 \text{ Wm}^{-1}\text{K}^{-1}$ for old snow with higher density and is 5-20 times lower than that of mineral soils (Zhang, 2005). Therefore, the snow cover can be seen as a **thermal insulator** which thermally decouples the ground from the atmosphere if it is sufficiently thick. Reported minimum snow depth thresholds for effective thermal insulation vary between 60 and 100 cm (Haeberli, 1973; Hanson and Hoelzle, 2005; Isaksen et al., 2002; Keller and Gubler, 1993; Luetsch et al., 2008; Zhang, 2005). The value is lower on smooth and flat surfaces than over coarse-blocky terrain and greatly depends on the density (ρ) and structure of the snow cover as well as on terrain roughness (Delaloye, 2004). Generally, the thermal insulation effect is most variable for shallow snow depths of a few dm (Isaksen et al. 2011). The definition of more reliable thresholds for the thermal insulation effect of snow would require a systematic comparison of the thermal resistance of the snowpack with snow depth records for different snow densities and terrain, and is still a gap in research.

For the European Alps, **typical densities** for fresh snow range between 100 and 300 kgm^{-3} and values between 300 and 500 kgm^{-3} are characteristic for the melting period between April and June (Jonas et al., 2009). The low density of fresh snow implies a high pore volume filled with air. If the snowpack is permeable and air circulating through, e.g. in funnels or at the contact zones to blocks or rock spurs, the snow pack may additionally cool this air mass before it reaches the ground surface. This leads to a strong cooling effect in the ground, e.g. on talus slopes where cold air is aspirated by the chimney effect (Sect. 2.1.3) as well as in coarse-blocky terrain which is very susceptible for convection in voids (Sect. 2.2.4). Moreover, **snow greatly influences the radiation balance** at the surface and therefore has a significant impact for mountainous ecosystems and phenomena like permafrost (Ishikawa, 2003; Luetsch et al., 2008; Zhang, 2005). The **albedo** of fresh snow is very high (up to 0.9), and even for old and wet snow it remains high (0.5-0.6) in comparison with bare bedrock (Pomeroy and Brun, 2001). The **high emissivity** of snow increases longwave backward radiation, particularly in clear-sky conditions during the night ("**autumn snow effect**", Keller and Gubler (1993)). For these reasons, the **snow situation in autumn can have a long-lasting effect** on the ground temperatures during the winter season as well as on the annual mean (Sect. 7.2.1).

The thermal insulation effect of snow is relevant for flat and gently inclined terrain as well as for near-vertical **rock walls** of high roughness, e.g. where snow accumulates on rock spurs. Since many rock faces are of variable inclination and aspect, snow may be more relevant at smaller spatial scales than on other periglacial landforms (Haberkorn et al., 2015; Wirz et al., 2011). Additionally, reflected radiation from surrounding areas may increase the daily amplitudes of rock surface temperatures in comparison with air temperature. Overall, the relative importance of the radiative and the insulating component is an ongoing debate (Hasler et al., 2011; Magnin et al., 2015).

In snow accumulation areas or after particularly snow-rich winters (e.g. the “avalanche winter” 1998-1999), as well as in years with limited snow melt in the summer season (as occurred in 1995 in the Swiss Alps), seasonal snow may persist and form **perennial snow patches** (Fig. 2.7b). Perennial snow patches have been used as topo-climatic indicators for permafrost (Haeberli, 1975; Keller, 1994), and for particularly shallow active layer depths (Krummenacher et al., 1998). However, this relation to permafrost is delicate. Snow may remain longer than one year due to massive accumulation by avalanches and wind, and its effect on the ground thermal regime depends on the local thermal and climatic conditions. Hence, sporadically occurring snow patches which only form after extreme avalanche events should not be directly treated as an indicator of cold ground conditions. If snow patches last longer than a couple of years, however, they may effectively point to the presence of permafrost.

Regarding changes in the **snow climatology**, a clear increase in winters with little snow has been observed by weather station data from lower elevation since the end of the 1980's without any clear trend over the past 10-15 years (Marty, 2008). Satellite-based studies from Hüsler et al. (2014) for the past three decades also confirm a decrease in the mean snow cover duration at lower elevation. However, the latter study did not find a significant change in the monthly snow cover area fraction for the high-mountain domain of the European Alps. Data from PERMOS (derived from GST measurements, Sect. 5.2) did not allow for sound conclusions about trends to date in the timing of the snow cover, mainly because the time series are short and inter-annual variability very large. Increased mean annual air temperatures do not necessarily lead to shorter snow cover durations, particularly for the high elevation band (Morán-Tejeda et al., 2013). This observation is reinforced by a recent study from Schmucki et al. (2014), where for the high-elevation station at Weissfluhjoch (2540 m asl) the increase in precipitation partly compensated the rise in air temperature regarding the mean snow duration and snow depth. However, for mountain permafrost, the timing of the snow is believed to be more important than the total snow duration (Delaloye, 2004).

In summary, **snow information is essential** for analysing the ground thermal regime and its influencing processes in detail. This information is usually only available for a few points (weather stations) which are not representative for all points of interest.

2.2.3 Heat and energy exchange as a function of subsurface characteristics

The **mass and energy fluxes at the ground surface** have been identified as the main drivers for changes in the thermal regime within the active layer and the permafrost below (Hoelzle et al., 2001). In this context, the most important physical processes are **heat conduction, convection** and **advection**. As with GST, the latent heat of fusion and changes in the heat capacity deserve particular attention when working with thermal data. With increasing depth, the properties of the subsurface become more and more relevant (Williams and Smith, 1989). Therefore, the maximum depth of daily and seasonal temperature variations depend on the structure and composition of the subsurface. A “buffering effect” is often attributed to ground material, which filters variations in the surface energy fluxes. This buffering effect mainly depends on the efficiency of the heat transfer and the occurrence of moisture in the form of water, ice or vapour (Williams and Smith, 1989).

The thermal parameters of a material can be described by its **thermal conductivity** k ($\text{Wm}^{-1}\text{K}^{-1}$) and **volumetric heat capacity** C ($\text{Jm}^{-3}\text{K}^{-1}$), which vary with the density and water content of the given material. Heat transfer by **conduction** is usually responsible for the largest part of the total heat transport in the ground (Williams and Smith, 1989). In massive, unfractured bedrock of homogeneous mineral composition, thermal conduction accounts for the entire energy flux. The energy flux is proportional to the negative temperature gradient within the material (Fourier’s law of heat conduction). Heat conduction is the main (and often unique) heat transport process included in many ground thermal models since it can be simplified by assuming linearity and taking constant literature values for k (Gruber and Hoelzle, 2008). In this case, the **ground heat flux** Q_g (Wm^{-2}) is:

$$Q_g = -k \left(\frac{\partial T}{\partial z} \right) \quad \text{Eq. 3}$$

where T is the temperature and z the depth (Williams and Smith, 1989). Assuming steady-state conditions and one-dimensional heat flow, the temperature at a given depth T_{d2} can be calculated as:

$$T_{d2} = T_{d1} + \left(\frac{Q_g}{k} \right) \cdot \Delta z \quad \text{Eq. 4}$$

where T_{d1} is the temperature at another depth and Δz is the depth difference (Williams and Smith, 1989). Conductive heat transport is most efficient for high, continuous temperature gradients and significantly reduced by layers of low conductivity (e.g. with large fractions of air), small temperature gradients (during isothermal conditions in the ground or in the snowpack) or temperature gradients overriding the point of fusion.

In reality, the subsurface is not a homogenous solid but fractured and filled with fluids (ice, water, vapour and dry air) in its cracks or voids. These fluids may thermally interact with each other and the surrounding ground materials by conduction, **convection** and **advection** (Williams and Smith, 1989). Convective energy fluxes by turbulent and radiative heat transfer, so-called **thermal radiation**, are particularly important in coarse-blocky material as well as in rock fractures and clefts (Delaloye, 2004; Harris and Pedersen, 1998; Mittaz et al., 2000; Scherler et al., 2014). Percolating water

transports energy by advection and is therefore important in any permeable substrate (Endrizzi and Gruber, 2012; Scherler et al., 2010). All these energy fluxes are interacting, non-stationary, three-dimensional and transient regarding past, current and future climate change (Noetzli and Gruber, 2009; Noetzli et al., 2007).

Because water ($\sim 4.2 \text{ kJkg}^{-1}\text{K}^{-1}$) and ice ($\sim 2 \text{ kJkg}^{-1}\text{K}^{-1}$) have high specific **heat capacities** compared to the other subsurface components (rock and air), more energy is required to warm water or ice. Phase changes at $0 \text{ }^\circ\text{C}$ further limit temperature gradients between the surface and the permafrost during the thawing season. Therefore, phase changes strongly influence the temperature of the surrounding material. Due to the large amounts of energy required for melting ice (enthalpy of fusion $\sim 334 \text{ kJkg}^{-1}$), ground ice may act as a heat sink. Hence, **ice-rich permafrost is expected to react less rapidly to ground warming** in terms of active layer deepening and permafrost degradation. But in situations with cold ice, a much stronger ground temperature increase may occur compared to situations where ice is close to the melting point. Changes in the ground ice content may be irreversible if the ground thermal regime is not in equilibrium with the climate (Marmy et al., 2015; Scherler et al., 2013). This was observed by increasing active layer thaw depths, high electric resistivities and increasing kinematic activity of many rock glaciers (PERMOS, 2013).

In summary, the thermal response of a permafrost mass to a warming within the active layer is mainly a function of the thermal conductivity and heat capacity of the surrounding subsurface materials (Harris et al., 2009; Osterkamp and Osterkamp, 1983), but may be influenced by convective and advective heat fluxes as well. In this context, the next section provides more information on landforms which consist of coarse-blocky material and show particularly high ice contents.

2.2.4 Characteristics of coarse-blocky and ice-rich substrates

The coarser the sediments at the ground surface are, the more the cooling of the ground is favoured (Gruber and Hoelzle, 2008; Harris and Pedersen, 1998). This is particularly the case under a snow cover, if voids in the ground remain connected to the atmosphere and act like “bypasses” for air circulation. An irregular topography as well as wind striking on the ground surface facilitate this exchange of air with the atmosphere, e.g. at the edges of large boulders or on ridges. Convection may act at many different scales from a few cm between blocks up to hundreds of meters in the particular case of the “chimney effect” (Sect. 2.1.3).



Fig. 2.8: Illustration of convective air circulation within coarse-blocky material, which may cause very rapid and intense ground cooling. Typically, the ground cooling and the formation of ground ice in rock glaciers and talus slopes profit from this process because voids beneath large blocks or boulders function as bypasses for circulating fluids. The photograph shows a part of a rock glacier at the Gemmi site; the large boulders in the front have diameters of ~1.5-2 m.

Fine ground material (in this context any substrate not coarser than gravel) is less permeable for air, but it is usually wetter and prone to phase changes in autumn, because the freezing of the water takes much more time than in dry substrate (Sect. 6.2). The reduced permeability of fine materials implies that melt water is more likely to refreeze in the close proximity. Since during the (re)freezing of water latent heat is emitted, it tends not to freeze unless it gets very cold (Williams and Smith, 1989). If water refreezes, this equates to a net warming in comparison to a rapid evacuation of liquid water out of the system as it is expected to happen in coarse-blocky material on inclined slopes. Therefore, a net heat loss e.g. by strongly negative temperature gradients is required to build new ground ice in fine-grained material of limited permeability.

Overall, the energy input into the ground in summer by conduction, convection and advection may be smaller in comparison to the potential heat loss during cold winter conditions. Such permafrost-favourable winter conditions are periods of little snow, little moisture remaining in the ground combined with cold air temperatures.

2.3 Mechanics of frozen ground materials and ice

In mountainous areas with high potential relief energy, changes in permafrost terrain are relevant for gravitational natural hazards and potential destabilisation of engineering infrastructures due to **slope stability issues** and changes in the **sediment yield** (Bommer et al., 2010; Fischer and Huggel, 2008; Gruber, 2004; Harris and Davies, 2001; Käab et al., 2005; Ravelin et al., 2010). The mechanics of frozen materials influence the processes and rates of sediment production and transport throughout the entire sediment cascade (Gärtner-Roer, 2012; Müller et al., 2014a). The mechanical behaviour of permafrost is complex and subject to intense research, particularly regarding rock-slope failures (Krautblatter et al., 2013) and rock glacier kinematics (Arenson et al., 2002; Haeblerli et al., 2006).

Slope stability for a specific mass can be characterised as the sum of the resisting forces divided by the sum of the driving forces. Assuming constant geometry, the most important driving forces for the deformation of unfrozen mountain slopes are increased pore water pressure or surcharge resulting in additional stress on the slope (Selby, 1993). Reduced shear resistance, e.g. due to lubrication or disruptions at the foot of the hillslope, may trigger a sliding, toppling or falling of land masses as well. An important resisting force for soils is **cohesion**, which results from physical cementation or attractive forces between particles and increases the stability of hillslope materials (Selby, 1993). The presence of water decreases the soil strength in case of positive **pore water pressure**, whereas cohesion is in most cases negligible for materials coarser than silts (Williams and Smith, 1989).

Since **permafrost is a complex multiphase system** consisting of solid particles (rock and ice) and fluids (water and air), its mechanical properties differ significantly from unfrozen ground material (Williams and Smith, 1989). Typically, materials are stronger when frozen or sealed by ice. Cementation by ice can lead to a bonding between particles which is several times larger than cohesion of unfrozen soils (Williams and Smith, 1989). Critical slope angles were found to be significantly lower for ice-free permafrost compared to permafrost containing ice (Rist et al., 2012). Yet, high ice contents can also cause deformation, e.g. in creeping landforms such as rock glaciers (Haeblerli et al., 2006). Moreover, frozen ground materials may break rapidly when being heavily strained (Williams and Smith, 1989). Abruptly applied stresses are rare but may occur, e.g. in deposition zones of rock slides, rock avalanches or snow avalanches. More commonly, **frozen ground material is deformed slowly and continuously in a ductile manner similarly to that of ice** (Williams and Smith, 1989).

When looking at idealized **pure ice** as a polycrystalline material, deformation takes place over very short distances. Ice crystals (mm – cm scale) and crystal aggregates are deformed elastically in response to stress, but they also slide or shear and grow or shrink by internal deformation (Williams and Smith, 1989). As long as the stress is applied, the deformation will continue and result in the **characteristic creeping behaviour**. The **rheology of ice is viscoplastic**, hence depending on its viscosity in response of influencing stresses and by dissipating mechanical energy into heat (Duval et al., 2010; Williams and Smith, 1989). **The viscosity of ice strongly depends on temperature** and therefore also on pressure and the shear rate (Kannan and Rajagopal, 2013). Glen (1955) found that

under uniaxial compressive stress, ice creeps in a similar manner to that of metals at high temperatures. Like other polycrystalline materials, ice exhibits three stages of deformation: an initial decelerating **primary creep**, a quasi-stationary **secondary creep** and finally a **tertiary creep** with a high strain rate (Duval et al., 2010). However, large ice masses like valley glaciers do not only move by internal deformation, but also due to **sliding** on the glacier bed (so-called “basal sliding”). This sliding effect is particularly pronounced when the ice is warm (close to 0 °C) or if liquid water is present (Duval et al., 2010; Williams and Smith, 1989).

The deformability of frozen ground material increases non-linearly if temperatures warm towards 0 °C, which is similar to glacial flow. However, the **mechanic behaviour of ice-debris-mixtures** is more complex than that of glacier ice and dependant on additional factors. In permafrost, voids are not necessarily saturated with ice and particles could lock into each other (“interlocking”), and thus increase the shear strength as discussed in Kannan and Rajagopal (2013). Arenson (2002) proposed several approaches to describe the creep potential of permafrost and tested them with pressuremeter tests using data from the boreholes Murtèl-Corvatsch, Pontresina-Schafberg and Muragl (Arenson et al., 2002). Consequently, he proposed the following exponential function to describe the **creep velocity v of a rock glacier** as

$$v = a \cdot e^{bT}, \quad \text{Eq. 5}$$

where a is a variable parameter depending on the rock glacier geometry, its internal composition and the slope angle. The parameter b characterises the reactivity of the rock glacier to changes in permafrost temperature T (K). This **temperature dependency of rock glacier creep** has been observed based on permafrost monitoring data (Delaloye et al., 2008, 2010) and additional results using the PERMOS data set are presented in Sect. 6.3 and 7.3. Arenson et al. (2002) showed with observations that 50-95 % of the total surface deformation actually happens within one or more relatively thin layers of minimal viscosity between 15 and 30 m depth. This observation was recently corroborated by a theoretical model applied to the Murtèl-Corvatsch rock glacier by Kannan and Rajagopal (2013).

In summary, the most important factors influencing the mechanics of frozen subsurface material are **ground temperature, pore-water pressure** and **gravitational forces** relative to the geometry of the landform, the underlying bedrock and potential surcharging masses of rock, snow or ice. Resisting as well as driving forces can be temporally and spatially variable because of the continuously changing geometry and hydro-thermal conditions. To improve the process understanding of mountain permafrost kinematics to changing ground temperatures, joint geotechnical, geophysical and hydro-mechanical research is required (Krautblatter et al., 2013).

PART II: DATA AND METHODS

3 Permafrost monitoring data

Mountain permafrost is still a young research field. For the European Alps only a handful monitoring time series are longer than 15 years. Surface and subsurface temperature data are the earliest, longest and still most common continuous permafrost observations available. Many of them were undertaken because of specific research questions (e.g. the mapping of the distribution of permafrost) and did not aim at monitoring the permafrost evolution over decades.

In the context of applied high-mountain and climate research, **monitoring** is substantially different from collecting measurements at a set of sites over a couple of years. Monitoring aims at a systematic observation and documentation of relevant variables and processes and their changes over long time scales. To achieve comparable data of high quality, standards are required for the setup and implementation of the measurements as well as the data processing and archiving. The practical realisation of such a monitoring programme in high-mountain terrain faces a variety of technical, scientific but also financial, personal and safety issues. For example, rock fall, avalanches, lightning, snow pressure, heavy wind events or rodents attacking cables might destroy equipment and provoke data loss. Some observations may need to be stopped because loggers risk being destroyed, getting lost or becoming inaccessible or for personnel safety reasons. The measured data need to be checked for quality aspects and homogenized (chapter 4). Technological progress leads to changes in the instrumentation and the data processing, so the properties and informative value of monitoring time series may change over time.

The Swiss permafrost monitoring network **PERMOS** has been operational since 2000 and in addition to temperature data it also comprises meteorological, kinematic and geophysical data. Within PERMOS and in the frame of the research project TEMPS, major effort was put into data management, the setup of an operational data base and the collection of meta-information over the past four years. Within the TEMPS project, data from additional study sites (Fig. 3.1 and Table 3.1) were available for this PhD thesis. The next section provides an overview on the different monitoring sites and it is followed by a description of the different data sets.

3.1 Permafrost monitoring sites

Given the spatial distribution of permafrost in the Swiss Alps (Sect. 2.1.1) and due to the history of mountain permafrost research in Switzerland, the majority of the current permafrost monitoring sites is located around the inner-alpine zone between the Valais and the Upper Engadine (Fig. 3.1, Appendix A1 for an overview on the region names of the Swiss Alps). The PERMOS network has been recently extended to the Ticino region and now comprises a total of 29 monitoring sites (the low-elevation station at Creux-du-Van in western Switzerland was not considered for the present project and is therefore not shown in Fig. 3.1). Other sites which are maintained by PERMOS partner institutions belong to the research project TEMPS (DIR, LDV, MDO, PMR, RTD and SAN). Site abbreviations and the measured parameters are listed in Table 3.1. Detailed information on the data set and the measured parameters is provided in the following sections.

Chapter 3: Permafrost monitoring data

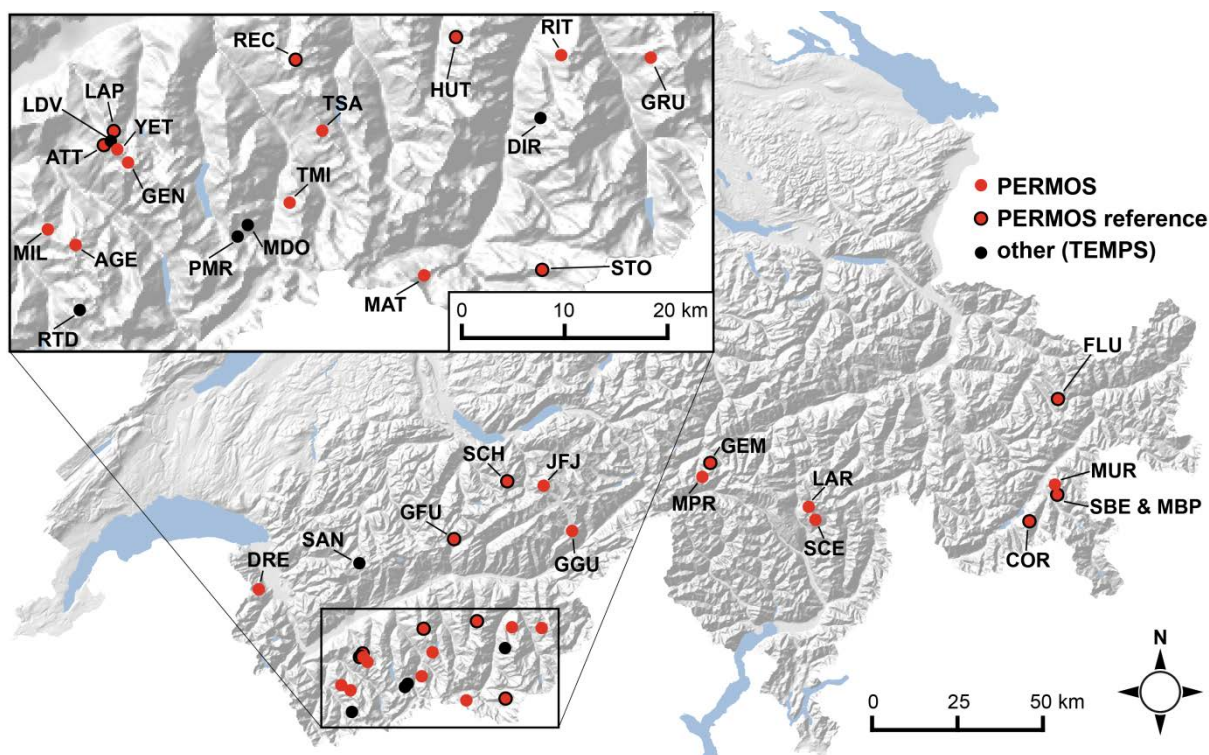


Fig. 3.1: Permafrost monitoring sites from which data were available for this PhD thesis. The inset map shows the sites of the Valais Alps in south-west of Switzerland in detail. Source background map: Federal Office of Topography.

Table 3.1: Permafrost monitoring sites overview: Site abbreviations in red correspond to the PERMOS sites shown in Fig. 3.1. The monitoring parameters are: meteorological stations (Meteo), borehole temperatures (BHT), ground surface temperatures (GST), basal temperatures of the winter snow cover (BTS), electrical resistivity tomography (ERT), refraction seismic tomography (RST), kinematic measurements (DGPS), aerial images (Airphoto). Data sources: PERMOS and UNIFR.

Abbr	Name	Alt. m asl	Landforms	Meteo	BHT	GST	BTS	ERT	RST	DGPS	Airphoto
AGE	Aget	2800 - 2900	rock glacier			x				x	
ATT	Les Attelas	2620 - 2800	talus slope	x	x	x		x	x		
COR	Murtel-Corvatsch	2500 - 3300	rock glacier, talus slope	x	x	x		x	x	x	x
DIR	Dirru	2350 - 2840	rock glacier					x	x	x	x
DRE	Dreveneuse	1560 - 1630	talus slope	x	x	x					
FLU	Fluela	2394 - 2501	talus slope, rock glacier		x	x		x	x		
GEM	Gemsstock	2850 - 2950	crest	x	x			x	x		
GEN	Gentianes	2870 - 2895	moraine	x	x	x		x			
GFU	Gemmi / Furggentälti	2460 - 2750	rock glacier, talus slope	x		x	x			x	x
GGU	Grosses Gufer	2200 - 2700	rock glacier			x				x	x
GRU	Gruben	2760 - 2900	rock glacier			x				x	x
HUT	Hungerlitaelli / Turtmanntal	2500 - 3000	rock glacier	x		x				x	x
JFJ	Jungfrauoch	2850 - 3750	crest		x	x					
LAP	Lapires	2380 - 2700	talus slope	x	x	x	x	x	x	x	
LAR	Stabbio di Largario	2240 - 2550	rock glacier			x				x	
LDV	Lac des Vaux	2720 - 2800	rock glacier			x		x		x	
MAT	Matterhorn	3250 - 3300	crest		x						
MBP	Muot da Barba Peider	2950 - 2980	talus slope	x	x	x					
MDO	Mont Dolin / Arolla	2760 - 2860	rock glacier, talus slope		x	x					
MIL	Alpage de Mille	2200 - 2500	rock glacier	x		x	x			x	
MPR	Monte Prosa	2440 - 2520	rock glacier			x				x	
MUR	Muragl	2480 - 2900	rock glacier	x	x			x	x	x	x
PMR	Petit Mont Rouge	2590 - 2700	rock glacier, talus slope		x	x					
REC	Rechy / Becs de Bosson	2600 - 3100	rock glacier	x		x	x	x		x	x
RIT	Ritigraben	2550 - 2900	rock glacier	x	x						x
RTD	Ritord	2500 - 2900	crest, rock glacier, moraine			x					
SAN	Sanetsch / Creux de la lé	2300 - 2400	moraine			x		x			
SBE	Schafberg	2730 - 2760	rock glacier		x	x				x	x
SCE	Valle di Sceru / Piancabella	2460 - 2560	rock glacier, talus slope			x				x	
SCH	Schilthorn	2400 - 3000	crest	x	x	x		x	x		
STO	Stockhorn	3390 - 3410	crest	x	x			x	x		
TMI	Tsarmine	2460 - 2600	rock glacier			x				x	x
TSA	Tsate	3030 - 3070	crest	x	x	x					
YET	Yettes Condja	2600 - 2800	rock glacier			x	x			x	

3.2 Temperature measurements

Since permafrost is defined thermally, ground temperature measurements are the most obvious monitoring parameter. Ground surface temperature (GST) records represent the thermal state at the boundary to the atmosphere, whereas ground temperatures (GT) are the only method to directly measure the thermal evolution of the permafrost at depth.

3.2.1 Ground surface temperatures (GST)

GST are commonly measured with miniature temperature loggers (Hoelzle et al., 1999) ~5-20 cm below the ground surface. The loggers record the sum of energy fluxes influencing the temperature of the near-surface ground material. The technique originates from the BTS-method (Haerberli, 1973), which was developed to measure the ground thermal signal from depth at the surface when the active layer is supposed to be in an isothermal state in late winter. **BTS** is most popular for permafrost mapping (Bonnaventure and Lewkowicz, 2008; Hoelzle et al., 1993) and it is used at some sites (LAP, REC, MIL) to assess the spatial and temporal distribution of GST in late winter (Delaloye, 2004). **Continuous GST measurements** have the advantage to cover entire years and they are independent of field work during winter. In contrast to skin surface temperatures which are widely used in remote sensing or climate modelling, the GST signal is only indirectly influenced by radiation and its diurnal amplitude is smoothed. This allows analysing the state and changes of the ground thermal regime and the snow cover with relatively little noise in the data (Sect. 4.1.1).



Fig. 3.2: UTL-1 and UTL-2 miniature data loggers measuring GST in the field.

Due to the different thermistors in use, typical GST **measurement intervals** vary between 30 minutes and 3 hours and the very first measurements were made at 4.5 h intervals. The most common **logger** types are Geotest UTL-1 (0.23-0.27 K precision, ± 0.1 K accuracy), Geotest UTL-3 (<0.1 K resolution, accuracy ± 0.01 K), Geoprecision M-Log5W minillogger with sensor PT1000 (0.01 K resolution, ± 0.1 K accuracy) and iButton (DS1922L, accuracy of 0.5 K as specified by the manufacturer but around ± 0.125 K near 0°C (Gubler et al., 2011), resolution 0.065/0.5 K) with accuracies ranging between 0.01 and 0.5 K. Wherever phase changes occur, offsets to 0 °C can be minimized to calibrate the sensors (Sect. 4.1.1). However, coarse sampling rates may reduce absolute accuracy.

The **placement** of loggers in the field is very important since the micro-climatic and terrain-specific conditions need to be kept over decades. Wherever possible, similar standards should be applied for all different loggers and sites regarding the placement depth, the orientation and setup of the logger.

Hence, it is a great advantage that the principal investigators delivering data to PERMOS maintain their loggers and sites for many years in a row. However, inconsistencies still arise if the terrain characteristics or the micro-climate are changing, e.g. on fast-moving rock glaciers.

The **GST data set** of the PERMOS/TEMPS data base is unique in terms of data quantity and covers time series from 273 different positions of variable length among which most are 5-15 years long (Fig. 3.3a). This data set is suitable to analyse the evolution of Alpine permafrost at a high temporal and spatial resolution, even though several GST time series are interrupted by gaps (particularly in summer, Fig. 3.3b-d). The homogenization of GST time series and handling of data gaps are discussed in Sect. 4.1.1 and 4.2.3.

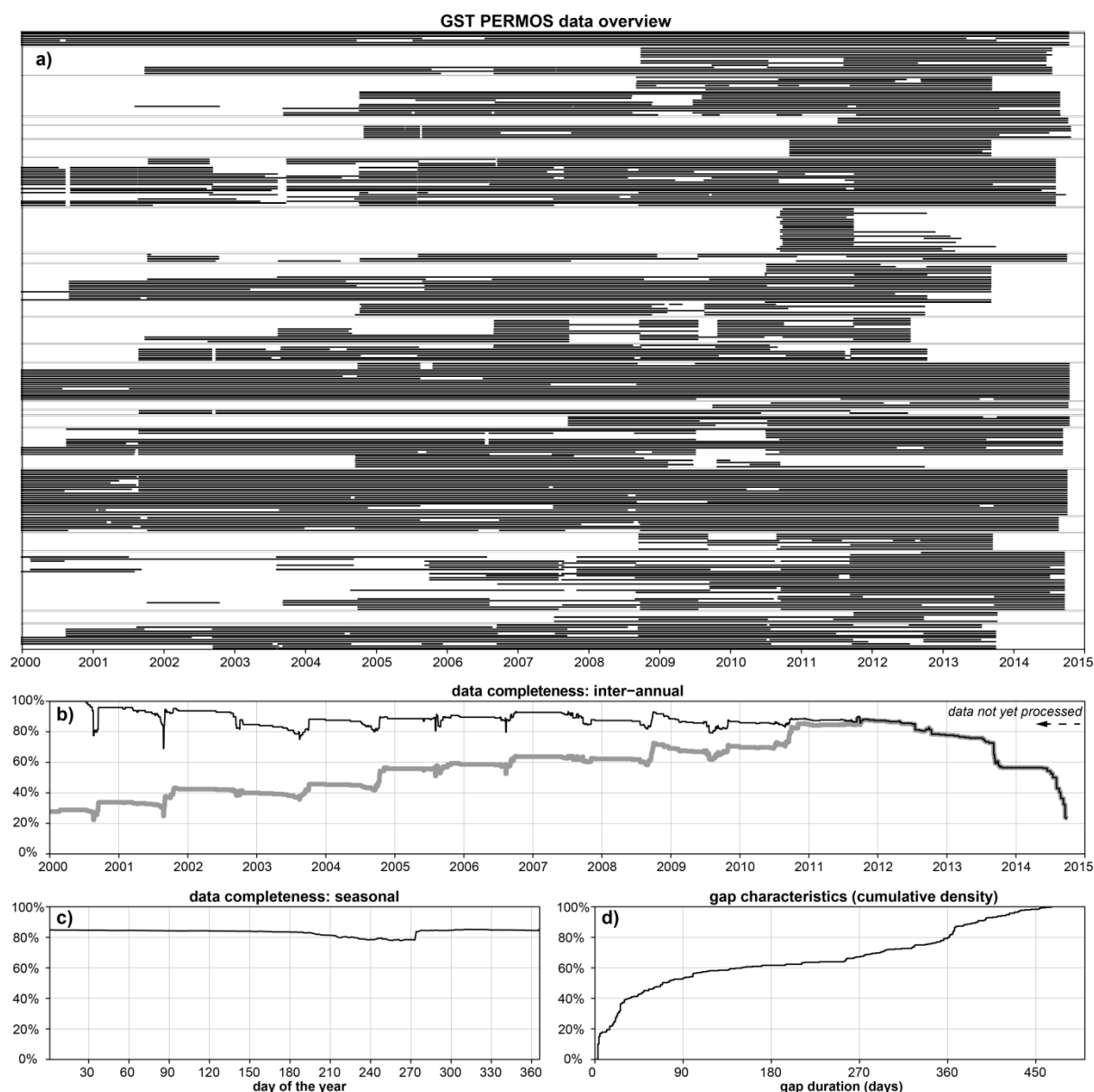


Fig. 3.3: Data completeness and gap characteristics of the GST monitoring data from 2000 until autumn 2014 (gaps shown after 2012 are mainly because data was not yet delivered). a) data availability overview for each GST logger (each line on the y-axis corresponds to one GST time series), black when data is available; b) data completeness in relation to the total number of GST series started (black line) and compared to the maximum number of GST loggers (grey line, 278 loggers first reached in 2012); c) seasonal pattern of data completeness (day 1 corresponds to January 1st); d) empirical cumulative density function of the gap duration for data gaps shorter than 500 days.

3.2.2 Ground temperatures (GT)

GT are usually measured in **boreholes** with thermistor chains (e.g. YSI Precision series 44000 and 46000) connected to multi-channel loggers (common types are Campbell CR10X, CR800, CR1000 or MADD logger). Typical accuracies of the thermistors range between ± 0.01 K and ± 0.2 K. Most PERMOS boreholes are percussion drillings (vertical, slope-perpendicular or horizontal) with a PVC tube inlet and sealed on top and at the bottom to prevent water intrusion. The resulting temperature profiles are one-dimensional and discontinuous. The **spacing** between the thermistors is either regular over the entire profile or at a finer resolution in zones of particular interest (e.g. at the permafrost table and base) ranging between a few cm to several meters. New technologies may in future allow a quasi-continuous measurement along entire profiles, e.g. by using fibre optics (Freifeld et al., 2008), even if it currently appears that thermal sensors are the most reliable method.

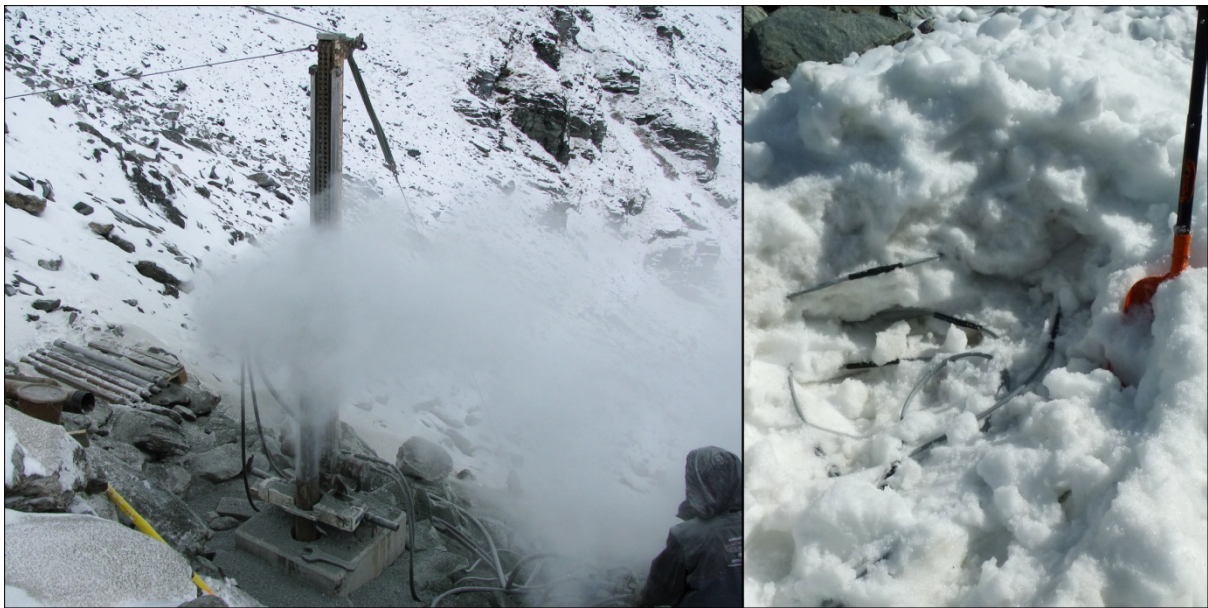


Fig. 3.4: Left: Drilling of a borehole at the Lapires site in October 2008 (Photo: C. Scapozza); right: calibration of a thermistor chain in the wet snow, at the Lapires site in June 2015 (Photo: A. Wiedmer).

The **temporal resolution** of GT measurements is very diverse, but several time series are recorded only once a day. Technically, one measurement per day is sufficient for resolving temperature variations at depth. Hourly sampling intervals, however, are beneficial for the representation of the uppermost meters, the comparison with GST data and for the interpretation of specific phenomena. Moreover, potential errors such as temperature offsets, drift or spikes are easier to detect and correct with data of higher temporal resolution (Sect. 4.1.1).

As with the GST loggers, also borehole thermistors need to be calibrated. But depending on the ground thermal regime, not all sensors are subject to phase changes (freeze-thaw-cycles) and hence the on-site calibration in the tube is often not possible (Sect. 4.1.1). The **calibration** of thermistors can be done either in the lab (before the installation or for maintenance) or directly in the field in spring when the snow cover is wet and at 0°C (Fig. 3.4). If the borehole is deformed (typically on rock glaciers) or frozen inside, the removal and replacement of thermistors may not be possible anymore.

The oldest PERMOS borehole COR_0287 at Corvatsch (Fig. 1.2) has been subject to this problem for many years and will be renewed in 2015. Fig. 3.5 provides an overview of the availability of ground temperature data from PERMOS and TEMPS. As with the GST data, most time series are interrupted by data gaps of variable timing and duration. Periods with complete data from all boreholes are rare. This complicates the calculation of aggregates and indices and renders the synergetic analysis of this data set demanding. The PERMOS borehole data and metadata is provided by PERMOS (2016)

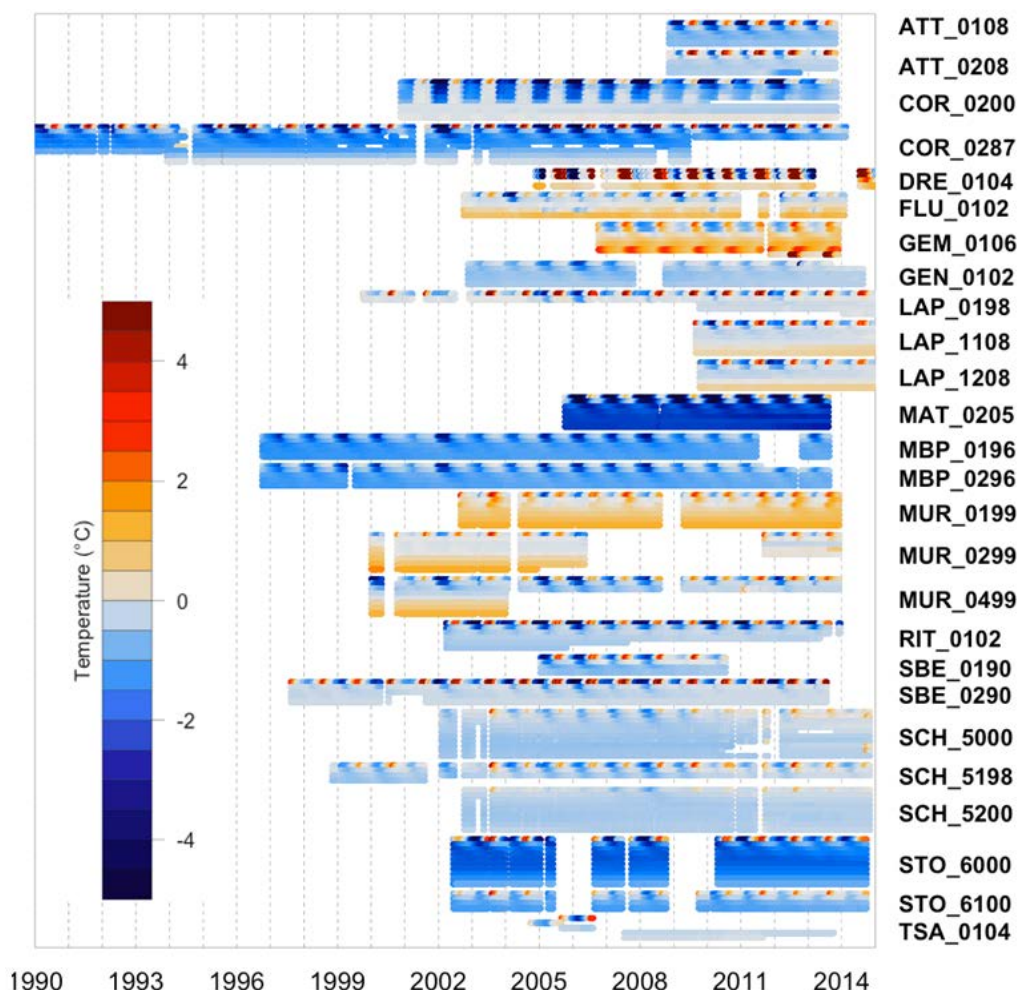


Fig. 3.5: GT data overview (figure kindly provided by J. Noetzli, PERMOS): For each borehole, contour plots are shown as time series. White areas indicate periods of missing data. On the right, the abbreviations of the boreholes are shown, among which the first three letters correspond to the site abbreviation (Fig. 3.1). For borehole meta data see Appendix A4.

3.3 Micrometeorological measurements

The site-specific climatic conditions are documented with **weather stations** at 17 of the PERMOS monitoring sites (Table 3.1). Most of these stations measure at least air temperature and shortwave incoming radiation. Additionally, a subset of 6 stations records the entire radiation balance, relative air humidity, wind direction and wind speed. Snow depth is measured either by ultrasonic (Campbell Scientific SR50 Sonic Ranging Sensor at 50 kHz, accuracy ± 1 cm) or snow poles equipped with thermistors (Delaloye, 2004; Lewkowicz, 2008) at 11 stations. A variety of different sensors is in use. Precipitation is not measured (except for the station Ritigraben), mainly because of power issues.

The **Alpine weather and climate** is also documented by the Swiss Federal WSL-Institute for Snow and Avalanche Research (SLF) and the Federal Office of Meteorology and Climatology (MeteoSwiss). The Intercantonal Measurement and Information System (**IMIS**, maintained by WSL, MeteoSwiss and Swiss cantonal and municipal authorities) measures various meteorological as well as snow depth at more than 160 sites in the Swiss Alps. Although many of these weather stations are not located on permafrost, this data is valuable for analysing snow depth at high elevation.

For this PhD thesis, **air temperature (AirT)** and **incoming shortwave radiation (ISR)** were mainly used to analyse other permafrost monitoring parameters such as GST or GT. Regarding AirT the radiation shield is of great importance and ventilated measurements have shown to be most reliable. Pyrradiometers are very sensitive to correct levelling. This is particularly important on moving landforms like rock glaciers, which are challenging for the long-term monitoring of the micrometeorological data. Innovative solutions have been found for this kind of problems, e.g. by using inclinable telescopic masts as shown in Fig. 3.6. However, the respective time series need to be carefully interpreted.



Fig. 3.6: Weather stations at the site Gemmi/Furggentälti: The station on the left is located on a solifluction lobe (Photo: Severin Schwab), the one on the right on a large boulder on the rock glacier nearby. A special tripod construction is used to equalize terrain movements. But due to large surface deformations, the station on the rock glacier needed adjustment almost every year. Since its installation in 2000, the station on the rock glacier moved > 50 m towards a zone of increased potential solar radiation.

Because of damage of the weather stations leading to data loss, the available meteorological data from PERMOS is interrupted by a multitude of gaps and erroneous values. For the **reconstruction of continuous time series** it proved to be inadvisable to extrapolate meteorological data from low-elevation stations due to the potential for inversions in many regions in Switzerland below ~1500-2000 m. For air temperature, good results could be obtained by using data from high-elevation stations such as Säntis (SAE, 2502 m asl, Fig. 1.1) or Grand St-Bernard (GSB, 2472 m asl). Moreover, the gridded data sets from MeteoSwiss (Frei, 2014) are valuable if a finer spatial resolution is required (Sect. 4.2.3). In the frame of the TEMPS project, Rajczak et al. (2015) developed methods for

the reconstruction of climate data with sparse observations and generated climate reanalysis time series (1981-2013) as well as downscaled climate scenarios (1961-2099) for the PERMOS sites SCH, COR, LAP, STO, RIT, FLU, GFU, CDV, GEM, MBP. This climate data is useful for permafrost modelling purpose (Marmy et al., 2015; Staub et al., 2015a).

3.4 Kinematic measurements

The **temporal evolution** of surface displacement rates on permafrost landforms is commonly measured by terrestrial surveys following markings on blocks, formerly with theodolites, nowadays mostly by means of real-time differential GPS (**DGPS**, Fig. 3.7a-b) or total stations. These measurements are mainly done during the summer period (on the same date \pm 2 weeks) when the ground is snow-free and document **inter-annual variations** of surface displacement rates (Delaloye et al., 2010; Lambiel and Delaloye, 2004; PERMOS, 2013). For a series of monitoring sites in the Valais Alps (maintained by the University of Fribourg), a **seasonal component** is additionally monitored by DGPS measurements in June at the end of the snow melt period as well as in October.

The **longest time series** of terrestrial surveys started in 1994 at the Gemmi (GFU) study site and the **most detailed measurements** (~70 DGPS campaigns since July 2004, every 2 months) exist for the Becs de Bosson rock glacier in the Vallon de Réchy (REC in Fig. 3.1). In general, a lot of DGPS data is available but most time series are shorter than those of GST or GT data. Occasionally, the boulders which contain the markings fall or topple. In consequence some targets need to be replaced because they become untraceable. This poses a great challenge for monitoring surface displacement rates on rock glaciers over long-term, particularly if the movements are fast (Sect. 4.1.3 and 4.2.5).

In addition to manual measurements, several rock glaciers are now equipped with (one or more) permanently installed GPS sensors (usually L1-single-frequency carrier phase modules, Fig. 3.7c) that continuously record their position. The use of **permanent GPS** devices for PERMOS is being evaluated during the period 2013-2015.

For analysing **spatial patterns** in more detail, DGPS measurements are only suitable when recorded very densely. Yet, other methods such as **photogrammetry** (based on aerial images taken from airplanes or drones), laser scanning (**LiDAR**) or terrestrial radar interferometry (**TRI**) perform well for the analysis of surface deformations at high spatial resolution (Caduff et al., 2015). For the application of these methods, the surface movements of interest need to be significantly larger than the resulting uncertainties. Therefore, mainly long time scales of several years were analysed by photogrammetry. Due to technical progress and the increase of the kinematic activity of many rock glaciers (PERMOS, 2013), movements over shorter time intervals may be quantified by photogrammetry in future (Kaufmann, 2012; Kenner et al., 2014; Müller et al., 2014b). For most areas in the Swiss Alps, **historic aerial images** allow the landscape evolution to be reconstructed back until the mid-20th century. Since permafrost creep has a strong climatic component, the analysis of the past kinematic activity of rock glaciers is of particular interest (Sect. 2.3).

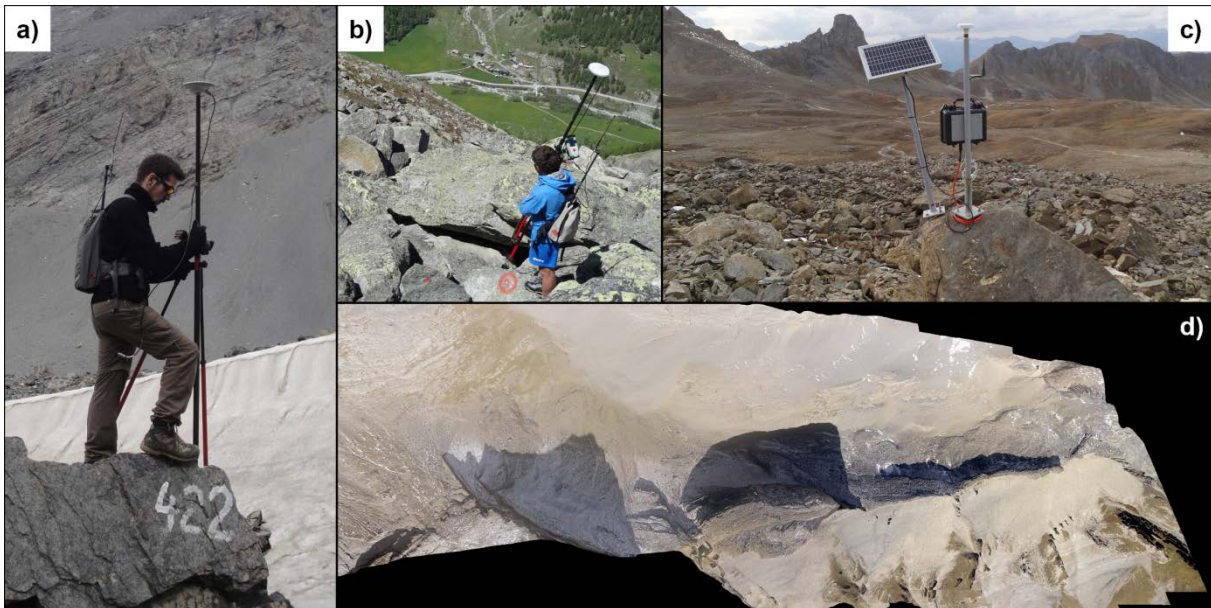


Fig. 3.7: Measuring displacement rates and surface changes on permafrost terrain: DGPS measurement at the Gemmi (a) and Tsarmine (b) rock glaciers; c) permanent GPS sensor installed on the Tsavolires rock glacier at the Réchy site; d) orthomosaic derived from aerial images (Gemmi site in 2007).

Additionally, **satellite data** (mainly ERS-1/2 DInSAR and TerraSAR-X) can be used for the detection of moving landforms. These techniques are particularly powerful for obtaining an overview of the spatial distribution of moving objects over large areas, e.g. to select landforms which should be investigated in detail by other methods such as DGPS (Barboux, 2014). DInSAR could be used to monitor slowly moving objects or to investigate seasonal variations in the surface deformation, but especially for landforms moving faster than 1.5 m per year, other methods are more suitable (Barboux, 2014). However, the technical possibilities in this domain are growing rapidly and will probably allow the monitoring of slope movements with increased temporal and spatial resolution over large areas (Caduff et al., 2015). For this PhD thesis, data from DGPS surveys, a few permanent GPS sensors as well as aerial images have been used to analyse rock glacier kinematics.

3.5 Geophysical measurements

As with temperature records, geophysical techniques have been used since in the beginning of permafrost observation in the Swiss Alps (Vonder Mühl et al., 2001b). The major **advantage of geophysical methods** is that they are **non-invasive** and **sensitive to temperature changes around 0 °C**. As illustrated in Fig. 3.8b, frozen and unfrozen materials as well as ice, water and air can be distinguished. Nowadays geophysical methods allow multi-dimensional monitoring of the ground properties by a systematic repetition of measurements (Hauck and Kneisel, 2008; Hauck, 2002). Only the currently most common methods, which have been used in the frame of the TEMPS project to gain additional information on ground properties, are described here: Electrical Resistivity Tomography (**ERT**) and Refraction Seismic Tomography (**RST**). Due to the material properties of permafrost (Fig. 3.8b) RST is particularly suitable to distinguish between air (acoustic velocity) and ice/permafrost, whereas ERT is very sensitive to ground water (which causes a low electrical resistivity signal).

By the **combination of ERT and RST** on the same profile at the same time it is possible to deduce the relative proportion of air, water and ice in the pore space of the ground around the rock material (Fig. 3.8). This can be done using the so-called 4-Phase Model **4PM** (Hauck et al., 2008, 2011). Regarding the quantification of the role of the snow melt on rock glacier kinematics, particularly the **self-potential** technique may be a suitable method because of its sensitivity to detect flowing water in the ground (Hauck, 2013; Scapozza et al., 2008). In the future, geophysical methods may be used to control intelligent systems of communicating measurement devices as discussed in Sect. 9.1.3.

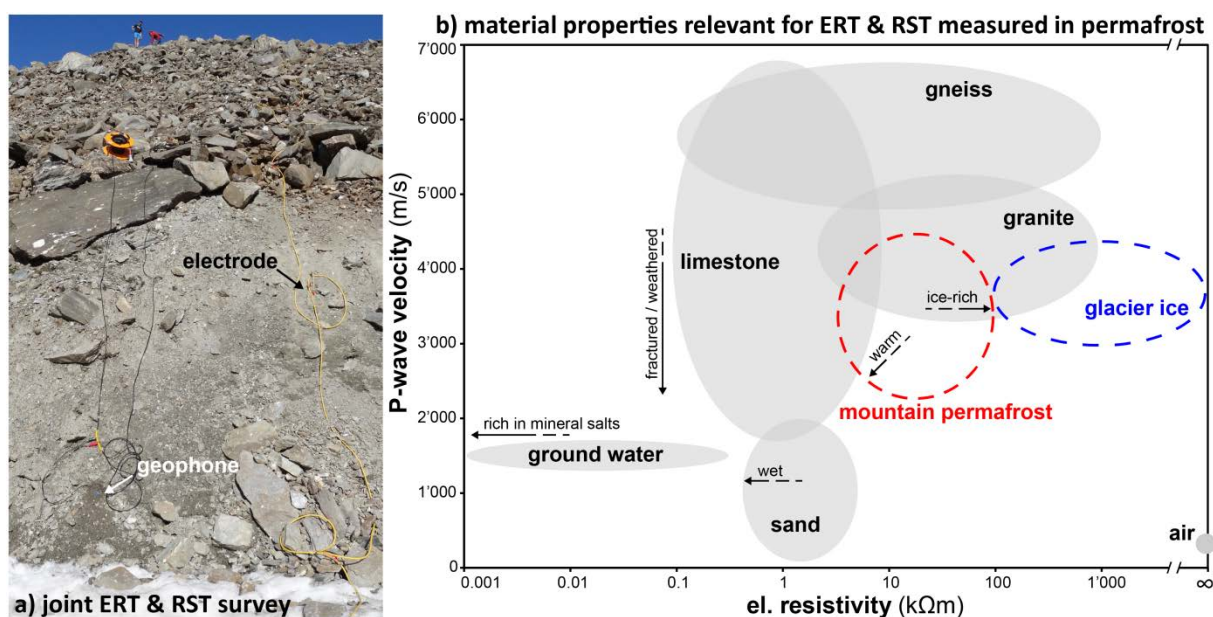


Fig. 3.8: Application of geophysical methods for mountain permafrost monitoring: a) simultaneous ERT and RST survey at rock glacier Tsavolires (site REC) in July 2012; b) Typical P-wave velocities and electrical resistivities for materials which are relevant for mountain permafrost according to Hecht (2000), Milsom and Eriksen (2011) and Schrott and Hoffmann (2008).

Geophysical methods are constrained by several disadvantages. The most important drawback is the **ambiguity of the inversion**, meaning that the result of one single measurement has a high uncertainty because the system is underdetermined (Hauck and Kneisel, 2008). Therefore, the reliability of geophysical data increases when it is coupled with other geophysical methods (e.g. RST in combination with ERT), complementary methods (like GST and GT measurements) or if it is repeated in the same setup over time (Hilbich, 2009; Hilbich et al., 2009; Vonder Mühl et al., 2001b). The latter implies that all surveys at one site need to be measured with exactly the same setup. For this reason and to save time with the installation of cables and electrodes, **permanent ERT profiles** have been installed at the sites SCH, COR, LAP, STO, and REC. The longest and most complete ERT monitoring (ERTM) data set from the Schilthorn currently counts more than 650 measured profiles and is therefore valuable for the analysis of temporal variations of ground properties. But broken cables, overvoltage by lightning, electrodes with bad coupling, changing topography etc. are typical issues for ERTM. It is very challenging to keep a permanent installation intact on moving landforms with differential surface deformations. As already done with considerable success at a few sites, remotely controlled measurements will most likely be the future of ERTM, but at this time many technical issues still exist and the data processing is very laborious (Sect. 4.1.4). Fig. 3.9 provides impressions from ERT monitoring in the field.

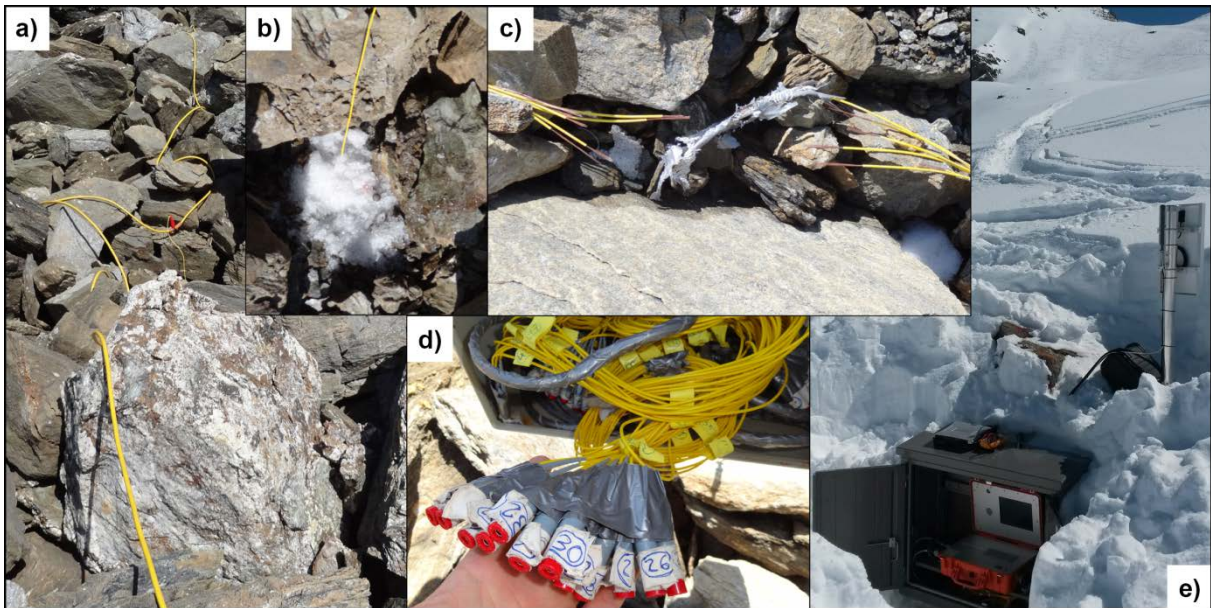


Fig. 3.9: Aspects of ERT Monitoring: a) ERT cable on coarse-blocky terrain; b) by putting water or snow, the ground coupling can be improved; c) broken permanently installed (self-made) ERTM cables due to rock fall or terrain deformation; d) cable jumble: keeping the overview is not always self-explanatory; e) high-tech ERTM installation at the Beccs de Bosson rock glacier in winter: rough conditions demand robust equipment with minimal energy consumption.

The following two chapters 4 and 5 describe the methods used for data processing and analysis.

4 Processing of observational mountain permafrost data

In observational research, field work and data processing are equally important steps building the basis for a comprehensive data analysis and interpretation. Standards have to be defined and strictly followed to finally achieve homogenized data, which are comparable among different study sites, measurement devices and over time. Often erroneous data or interesting phenomena are discovered during the steps of data correction, homogenization or gap filling. Systematic data processing routines help to periodically reconsider and improve the monitoring setup. Previous work as well as new ideas developed in the frame of this PhD thesis and the TEMPS project are summarised hereafter as a suggestion of best practice processing of observational mountain permafrost data to obtain comparable and homogenised data sets.

4.1 Processing and homogenization of raw data

The quality of the acquisition of the data in the field and the correction of the raw data was ensured by the principal investigators who delivered the data to PERMOS. The homogenization of this data was then part of the research project TEMPS. First, a few considerations about the terms **accuracy** and **precision**: as visualised in Fig. 4.1 with hits on target circles, a set of data points may be very accurate even if single measurements are of lower precision and vice versa. Transferred to permafrost monitoring data, modern thermistors such as UTL-3 are of high accuracy and precision (type a) while the older UTL-1 is accurate regarding the mean of an ensemble of values, but with limited precision due to its coarse precision (type b). Uncorrected DGPS data might initially be categorized as type c (i.e. precise but not accurate) and after correction as type a. Data which is neither precise nor accurate, (type d) should be avoided wherever possible, otherwise large systematic as well as stochastic errors complicate the data analysis and interpretation.

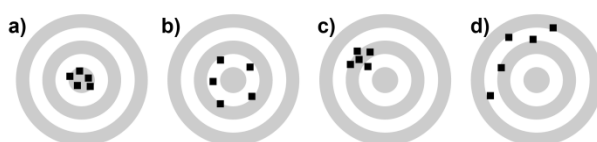


Fig. 4.1: Accuracy and precision of data points: In the optimal case a) all data points are of high accuracy (close to the real value) and high precision (small variations among samples). Situation b) is accurate regarding the mean, but the samples are of low precision. Situations c) and d) contain systematic errors (low accuracy), with high and low precision, respectively.

Even the most sophisticated data analysis techniques cannot compensate for erroneous measurements. Common adjustments are the correction for potential systematic biases and offsets, the removal or correction of spikes and artificial trends (e.g. due to logger and sensor drift), whereas corrections for resampling or smoothing are optional.

4.1.1 Ground temperature (GT) and ground surface temperature (GST) data

Thermistor chains in boreholes are usually installed permanently, whereas miniature data loggers used for recording GST are placed loosely between blocks at the ground surface (Fig. 3.2). The latter need to be replaced every year after data download and maintenance. The GST variability depends on the placement depth of the data loggers below the surface, particularly the diurnal amplitude in

summer. Therefore, and because deviations cannot be corrected afterwards, the **placement** of the thermistors and miniature loggers must be kept constant. There are three main potential issues regarding GST raw data: First, systematic changes for entire years due to different logger placement or confusion of loggers. Second, GST records which do not represent the thermal regime at the field site but of a backpack or office (“backpack-temperatures” in Fig. 4.2) if the loggers were programmed at the office and just exchanged in the field. Third, data gaps occur, e.g. if the loggers were broken or if the maintenance did not ensure a direct replacement or reprogramming of the logger. In this regard, **metadata** is highly important for data processing and homogenisation.

Systematic errors, typically caused by constant logger or thermistor offsets, can be corrected by calibration under conditions of known temperature or during **zero curtain** periods (Sect. 2.2.2). Usually, the snow melt period in spring is used for calibrating systematic GST offsets, because they are most pronounced during this time period (Fig. 4.2). Especially for miniature data loggers of lower accuracy and resolution such as UTL-1 and iButton (Sect. 3.2.1), this temperature offset can be large (up to ~ 0.5 K). Data recorded with UTL-1 devices did usually not show a thermal drift over time.

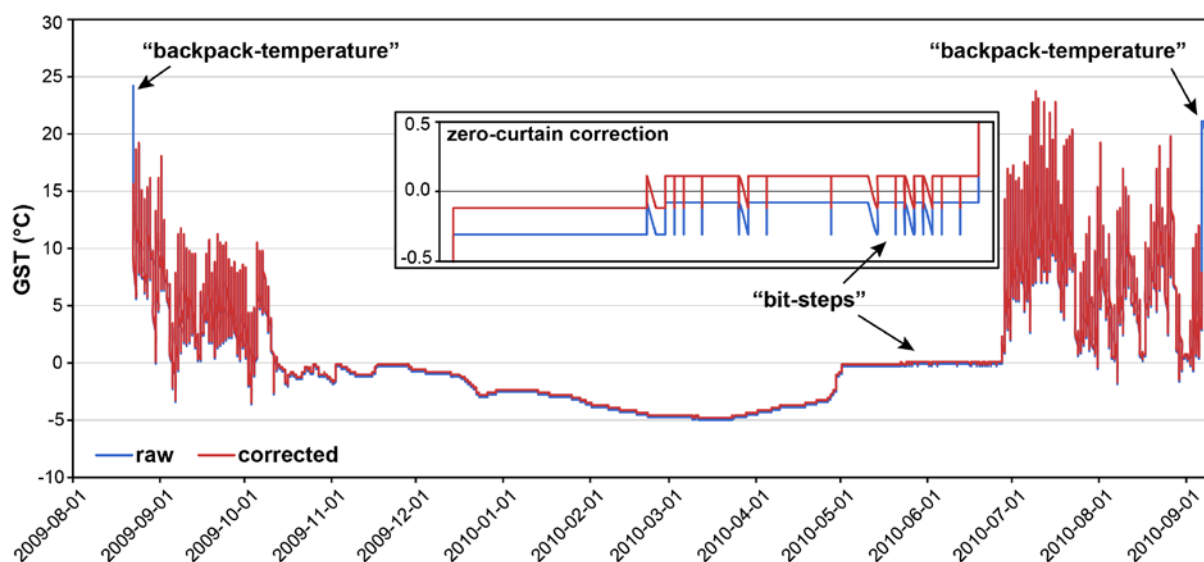


Fig. 4.2: Raw (blue) and corrected (red) data at 2-hour resolution is shown at the example of logger GFU_S010 for the time period 2009-2010. The zoom-in shows the period of snow melt in May and June). Systematic offsets can be quantified during zero curtain periods. The spring zero curtain was oscillating between two different temperatures, here called “bit-steps” due to the limited precision of the UTL-1 logger. This makes the correction challenging, and it is advisable to correct for the mean offset during the zero curtain. Additional zero curtains in early winter may be used for calibration as well. Moreover, at the beginning and the end of a time series, the raw data may be influenced by other thermal signals which need to be removed (“backpack-temperatures”), measured on the way between the office and the field.

Not all temperature records show distinct zero curtains. Often zero curtains are missing when the snow cover in winter was absent or thin, if the ground is dry and porous or if the melting point was not exceeded. The latter is typically a problem for borehole thermistors within or below permafrost. If the thermistor chains can be removed from the casing safely, they may be **calibrated** in the field in the wet snow in spring, or in the lab by using an ice-water mixture or specific calibration solutions. However, due to shearing or intrusion of moisture, thermistor chains may be locked in or frozen into the borehole tube. Consequently, a re-calibration of these thermistors is not possible and issues of **thermistor or logger drift** may be laborious to detect and almost impossible to correct.

The **correction of GT** data is particularly challenging when the temperature variations (signal) are of the same magnitude or even smaller than the **thermal resolution** (accuracy + precision or “noise”) of the thermistor. Such a problem had to be solved for the data from borehole LAP_0198 in Lapires, where permafrost temperatures are very close to the melting point, but showed strong fluctuations. Since this data was needed for the calibration of a ground thermal model (Staub et al., 2015a), any physically implausible phase changes due to imprecise measurements would have negatively influenced the model performance. The correction of these **implausible GT variations at borehole LAP_0198** is illustrated in Fig. 4.3. Additional information on the subsurface from geophysical measurements and the drilling proved to be very valuable for performing this GT correction.

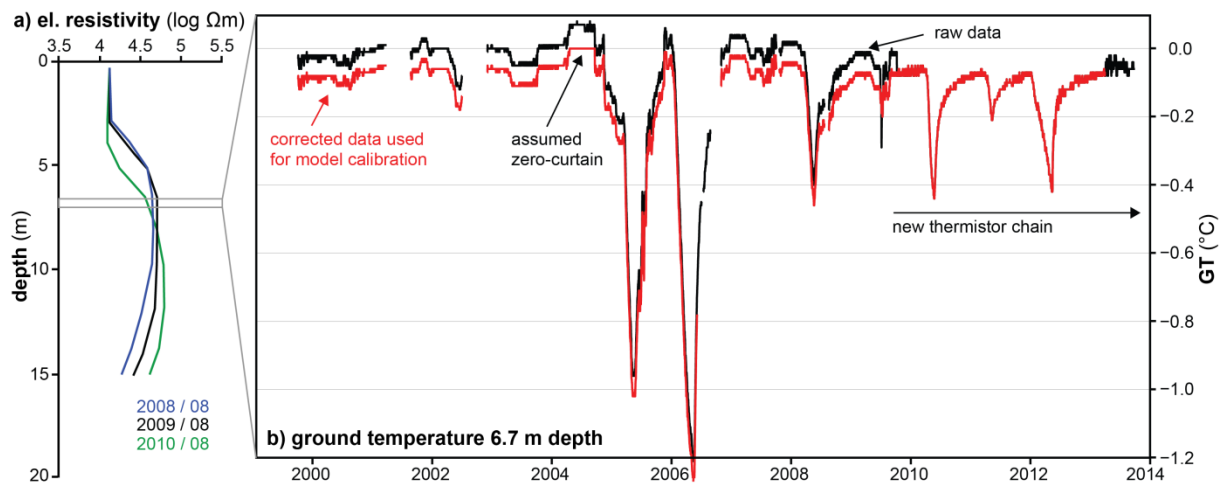


Fig. 4.3: Correction of GT data measured in the LAP_0198 borehole: a) ERT monitoring data clearly indicate the presence of massive ice below ~ 5 m depth (PERMOS, 2013), in b) raw and corrected GT data at 6.7 m depth are shown: the offset observed after the installation of a new thermistor chain in 2009 was plausible regarding a zero curtain period in 2004.

For the **Lapires talus slope** it is known from excavations in 1998 (Delaloye et al., 2001; Lambiel, 1999) and drillings in 1998 and 2008 (Scapozza, 2013) that a thick and ice-rich permafrost layer is present below a porous and coarse-blocky active layer of approximately 5 m around borehole LAP_0198. Very high electrical resistivities ($> 45'000 \Omega\text{m}$, Fig. 4.3a) and fast seismic velocities (~ 3500 m/s) indicate a high ice content between 5 and 20 m depth (Delaloye, 2004; Hilbich, 2010; Lambiel, 2006; Scapozza, 2013). Even though water might coexist along with ice, the occurrence of positive temperatures within the permafrost is still very unlikely due to the high heat capacity of ice. To correct the GT raw data, a constant linear shift was detected which exactly fitted to measurements performed after 2009 with a new, calibrated thermistor chain (Fig. 4.3b). The same linear shift for correction fitted with a zero curtain period in 2004, for which the raw data showed positive GT. Hence, positive temperatures within the permafrost body could be excluded for the model calibration (Staub et al., 2015a). However, this type of data correction is very time consuming and only feasible for individual case studies.

To achieve a **homogeneous data basis** on which different sites and time series can be compared, the corrected measurement data need to be of **similar temporal resolution**. Because of differing sampling intervals (minutes to days, Sect. 3.2), **daily means** were chosen as compromise on which basis most processes can be analysed. However, daily means can either be calculated directly as the

arithmetic mean of all measurements of one day, or by **resampling** the data first into regular time steps by linear interpolation, e.g. into hourly means. The latter was done for all GST time series in order to consider the diurnal GST amplitude in a standardized way. Most GST raw data was sampled every two hours. For many older boreholes only daily means are available, hence no resampling at the hourly scale could be done in these situations. Days with missing temperature values were consequently set to 'NA' and were then reconstructed in a second step as described in section 4.2.3.

For the **quantification of uncertainties** in later steps of data aggregation and analysis, uncertainty estimates for each daily mean value as well as information on the nature of these errors are required. The quantification of uncertainties is a demanding task because the measurement and calibration errors may be systematic or stochastic. In this context, the **effects of the thermal resolution** (temperature range / bit-depth) of a thermistor are of particular interest. These effects were assessed from a theoretical perspective with synthetic GST data consisting of a sine curve amplified for a realistic annual temperature pattern with a 30-day zero curtain in spring (Fig. 4.4a-). By resampling this temperature curve to the mean resolution of an UTL-1 logger (± 0.27 K), stochastic as well as systematic errors were quantified (Fig. 4.4c-d). This experiment revealed systematic errors of ± 0.05 - 0.1 K and stochastic errors of ± 0.1 - 0.2 K. Hence, the correction of the zero curtain offset did not reveal perfect temperature measurements. The remaining errors were of the order of the logger accuracy (± 0.1 K for UTL-1) and were expected to propagate in aggregates and indices.

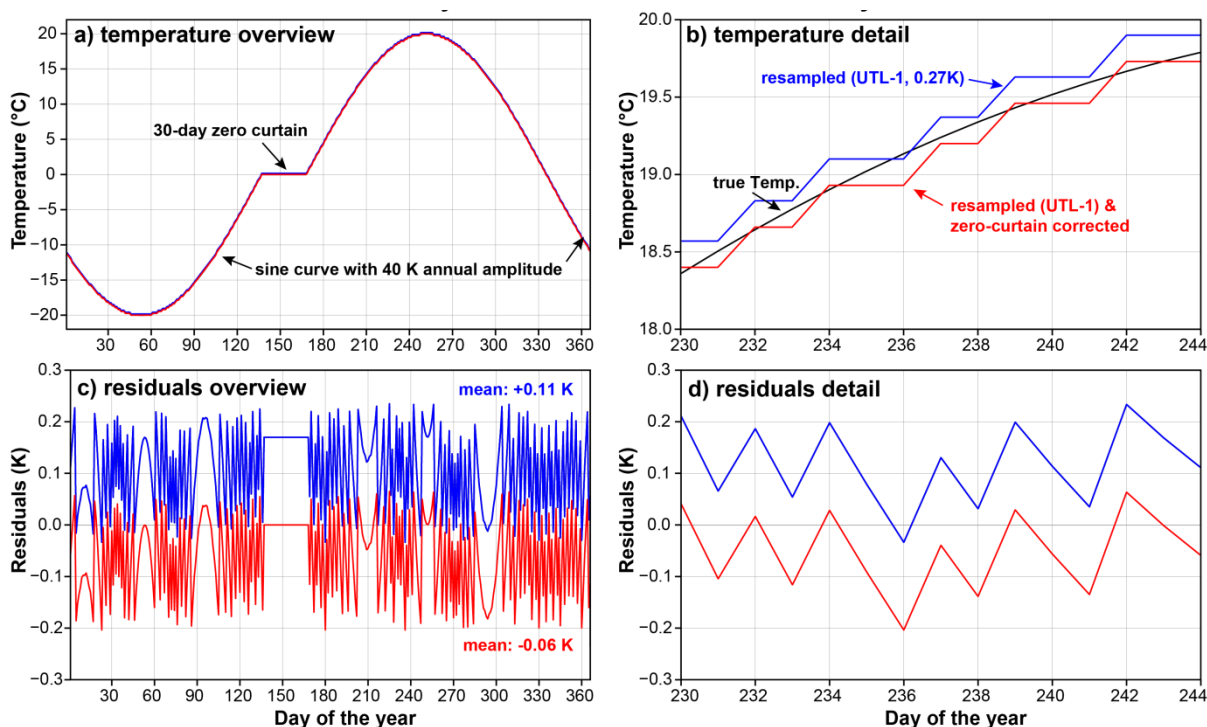


Fig. 4.4: The influence of the precision of a UTL-1 thermistor on the measurements, assessed with synthetic GST data. A sine curve with an annual amplitude of 40 K combined with a 30-day zero curtain (at 0°C) were assumed to be true daily mean GST values (black curve in a and b). This synthetic temperature curve has been resampled with a precision of five digits to the precision of a UTL-1 data logger (8 bit, 256 values between -39 and +40 °C) at 0.1°C accuracy (in blue). Additionally, the resampled curve was corrected for the systematic offset during the zero curtain (red curve). The residuals (c and d) show a stochastic behaviour without a clear seasonal pattern and mean values in the order of 0.05-0.1 K.

In summary, a **systematic and standardised data processing** is required for the following steps of data aggregation, analysis and interpretation. For thermal data, the most important step is the correction for systematic measurement errors. This is usually feasible using zero curtain periods occurring in spring and/or autumn close to the ground surface. The remaining uncertainties of the corrected values are in the order of the accuracy of the measurement devices but potentially larger if the thermistors cannot be calibrated regularly. Moreover, different dynamic and temporal resolutions need to be transformed to a comparable aggregation level. The reconstruction of missing values is described in Sect. 4.2, whereas the data aggregation and computation of indices are the subject of Sect. 5.1.

4.1.2 Meteorological data

Within the TEMPS project, major effort was put into the inspection and the homogenization of meteorological data acquired by automatic weather stations at the PERMOS sites. However, for this thesis only the parameters **air temperature (AirT)**, incoming **shortwave radiation (ISR)** and **snow depth** were used. As for GST, the meteorological data were recorded at differing temporal resolution and daily means were computed to achieve a comparable data basis. Some time series are interrupted by gaps or contain erroneous values due to technical issues (e.g. ice or snow on sensors). The PERMOS/TEMPS meteorological data was mainly used for specific questions at individual sites. In addition, data from MeteoSwiss and SLF was considered, if complete and spatially distributed data was required. How continuous AirT and ISR time series were computed for PERMOS sites is described in Sect. 4.2.4.

4.1.3 Kinematic data

As mentioned in Sect. 3.4, three different methods of kinematic monitoring data were used: DGPS surveys, permanently installed GPS devices which continuously record their position at a given point, and aerial photographs to consider larger areas at high spatial resolution. The processing of these different data sets is described hereafter. All methods have in common that they need to be **corrected for systematic errors** against a reference and possibly transformed into a common **coordinate reference system (CRS)**.

For the most relevant category, the **DGPS surveys**, the movement of a set of pre-defined markings at the ground surface was measured over time. Either one or more landforms can be reached within one single campaign using the same reference station, to correct errors in the GPS signal in real-time. Ideally, the reference station is located on a fixed point with known coordinates. Depending on how precisely the reference station is set, a **systematic bias** (3D shift) will result during the entire measurement campaign. To correct for this bias, control points in stable terrain need to be measured in parallel. By minimizing the residuals of the control points for each of the surveys according to a reference survey (or to the respective mean from several surveys), all measurements from a given site can be corrected with final accuracies of 2-3 cm. This process is illustrated in Fig. 4.5. The procedure assumes that all coordinates have been measured in the same CRS and using the same elevation model (e.g. ellipsoid or geoid).

Manual DGPS measurements bear the uncertainty of **human and technical errors**. Those are usually not systematic and therefore complicated to correct. In the case of DGPS surveying, typical errors relate to the levelling and height setting of the rover antenna (Fig. 3.7a-b), motion of the reference station during the survey or confusion of point numbers. In any case, stochastic measurement errors of 1-3 cm will remain. Confusion of point ID's is easiest to correct using GIS tools and by checking the displacement, azimuth and slope values for outliers.

On fast-moving landforms with large surface deformations some markings e.g. close to the rock glacier border or front may be measurable only for a limited time period because boulders fall or tilt. A strategy for the **renewal of points** is to add new points at locations close to the old ones, ideally before the latter become inaccessible. By keeping the same point ID with a suffix (e.g. *_b*, *_c*, *_d* etc.), the connection between former, actual and future points can be guaranteed. However, changes in the morphology and dynamics of rock glaciers over decades need to be taken into account. For this project, representative points within functional zones were grouped together, e.g. for the rock glacier tongue, its centre and the rooting zone.

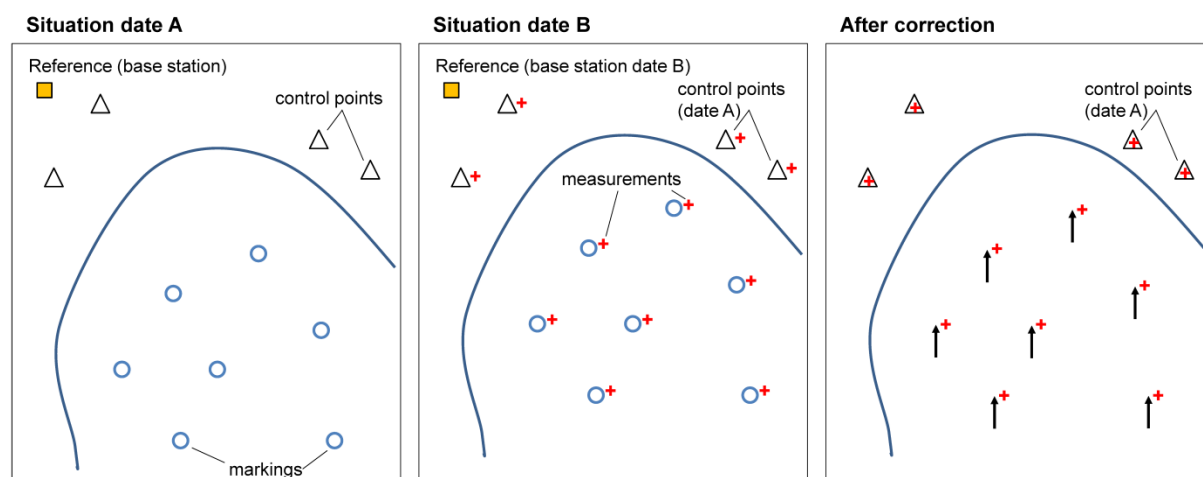


Fig. 4.5: Illustration of raw and corrected DGPS measurements from two measurement campaigns on dates A and B: By minimizing the residuals of the control points in stable terrain in reference to known coordinates (e.g. from the first campaign), all other measurements can be corrected and displacement vectors calculated (illustration on the right).

Permanently installed GPS devices (Fig. 3.7c) aim at recording terrain movements at very high temporal resolution for one point, typically at 0.5-1 Hz. Within this PhD thesis, data from these devices was mainly used to assess the influence of the snow melt on the kinematic activity of rock glaciers at the weekly to monthly scale (Sect. 6.3, 7.3 and 7.3.2). Single data points are of limited accuracy in the order of cm-m (due to GPS clock or orbit errors, ionospheric and tropospheric delay etc.), but daily solutions at the mm to cm-level are technically possible (Wirz et al., 2014). In this context, the separation of the movement signal from background noise is a crucial processing step before the data can be analysed. For this PhD thesis, pre-processed GPS data at hourly resolution was used for the rock glaciers Beccs de Bosson and Tsavolires (Val de Réchy) as well as Tsarmine (Val d'Arolla). Additionally, spikes in the hourly data were removed using a running median filter and the remaining values aggregated to daily mean values. Depending on the signal-to-noise ratio, the mean coordinates could be smoothed in a moving time window (Wirz et al., 2014).

For measuring spatially distributed displacement rates based on aerial photographs, state of the art **photogrammetry techniques** have been used. See Kraus (2007) and Paine and Kiser (2012) for the theoretical background of aerial triangulation, orthorectification and image correlation. It proved to be crucial to keep a common CRS within a set of stable ground control points (GCP) for the successful long term monitoring of morphological changes (Staub et al., 2015b). A precise net of GCP with at least 4-5 well distributed points, resulted in a significantly improved accuracy of the orthorectification compared to direct georeferencing using GPS/IMU data recorded during the flight. Resolutions and accuracies of the final orthomosaics in the order of 10-15 cm can be attained with digital sensors and an adapted flight planning, i.e. by flying at low elevation in periods with minimal snow coverage and ensuring a high overlap between the images. By means of drones the ground sampling distance (GSD) of the raw images could be reduced to a few cm, but with the drawback of having many more images to process in the steps of aerial triangulation and orthorectification. Moreover, image processing techniques such as **feature tracking** by image correlation (Sect. 5.6) were used to quantify the accuracy of orthophotos in stable terrain. Although rapid technological progress is expected in this domain, the snow cover remains an issue for any optical methods.

4.1.4 Geophysical data

Geophysical data requires several processing steps between data acquisition and its analysis. First, the **topographic information** on elevations and distances for each electrode or geophone has to be inserted to correct for irregular spatial distances within the half-space. Second, **erroneous measurements**, e.g. caused by insufficient coupling of an electrode or a geophone to the ground, need to be removed. Third, due to the ambiguity of the **inversion process**, one optimal solution has to be identified among many other potential solutions (Loke and Barker, 1996). State of the art procedures are described very nicely in Hilbich (2009) and further theoretical background and practical information on the use of geophysical methods for mountain permafrost monitoring and research can be found in Hauck and Kneisel (2008) and Hauck (2013). In the following, only some particularly important points for ERT monitoring (ERTM) are discussed.

The **processing of ERTM data** using mathematical inversion still requires at least manual control after processing. Regarding the integration of topography it could be beneficial to switch from relative length-elevation profiles to **spatially referenced profiles** using real-world coordinates to ensure spatial coherence within different surveys. This approach could be particularly useful also for archiving the data in a consistent way. Moreover, it is in the nature of the data, that 'NA' values occur occasionally, e.g. because of a bad ground coupling or if not the entire profile has been measured. Technical improvements are likely to be implemented in future which may lead to longer and three-dimensional profiles and shorter time intervals. Thus, data processing will have to be adapted to these developments. A possibility to **homogenize different surveys** at varying spatial resolutions could then be to resample the measured or pre-processed values into common grids of coarser resolution. Very favourable for geophysical monitoring is the fact that **relative values** (differences of electrical resistivities as well as seismic velocities between two measurements) are much more accurate than the absolute values itself (Hilbich, 2009; Hilbich et al., 2009).

4.2 Reconstruction of missing data and quantification of uncertainties

Many GST and GT time series within the PERMOS network are 10-15 years long, but interrupted by gaps of different duration (Fig. 3.3 and Fig. 3.5). To **increase the amount of complete time series** for comparison between loggers, sites and years, the data needed to be homogenized and gaps needed to be filled. Gaps may either be filled with a representative mean value or at the aggregation level of the homogenized data (e.g. daily means). Both approaches have their use. Yet, keeping the original aggregation level is preferred, because it makes further calculations more flexible (Sect. 5.1). As long as other complete time series of similar variance are available, empirical statistical approaches can be used to reconstruct missing data. Additionally, physically based models could be used. Depending on the research questions, the data and gap characteristics and the level of aggregation, various techniques may be adequate.

The following sections present the **development and evaluation of different gap filling approaches** for GST and GT data recorded close to the surface (< 1-2 m depth), on which basis aggregates and indices can be calculated. A special focus is on the **quantification of uncertainties**, because this represents a major improvement made in the frame of this thesis. A sophisticated approach for the downscaling and bias-correction of meteorological data was developed by Rajczak et al. (2015) in the frame of the TEMPS project. On the basis of annual mean values, gaps in surface displacement rates of rock glaciers have also been filled. Generally, gap filling was carried out **based on homogenized data** as described in Sect. 4.1. Due to the ambiguity of the methods, the complexity of subsurface processes and the limited amount of data available, no gap filling was performed for geophysical data. If not stated differently, the sections reference to Staub et al. (subm.).

4.2.1 Comparison of approaches

Dealing with missing data is one of the major common problems of many different research disciplines and the **need for standardization** had been identified previously (Falge et al., 2001; Gudmundsson et al., 2012). The list of potential approaches ranges from process-based models to empirical-statistical transformations. The requirements regarding input data as well as the applicability of the gap-filled values are different for each approach (e.g. Moffat et al., 2007). So far little information was available on how gaps in permafrost monitoring data could be treated.

Process-based models (Jansson, 2012; Lehning et al., 2006; Westermann et al., 2013) are not suitable for filling gaps in large data sets of permafrost observations, because of the high requirements on the meteorological input variables and the calibration parameters (e.g. as the density of the snow or the porosity and thermal conductivity of the substrate) and the high computational effort (Ekici et al., 2015; Marmy et al., 2015). The group of **empirical statistical methods** is more appropriate to the problem statement of the present thesis and regressions and statistical transformations are most commonly used for bias correction and spatial transfer of meteorological parameters (Gudmundsson et al., 2012; Rajczak et al., 2015; Tardivo and Berti, 2014). Up to now, **linear regression (LR)** has been used to fill missing monthly means of reference GST time series for the visualisation of running annual mean values for PERMOS data (PERMOS, 2013). A widely used method for the downscaling and spatial transfer of meteorological parameters (Rajczak

et al., 2015) is **quantile mapping (QM)**. QM is a nonparametric statistical transformation technique, which statistically corrects for bias between two time series based on the quantile distribution of the data, without presuming a linear relationship or a specific distribution (Gudmundsson et al., 2012; Themessl et al., 2011). QM reproduces the mean conditions for all quantiles very accurately. If gaps are short and the data is autocorrelated, **linear interpolation (LI)** also performs well. In any case, gap filling has to account for local characteristics, seasonal and inter-annual patterns. Tardivo and Berti (2012) recommend to treat each gap individually and Rajczak et al. (2015) conducted the bias correction separately for each season.

4.2.2 Uncertainty assessment and error propagation

Depending on the original data, aggregates also remain uncertain to some degree and gap-filled data is subject to uncertainty anyway. Generally, uncertainty can be estimated based on observed variability or based on residuals between true and synthetic values. The **estimation and propagation of uncertainties** depends on the data and the gap filling method and on the characteristics of these uncertainties as well. Normally distributed, **stochastic errors** (σ_{sto}) are assumed to compensate with larger sample sizes, whereas **systematic errors** (σ_{sys}) need to be averaged for aggregates. According to error propagation laws, the mean uncertainty of an entire gap (σ_{gap}) can be calculated as:

$$\sigma_{gap} = \pm \sqrt{\left(\frac{\sigma_{sto}}{\sqrt{n_{sto}}}\right)^2 + \sigma_{sys}^2} = \pm \sqrt{\left(\frac{\frac{1}{n_{sto}} \sum_{i=1}^{n_{sto}} \sigma_{sto,i}}{n_{sto}}\right)^2 + \left(\frac{1}{n_{sys}} \sum_{j=1}^{n_{sys}} \sigma_{sys,j}\right)^2}, \quad \text{Eq. 6}$$

where n_{sto} and n_{sys} are the sample numbers and i and j correspond to specific dates for stochastic and systematic errors, respectively. The characteristics of the gap data are assumed to be influenced by similar processes as during the calibration period, e.g. regarding the influence of snow or global radiation. However, this assumption might not be fully correct because of large inter-annual variations (Sect. 6.2). Ideally, an independent subset of common observations should be used for cross-validation, but this was not done here because of the short time series. Possibilities for considering inter-annual variations for uncertainty estimation are mentioned in Staub et al. (subm.).

4.2.3 Procedures for filling gaps in thermal data

Within this PhD thesis an algorithm for the filling of gaps in GST time series was developed to increase the amount of complete hydrological years (Oct-Sept) available for integrative data analysis (Sect. 5.1). It is based on homogenized daily means as input data (Sect. 4.1.1) and makes use of the high probability of finding similarities among different time series. The algorithm provides estimates for missing daily mean GST values as well as the respective uncertainty. Using a large number of randomly generated artificial data gaps of variable duration and timing (~18'000 gaps and >2.5 million daily mean values), the performance of the gap filling routine was validated. Most challenging are the highly variable snow conditions, which often substantially vary even over short spatial distances. The complete description and validation of the procedure can be found in Staub et al. (subm.).

The procedure for filling gaps in thermal data is based on the two methods LI and QM (4.2.1). LI uses mean values before (GST_{prior}) and after the gap (GST_{after}) and has the great advantage of being independent of any other time series. But changing meteorological and ground thermal conditions cannot be considered. Therefore the procedure is mainly applicable to fill short data gaps of a few days only. The **expected GST values** (GST_{synt}) were calculated by LI as described in Eq. 7:

$$GST_{synt,i} = GST_{prior} + \left(\frac{GST_{after} - GST_{prior}}{n + 1} \right) \cdot i, \text{ with } i = \{1, 2, \dots, n\} \quad \text{Eq. 7}$$

Where n is the number of missing values (gap duration) and i corresponds to a specific date. Data gaps of only one day are ideally interpolated between the two nearest neighbours, whereas longer gaps require longer aggregation windows before and after the gap (Fig. 4.6c). Therefore, the length m of the aggregation windows was defined dynamically as a function of n :

$$m = \left\lceil \frac{n}{2} \right\rceil \in \mathbb{N} \quad \text{Eq. 8}$$

The mean uncertainty of the gap-filled values can be estimated based on the standard deviation (SD) calculated for the time span of GST_{prior} and GST_{after} . This method accounts for differences in the short-term GST variability, resulting in greater uncertainties if SD is large (Fig. 4.6a-b). These uncertainties are presumed to be stochastic and hence partly self-compensating. As a consequence, the mean uncertainty of aggregates can be divided by the square root of observations (Eq. 6).

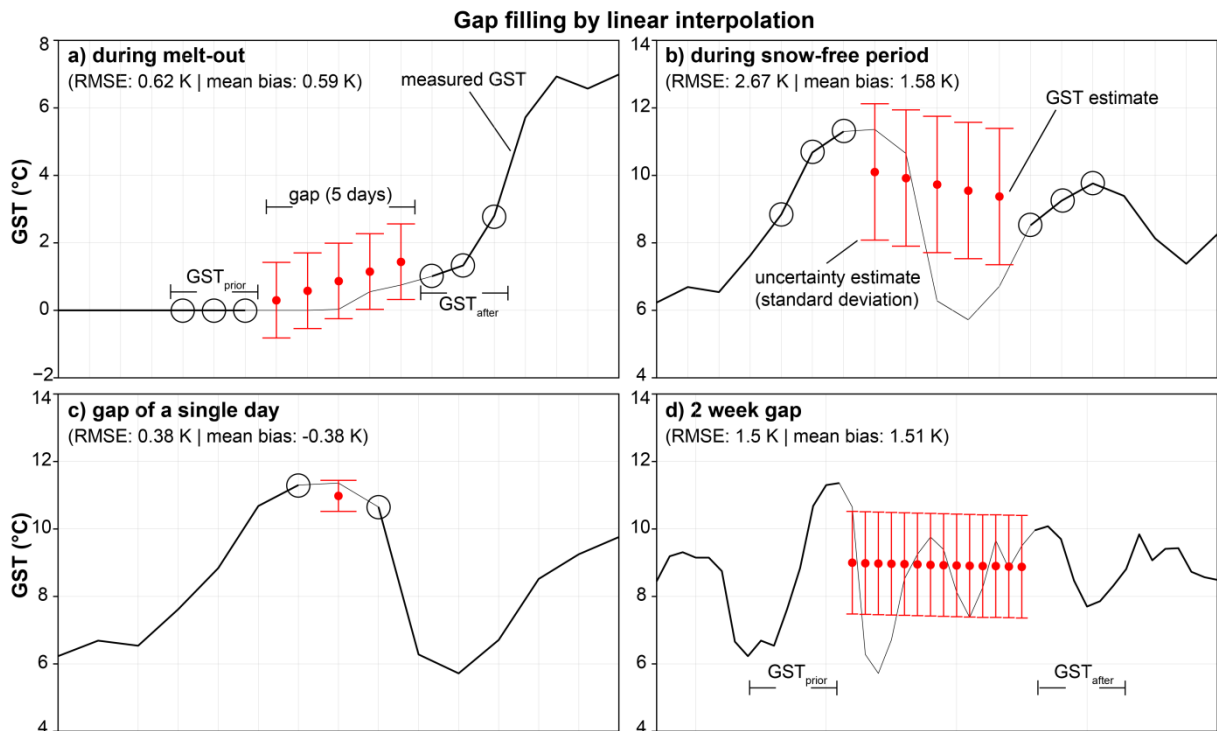


Fig. 4.6: Examples for artificial gaps filled using linear interpolation: a) 5-day gap in a typical situation at the end of the snow melt period in early summer, and b) for mid-July when the ground is completely snow-free, c) for a data gap of only one day, d) a gap of 2 weeks. The red dots represent the interpolated GST values, uncertainties were approximated based on the standard deviation of GST_{prior}/GST_{after} . The x-axis represents time (days).

During snow-covered periods, as the ground is thermally insulated from air temperature variations, GST data is highly autocorrelated and LI would technically be suitable also to fill gaps of up to several weeks duration. However, this type of data gap was not observed in the PERMOS GST data. Gaps starting in winter usually last until the maintenance in the following summer, since there is no remote-control and no access to replace the logger. In GT data the observed short-term variations are much smaller than in GST data and the LI method is suitable to fill gaps of up to several weeks.

For GST data gaps of several weeks or months, the **QM** technique was used based on other, complete so called regressor time series. Although the statistical transformation of QM corrects for errors in the mean and percentiles (Fig. 4.7d), it is not capable of correcting for daily correspondence between the regressor and the target logger (Rajczak et al., 2015). By adjusting the distribution of GST values of the most similar regressor logger with maximum covariance to the GST values of the target logger, synthetic GST data (GST_{syntr} , fitted values) can be generated to fill the gap. As long as the regressor logger is simultaneously exposed to the same atmospheric and snow conditions as the target logger, the method accounts for the high temporal variability of high-mountain GST realistically (Fig. 4.7e). The **selection of an adequate regressor logger** is the most important step for the successful application of the QM technique, particularly because of the spatially heterogeneous snow conditions and subsurface properties. The selection is based on the coefficient of determination (R^2) of the daily mean GST values. See Staub et al. (subm.) for the detailed description of the regressor selection procedure and its optimization for minimizing the computational effort.

For gaps filled by the QM approach, **uncertainties** were estimated for each day of the year based on the residuals between the observations and the fitted values during the common observation period. Assuming that the observation period covers different meteorological and snow conditions, the inter-annual variability is at least partly included in the uncertainty estimate. The covariance between the target and regressor logger proved to be highest in the snow-free state. The respective residuals during the snow-free period are stochastic (σ_{sto}), whereas the residuals during snow-covered periods are potentially systematic (σ_{sys}). The different steps of the QM method from the calibration to the uncertainty propagation are illustrated in Fig. 4.7.

The **comparison of the LI and QM approach** using artificial gaps of ≤ 30 days duration revealed that the QM method performs significantly better (significance level 95 %) than LI regarding the expected GST value for gap durations ≥ 4 days. Hence, gaps < 3 days are more efficient to fill with the LI method. For longer gaps, the QM method performs significantly better regarding the estimated GST values, even though the uncertainty estimates are sometimes critical (Staub et al., subm.). Both approaches are designed for operational use with a GST data base.

In **summary**, data gaps during the snow free period or of a duration shorter than 2 months (~ 60 % of all gaps) could be filled with uncertainties which influenced the annual mean less than 0.25 K. For gaps of 6-8 months duration, the resulting errors on the annual mean were with a likelihood of 95 % smaller than 0.5 K, in the best 50 % of instances even below 0.25 K (precision of the UTL-1 logger).

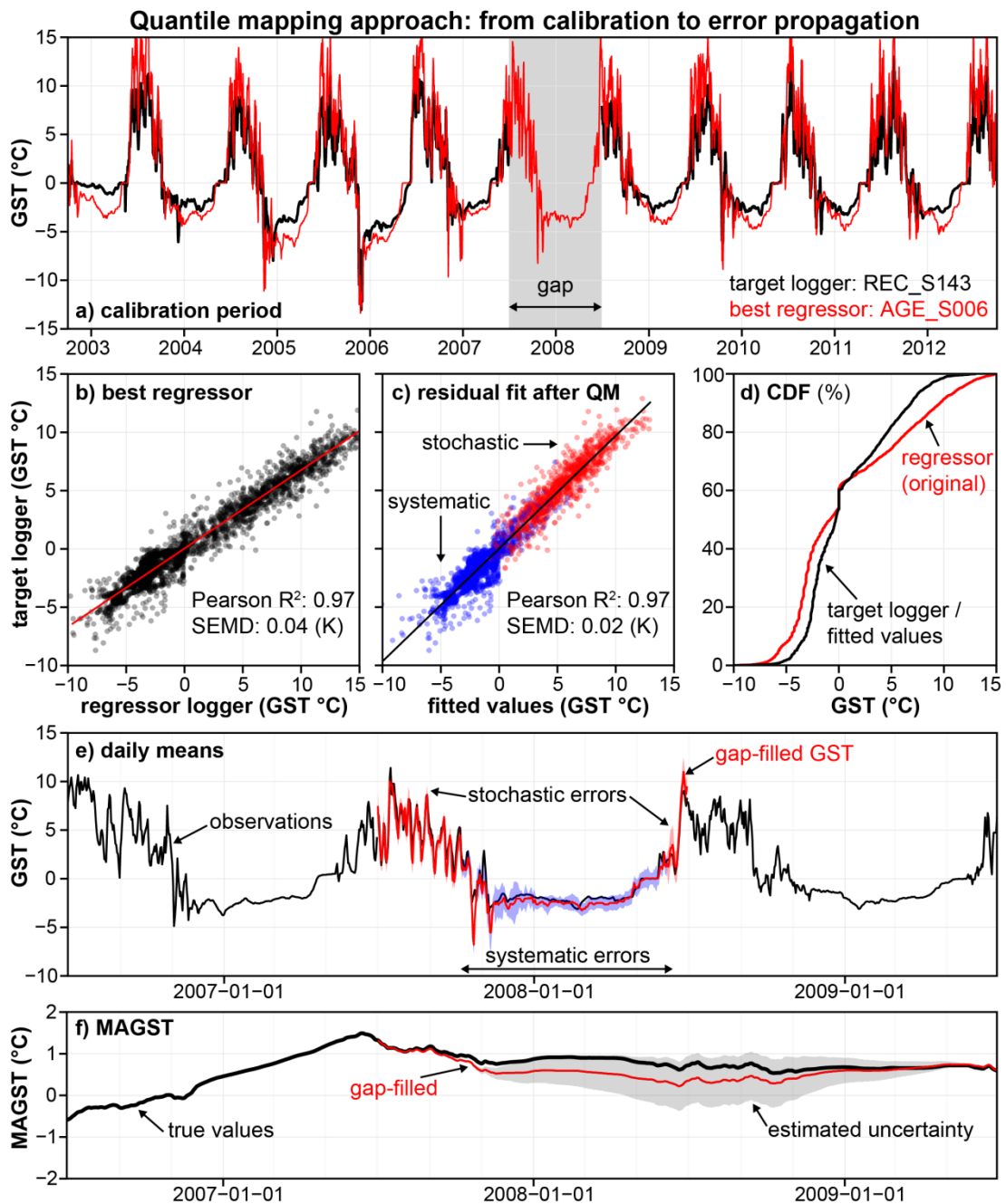


Fig. 4.7: Illustration of the quantile mapping (QM) approach to fill data gaps at the example of an artificial 365-day gap: a) and b) compare the target logger and the best regressor for the entire calibration period (SEMD: standard error of the mean differences); c) comparison of the fitted values after the QM transformation, based on the remaining residuals, stochastic and systematic uncertainties are quantified; d) illustration of the cumulative density function (CDF) of the regressor and the target logger; the results of the gap filling are illustrated as daily means in e) and as running MAGST in f) in comparison with observations (black).

4.2.4 Procedures for meteorological data

The climate at high elevation substantially differs from that below ~2000 m asl. Most relevant for the integrative analysis of mountain permafrost are the parameters **air temperature (AirT)**, **incoming short wave radiation (ISR)** and **snow depth (SD)**. Yet, as illustrated in Sect. 3.3, meteorological data at the points of interest are sparse and prone to gaps or erroneous values. To characterise atmospheric and snow effects on the ground and respective seasonal, inter-annual or spatial variations, relative values turned out to be suitable.

Within TEMPS, **meteorological data** has been reconstructed based on an ensemble of Regional Climate Models (RCM) for a selection of PERMOS sites (COR, LAP, RIT, SCH, STO, CDV, DRE, FLU, GFU, GEM, MBP), for which micrometeorological measurements were available. The procedure is described in Rajczak et al. (2015) and the work flow is illustrated in Fig. 4.8. Briefly, the climatic conditions had in a first step been reconstructed for stations with long-term observations (bias correction) and were in a second step transferred to the target sites (spatial transfer). Because the data is based on a reanalysis of RCM data between 1981 and 2013, it is not very accurate at the daily scale and regarding single meteorological events (Fig. 1.2a), but it represents the characteristics of the climate well at larger aggregation levels. The major advantage of this reconstructed meteorological data is that projections until the end of the 21st century are available based on the same procedure. These climate scenarios were used to drive ground thermal modes at PERMOS sites (Marmy et al., 2015; Staub et al., 2015a). However, local measurements are required for the spatial transfer and bias correction, and such data is not available for all sites of interest.

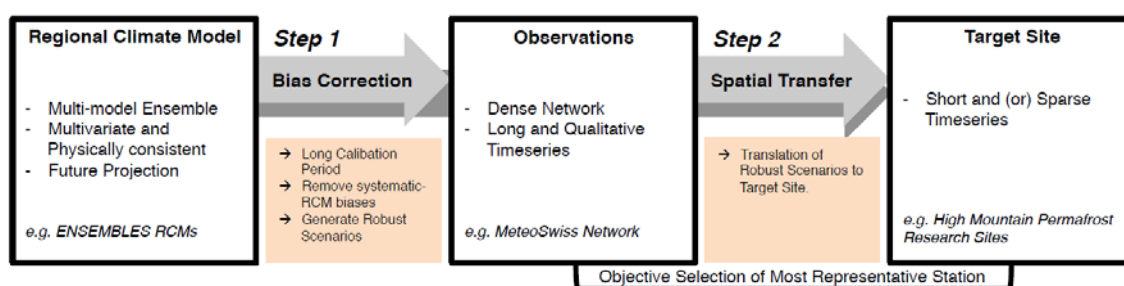


Fig. 4.8: Two-step bias correction approach for meteorological parameters (Rajczak et al., 2015).

The **gridded data products** provided by MeteoSwiss (Frei, 2014) have shown to be useful, particularly in combination with large and spatially distributed data sets as the ones from PERMOS. Gridded data is available e.g. for daily mean air temperature (TabsD), daily precipitation sum (RhiresD) and relative sunshine duration (SrelD) at a spatial resolution of ~ 2 km. The data provided by MeteoSwiss are interpolated from station observations, represent the spatial pattern and are based on state of the art techniques and high-quality observational data. Especially for AirT, which is a spatially homogeneous parameter at high elevation, the use of gridded data sets from MeteoSwiss is straightforward if on-site records are lacking or if many different locations should be compared efficiently. The use of the gridded data guarantees a consistent data basis and allows for the reconstruction of past meteorological conditions until 1961. The data from 1980 are more accurate because more stations were available for the grid interpolation.

For any spatial transfer of air temperature, the **lapse rate** is important to correct for elevation differences. Therefore, typical lapse rates for high-mountain areas were analysed based on homogenized station observations from MeteoSwiss (10 stations >1400 m asl) and the elevation dependency of TabsD gridded values for grid cells above 2000 m asl (Fig. 4.9). Lapse rates are subject to distinct seasonal patterns as well as a high short-term variability (e.g. Gao et al., 2012; Rolland, 2003). As a good compromise between a practicable method and a reasonable improvement of the lapse rate correction, the approximation shown in Fig. 4.9 as a function of the day of the year was used to correct for the seasonal pattern.

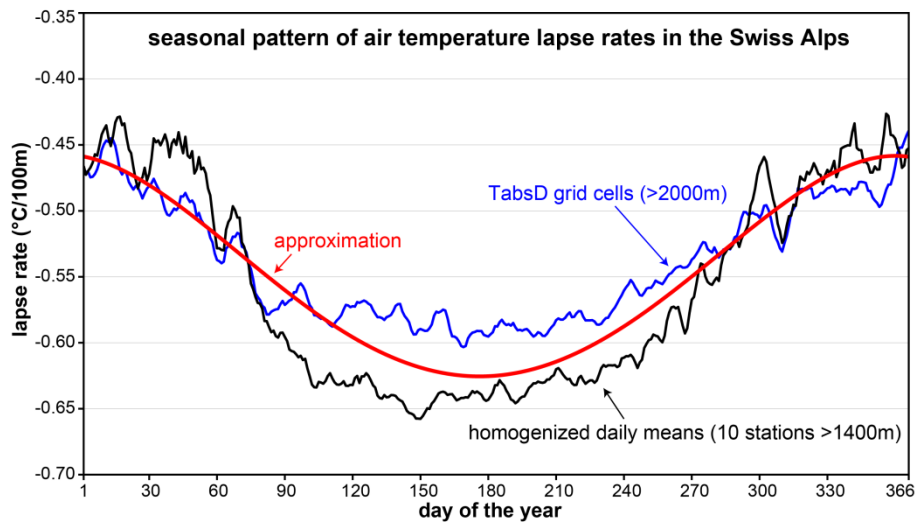


Fig. 4.9: Seasonal pattern of air temperature lapse rates in high-alpine terrain analysed using data from MeteoSwiss. In black, the median of all lapse rates for each day of the year from 10 meteorological stations measured at elevations above 1400 m asl is shown (period 1980-2015). In blue, median lapse rates derived from grid cells above 2000 m asl (TabsD data, n: ~3'000) are shown for the same period. Based on both data sets, the red line illustrates a best approximation in the form of a 4th order polynomial fit.

The comparison of approximated air temperature based on the gridded data TabsD with local observations revealed a very good agreement between estimated and measured daily mean air temperature (Fig. 4.10) with highly significant correlation ($R^2 \gg 0.9$). RMSE values in the order of 1-2 K suggest that some scatter occurred due to local effects which are not represented by the TabsD data. To a small extent, this bias may be due to measurement errors. Compared to the lapse rate correction using homogenized data from single stations (e.g. Säntis), the approximation using TabsD data revealed a better overall performance with smaller RMSE values.

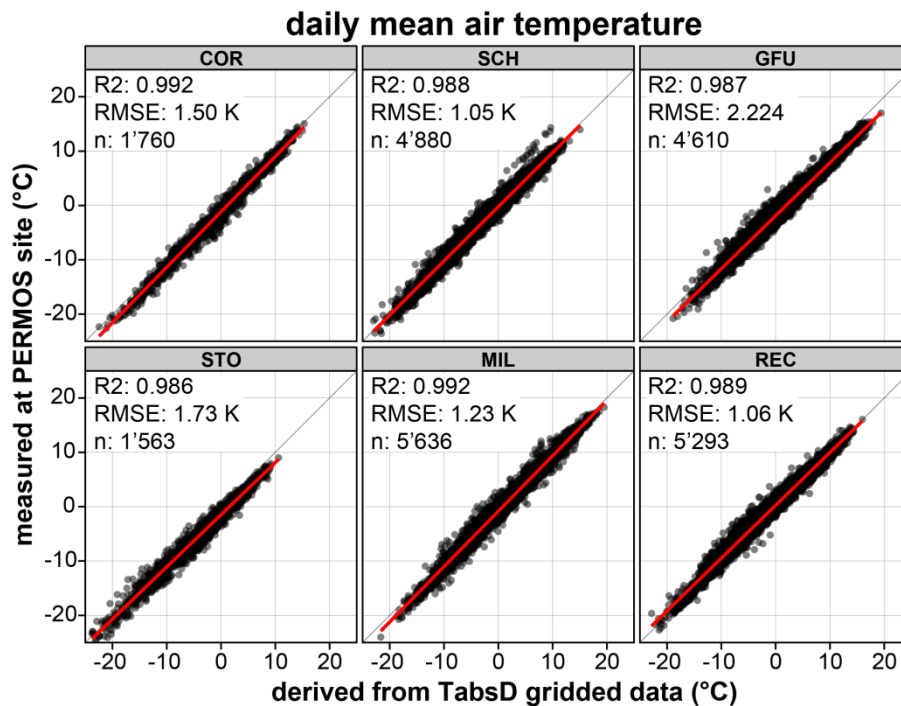


Fig. 4.10: Comparison of grid-derived air temperature with observations at the example of 6 PERMOS weather stations (COR, SCH, GFU, STO, MIL, REC) in different regions of the Swiss Alps. The red lines illustrate linear regressions. Estimated and measured values are in good accordance.

ISR is spatially more variable and is therefore more challenging to reconstruct for points without measurements than AirT. Yet, ISR is strongly related to the sunshine duration and is to some degree correlated with AirT. The dependency on the position of the sun and shading effects by topography enable the approximation of daily, spatially precise potential ISR maxima (PISR, Fig. 4.11a) for each location using digital elevation models and GIS techniques (Olaya, 2009). With quartic polynomial fits based on 20 days of computed PISR values distributed over the year (30 min time step, entire Swiss Alps in 25 m resolution), daily PISR time series have been approximated (Fig. 4.11b). Pearson correlation between approximated and computed PISR is very high ($R^2 \gg 0.95$) and RMSE of the residuals in the order of 2-5 % of the respective PISR values. Sunshine duration, available as gridded data provided by MeteoSwiss (SrelD), is a good proxy for the temporal variance in relative shortwave incoming radiation (Fig. 4.11c). By combining the spatial and temporal data sets, ISR time series can be approximated for any points by Eq. 9 (Fig. 4.11d):

$$ISR \cong SrelD \cdot PISR \Leftrightarrow ISR \geq PISR \cdot 0.2 \quad \text{Eq. 9}$$

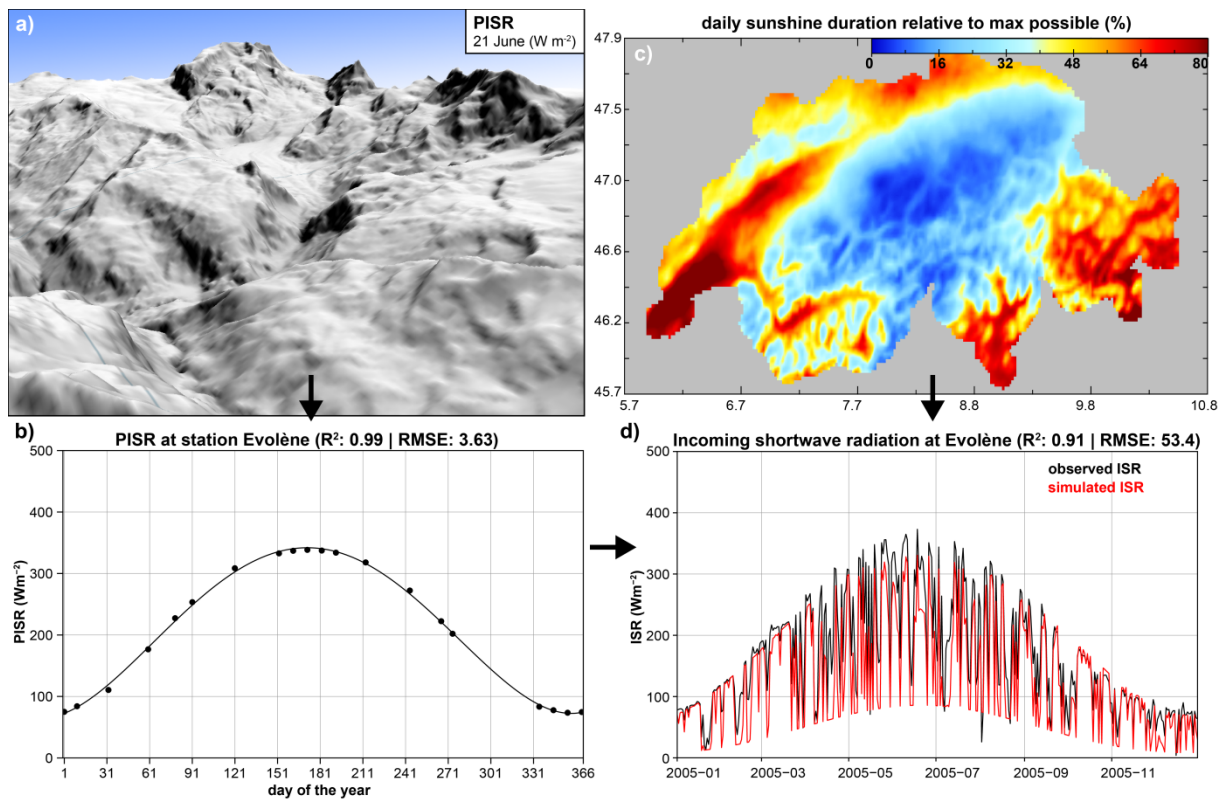


Fig. 4.11: Approximation of the incoming shortwave solar radiation (ISR Wm⁻²) for points of interest by means of spatially precise potential maxima (PISR) and relative daily sunshine duration (SrelD): a) Raster output of PISR at 25 m resolution for the 21st of June simulated with SAGA GIS (PISR is highest in white areas); b) approximated seasonal pattern of PISR for a specific point based on 20 days of calculated PISR values; c) SrelD gridded data from MeteoSwiss (2 km resolution), which was used to integrate the temporal variance for the computation of time series of daily ISR estimates according to Eq. 9 (d).

Since SrelD defines sunshine when the direct solar irradiance exceeds 200 Wm^{-2} , the final result of Eq. 9 can be improved when constraining the minimum value to 20 % of PISR. The correspondence of estimated and observed ISR was best for cloud-free days with high SrelD (Fig. 4.11d). Although absolute values are subject to a uncertainty of $\pm 25 \%$, relative variations of ISR at the weekly-monthly scale were still well captured (R^2 : 0.8-0.95).

Snow has been identified as a key parameter for the evolution of the ground thermal regime because of its heterogeneity and influence on the surface energy balance (Sect. 2.1.2 and 2.2.2). However, snow depth records are sparse (Fig. 2.4) and their high variability complicates the spatial transfer between stations. Remote sensing products may deliver additional insights and possibly assist for gap filling tasks in near future. Today, the snow climatology of the past three decades can be reconstructed only at the km-scale (Hüsler et al., 2014). Therefore, the **lack of snow information** is a central issue. For specific tasks in the present thesis where snow data was required (Sect. 5.2), either PERMOS data and/or IMIS/SLF snow data was used at daily resolution without correction or gap filling.

4.2.5 Procedures for kinematic data

Missing data is unavoidable in long-term monitoring for many reasons. But especially for analysing the temporal evolution of the kinematic behaviour of different zones on rock glaciers, it is crucial to represent the same sets of surveying points in all time steps. It was therefore necessary to estimate missing values and to restrict the data to subsets of reasonable completeness to **increase the number of representative annual mean values** for different rock glaciers or zones on rock glaciers regarding horizontal and three-dimensional surface displacement rates.

Potential approaches to fill gaps in DGPS data are linear regression (LR), multiple linear regression (MLR) or QM by using 2D or 3D displacement rates of other surveying points (Sect. 4.2.1). To account for the small number of common observations (5-15 for annual data) and to keep the approach as simple as possible, LR was used based on other points of highest covariance.

The better the goodness-of-fit of the statistical transformation and the more data points available, the higher the probability to achieve a good approximation for the missing data point or the missing displacement over a given time interval. Experience showed that a minimum number of 5 common observations should be available for robust estimates. Usually the creep velocities of the most suitable regressor points correlate with R^2 in the order of 0.8-0.95. To quantify uncertainty estimates, the 95 % quantile of the remaining residuals (fitted values – observations) was used. As Fig. 4.12 illustrates, the gap filling of the expected surface displacement rates was very promising whereas the uncertainty estimation was less reliable due to high inter-annual variability. Geomorphological expertise is required to group surveying points into zones of similar kinematic behaviour and to compare the movements of different landforms. In addition, the high kinematic activity in recent years raises doubts on the transferability between past, current and future creep velocity relationships among survey points due to potential systemic changes of the movement behaviour and partial destabilization of rock glaciers (sections 7.3 and 8.3).

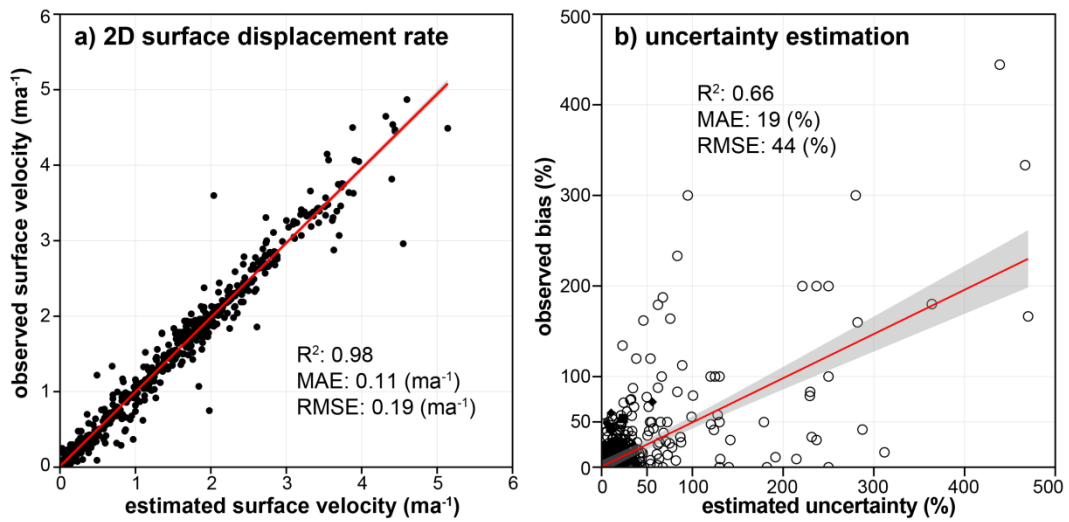


Fig. 4.12: Gap filling of kinematic data and uncertainty estimation for reconstructed values for the example of the Gemmi/Furggental rock glaciers using artificial gaps. The expected horizontal surface displacement rates could be filled with high accuracy (a), whereas the uncertainty estimation for the reconstructed values were less reliable. On average, estimated uncertainties were slightly higher than the absolute bias between gap-filled and observed displacement rates.

For continuous GPS measurements, no gap filling was applied because the few time series available are still short. LR and QM would be suitable approaches, e.g. for weekly or monthly aggregates. For **coordinates or displacement vectors measured by photogrammetry**, gaps typically arise from snow-covered areas or from the insufficient image contrast over shady or steep terrain.

5 Integrative analysis of permafrost monitoring data

In integrative data analysis different methods and data sets are used to maximize the informative value of each parameter for answering specific research questions. The goal was to achieve a quantitative picture of the evolution of mountain permafrost during the observation period, for all variables which are potentially responsible for changes in the ground thermal regime and in kinematic activity. To improve the process understanding, several study sites, landforms and topoclimatic conditions were compared. This chapter provides the methodological approach on which the results (Part III) and synthesis (Part IV) are built on.

5.1 Addressing different scales in time and space with aggregates and indices

The response time of the ground to meteorological events and heat and energy exchange processes differs considerably. In contrast to variations in AirT in the order of a few days, whose influence is restricted to the uppermost ground layers and to the snow-free period, infiltrating water from snow melt or precipitation can have a more immediate impact and also deeper in the ground. **By aggregation, the explanatory power of data can be increased.** Aggregates facilitate the comparison among several time series because the signal-to-noise ratio is increased. **Indices** are data aggregations or single data points which are commonly used in the scientific community, e.g. annual mean values of AirT (MAAT) or GST (MAGST) or the basal temperature of the winter snow cover (BTS). Indices are state of the art representations of a specific type of data in a standardized form. Key aggregates and indices for analysing the surface energy balance with GST data are discussed in the following. The glossary on page xv provides an overview of the abbreviations.

At **daily resolution**, single weather patterns dominate the temperature close to the ground surface and many processes are still visible in the data, such as the thermal insulation of the ground by snow or the infiltration of water. To make changes over long time scales visible, **weekly, monthly or annual mean values** are appropriate. In **aggregates over running (moving) time windows**, imposed limits like calendar days or months do not bias the result. Another advantage of running windows is that many data points are available, e.g. compared to annual means for calendar years. Also, **standard deviations (SD), sums or quantiles** can be computed over running windows.

For specific permafrost-relevant parameters and processes it is necessary to aggregate e.g. thermal or kinematic data, over the entire snow-free period, during zero curtains or to summarize only positive or negative values. Popular examples are thawing (**TDD**) and freezing degree days (**FDD**), which summarize positive or negative daily mean GST over entire hydrological years. Also, the comparison of different monitoring parameters, namely temperature differences between the ground surface and the air (so called surface offset **SO**) or between a specific depth in the ground and GST (thermal offset **TO**), belong to this kind of temporal-thematic aggregates. TDD, FDD, SO and TO can also be calculated in running windows, e.g. of 365 days. For the comparison of heterogeneous time series, the calculation of **anomaly values relative to a common observation period** (in the following with suffix a) is advisable. Fig. 5.1 illustrates aggregates and indices using GST data.

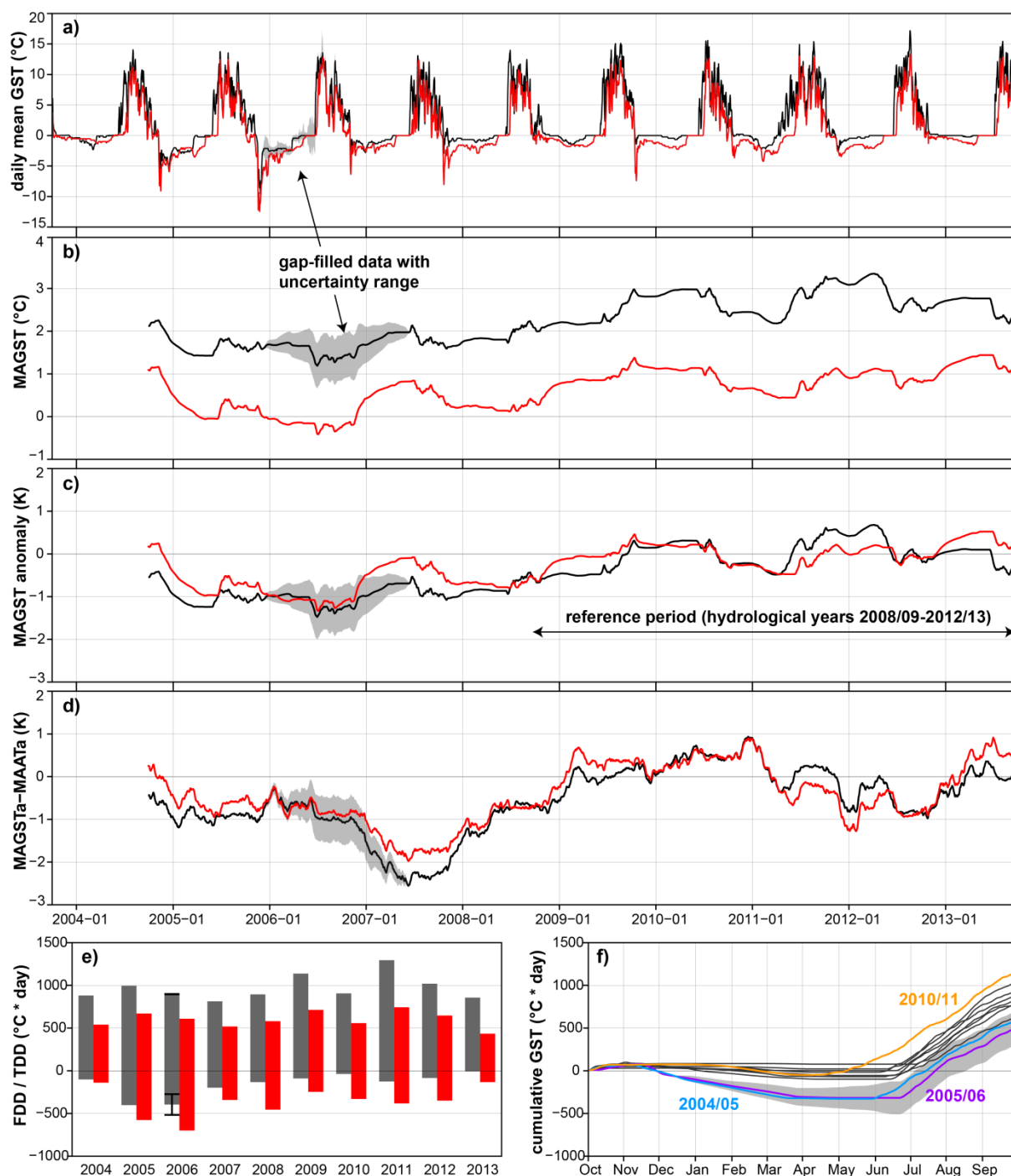


Fig. 5.1: Aggregates and indices for GST data, exemplified by two time series for two measurement locations situated on talus slopes 1.5 km apart from each other (in red LAP_S015 at 2500 m and in black/grey ATT_S002 at 2700 m asl): a) daily mean GST (with uncertainty range in grey, where data gaps needed to be filled); b) running annual means (rMAGST) with respective uncertainty range resulting from the filling of data gaps; c) rMAGST anomaly values showing inter-annual variations relative to the mean value of the respective series in a specified reference time window; d) running annual means of the surface offset (rMASO, rMAGSTa-rMAATa); e) thawing (TDD) and freezing degree days FDD for different hydrological years (Oct-Sep, the indicated years correspond to the end of the respective hydrological year); f) cumulative degree days (CDD) for the logger ATT_S002.

Other GST indices such as the basal temperature of the winter snow cover **BTS** (Haeberli, 1973) are **only valid under specific ground thermal conditions**, namely when the active layer is in a quasi-isothermal state in late winter. The same holds for the winter equilibrium temperature (**WEqT**). While BTS only represents a snapshot of one single survey (some hours during a 1-day field

campaign), WEqT can be arbitrary defined for a longer time period before the snow melt. BTS and WEqT are theoretical values that aim at capturing the thermal signal from the permafrost at the ground surface. However, the assumption of a thermal equilibrium within the active layer is problematic because the thermal insulation by the snow cover is often not ensured. In many cases the snow melt starts before an equilibrium state is reached and the BTS or WEqT value of one single year might not be representative for the ground thermal characteristics. Therefore, a **numerical detection of WEqT** from GST data was introduced in order to consider the probability of having reached thermal equilibrium. The last period of quasi-stable GST before the start of the melting period was used. Possibly, the terminology **late winter surface temperature (LWST)** would be more appropriate for this type of aggregate. The median GST over a period of 1 month two weeks before the snow melt starts was used to approximate LWST. The spatial variability and temporal evolution of BTS, WEqT and LWST are illustrated in Fig. 5.2. To assess the validity of these values, the snow thermal indices can be used (Sect. 5.2).

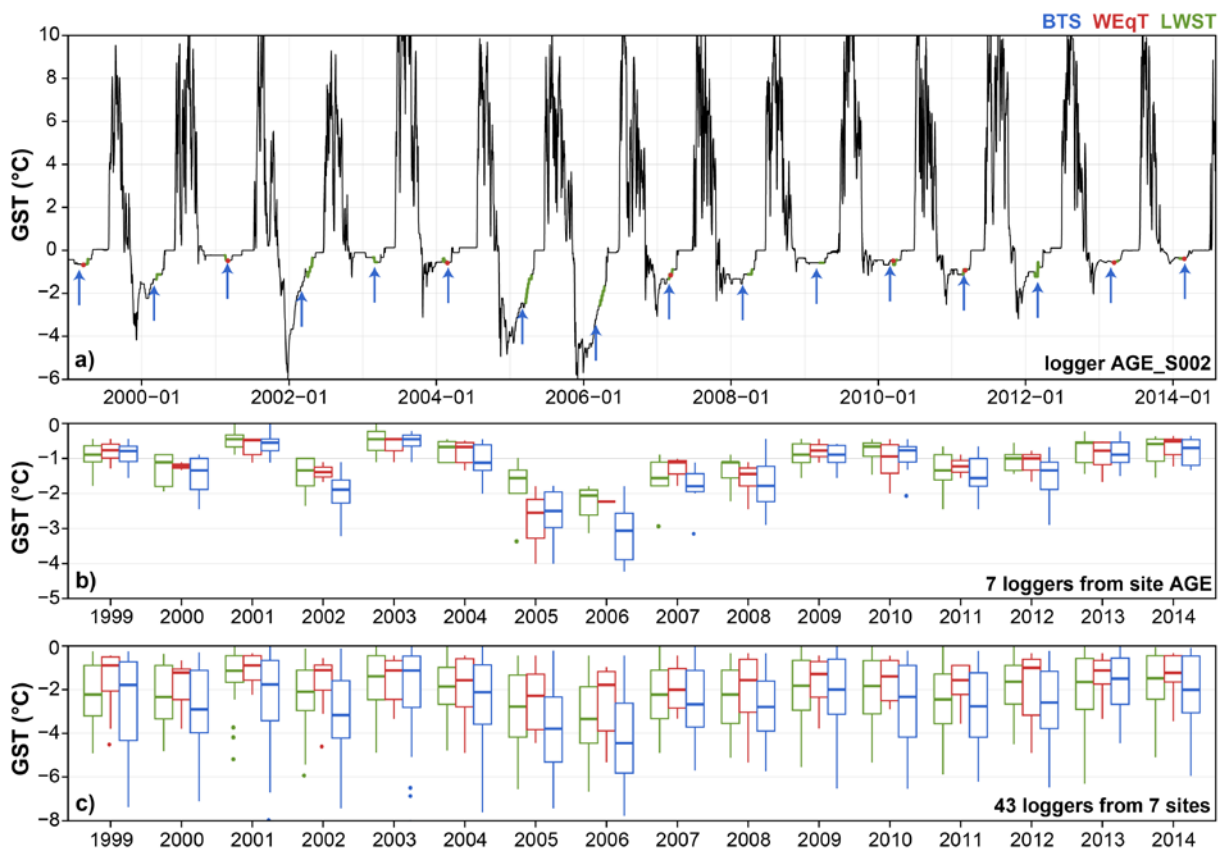


Fig. 5.2: BTS, WeQT and LWST values derived from daily mean GST from a set of 43 complete time series from 7 different field sites: a) comparison of the indices at the example of logger AGE_S002. Arbitrary defined BTS values in blue always represent GST data for the 1st of March, WEqT values are shown in red if they were computable, and LWST in green represent the median during a 30-day period two weeks before the zero curtain starts); b) comparison of the same values for all 7 loggers from the AGE field site; c) comparison of 43 complete time series from 7 field sites.

From GT measured in boreholes, additional indices were derived. The zero annual amplitude (**ZAA**) represents the maximum depth to which seasonal temperature variations are detectable (usually ~20 m). The depth of seasonal thawing and refreezing (Fig. 2.6) characterises the active layer thickness (**ALT**). Usually ALT is greatest in October when the ground surface started freezing.

ALT variations have a spatial (among boreholes), seasonal and inter-annual component. Many temporal aggregates (e.g. MAGST, FDD or LWST) also proved to be useful for **spatial comparison** of field sites and loggers.

For **kinematic data**, aggregation was done spatially over different sets of measurement points or zones on rock glaciers (i.e. the most rapidly moving central part). Aggregation over different time windows was meaningful only for high-frequency data, recorded by permanent GPS, e.g. for comparison with manually measured coordinates at greater time intervals. **Geophysical data** like ERT was resampled to grids of coarser spatial resolution to reduce the uncertainty of the measurements and of the inversion process. Moreover, anomaly values (i.e. changes in apparent resistivity or p-wave velocity) were used to visualize changes over time and to compare different field sites of kinematic and geophysical data.

5.2 Deriving snow information based on GST data

Snow was identified decades ago as a **dominant factor for the permafrost evolution** because it highly influences the energy balance at the ground surface while being temporally and spatially highly variable (Sect. 2.1.2). Since snow data is sparse, usually restricted to the parameter snow depth and only representative for the exact position of the measurement (Fig. 2.4), other sources of information are required to assess the spatial and temporal variability of snow characteristics and their influence on permafrost.

Since GST data is influenced by the **local snow characteristics**, this large data set was used to extract snow information for the explicit points of interest. Methods for deriving snow characteristics, such as the **thermal insulation effect, the timing of the onset, melt and disappearance of the snow and the snow melt rate**, from GST monitoring data are discussed in detail in Publication I (Staub and Delaloye, 2016). Only the key elements are shown here, and how integrative mountain permafrost research can benefit from GST-derived snow information.

5.2.1 Generalities and GST-derived snow information

Semi-quantitative information on the thermal insulation effect by the snow cover and periods of phase changes can be **derived from short-term GST variations**. In the Swiss Alps, the daily standard deviation (SD) of AirT ranges between 0.5-5 K with little seasonal change. As long as the ground is not thermally insulated and dry, daily SD of GST (GST_{SDday}) are in the same order of magnitude. GST_{SDday} are slightly higher if recorded at (“skin surface temperature”) or very close to the ground surface, and slightly lower if measured 10-20 cm below the surface. As Fig. 5.3 illustrates, the presence of an insulating snow cover reduces GST_{SDday} by a factor of at least 5-10 times. Similar values were reported from the area of Corvatsch, eastern Switzerland, where during the winter period GST_{SDday} were smaller than 0.2 K (Schmid et al., 2012). Schneider et al. (2012) used a threshold of 0.4 K for the daily GST amplitude to delineate snow-covered from snow-free periods.

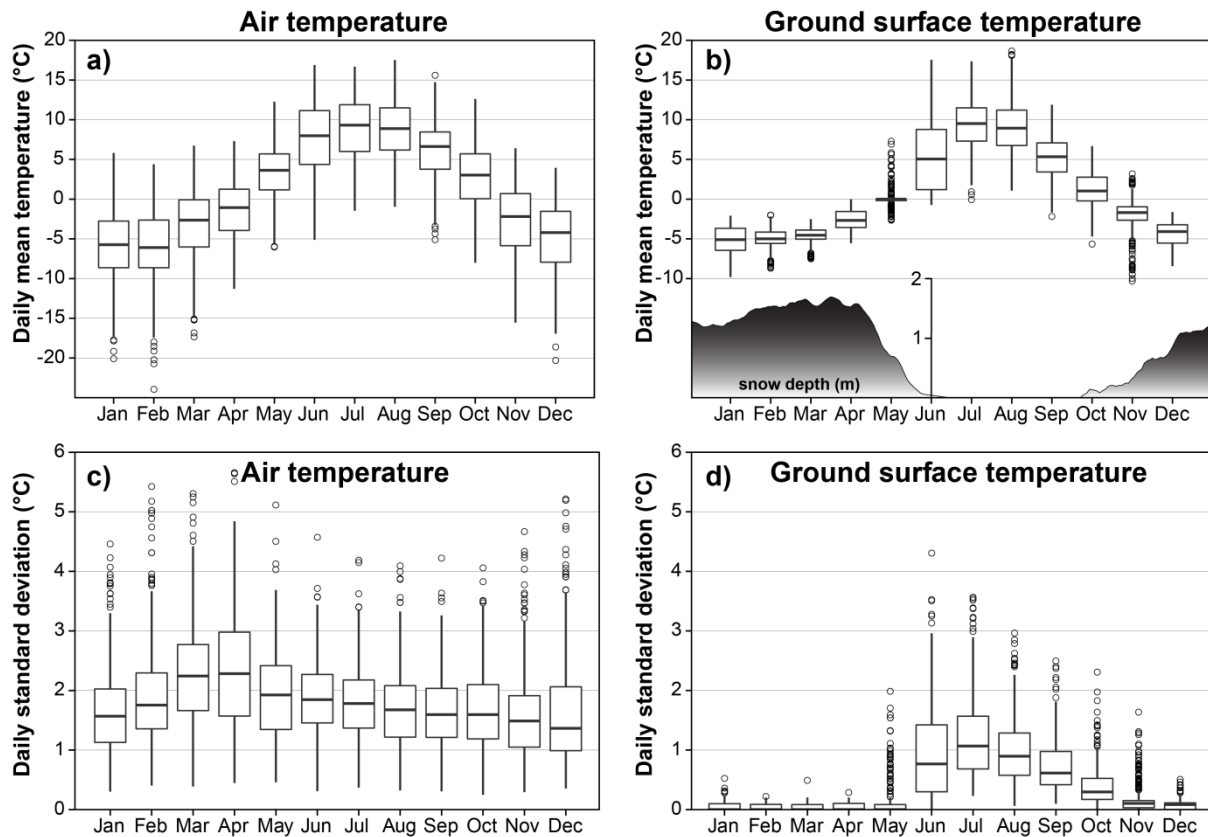


Fig. 5.3: Seasonal patterns of AirT (~ 2 m above ground) and GST (~ 20 cm below the surface) at the rock glacier “Alpage de Mille” (2400 m asl, MIL in Fig. 3.1) over the period 1997-2014: a) and b) visualize daily mean temperatures as well as the average snow depth measured at the same site, c) and d) illustrate the high influence of the snow on the daily GST standard deviation ($GST_{SD\text{day}}$) in terms of reduction of $GST_{SD\text{day}}$.

The methods described in Staub and Delaloye (2016) enable the following snow information to be derived from GST data:

- The **delineation of zero curtain (ZC) periods** when phase changes dominate the GST signal, and the start of the snow melt in spring (**basal ripening date RD**) and the **snow disappearance date (SDD)**.
- Snow thermal indices** ranging from 0 to 1 which characterise the thermal insulation effect of the snow cover based on GST variability. Three indices were developed for different input data: $snow_1$ takes hourly or bi-hourly GST values, $snow_2$ daily GST values, and $snow_3$ GST and AirT time series at hourly or daily resolution. $snow_3$ is based on an algorithm proposed by Hipp (2012), originally developed for the automatic detection of snow depths from snow poles instrumented with iButtons (Lewkowicz, 2008).
- The first day with detectable snow (**snow onset date SOD**), the start of the high insulation period (HTI_{start}), and the period without meaningful thermal insulation by the snow (between SDD and HTI_{start}).
- The **snow melt rate (SMR)** as snow water equivalents (SWE) in mm per day during the spring zero curtain using AirT as a proxy.

For additional details and the validation of the methods see Publication I (Staub and Delaloye, 2016). Examples of the snow thermal indices are illustrated and commented in Fig. 5.4.

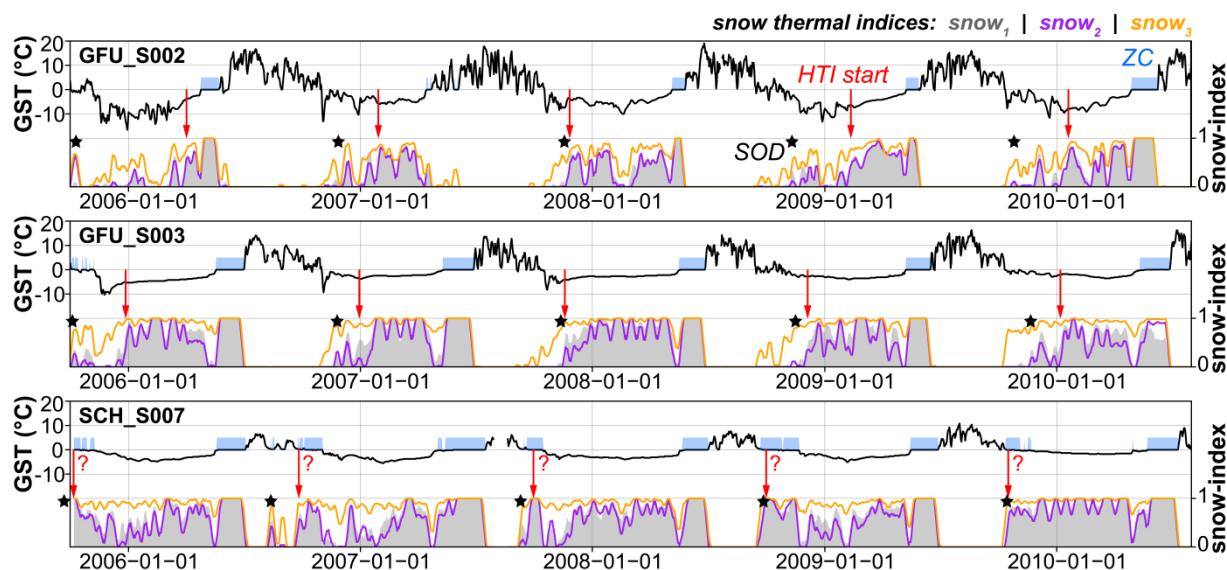


Fig. 5.4: Comparison of GST and snow indices for selected GST time series from the sites Gemmi (GFU) and Schilthorn (SCH). Black line: daily mean GST; blue areas: periods with phase change (zero curtains); grey areas: snow index snw_1 ; purple line: snow index snw_2 ; orange line: snow index snw_3 ; black stars: snow onset date (SOD) based on snw_1 ; red arrows: start of the high-insulation winter period (HTI_{start}) based on snw_1 . Thermal insulation by the snow cover is approximated gradually from 0 (no insulation) to 1 (very high thermal resistance). HTI_{start} may occur at the same time as SOD or much later in the season, depending on the evolution of the snow cover in the course of the winter.

5.2.2 Use and limitations of the methods

The snow indices are **designed for permafrost terrain**. Based on GST data they characterise the probability of the presence of a thermally insulating snow cover. Negative GST during the winter season are required for the successful determination of the melting period and RD. For GST data measured at permafrost-free sites, it is likely that the spring zero curtain is not distinguishable from other periods of freezing or thawing. Although during periods of phase change, the variation of GST is completely decoupled from those of air temperature, the ground remains influenced by the basal temperature of the snow and the advection of latent heat. **ZC** can occur at the ground surface during:

- the melt of snow when the active layer is frozen (spring zero curtain);
- the melt of fresh snow on unfrozen ground (as often occurs in autumn, particularly on fine-grained and humid substrate);
- ground water freezing;
- after rain on snow events, when water percolates through the snowpack and refreezes at the surface or in the subsurface (Westermann et al., 2011; Wever et al., 2014).

In these situations, the GST signal is dominated by phase changes which happen in proximity to the ground surface. However, limited information about the intensity of the heat fluxes could be derived directly from GST data. Generally, **the spring zero curtain can be seen as a phase of net ground warming** due to the infiltration of water (Sect. 2.2 and Fig. 7.4). The approximation of snow melt rates is a first step towards a more quantitative analysis of the influence of the melting period on the ground thermal regime. Phase changes which occur during ground freezing or the melting of snow on warm ground are more challenging to analyse quantitatively based on GST data, since the amount of latent heat and the energy fluxes in the ground are not known. By means of the concepts of surface

and thermal offsets (SO and TO, Sect. 5.1), however, the **efficiency of ground freezing** could be described semi-quantitatively. The higher the temperature gradients are, the higher the heat fluxes are expected to be (Sect. 2.2.3). Studying SO and TO is particularly interesting at sites which are prone to the chimney effect (Sect. 2.1.3).

5.2.3 Potential improvements of the melt-index by considering global radiation

The approximation of SMR was improved by considering more detailed information on the meteorological conditions, the site-specific terrain and snow characteristics. By using on-site air temperature records, potential bias due to the downscaling and spatial transfer of gridded data could be eliminated. Additionally, incoming shortwave radiation (ISR), the second important parameter controlling snow melt, was introduced. As described in Sect. 4.1.2 and 4.2.4, ISR values can be approximated by considering potential ISR (PISR, spatially accurate) and the relative sunshine duration (temporally accurate). Hence, the melt-index (Equation 6 in Staub and Delaloye (2016)) can be complemented by a radiation term as in Eq. 10:

$$melt - index_2 \cong \frac{\Delta h s \rho}{\Delta t} \cong \frac{A \sum_{t=RD}^{SDD} AirT^+ + B \sum_{t=RD}^{SDD} ISR}{\Delta t_{(SDD-RD)}} \quad \text{Eq. 10}$$

The parameters A (AirT factor) and B (ISR factor) in Eq. 10 were calibrated using IMIS snow data as a proxy for the true snow melt by assuming a constant snow density (ρ) of 400 kgm^{-3} . Optimal values for A and B were 2.0 and 2.1, respectively. The explanatory power of both terms is significant (p-values < 0.01, n: 934) and the introduction of the radiative component slightly improved the overall performance compared with the original melt-index. R^2 with cumulative snow depth loss is ~ 0.9 (0.84 if only the AirT is included in the calculation) and the RMSE of the residuals is about 20 % lower. Since the IMIS snow stations are mostly located in open terrain with strong direct solar radiation (mean values for June 21: PISR: 333 Wm^{-2} , ISR: 163 Wm^{-2}) compared with the GST data from PERMOS (mean values for June 21: PISR: 292 Wm^{-2} , ISR: 146 Wm^{-2}), the spatial transfer of this calibration would need to be analysed carefully. However, the increased complexity of melt-index₂ compared with the simple temperature-index model most likely does not justify its potential increase in accuracy. Therefore it was not included in Staub and Delaloye (2016).

5.3 Quantification of the time lag between GST and GT at depth

With increasing depth below surface, GT becomes less variable over time and the seasonal component diminishes. However, over time scales of years, the integral of the surface energy balance dominates the thermal evolution even at depth (Sect. 2.2). The thermal conditions at depth are expected to be relevant to the hydro-mechanical and creep behaviour of permafrost (Sect. 2.3). Therefore, the **time lag of the thermal signal** between the surface and specific depths as well as the **intensity of the ground thermal reaction** to GST variations needed to be quantified.

Assuming two sine curves of similar wavelength with an offset in time, this offset can be quantified by applying systematic shifts in time (time lags) and maximizing the **coefficient of determination (R^2) of the cross-correlation** (Fig. 5.5). Transferred to GT data this means that the time lag between two thermal signals can be estimated if the **seasonal signal** dominates over inter-annual variations. The amplitude of the two time series does not matter as long as the seasonal component outbalances other variabilities. GT also show inter-annual variations and are influenced by meteorological events and lateral disturbances at various time scales. A pre-condition for a time lag analysis is that the data is continuous and of the same aggregation level. To study the effect of inter-annual variations, the procedure was repeated for subsets of 3-5 years duration and by analysing daily mean values at greater depth (Fig. 5.5c-e).

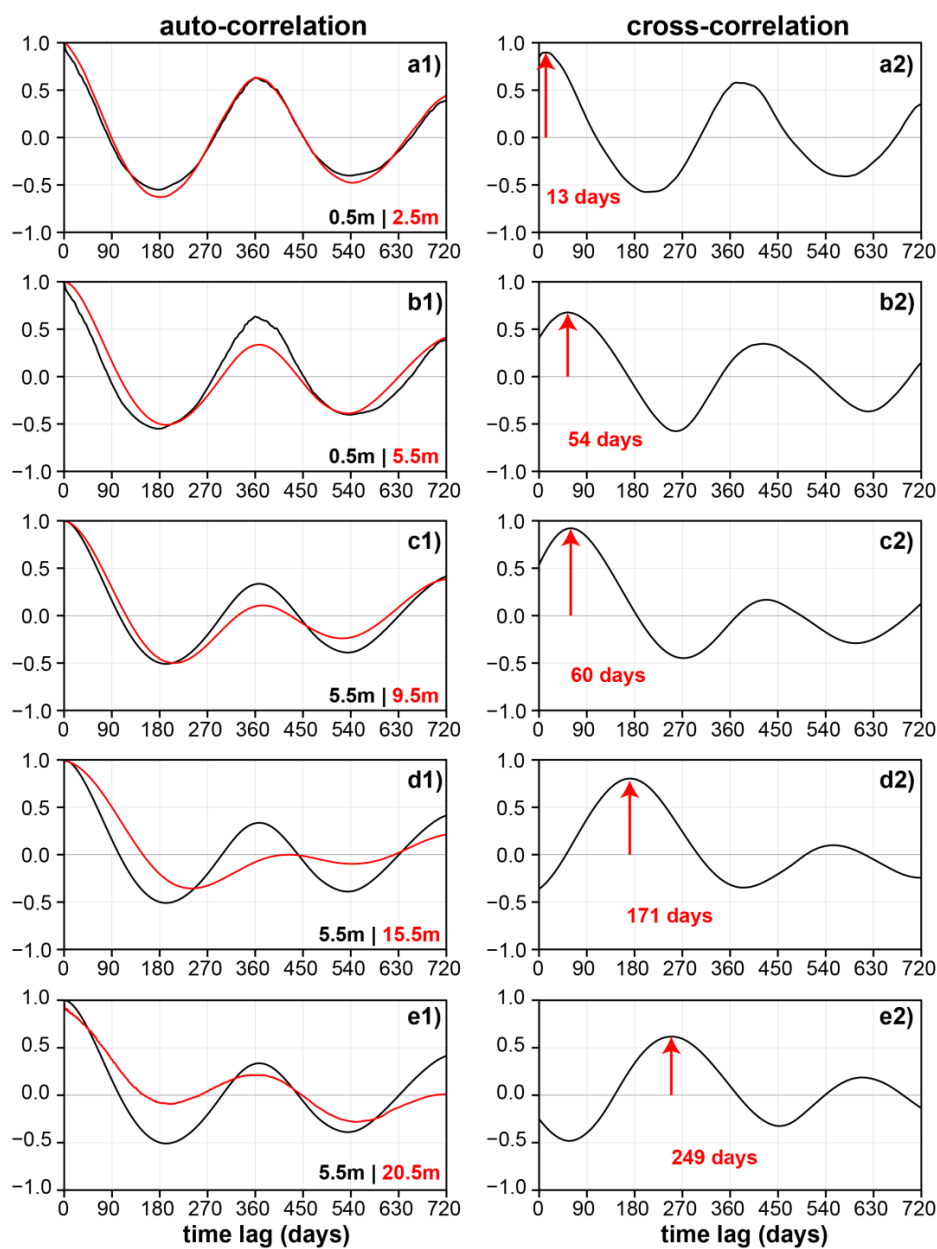


Fig. 5.5: Analysis of the time lag of the surface temperature signal at different depths for borehole COR_0278 for a period of continuous data between 2010 and 2013: On the left, auto-correlation between the thermistor pairs (upper and lower thermistors indicated on the plots) are shown, and on the right the respective time lag at maximum cross-correlation (red arrow): a) within the active layer, b) between the surface and the permafrost, c-e) in the permafrost. To reach 10 m depth, the GST signal needs approximately 4 months, and for 20 m depth about 10 months.

Depending on the relative importance of the seasonal signal, the superposition of inter-annual, seasonal and short-term variations and the degree of conductivity within the active layer, the calculation of the time lags was straightforward. In most cases, reasonable R^2 values $\gg 0.5$ were obtained within the active layer (Fig. 5.5a-b). At greater depths the relationship between GST and GT was usually more complex because of phase changes and differences in the thermal resistance of the subsurface due to the variable composition and material properties. By choosing a thermistor e.g. at 5 or 10 m depth, the propagation of the thermal variations with increasing depth could be analysed down to the ZAA. When systematically applied to all thermistors of a borehole, the relation between depth and the time lag can be visualized as in Fig. 7.5. The same approach could also be used at a coarser aggregation level to analyse the time lag of inter-annual GT variations, at depths below the ZAA. However, for this purpose the time series are still too short. In addition to the time-lag analysis, the relative importance of heat conduction on the total heat and energy exchange in the ground was assessed. This is subject of the next section.

5.4 Visualization of the degree of conductivity with thermal orbits

As mentioned in Sect. 2.2, conduction is the most important heat transport mechanism in the ground and is relatively simple to describe mathematically. However, turbulent fluxes of fluids in voids temporally superimpose on the effects of heat conduction. To visualize how the conductive heat transport is influenced by other processes, so-called **thermal orbits** were applied. Thermal orbits, which were introduced originally by Beltrami (1996), are based on scatterplots of two temperature time series. The resulting data points are assumed to be of perfect oval shape in the case of purely conductive heat transport between the two thermistors at different depths. As illustrated in Fig. 5.6, phase changes as well as advective and convective processes cause additional scatter within the active layer. Additionally, the shape of these orbits could be quantitatively analysed (Smerdon et al., 2009). The next section will demonstrate how the information on the time lag and the degree of conductivity can be used to derive knowledge about the kinematic activity of rock glaciers.

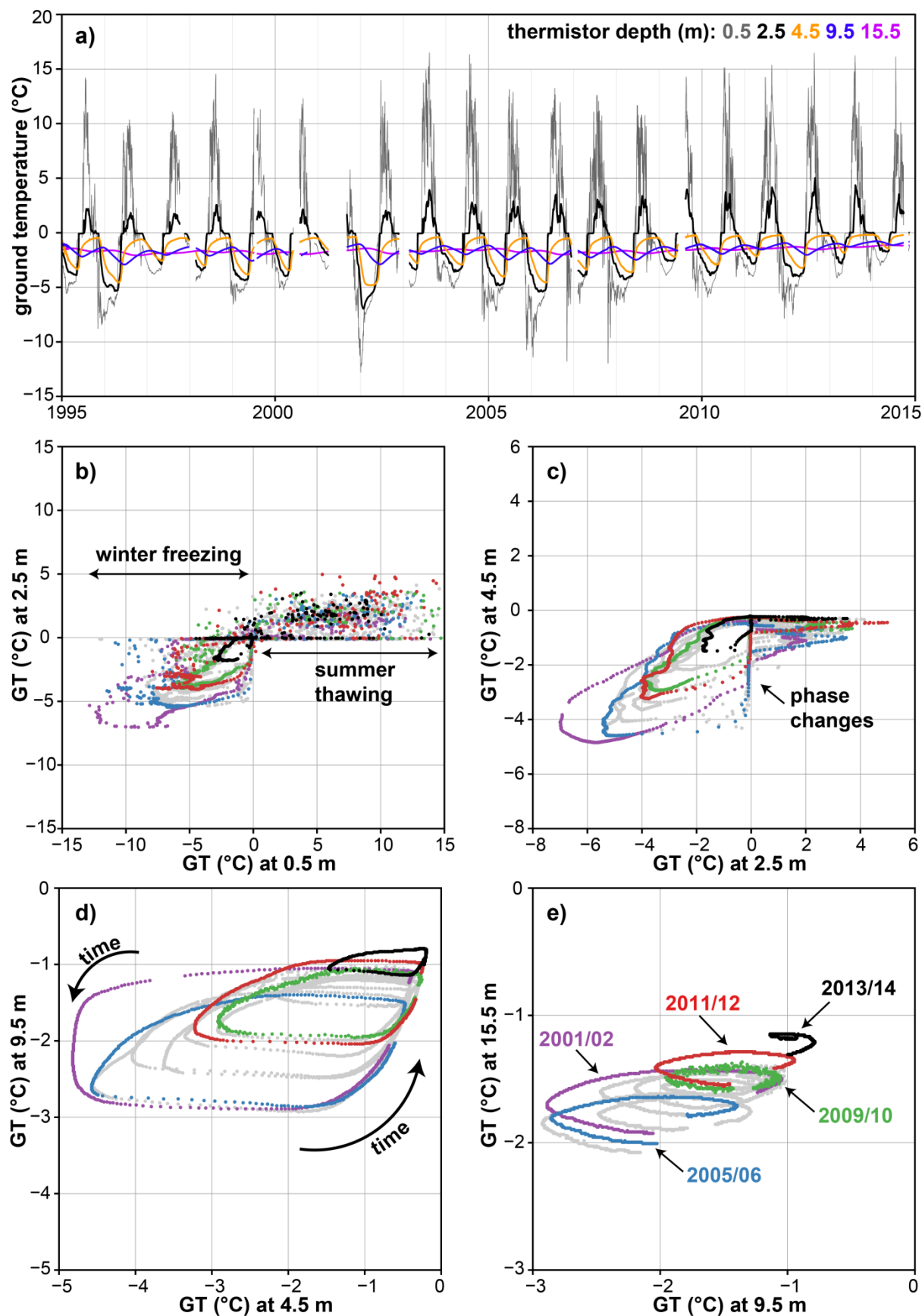


Fig. 5.6: Thermal orbits comparing different thermistor combinations at the example of borehole COR_0287 on rock glacier Murtèl-Corvatsch. Panel a) provides an overview on temporal GT variations between 0.5 and 15.5 m depth; panels b-d show thermal orbits for the same thermistors: b) the active layer close to the surface; c) between the active layer and the permafrost; d-e) in the permafrost. Only hydrological years with > 90 % complete data were selected, different years are indicated with different colours. At 10-15 m depth, the large inter-annual variations and current maxima are visible.

5.5 Approximation of GT variations from GST data for analysing rock glacier kinematics

The viscosity of ice and ice-containing subsurface material is temperature dependant (Sect. 2.3). Therefore, variations in kinematic activity are expected to correlate with GT variations at the respective depth of the shear horizon, where 50-95 % of the total deformation takes place (Arenson et al., 2002; Wagner, 1992). Based on inclinometer data for three rock glaciers in the south-east of Switzerland, Arenson et al. (2002) found that the shear horizon is located at 15-30 m below the surface. Besides GT, other factors such as geometry, water infiltration, and surcharge by snow or rock deposits may influence rock glacier kinematics (Sect. 2.3). More data on this hydro-thermal-mechanical relationship is required for a multitude of different rock glaciers to improve the process understanding. If GT data is lacking, as is usually the case on rock glaciers, GST can be used to approximate relative GT variations at various depths.

Since the thermal signal in the ground is delayed (Sect. 5.3), a time lag as well as a filter needs to be introduced to modify the GST variations. In the most simple case, GT variations at depth can be approximated based on GST means over one or more years. As shown in Fig. 5.5, the respective time lag (*tlag*) at 15 m depth is sometimes less than 12 months, whereas at 30 m it can be assumed to be between one and two years (Fig. 7.5). In order to reconstruct GT variations within rock glaciers without relying on borehole data, a method to calculate synthetic GT anomaly values (GT_{synt}) for arbitrary time intervals (*n*) was developed. It is based on monthly mean GST values (GST_{month}) and GST reference values (GST_{month_ref}) as described in Eq. 11. GST_{month_ref} corresponds to the mean GST value of several years of the respective month. The approach benefits from the fact that seasonal GST variations are several factors larger than inter-annual GST variability.

$$GT_{synt} \cong \frac{1}{n} \sum_{-tlag}^{n-tlag} (GST_{month} - GST_{month_ref}) \quad \text{Eq. 11}$$

The procedure was validated by comparing running mean values calculated over 1, 2 and 3 entire years with respective GT_{synt} (*n*: 365, 730, 1095 and *tlag*: 0). As shown in Fig. 5.7a-c, the method performed well with R^2 of 0.99 and RMSE values in the order of ~3 % of the maximum inter-annual variability. To facilitate the comparison with other data, the monthly means of GT_{synt} were linearly interpolated to daily values. In Fig. 5.7d-f GT_{synt} are compared with observed GT from the rock glaciers Murtèl-Corvatsch (GT at 15 m), Ritigraben (16 m) and Pontresina-Schafberg (17 m). For GT close to the melting point, the correlation between GT_{synt} and observed GT may be affected by phase changes (Fig. 5.7e). But increased amounts of liquid water possibly cause acceleration or rock glacier displacement rates (Delaloye et al., 2010; Ikeda et al., 2008). Therefore, variations in GT_{synt} may be an even better proxy than GT observations to describe variations of rock glacier creep. The method is applied in Sect. 7.3 to assess the kinematic response to meteorological events.

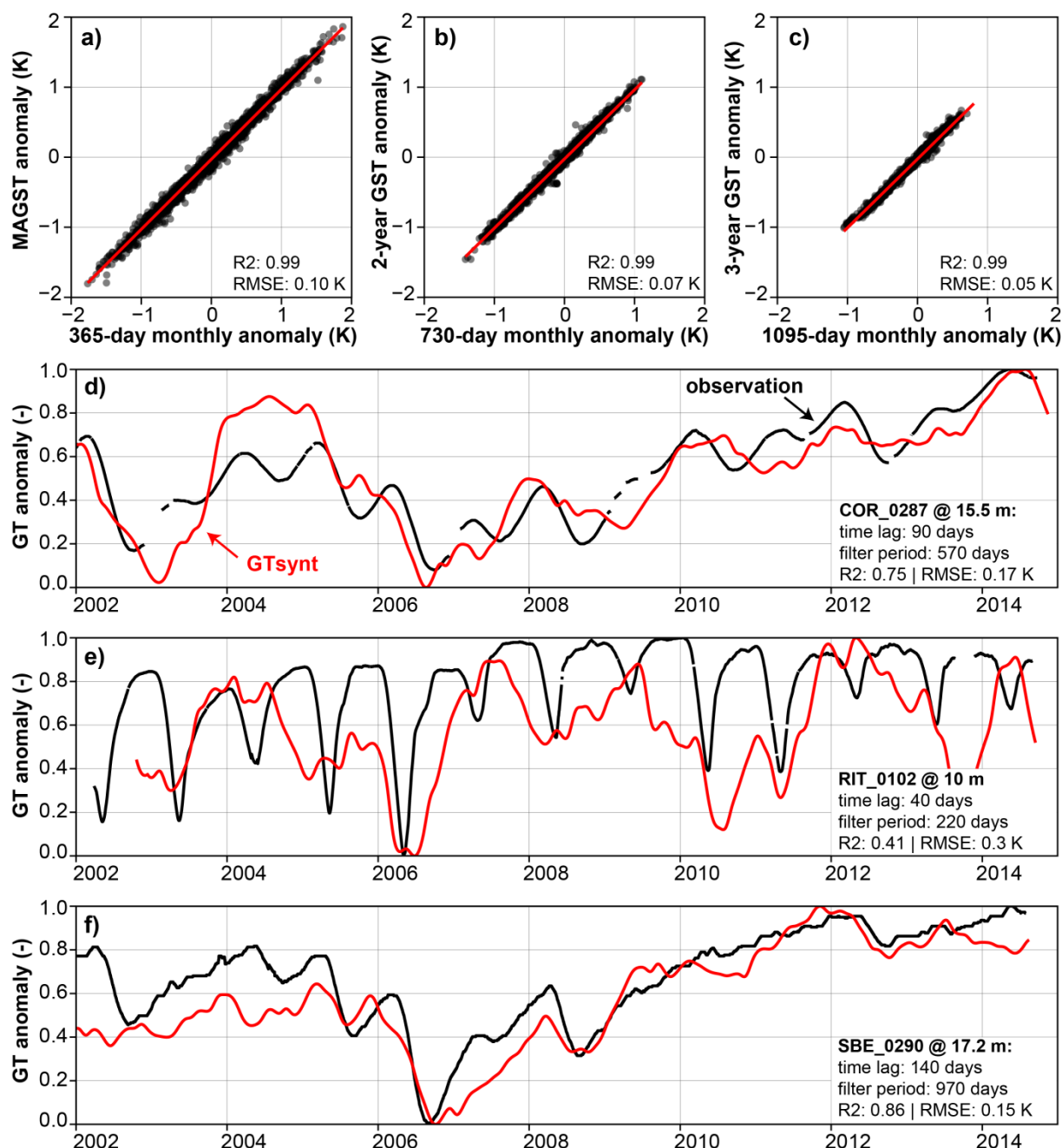


Fig. 5.7: Comparison of GST-derived, synthetic GT data (GT_{synt}) with GST and GT observations. Panels a-c show the results of the validation of the approach described in Eq. 11 using GST data from 26 complete time series between 2002 and 2012. On the x-axis, the respective mean GST are calculated with a time lag of 0 days and the indicated filter window. On the y-axis, the corresponding running mean is shown calculated from daily mean GST. The panels d-f compare GT_{synt} (red) with GT observations (black) from boreholes at the example the three rock glaciers Murtèl-Corvatsch (COR), Ritigraben (RIT) and Pontresina-Schafberg (SBE). The result with the highest Pearson R^2 is shown and the respective time lags and filter window are indicated in the figure. The time lags are lower than those in Fig. 5.5 due to the long filter time windows, which are aligned at the end of the respective period. For this reason, the effect of GST variations observed at the surface is significantly delayed (e.g. cold winters 2004/05 and 2005/06 appear in late 2006).

The next section explains how spatial patterns of horizontal surface displacement rates were analysed and quantified by means of aerial photogrammetry and GIS techniques.

5.6 Image correlation methods for the analysis of rock glacier kinematics

The major advantage of aerial images and photogrammetric techniques is that terrain movements can be quantified at high spatial resolution with excellent precision (cm-scale) and reasonable accuracy (dm-scale). Therefore photogrammetry was considered in the frame of this thesis. However, the manual stereo-analysis of multi temporal aerial images is very time consuming and the quality of the results strongly depends on the experience and stereovision of the operator. Automated techniques which track features or zones of similar image characteristics can be used to measure surface deformation on moving landforms more efficiently (Bollmann et al., 2015; Fey et al., 2015; Käab et al., 1997; Kenner et al., 2014).

In addition to manual stereo measurements the image correlation approach of Fahnestock et al. (1992) and Scambos et al. (1992) was used for this thesis. The latter is based on Fast Fourier Transformation (FTT) and available as a SAGA GIS module (IMCORR). IMCORR is a sophisticated tool to quantify systematic and stochastic shifts in geographic raster data, either to measure displacements or to assess uncertainties of georeferenciation and orthorectification. This technique was applied to a series of high-quality aerial images covering three rock glaciers at the Gemmi field site. Long time series of geodetic and photogrammetric rock glacier surface displacement rates have been reprocessed and jointly analysed to study morphological changes (Krummenacher et al., 1998, 2008; Staub et al., 2015b). Fig. 5.8a shows extracted displacement vectors around a shear zone between very fast displacement rates in the rock glacier centre to an inactive part on its orographic right border. Fig. 5.8b compares the respective velocities in the surrounding area of DGPS points for three time periods. Although the overall agreement is reasonable, the correlation between geodetic and photogrammetric displacement rates is not ideal because the time points of the terrestrial DGPS surveys and the aerial images differ. The application of the IMCORR tool in presumably stable terrain revealed uncertainties in the order of ± 15 cm based on four image strips (2010-2014) recorded with a UltracamX sensor at a ground sampling distance of ~ 15 cm. This uncertainty is similar to the RMSE of the residuals after the bundle block adjustment of the image strips during the process of orthorectification. The IMCORR tool could also be used to validate orthophotos, digital elevation models or derivatives which often come without detailed information on the orthorectification process.

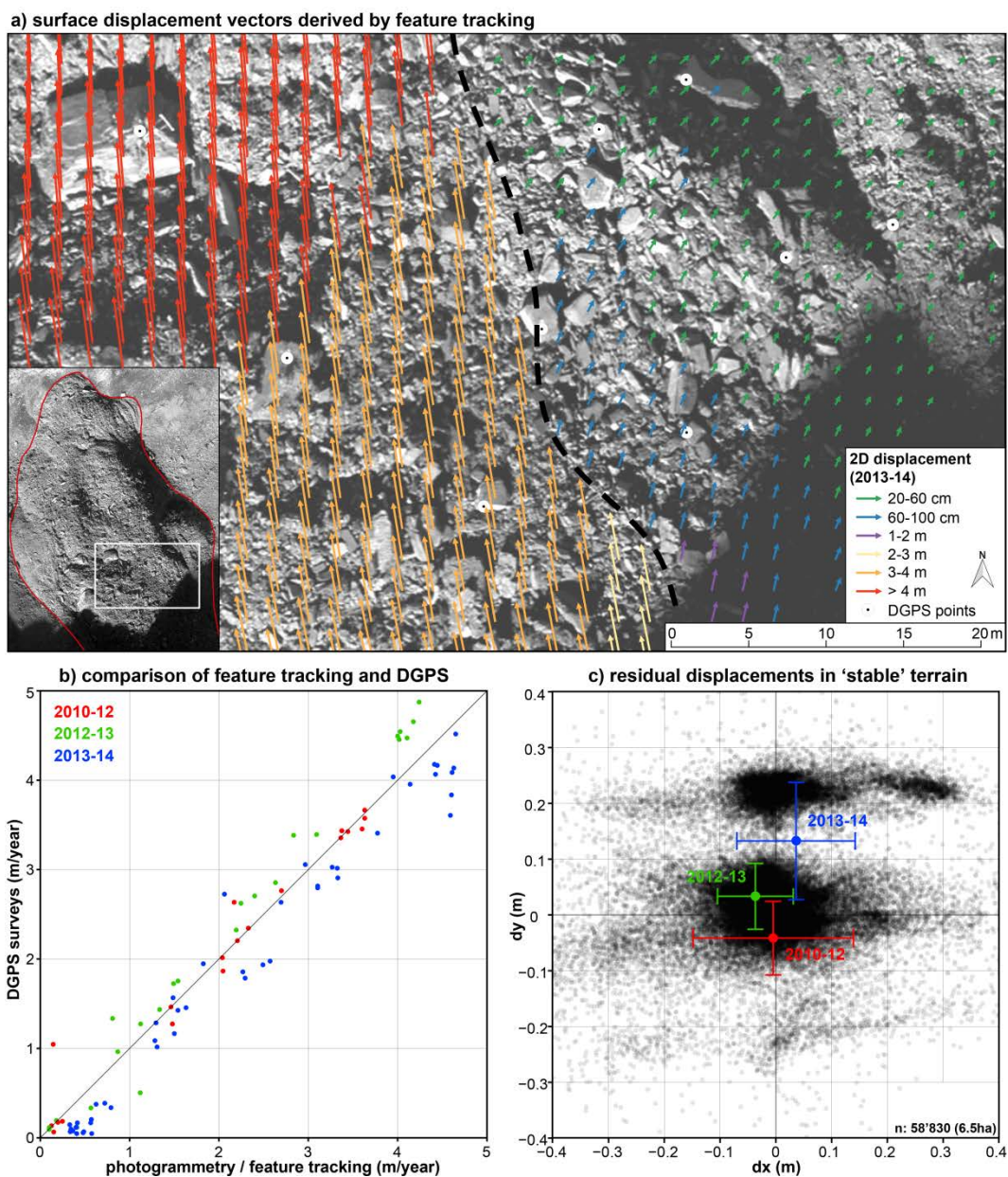


Fig. 5.8: Applications of the image correlation module IMCORR which is implemented in SAGA GIS on high-resolution orthophotos of the Gemmi rock glacier. In a) displacement vectors around a narrow shearing zone (dashed black line) where the velocities drop significantly towards a side lobe of the rock glacier. b) represents the comparison of photogrammetric derived horizontal velocities with the respective values measured by DGPS surveys between 2010 and 2014. In c) residuals of the multitemporal orthophotos in presumably stable terrain around the rock glacier are depicted.

PART III: RESULTS

6 Evolution and variability of mountain permafrost parameters

This chapter summarises the contribution of the research work of this thesis on the **temporal and spatial variability of thermal, kinematic and geophysical permafrost monitoring parameters** in the geographic region of the Swiss Alps. Temporal variations are jointly analysed with the spatial variability to address the diversity of permafrost landforms, the heterogeneous subsurface and topoclimatic characteristics. Furthermore, this allows the observed permafrost variability to be placed in the context of climate change.

6.1 Meteorological and snow data

In the Swiss Alps, **mean annual air temperatures** (MAAT) increased rapidly in the late 1980ies and remained at a higher level since then (Fig. 1.1). The strongest air temperature (AirT) increase occurred in spring and autumn (MeteoSwiss, 2014). As Fig. 6.1a illustrates for the period between 1995 and 2014, considerable inter-annual variations in MAAT anomalies (SD: ± 0.5 K) were observed, but the variability between different sites was small (SD: ± 0.1 K). The most distinct warming peak in AirT could be attributed to the period between June 2006 and May 2007, whereas the summer heat wave in 2003 had only limited influence on MAAT. No clear trend of increasing AirT can be found during the past 20 years, even though 17 of the 20 warmest years ever observed occurred in this period (MeteoSwiss, 2014). Focusing on the months June to September, the period when the atmosphere has the most direct influence on the ground temperature, the heat wave in 2003 was most distinct regarding cumulative AirT degree days as well as global radiation (Fig. 6.1d-e). The inter-annual variations of **incoming shortwave radiation** (ISR) showed a distinct pattern with maximum deviations of $\pm 15\%$ compared to the mean values (Fig. 6.1b). Generally, the temporal variations of ISR anomalies were larger (SD: ± 33 Wm⁻²) than the spatial variability between sites (SD: ± 16 Wm⁻²). However, ISR anomalies correlated only moderately with AirT anomalies (R^2 : 0.36) and in several periods there was no correlation at all between these two parameters (e.g. in 1995-1996 or 2007).

Regarding **snow depth**, large inter-annual differences are present, such as between the snow rich winters of 1994/1995 and 1998/1999 (“avalanche winter”) and the snow-poor winters of 1995/96, 2005-2007 or 2010/11 (Fig. 6.1c). A ratio of 1:2-5 to 1:3 could be found between maxima in a snow poor and snow rich years. The snow onset and disappearance also showed large temporal variability (Fig. 6.1b). The spatial variability of snow depth was at least twice as large as the inter-annual variations and corresponded to approximately 50 % of the mean snow depth for the IMIS stations analysed here. Maximum snow depths were usually much greater than 1 m, so they probably contributed to an effective thermal insulation of the ground for at least several weeks. However, this may not have been the case at other points of interest (Fig. 2.4 and Sect. 5.2).

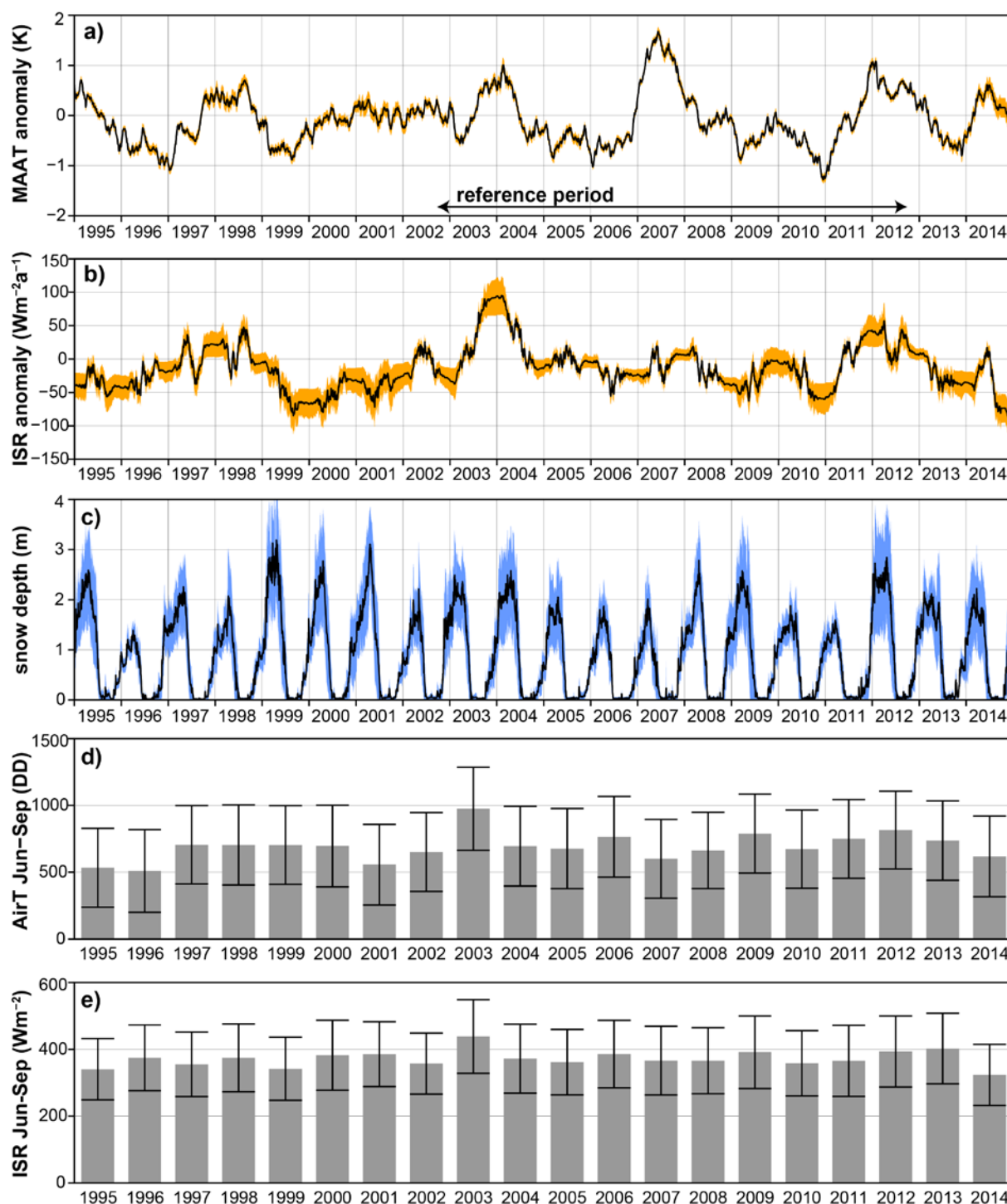


Fig. 6.1: Evolution of air temperature and snow depth from 1995 to 2014 at 33 permafrost monitoring sites from PERMOS and TEMPS (Fig. 3.1): a) mean annual air temperature (MAAT) anomalies relative to the reference period of the hydrological years 2002/03-2011/12 based on gridded air temperature data (TabsD, source: MeteoSwiss), in orange the standard deviation (SD) between monitoring sites; b) incoming shortwave radiation (ISR) approximated by potential incoming radiation and relative sunshine duration, the SD between sites is illustrated in orange; c) mean snow depth data from 8 IMIS snow stations with complete data sets (ATT-2, BED-2, CMA-2, GOR-2, MAE-2, PMA-2, TIT-2, WFJ-2, source: SLF), the SD between stations is indicated in blue; d) sum of air temperature degree days (DD) for the potentially snow-free months June – September, error bars represent spatial variability (SD); e) sum of the global radiation (Wm^{-2}) from June to September, error bars represent spatial variability (SD).

In the following sections the evolution and variability of ground thermal data is described to contribute to the understanding of the permafrost response to meteorological events (Chapter 1).

6.2 Temporal evolution and variations observed in ground temperature data

Due to the high impact of the snow cover on the surface energy balance, **the evolution of mean annual ground surface temperatures (MAGST) significantly differs from variations in MAAT**. This is visualized in Fig. 6.2a-b on the basis of the surface offset (SO, $MAGSTa - MAATa$). In periods with increasing SO, MAGSTa was warmer compared to MAATa, e.g. after early snow disappearance. Periods of decreasing SO traced back to late or very limited thermal insulation in winter and/or an early snow disappearance, respectively. The snow cover duration and its thermal insulation effect is visualized in Fig. 6.2c as running annual means of the snow thermal index $snow_1$ (Staub and Delaloye, 2016). From late 1999 to early 2003, MAATa remained close to zero (Fig. 6.1a) and variations in SO were almost exclusively due to variations in snow coverage. The temporal variability of MAGSTa and SO were in the order of ± 0.5 K, hence similar to the temporal variability of MAATa.

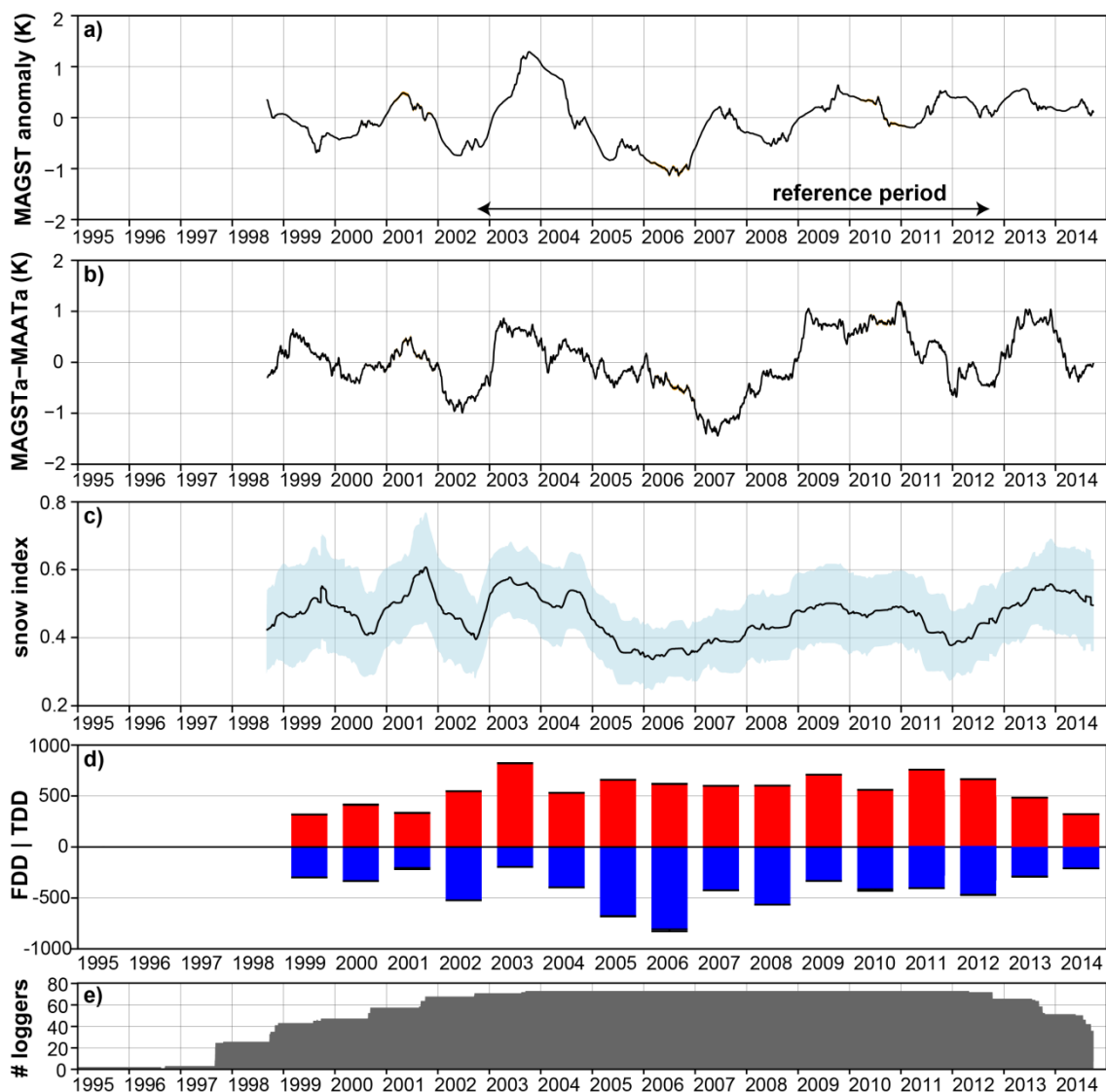


Fig. 6.2: Temporal evolution of GST aggregates and indices using the 73 GST loggers from 10 sites: a) mean annual ground surface temperature (MAGST) anomalies relative to the reference period of the hydrological years 2002/03 – 2011/12; b) mean surface offset ($MAGSTa - MAATa$); c) mean annual snow index ($snow_1$, Staub and Delaloye (2016)) and the standard deviation among the different loggers (blue area); d) mean freezing and thawing degree days per hydrological year (e.g. 2014 for Oct. 2013 – Sept. 2014); e) the quantity of available time series. Because the most complete GST time series have been used, the uncertainties of the gap-filled values (orange areas in a and b as well as the error bars at the ends of the bars in d) are not visible since they are very small.

On average, the Pearson correlation between MAGSTa and MAATa was weak (R^2 : 0.37). However, this was very **different for snow-free or snow-poor locations**. In steep rock walls, R^2 between daily mean GST and AirT were in the order of 0.8, and 0.6 between MAGSTa and MAATa, respectively. To characterise point-specific snow properties, the snow index $snow_1$ was used (Staub and Delaloye, 2016). For the GST loggers selected for Fig. 6.2, among which the great majority were placed in snow-rich locations, the correlation between MAGSTa and annual mean snow-index was higher (R^2) than between MAGSTa and MAATa. This implies that higher thermal insulation by snow tends to cause a relative ground warming.

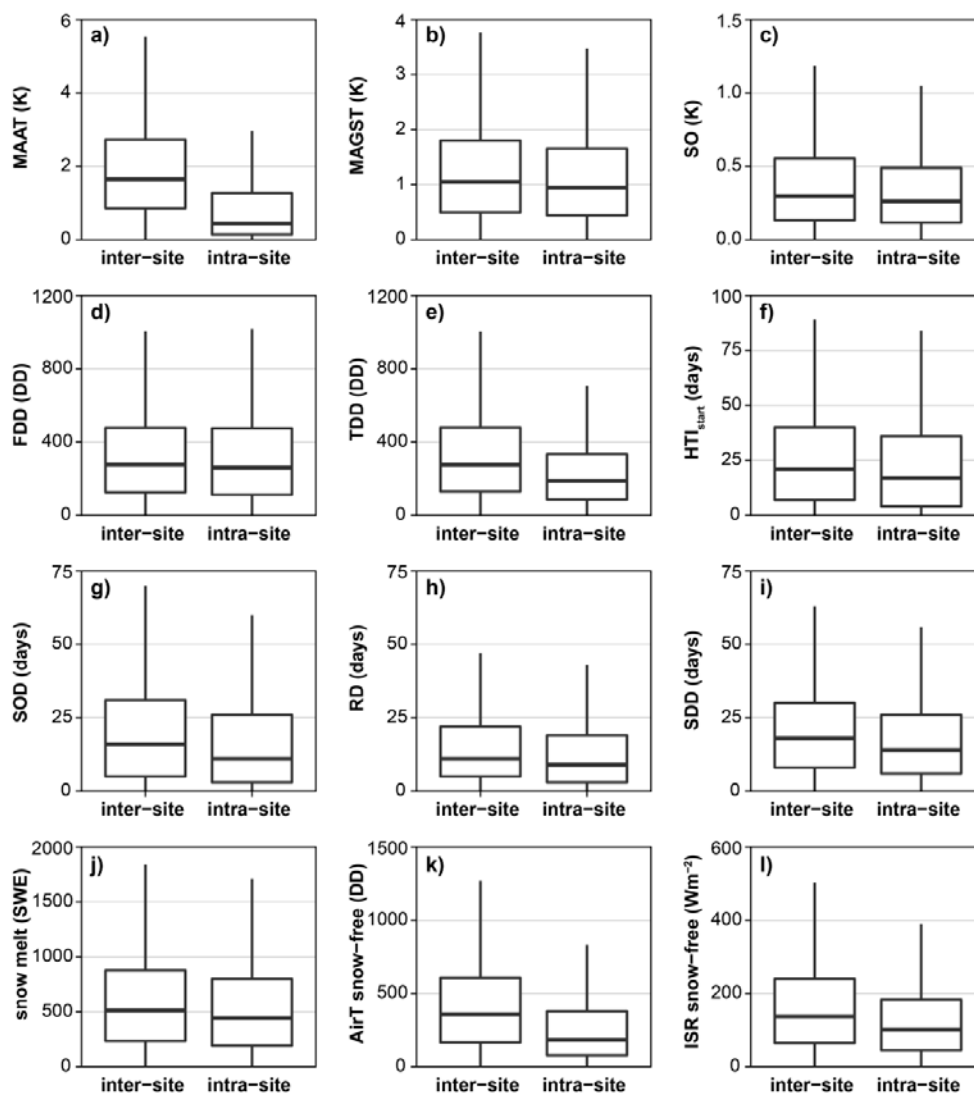


Fig. 6.3: The spatial variability of permafrost-relevant indices and aggregates based on 198 GST loggers and the hydrological years 2002/03–2012/13. Daily mean values were aggregated to hydrological years. The category “inter-site” represents differences in the respective values for all logger combinations between sites (n: 121’859, mean distance between loggers ~62 km), the spatial variability among different loggers located on the same site is illustrated in category “intra-site” (n: 11’366, mean distance: 487 m). Absolute differences of the following indices and aggregates are shown: a) mean annual air temperature (MAAT); b) mean annual GST (MAGST); c) mean surface offset (MAGST-MAAT); d) freezing degree-days (FDD); e) thawing degree-days (TDD); f) start of the high-insulation period by snow (HTI_{start}); g) snow onset date (SOD); h) snow ripening date (RD); i) snow disappearance date (SDD); j) cumulative snow melt rates during spring zero curtain (mm SWE); k) cumulative AirT degree-days during the snow-free period; l) shortwave incoming radiation (ISR) accumulated during the snow-free period. The snow characteristics (f-j) were defined using the indices $snow_1$ and melt as described in Staub and Delaloye (2016).

Freezing and thawing degree days (FDD and TDD in Fig. 6.2d) are also good proxies for assessing the thermal effects of snow. FDD were mainly influenced by the snow evolution throughout the winter season, particularly in early winter. TDD were dominated by the snow disappearance in summer and, additionally they were influenced by the weather conditions during the snow-free period (Fig. 7.7). Inter-annual variations of FDD (SD: ± 180) were larger compared than those of TDD (SD: ± 140). The spatial variability was larger than the temporal variability for the two indices (SD: ± 255 for FDD and ± 230 for TDD, respectively). The start of the highly insulated period (HTI_{start}) was temporally more variable than the snow disappearance date SDD (Fig. 7.1). More information on the temporal variability of the snow cover is provided in Sect. 7.1.

Fig. 6.3 illustrates the quantification of the **spatial variability of GST** aggregates and indices which characterise the point-specific surface energy balance. This analysis was based on entire hydrological years of 198 time series of different field sites that represent various topo-climatic conditions and subsurface properties. In general, these observations confirmed the expected high variability of ground surface properties (temperature, snow coverage) at small spatial scales i.e. on one landform (intra-site variability, some hundreds of meters). The inter-site variability of MAAT was larger than the respective intra-site variability because elevation differences were larger between sites than within one site (Fig. 6.3a). Overall, the intra-site variability was almost as large as the inter-site variability, especially for variables which are directly or indirectly affected by snow. This implies that over large distances, very similar ground thermal characteristics existed. However, due to the delayed and filtered response to temperature changes at the ground surface, ground temperatures (GT) could be assumed to be spatially less variable at greater depth than at the surface, at least within zones or layers of comparable thermal conductivity and ice and water content.

Looking at the **temporal evolution of permafrost temperatures at depth** based on borehole data, there are two main aspects to point out. First, GT showed distinct seasonal and inter-annual variations (Fig. 6.4). Second, most borehole thermistors showed an overall warming, especially before 1995 (only Murtèl-Corvatsch), between 2000 and 2004 and since 2009 (Fig. 6.5). Most GT time series reached their highest values at the end of the analysed period (2014). This can be explained by the higher temperatures at the ground surface since 2009, which have now reached layers below the ZAA. Distinct periods of decreasing GT occurred in the snow-poor winters between 2005 and 2007. Generally, inter-annual GT variations were particularly prominent at locations where GT was rather cold (i.e. below $-1\text{ }^{\circ}\text{C}$). If GT are very close to the melting point (e.g. at LAP, SBE or SCH), the potentially increasing fraction of water in the ground prevents GT from increasing by phase changes. But as can be seen in Fig. 6.4, particularly at the sites of warm permafrost, the GT minima in winter are also high.

The following section illustrates the temporal and spatial variability of rock glacier surface displacement rates, which relate to GT variations at the depth of the shear horizon. The relationship between ground temperature and the kinematic activity of rock glaciers is discussed in Sect. 7.3.

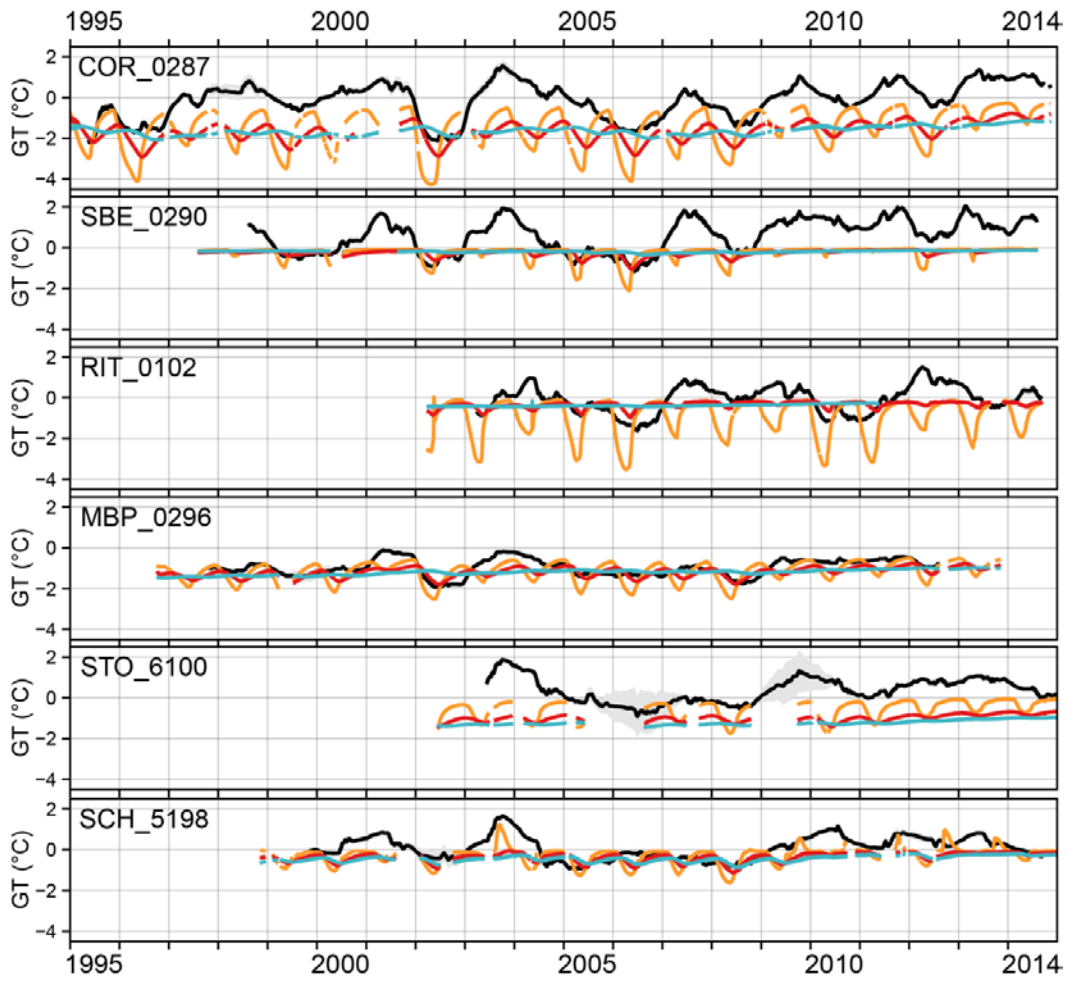


Fig. 6.4: Evolution of GT at seven selected PERMOS boreholes. COR_0287, SBE_0290 and RIT_0102 were drilled in rock glaciers, MBP_0296 in a talus slope, STO_6100 was drilled into a flat rock plateau and SCH_5198 on the north slope of a mountain peak. MAGST (black lines using the uppermost thermistor, estimated uncertainties due to gap filling in grey) is shown together with daily mean GT at ~5 m depth (orange), ~10 m (red) and ~15 m (blue).

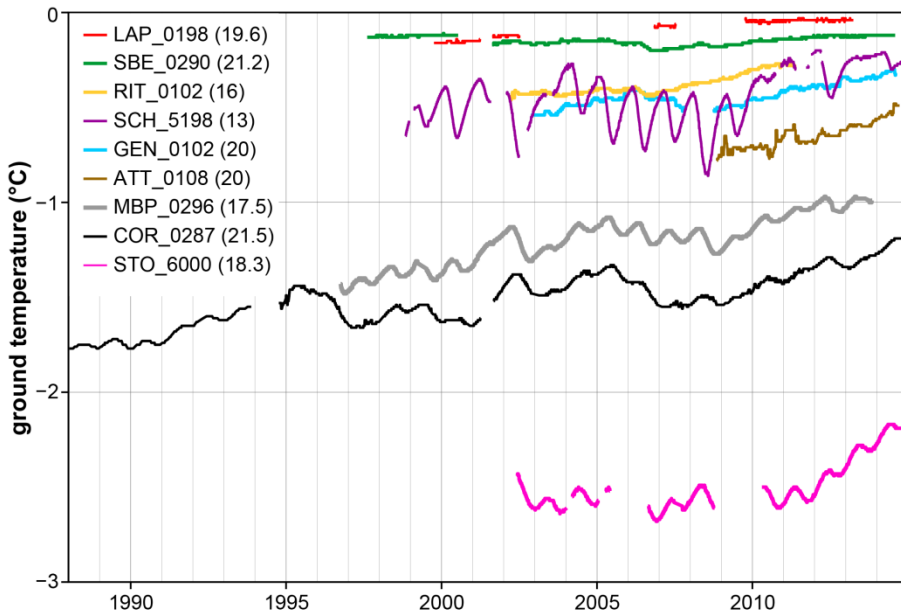


Fig. 6.5: Thermal evolution of GT around the zero annual amplitude (ZAA). Except for some very warm or humid sites (Lapieres, Schafberg, Schilthorn), several periods of clear GT increase are visible.

6.3 Evolution of rock glacier creep activity

The **strong increase of horizontal surface displacement rates of rock glaciers** is illustrated in Fig. 6.6 based on photogrammetric data for three rock glaciers at the Gemmi study site (Krummenacher et al., 1998, 2008; Staub et al., 2015b). In 2014, these rock glaciers moved up to 200 to 600 % faster than between 1990 and 1995 (overview map in Appendix A3). Although the range of absolute deformation rates was large, the velocity changes over time relative to a common reference period were similar for these three landforms. Two distinct peaks of high creep velocities could be identified: a first peak between 2000 and 2005 and a second peak between 2013 and 2014. For the three rock glaciers at the Gemmi site, the mean velocities between 2010 and 2014 clearly exceed those of the period 2000-2005.

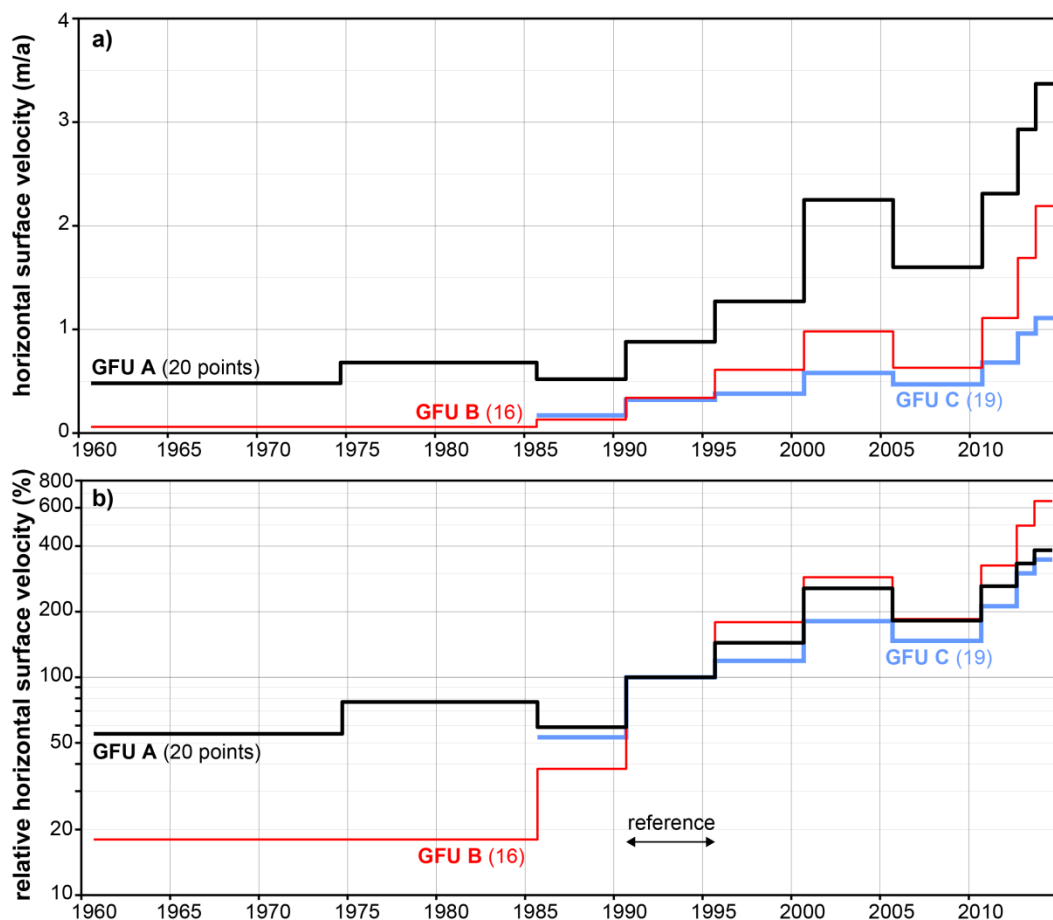


Fig. 6.6: Photogrammetric reconstruction of horizontal rock glacier creep velocities since 1960 exemplified by a photogrammetric reconstruction of three rock glaciers located at the Gemmi site: a) mean horizontal displacement rates (m a^{-1}); b) anomaly values relative to the period 1990-1995. In brackets the number of monitoring points is indicated. The data until 2000 was quantified by Krummenacher et al. (1998) and Mihajlovic et al. (2003).

The evolution of mean annual surface displacement rates was analysed based on geodetic data for a 13 rock glaciers. Although absolute displacement rates range from a few cm to several m per year (Fig. 6.7a), **large resemblances between relative inter-annual velocity changes emerged** (Fig. 6.7b). This indicates a similar kinematic reaction to common influencing effects, which are the subject of Sect. 7.3. In addition to the homogeneous pattern of relative velocity changes, some rock glaciers showed **distinct morphological changes** due to fast or uneven deformation. The common patterns

comprise a **first velocity maximum in 2004**, followed by a rapid **deceleration between 2005 and 2007**, and very high kinematic activity in recent years. For most of these rock glaciers, **surface velocities were greatest between 2013 and 2015**. Exceptions to this general pattern are the decelerating rock glacier AGE (2013/14 = 50-60 % of the velocity in 2003/04) as well as intermittent deceleration phenomena around 2010 at rock glaciers TMI, GGU and HUT.

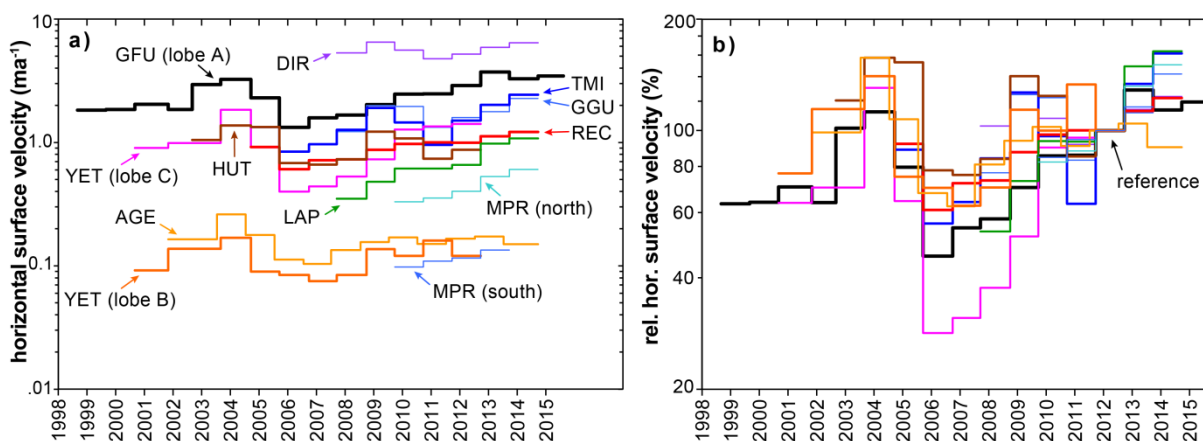


Fig. 6.7: Evolution of horizontal surface velocities of 13 different rock glaciers derived from geodetic data (annual measurements, data correction as described in Sect. 4.1.3). In a) the large range of mean annual surface velocities is shown from the slowly moving lobe B at YET to very rapidly moving rock glaciers such as Dirru (DIR), Gemmi (GFU), Tsarmine (TMI), Grosses Gufer (GGU). In b) relative deviations of the same data are shown compared to the reference period 2011/12 (= 100 %). Data source: PERMOS and University of Fribourg.

The **observed velocity variations fit well with the GT variations** shown in Fig. 6.5 (Sect. 7.3). However, despite the similarities, there was also considerable variability in rock glacier creep velocities, which demonstrates the complexity of the related thermo-hydro-mechanical processes. Site-specific conditions such as the geometry relative to the bedrock, subsurface properties like ice and water content or the size of the particles, the depth of the shear horizon as well as interactions with other landforms are potential influencing factors (Bollmann et al., 2015; Delaloye et al., 2005, 2010, 2013; Perruchoud and Delaloye, 2007; Roer et al., 2005, 2008). The effects of temperature and snow melt are discussed in Sect. 7.3.2.

6.4 Temporal and spatial variability of electrical resistivity

Electrical resistivity tomography (ERT) is very sensitive to water and temperature changes around the melting point and particularly suitable to monitor changes in warm and degrading mountain permafrost (Fig. 3.8b). Seasonal and inter-annual variations in **apparent electrical resistivity (ρ_a)** were analysed using data from a horizontal ERT-monitoring profile on the north flank of the Schilthorn, a unique time series of more than 300 data points originating from ERT surveys and automatic measurements made between 1999 and 2010 (Hilbich et al., 2011; PERMOS, 2013). Compared to inverted specific electrical resistivities, ρ_a values are particularly suitable for analysing changes in near-surface changes such as the infiltration of melt water because no inversion artefacts occur (Hilbich et al., 2009).

Fig. 6.8 shows the temporal evolution of ρ_a over the seasons for different calendar years. The first measurement in September 1999 corresponded to the highest ρ_a value obtained in autumn, whereas the measurements of the year 2010 showed the lowest ρ_a values for all seasons. This result is consistent with the observed general increase in GT (Sect. 6.2), even though the GT increase was limited for the Schilthorn measurement site due to the generally warm ground conditions and the high influence of phase changes (Fig. 6.4). Inter-annual variations in the subsurface temperature and water content were characterised by low ρ_a values after the 2003 heat wave which were followed by a distinct increase in ρ_a as a consequence of the cold winters between 2004 and 2007. Regarding the seasonal pattern, generally ρ_a reached a maximum before the snow melt period started and decreased during the entire thawing season. The initial decrease in ρ_a is linked to water infiltration resulting from snow melt, because 6-8 months of precipitation are discharged within 1-2 months. Progressive thaw of the active layer then increased the fraction of liquid water and led to decreasing ρ_a until the ground surface started to freeze again. The slope of rising ρ_a values in early winter can be used as a measure of the effectiveness of ground cooling. Finally, small seasonal amplitudes of ρ_a may indicate a reduced ability of the subsurface for the regeneration of ground ice, because a high subsurface water content diminishes ground freezing.

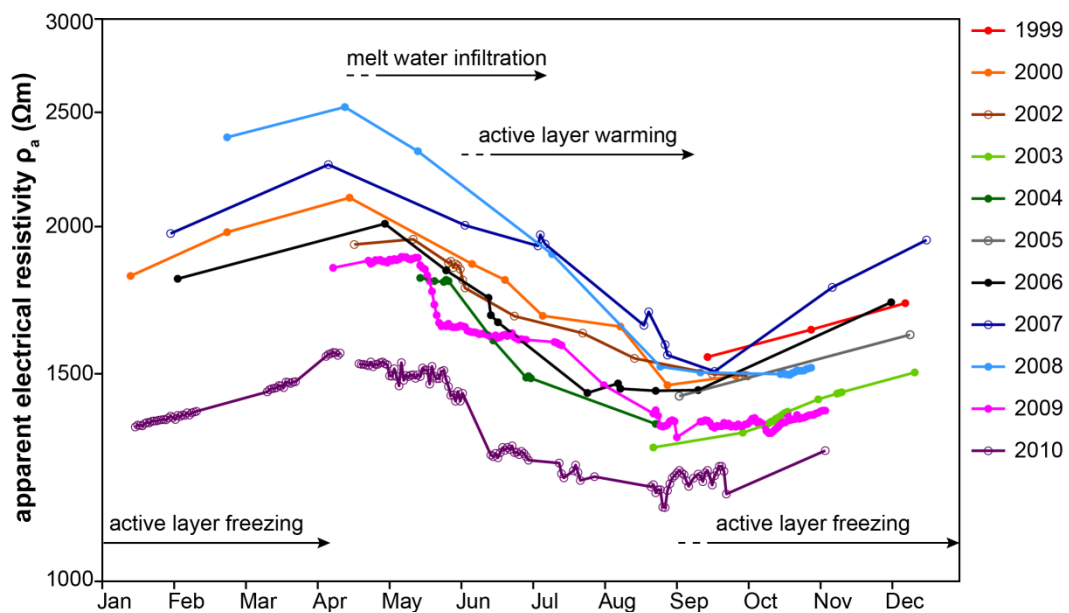


Fig. 6.8: The seasonal pattern of mean apparent electrical resistivity (ρ_a) measured at the Schilthorn between 1999 and 2010. The data of different years are plotted in differing colours. ρ_a maxima occurred before the snow melt and were followed by a distinct decrease in ρ_a during the thawing period due to water infiltration and ground warming in the course of the summer season. Minima occurred in autumn when the active layer reached its maximum thickness and before the ground surface started to freeze again. The inter-annual variations point to an increase in the liquid water fraction in 2003, a strong decrease during the cold winters between 2004 and 2007 (with particularly rapid ground cooling) and a second, continuing increase since summer 2008. Modified from Hilbich et al. (2011) and PERMOS (2013).

The same ρ_a time series was analysed in direct **comparison with GT data** from borehole SCH_5198 from the Schilthorn (at 7 m depth, the uppermost thermistor below the permafrost table). For the period of most complete ERT data between 2005 and 2010, the ρ_a values were linearly interpolated to daily resolution (Fig. 6.9a) and running annual means of GT (MAGT) and ρ_a (MAAR) were computed. Strong decreases in MAAR in 2009 and 2010 coincided with the start of the most recent

period of (ongoing) ground warming (Fig. 6.9). Although MAGT does not yet show positive temperatures at 7 m depth, averaged on a larger spatial area MAAR indicates ongoing permafrost degradation. Moreover, a strong negative correlation between MAGT and MAAR (R^2 : -0.89) was found for this time period. Hence, permafrost degradation appears to be detectable by ERT monitoring time series before GT records get positive.

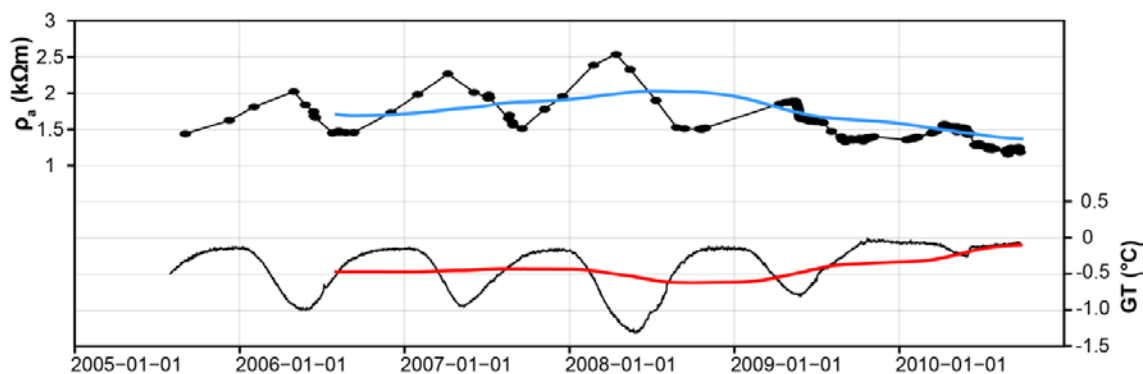


Fig. 6.9: Evolution of apparent electrical resistivities (ρ_a , upper part) in relation to ground temperatures (GT, lower part) at 7 m depth for the horizontal ERTM-profile at the Schilthorn site (Hilbich et al., 2011). Running annual mean values of ρ_a (MAAR, blue) and GT (MAGT, red) show an inverse evolution over time (R^2 : -0.89). Data source: Hilbich et al. (2011) and PERMOS (2013).

Geophysical data permits the **spatial variability of structural subsurface properties** to be investigated. This information cannot be derived from any other monitoring technique without disturbing the substrate. A general observation from ERT and RST surveys made in the frame of the TEMPS project on rock glaciers (Réchy, Tsavolires, Gemmi, Lac des Vaux, Dirru, Murtèl-Corvatsch), talus slopes (Lapires), moraines (Sanetsch) and highly fractured rock (Schilthorn), is that a high spatial variability of electrical resistivities and seismic velocities occurs at the scale of several tens to a few hundreds of meters. This variability can mainly be explained by structural differences between ground layers and it was most pronounced between the permafrost and the unfrozen zones above and below. Considerable lateral variability could also be observed, however, e.g. due to irregular melt water infiltration during periods of ground thawing (Hauck et al., 2015).

6.5 Spatial variability of permafrost-relevant topo-climatic parameters

Permafrost parameters were measured at a variety of field sites (Fig. 3.1), but the data obtained remain a snapshot of the domain of potential permafrost occurrence in the Swiss Alps. GIS techniques were applied to assess to what extent the PERMOS GST and GT monitoring sites are representative of the **spectra of topo-climatic conditions of the total area potentially affected by permafrost in Switzerland**. As a reference for the domain of potential permafrost occurrence, the APIM permafrost-index map from Boeckli et al. (2012b) was used. Within grid cells with an APIM-index ≥ 0.1 , the topo-climatic variables elevation, potential incoming shortwave radiation (PISR) and slope were sampled based on the DEM SwissAlti3D from Swisstopo at 25 m spatial resolution for more than 5.5 million points. Elevation was used as a proxy for AirT, PISR for the direct exposure to global radiation and slope for the accumulation and re-distribution of snow. These topo-climatic variables were sampled for the positions of all GST and borehole locations as well. The results

showed that the elevation range covered by the GST and GT data from PERMOS and TEMPS was similar to that of the APIM data set (Fig. 6.10). The distributions of the terrain slope of the GT and the GST locations were very similar, but steep slopes were underrepresented in the current monitoring setup in comparison with the APIM data. Although many sites were located in shady areas, the GST and GT locations received more solar radiation compared with the APIM data. The lack of locations with very little direct insolation situated on steep slopes in the current permafrost monitoring setup is explained by the difficult access to oversteepened mountain flanks, which makes the installation and maintenance of ground thermal monitoring very challenging.

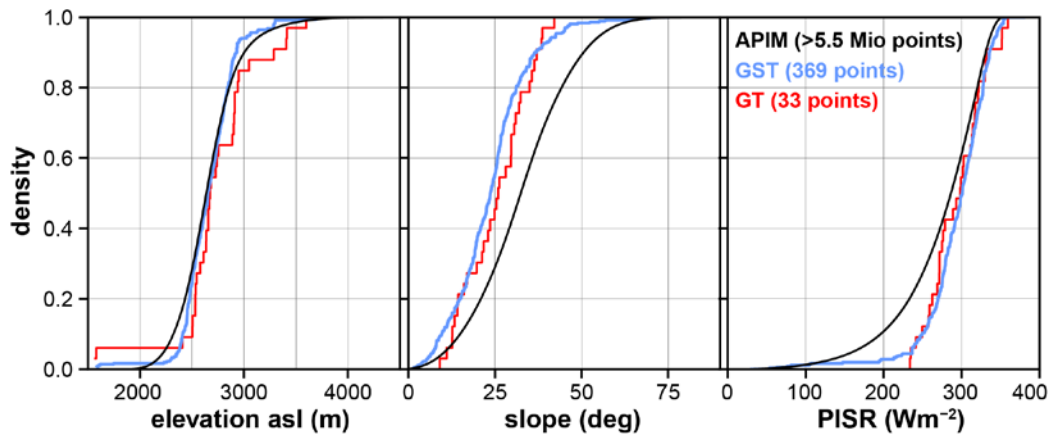


Fig. 6.10: The representativeness of GST and GT observations in relation to topo-climatic characteristics. The panels show the cumulative density function of elevation, slope and potential incoming shortwave radiation (PISR) sampled from the APIM data (black) for the 21st of June as well as for the positions of the PERMOS and TEMPS GST (blue) and GT (red) measurements. To approximate typical permafrost areas for comparison, the APIM data set (Boeckli et al., 2012a) was used (areas of APIM-indices ≥ 0.1).

6.6 Concluding remarks

The results regarding the evolution and variability of permafrost variables revealed **distinct changes, and inter-annual, as well as seasonal, variations in thermal, kinematic and structural parameters** (such as the subsurface ice or water content). GST did not show a clear warming trend during the observation period, whereas GT increased at the majority of the monitoring sites. The ground warming was the largest at boreholes with lower GT or in case of active layer thickening (lowering of the permafrost table, Fig. 2.6). If GT were close to the melting point, geophysical methods such as ERT monitoring proved to be useful because they indicated changes in the relative fraction of ground water before they were thermally detectable. Generally, **the permafrost observations highlighted the high spatial heterogeneity of the ground properties**. Overall, the small-scale variability of thermal and snow properties at a single monitoring site was almost as large as the variability at the regional scale between several sites. Snow and its effects on the ground surface energy balance (e.g. clearly negative FDD in case of reduced insulation) showed particularly great small-scale variability, whereas AirT and ISR were slightly less variable. Surface deformation rates of most rock glaciers were significantly faster between 2012 and 2015 than before 2000 and showed distinct inter-annual variations similar to those observed for the GST and GT time series.

Chapter 6: Evolution and variability of mountain permafrost parameters

The following Chapter focusses on meteorological events and aims at quantifying the relative importance of air temperature and snow cover on the thermal and kinematic permafrost response.

7 Thermal and kinematic response to meteorological events

Chapter 6 provided an overview on the temporal and spatial variability of various permafrost-relevant parameters. The **permafrost response to meteorological events** is assessed in this chapter. Therefore, characteristic meteorological events, i.e. weather conditions which showed a strong impact on the surface energy balance, are identified below. These characteristic meteorological events turned out to be mainly described by variations in air temperature and snow coverage. The thermal insulation effect was derived from the index snow_1 (Staub and Delaloye, 2016).

7.1 Important meteorological events between 2000 and 2015

Inter-annual variations in GST were homogeneous across a multitude of locations and field sites, even if they lie far apart (Fig. 7.1a). This implies that there exist regional or even Alpine-wide weather variations, here called “meteorological events”, which similarly influenced the energy balance at the ground surface. Such meteorological events can occur within the time frame of a few days (e.g. snow or rain events), weeks (e.g. summer heat wave or dry fall conditions) or several months (e.g. anomalies in AirT or ISR). The effect of such meteorological events on the ground thermal regime can be of very different intensity and persistence (Sect. 7.2). The most important meteorological events are displayed in Fig. 7.1 in combination with the ground thermal and kinematic response of the permafrost. The following description of the meteorological conditions is ordered chronologically and based on the results obtained in chapter 1. The focus is on the timing of the snow onset and disappearance because most study sites were at least partly influenced by snow. Further information on regional differences e.g. on the snow cover can be found in the official PERMOS reports (PERMOS, 2009, 2010, 2013; Vonder Mühll et al., 2001a, 2004, 2007).

The **hydrological year 2000/01** started with particularly early snow falls which rapidly caused a high thermal insulation of the ground surface. This early snow onset greatly limited ground freezing (Fig. 6.2d), especially in the southern and eastern part of Switzerland. Since the snow free period in 2001 was delayed and only little snow fell in November and December 2001 (Fig. 6.1c), the **hydrological year 2001/02** was characterised by an intense winter cooling which counterbalanced the effect of the winter 2000/01. Moreover, some summer snow events occurred in 2002. This resulted in a distinct decrease in MAGST anomalies (Fig. 6.2a) whereas MAAT anomalies remained around zero (Fig. 6.1a). The most intense ground cooling was observed in the Upper Engadine (Appendix A1) at the monitoring sites COR and MBP (Fig. 6.4). The **hydrological year 2002/03** started with an early snow onset with HTIstart 30-40 days earlier than usual (Fig. 7.1b). This led to the most limited ground cooling (warmest FDD) since the start of the measurements (Fig. 6.2d). The snow melt started early and was followed by the extreme heatwave of summer 2003 (Gruber, 2004; Schaer and Jendritzky, 2004). The TDD sum was the highest observed in the period 2000-2014 (Fig. 6.2d). Besides the early melt-out and the particularly warm AirT, the positive ISR anomaly is likely to have contributed to the high TDD values (Fig. 6.1). The superposition of warm winter conditions and intense and long-lasting summer thawing led to MAGST maxima in autumn 2003 (Fig. 6.2a). The GST maxima of 2003 were not surpassed at most locations until 2014.

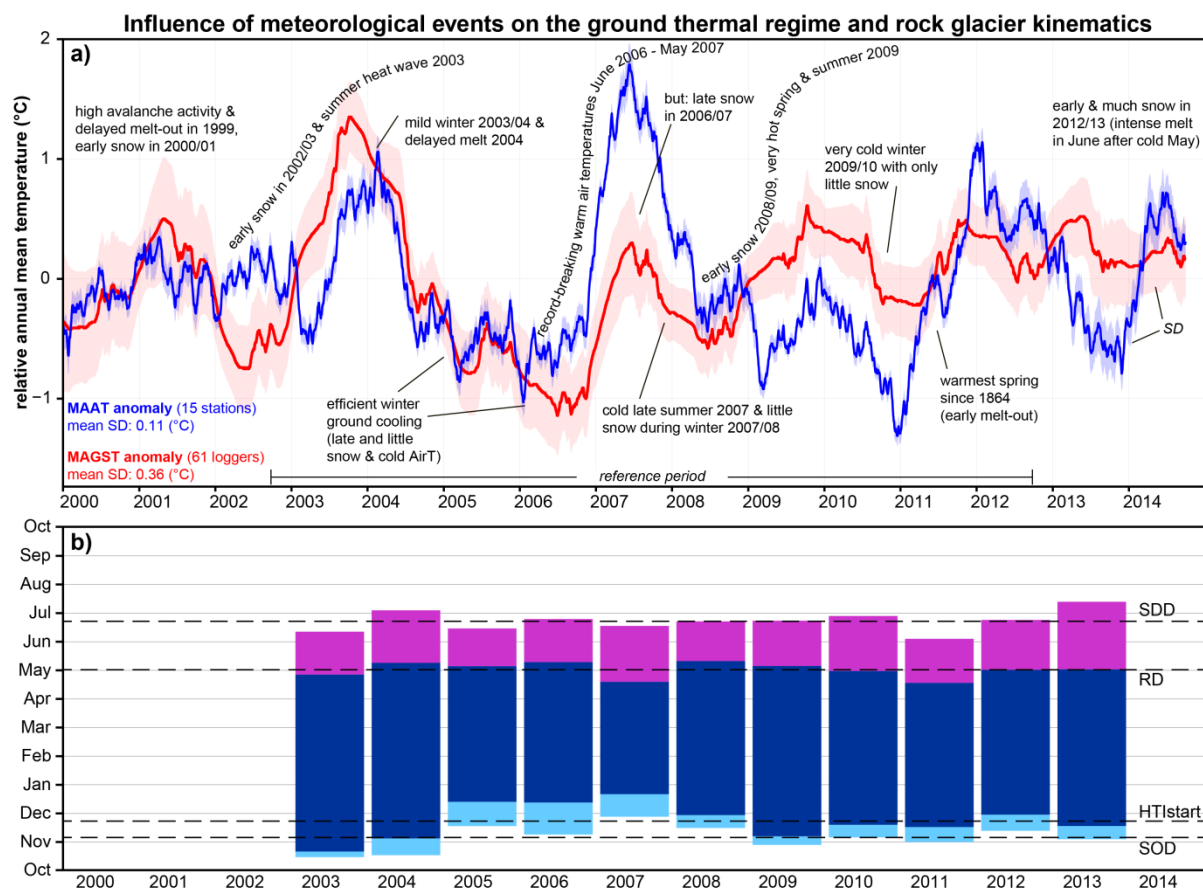


Fig. 7.1: The influence of meteorological events on the ground thermal regime: a) compares mean annual air (MAAT) and ground surface temperature anomalies (MAGST) and illustrates by a non-exhaustive number of meteorological events. In panel b), the timing of the snow onset (SOD), the start of the high insulation period (HTI_{start}), the basal ripening date at the start of the snow melt (RD) and the snow disappearance date (SDD) are shown for years with sufficient data (≥ 40 gap-less GST time series for which snow-indices could be calculated). The colours symbolize the different stages of snow thermal insulation: weak insulation (light blue), effective thermal insulation (dark blue), snow melt (purple).

Starting with warm ground thermal conditions, the **hydrological year 2003/04** was characterised by a mild winter with average snow depths but a very long snow covered period with an early snow onset and a delayed melt-out in summer 2004 (Fig. 7.1b). This caused a rapid reduction of MAGST anomalies during the second half of 2004, which continued until 2006 because of particularly snow-poor winters in the **hydrological years 2004/05 and 2005/06** (Fig. 6.2a). Due to the late start of the high thermal insulation period (HTI_{start}) and the relatively cold winter AirT (Fig. 6.1a and Fig. 7.1b), FDD of the winters 2004/05 and 2005/06 belong to the coldest ever measured (Fig. 6.2d). AirT were particularly cold between January and March 2005 and December 2005 and January 2006. Because of the strong cooling effect, which was detected even deep in the ground (Fig. 6.4), the early snow disappearance in June 2005 only had little influence on MAGST. However, exceptionally warm AirT between June 2006 and May 2007 (Fig. 6.1a, despite August 2006) introduced a trend reversal to increasing MAGST anomalies for the first half of the **hydrological year 2006/07** (Fig. 6.2a). Subsequent to this peak in MAAT anomalies, AirT was colder again between July 2007 and December 2007. Because snow depth remained shallow until February 2008, the heat accumulated within the active layer could continue to leave from the ground. As a result, FDD were slightly colder than the long-term average and caused a decrease in MAGST for the **hydrological year 2007/08**.

The **hydrological year 2008/09** can be seen as the start of the most recent and long-lasting period of almost continuous positive MAGST anomalies to date. The main causes for this ground warming were the early snow onset in October 2008, which led to the warmest FDD compared with the five preceding years, despite the very cold AirT in January 2009. The warm and dry spring initiated an intense and early snow melt (Fig. 7.1b) and with an above-average summer AirT, TDD were higher than in the preceding five years. Starting at a positive MAGST anomaly value, the **hydrological year 2009/10** brought intermediate cooling of the ground thermal regime and MAGST decreased towards the reference mean. The main causes were below-average snow depths which led to high FDD and average TDD in summer. Low AirT and little precipitation in September and October 2010 led to continued ground cooling during the first part of the **hydrological year 2010/11**. Moderate snow depths and the warmest spring since the first AirT records in 1864 with much less precipitation than usual, caused a timely start of the snow melt and the earliest snow disappearance of the time series (Fig. 7.1b). Even though July 2011 was cold and wet, TDD were higher than average. Autumn 2011 was particularly warm and in the northern Alps also very dry. A snow event in Mid-September caused an early onset of the snow cover at high elevation, but many monitoring sites became snow-free again in October. Because of greatly reduced precipitation until the end of 2011, FDD were colder in the **hydrological year 2011/12** compared to the preceding three years (Fig. 6.2d), although heavy snow falls occurred in the second half of the winter. Cold AirT in February 2012, which caused the freezing of lakes at low elevation, favoured intense ground cooling at the position of the GST measurements. As in 2011, spring 2012 was hot and dry, but the snow disappearance was close to the long-term average (Fig. 7.1b).

The **hydrological year 2012/13** started with early snow onset which limited ground cooling despite cold AirT from February to March. At some PERMOS monitoring sites, snow melt had already started in April, but heavy snow falls in May and cold AirT led to an extraordinarily thick snow cover in late spring. A heat wave in mid-June caused a very intense snow melt (Fig. 7.1b). The zero curtains derived from GST measurements were significantly longer compared to other years and the snow disappeared even later than in 2004. Overall, these conditions caused an increase in MAGST until spring 2013 followed by a MAGST decrease because of reduced TDD. However, MAGST anomalies remained positive afterwards because snow arrived early in the **hydrological year 2013/14**. Snow depths were greatest on southern slopes of the Alps but remained below-average until Christmas in other regions. 2014 was characterised by much precipitation during the summer months (mainly in the form of rain) and a significant decrease in global radiation (Fig. 6.1b). Although 2014 may be remembered by the general public as a year without any summer, AirT were oscillating around the reference mean (Fig. 6.1a).

The most recent development in the **hydrological year 2014/15** was characterised by below-average snow depths until the turn of the year followed by intense snow falls in the second half of the winter. AirT was warm in spring and the summer of 2015 was the second warmest ever measured after 2003. At the study site Gemmi in the northern Alps, several snow patches and cornices, which had lasted at least for three years in a row, completely disappeared by mid-August. Especially at snow-rich locations where the snow usually disappears only in July or August, early SDD can be expected

for 2015. Due to a significant lack in precipitation, ground conditions were very dry, especially in July. According to first observations from field work, GST were much warmer between June and August 2015 than during the 10 preceding years and similar to those measured in 2003.

7.2 Thermal response

The observation-based analysis of the permafrost response to meteorological events represented a challenging task, because various influencing effects were superimposed in the GST and GT measurements. Generally absolute **differences in MAGST cannot be explained by MAAT directly** as long as the surface energy balance is temporally modified by the snow cover (Fig. 7.2a). Changes in MAGST (Δ MAGST) showed a significant relation to MAAT anomalies (p-value < 0.05), but there are obviously other important influencing factors (Fig. 7.2d). Regarding the relationship of Δ MAGST to FDD and TDD anomalies, it was not clear whether the winter or the summer season had the stronger effect on MAGST changes (Fig. 7.2e-f). Overall, the most positive Δ MAGST occurred in the hydrological year 2002/03, where the warmest FDD and TDD ever measured were superimposed.

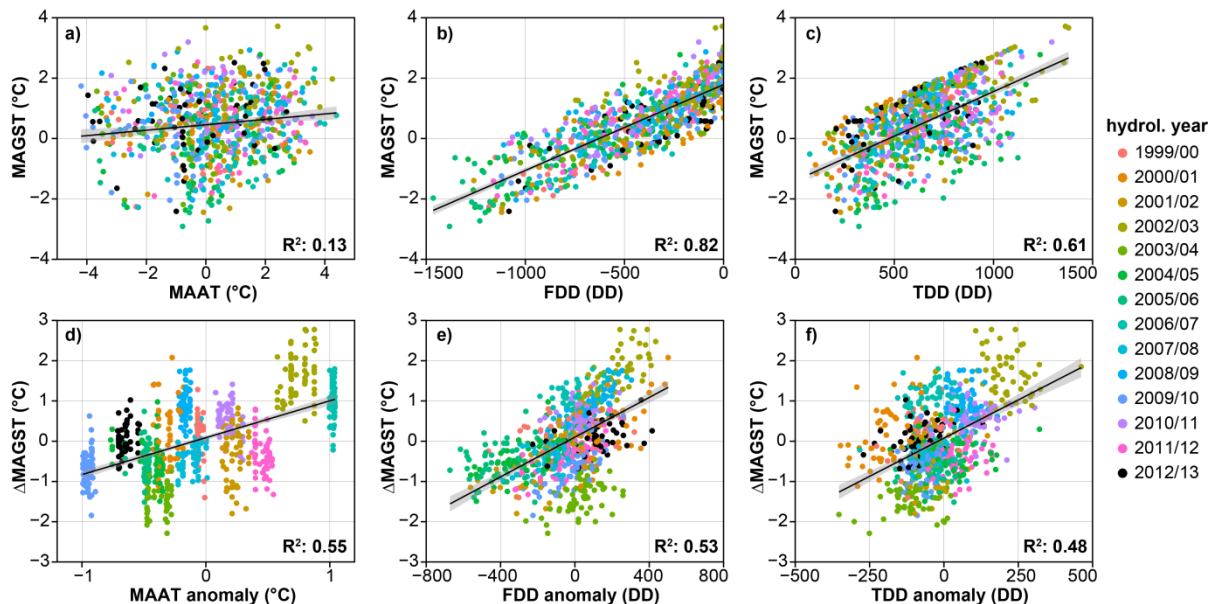


Fig. 7.2: Comparison of MAGST and MAGST changes (Δ MAGST) compared to MAAT, freezing (FDD) and thawing degree days (TDD) and respective anomaly values. Each point characterises data from one GST time series of one complete hydrological year (total: 62 loggers). The black line illustrates the linear regression through all data points, the grey area corresponds to the respective 95 % confidence interval. The hydrological years 2006/07-2010/11 were used as the reference period.

In the following, the thermal response of mountain permafrost to meteorological events is described in relation to the response time (time delay) and the persistence (effect duration) at the ground surface as well as in the subsurface. Second, the relative importance of AirT and snow variations for the ground thermal regime and the reversibility of inter-annual GST and GT variations are discussed.

7.2.1 Response time and persistence of meteorological events

Changes in the heat and energy exchange between the ground and the atmosphere affected directly **the ground surface**. The response time as well as the intensity of the ground thermal reaction depended on the timing of the meteorological event and its influence on the surface energy balance.

During the snow-free period, the reaction of GST to variations in AirT was almost immediate and the response time in the order of hours. Snow falls influenced the surface energy balance for several days, weeks or months.

At depth the thermal reaction diminished compared to the ground surface, but it potentially lasted longer. With increasing depth below the surface, the thermal effect of several days of extremely high AirT are delayed, similar to the propagation of the seasonal GST variations illustrated in Sect. 5.3. A precipitation event or intense snow melt can cause a rapid thermal response due to water infiltration, e.g. if the water refreezes in the ground or if it contributes to the thawing of the active layer during snow melt.

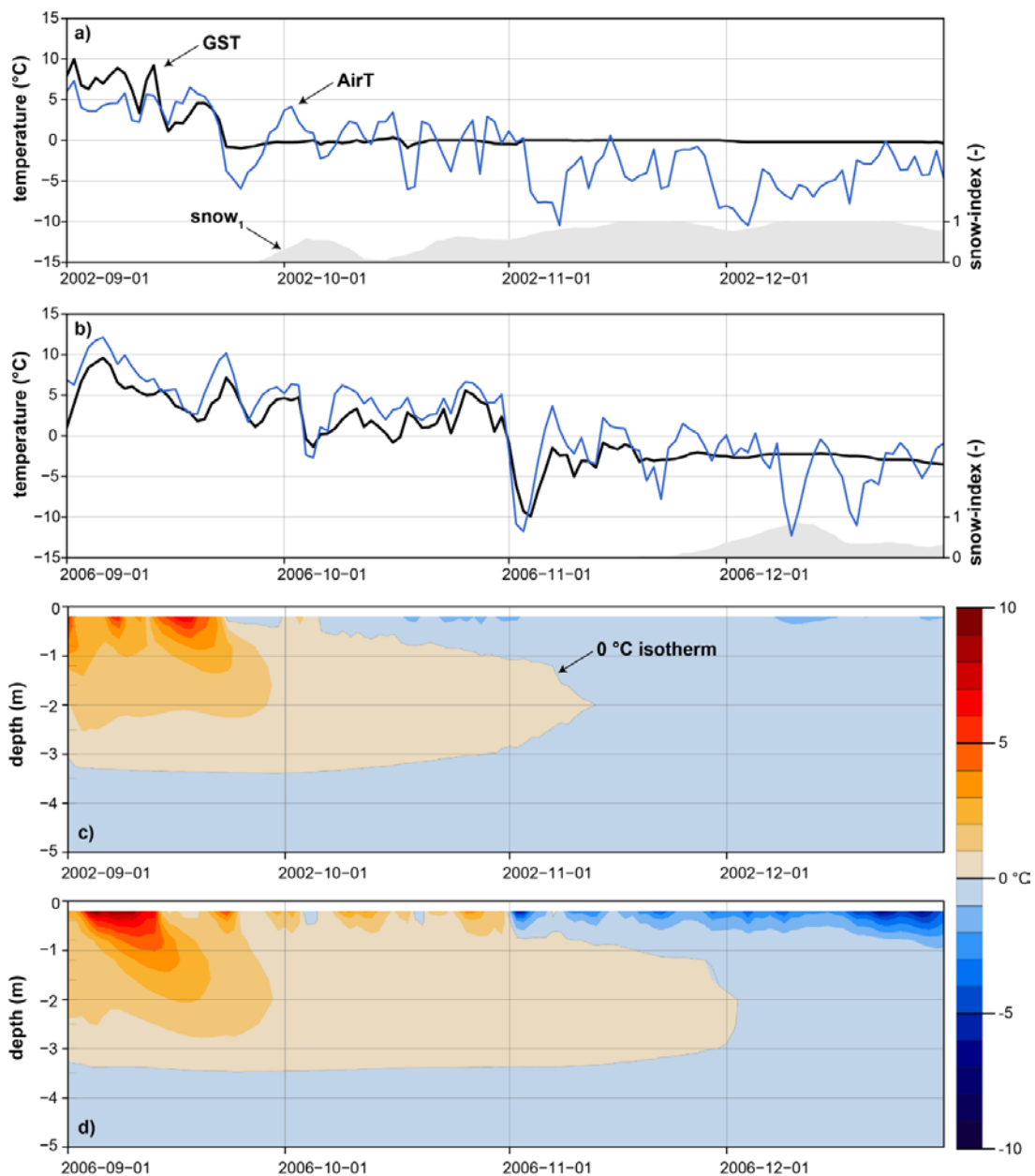


Fig. 7.3: The ground thermal response to early and late onset of the insulating snow cover. Panels a) and b) illustrate the thermal reaction of the ground surface at the example of logger GFU_S007 on the Gemmi rock glacier. Daily mean GST and AirT are shown in combination with the snow-index snow_i. In c) and d), the thermal reaction within the same time period is displayed for the uppermost 5 m of borehole STO_6100 at the Stockhorn. GT is indicated by a colour gradient.

The long-lasting ground thermal effect of snow events in autumn and early winter are illustrated in Fig. 7.3 for **the winters 2002 and 2006**, which differed greatly in relation to the prevailing snow conditions. As displayed in Fig. 7.3a and b, GST and AirT show high covariance as long the ground is snow free. The differences in the thermal insulation effect of the snow of these two years are characterised by the snow-index $snow_1$ Staub and Delaloye (2016). Although the summer 2006 was particularly warm (also between September and December mean AirT were ~ 2.5 °C warmer in 2006 than in 2002), the ground freezing was much more efficient in 2006. Due to the efficient winter cooling (Fig. 6.2d), the unusually warm AirT between June 2006 and June 2007 (Fig. 6.1b) did not cause a stronger ground warming. The response to the intense ground freezing in 2006 was rapid even at greater depth (Fig. 6.4).

In contrast to the delayed response of GT to thermal signals at the ground surface, the **infiltration of melt water can cause an immediate thermal and structural reaction at depth**. This is shown in Fig. 7.4 using data from borehole SCH_5198 from the Schilthorn in combination with the ERT monitoring data and the approximate snow melt rates derived from the closest GST logger SCH_S011. After an intense period of snow melt between the 21st and 26th of May 2009, infiltrating water caused an increase of the water saturation in the subsurface, although large parts of the melt water probably drained off on the slope. The 0 °C isotherm first arrived around the thermistors at 1.2 and 1.6 m depth and the thermistors above and below measured $GT \geq 0$ °C only with 2-8 weeks later (Fig. 7.4). The exact position of the 0 °C isotherm is subject to uncertainties due to limited accuracy and precision of the data. However, the increasing fraction of water at 1-1.5 m depth was detected simultaneously by GT and ERT data shortly after melt water infiltration at the ground surface. As shown for the seasonal and inter-annual scale in Fig. 6.9, the inverse relationship between GT and ρ_a can also be observed at the scale of days to weeks (Fig. 7.4a).

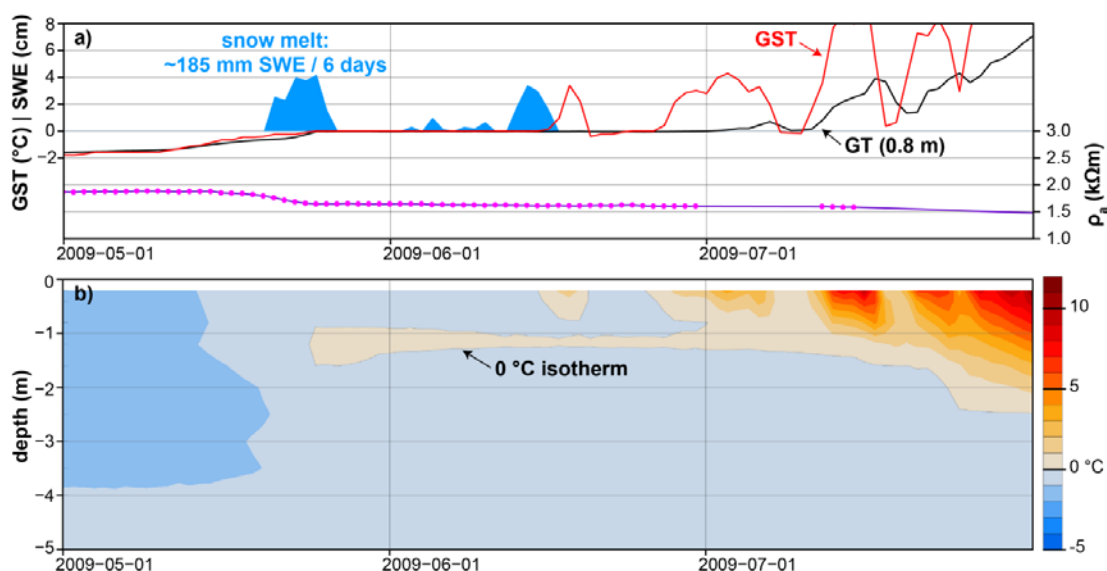


Fig. 7.4: Ground thermal effect of the snow melt illustrated with data from the Schilthorn monitoring site between May and July 2009: a) GST (red) and GT (black, 0.8 m depth), snow melt-index (blue area, SWE), apparent electrical resistivity ρ_a (purple dots, data source: Hilbich et al. (2011) and PERMOS (2013)); b) contour plot of the Borehole SCH_5198 for the uppermost 5 m. An intense snow melt between the 21st and 26th of May caused a rapid increase in the moisture content, which can be seen in the rapid decrease in apparent resistivity and the positive GT around 1.2 m depth. Later in July, intermediate periods of cold GST limited the ground warming.

The response time of GT at depth to GST variations has been analysed for all boreholes of the PERMOS-TEMPS data base as described in Sect. 5.3. The results are displayed in Fig. 7.5. The majority of boreholes showed an **almost linearly increasing thermal delay with increasing depth**, at least in parts of the profile. On average, the time delay at 10 m was in the order of 4-5 months, and at 20 m depth, 10-11 months. Deviations from this linear relationship point to non-conductive heat transport, phase changes or differing thermal conductivity at the boundary of layers, e.g. at the permafrost table or the permafrost base. Moreover, site-specific effects such as the circulation of air or water in the substrate could possibly explain decreasing time lags at depth.

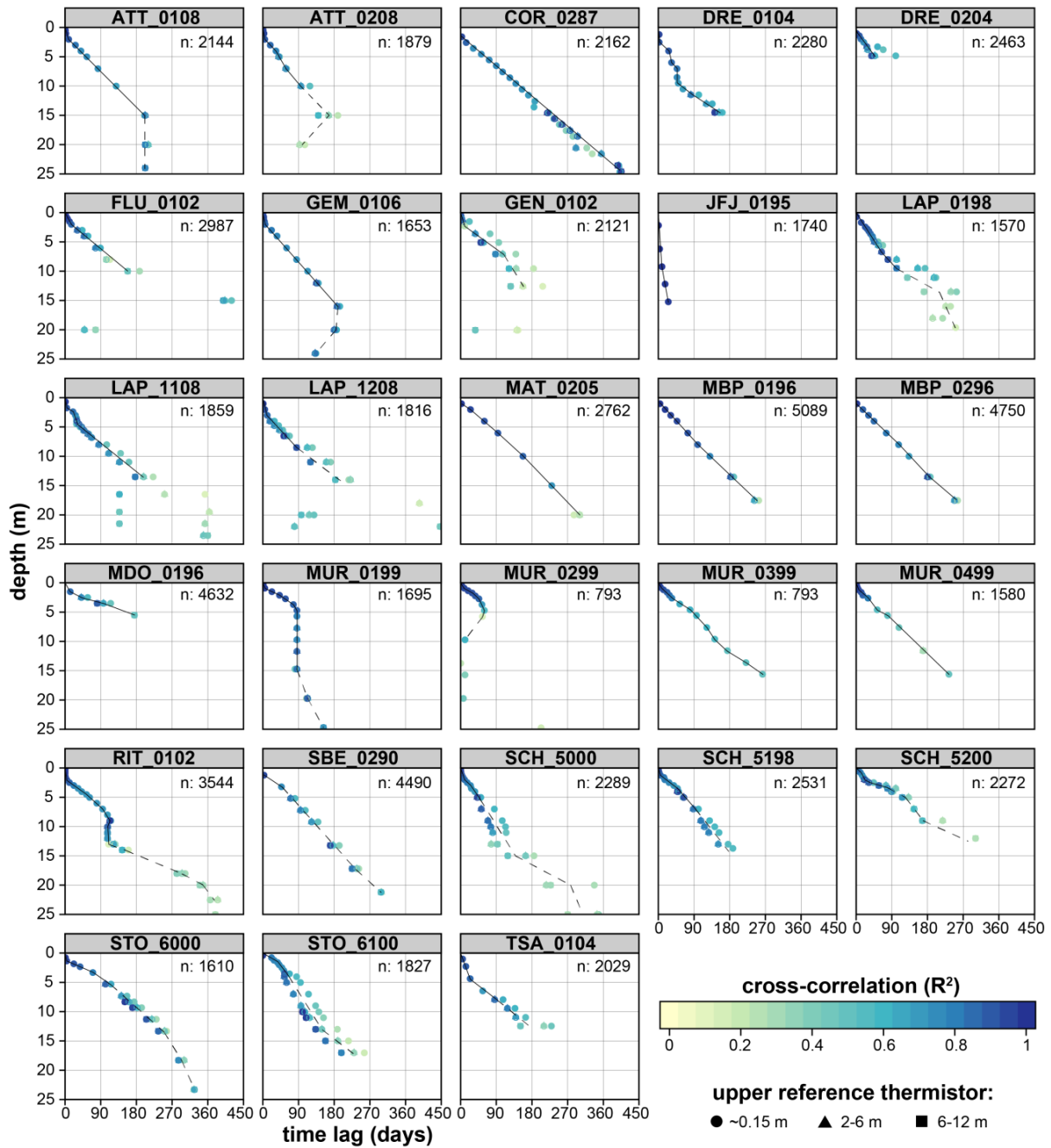


Fig. 7.5: Thermal delay of GT compared to the uppermost reference thermistor (0-0.5 m, 0.15 m on average) for all PERMOS/TEMPS boreholes (for meta data see Appendix A4). The analysis is based on the longest continuous period with data (number of days indicated in the upper right corner of each panel) and the method is described in Sect. 5.3. To reach greater depth, the time lag analysis was done in three steps using the uppermost as well as two other reference thermistors between 2-12 m with $R^2 \geq 0.6$, indicated with different shapes. The black lines illustrate generalized depth-time lag profiles.

Overall, the thermal response was delayed at depth compared to the ground surface, except during the infiltration of melt-water which may have led to rapid thermal and structural disturbance. The persistence of meteorological events tended to increase with increasing depth. Therefore and because of the transient memory of colder times contained in GT, GT records showed a clear temperature increase since the start of the measurements, whereas GST data mainly indicated strong seasonal and inter-annual variations as well as a long-lasting positive temperature anomaly since 2009. Snow was particularly important for the evolution of GST because it influenced the surface energy balance for several months in a row. The relative importance of snow and AirT for the ground thermal regime is discussed in the following section.

7.2.2 Relative importance of air temperature and snow on the surface energy balance

The relative importance of AirT and snow for inter-annual variations in the ground thermal regime over mountain permafrost is a long and still ongoing debate (Sect. 2.2.2). The description of important meteorological events in Sect. 7.1 provided several examples where either the snow conditions or summer AirT or both caused a particular ground thermal reaction. The GST data was used in combination with the snow-index snw_1 presented in Staub and Delaloye (2016) to assess the thermal effect of the snow on GST.

As illustrated in Fig. 7.6, **variations in FDD were clearly related to the timing of the snow onset whereas variations in AirT have a minor effect on the ground freezing.** Higher mean snow-indices as an indicator for higher or longer thermal insulation by the snow cover, correlate with warmer FDD values. This relationship is statistically significant at the significance-level of 95 % (p -values < 0.05). Moreover, variations in AirT were apparently not the cause for early or late snow onset, as the weak covariance with AirT anomalies from October to December shows (Fig. 7.6d-f).

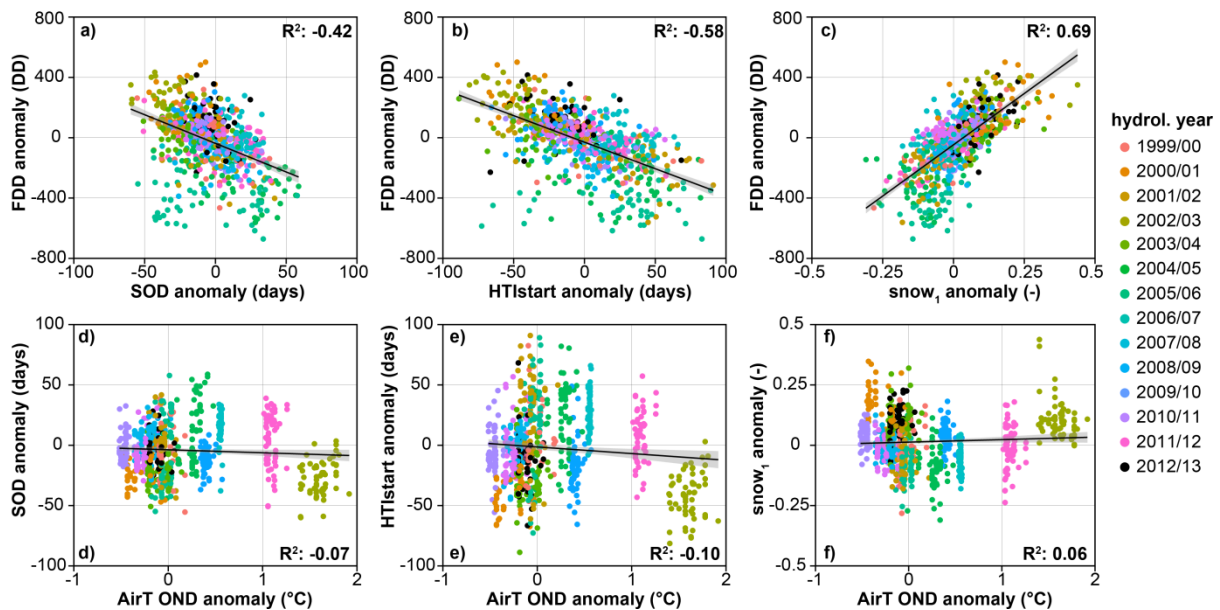


Fig. 7.6: The influence of the snow onset on the ground freezing. FDD anomalies are significantly correlated with a) the snow onset date (SOD), b) the start of the high-insulation period (HTI_{start}), and c) the mean snow-indices (here: snow₁). On the other hand, varying snow characteristics cannot be explained by AirT anomalies from October-December (AirT OND) as the panels d-f illustrate (p -values > 0.05). The plots are based on the same time series as shown in Fig. 7.2.

Concerning the **thawing season**, a clear relation was present between the timing of the snow melt (Fig. 7.7a) as well as AirT (Fig. 7.7d) and ISR (Fig. 7.7f) during the snow-free period. Again, TDD variations could not be explained by variations in AirT (Fig. 7.7c) or ISR alone (Fig. 7.7e). Below-average quantities of melt water (derived from the melt-index, Sect. 5.2) showed a weak negative correlation with TDD (Fig. 7.7b). No significant relationship between HTI_{start} and SDD could be found. Hence, snow in early winter seems to have a very limited influence on the snow disappearance date. Probably, precipitation in late winter as well as AirT between April and September are the most important factors which cause inter-annual TDD variations. Therefore, the superposition of early SDD and warm AirT during the snow-free period caused particularly high TDD values, such as in 2003.

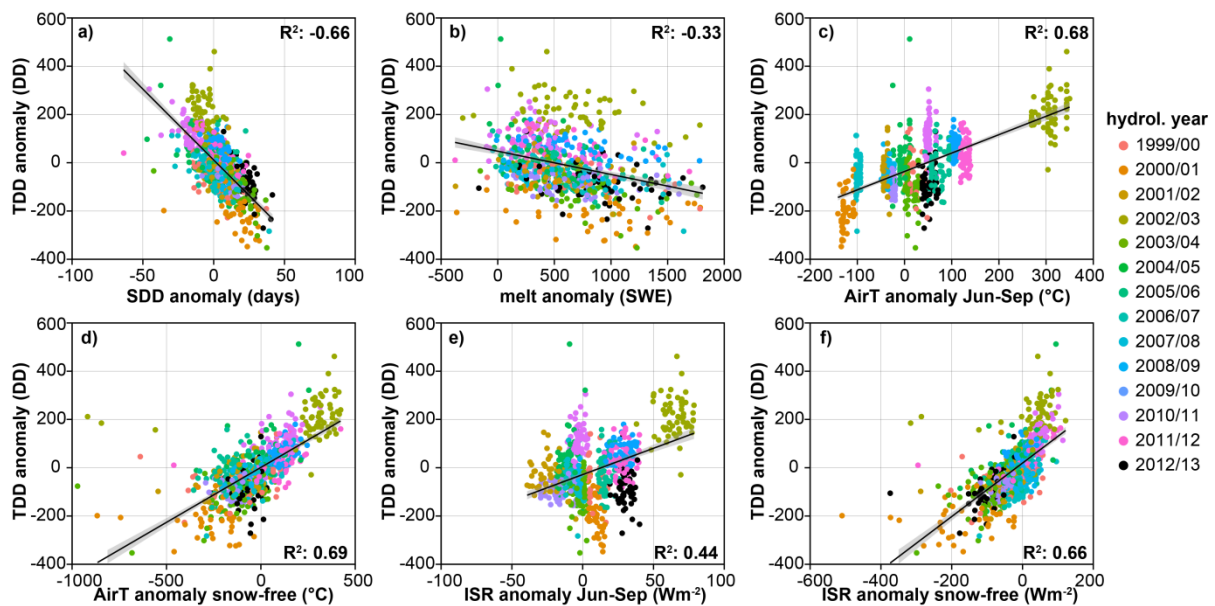


Fig. 7.7: The influence of the snow disappearance date (SDD), AirT and ISR on ground thawing, represented as TDD anomalies. TDD anomalies are significantly (p -values < 0.05) correlated with a) SDD; b) the snow melt anomalies (approximated SWE using the melt-index); c) the sum of daily mean AirT between June and September; d) the sum of daily mean AirT during the entire snow-free period; e) the global radiation sum between June and September; and f) the global radiation sum during the entire snow-free period. The plots are based on the same time series as Fig. 7.2.

7.2.3 Reversibility of GST and GT in function of the snow thermal insulation

The analysis of GST indices revealed that the ground surface is mainly influenced by the atmosphere and the snow cover. Meteorological events caused a rapid and strong thermal reaction in seasonal and inter-annual GST variations. In contrast to the subsurface, structural changes at depth like the deepening of the active layer or the increase of the liquid water fraction did not affect GST. Also in periods of warm AirT, particularly strong ground cooling could still occur with favourable snow conditions, i.e. a late snow onset. This implies that the **temperature at the ground surface is reversible**. However, the **reversibility of the subsurface** to regenerate cold ground conditions after positive temperature anomalies **greatly depends on the thermal evolution at the ground surface**.

As illustrated in Fig. 7.3 and discussed in Sect. 7.2.2, the active layer freezeback proved to be strongly influenced by the snow conditions in early winter, and so it varied from year to year. Additionally, locations which are less influenced by snow, e.g. due to exposure to wind or a rough surface, remained thermally less insulated.

The spatial variability of ground cooling and ground warming in relation to of the snow thermal index $snow_1$ was analysed by means of cumulative degree days (CDD, Fig. 5.1f) and using numerous GST time series. Fig. 7.8 illustrates the seasonal CDD evolution separately for each hydrological year and with a colour gradient which represents the $snow_1$ values. With numbers, the mean CDD difference between December and April as well as between June and September are indicated together with the SD of the spatial differences.

In contrast to ground freezing, ground **thawing was more homogeneous at all locations**, as shown by the slope of the CDD curves in Fig. 7.8. Exceptions might be due to remaining snow in summer, e.g. after massive snow accumulation by avalanches (coloured straight lines in Fig. 7.8). Winters with more snow (dark violet colours) were characterised by much warmer CDD in late winter and a reduced spatial variability, e.g. in 2000/01 or 2002/03. Because the ground warming in spring started at a less negative CDD values, large CDD values at the end of the hydrological year were more likely. In contrast, in winters with late or little snow (grey and light-blue colours) ground freezing was much less homogeneous at different locations. At the coldest locations, the ground freezing was several times more intense compared to the warmest winters. This implies that **snow conditions are dominant for the ground freezing**, particularly in the first half of the winter. Moreover, intense ground cooling is favoured on terrain which require more snow to be thermally insulated by snow such as coarse-blocky or very rough surfaces.

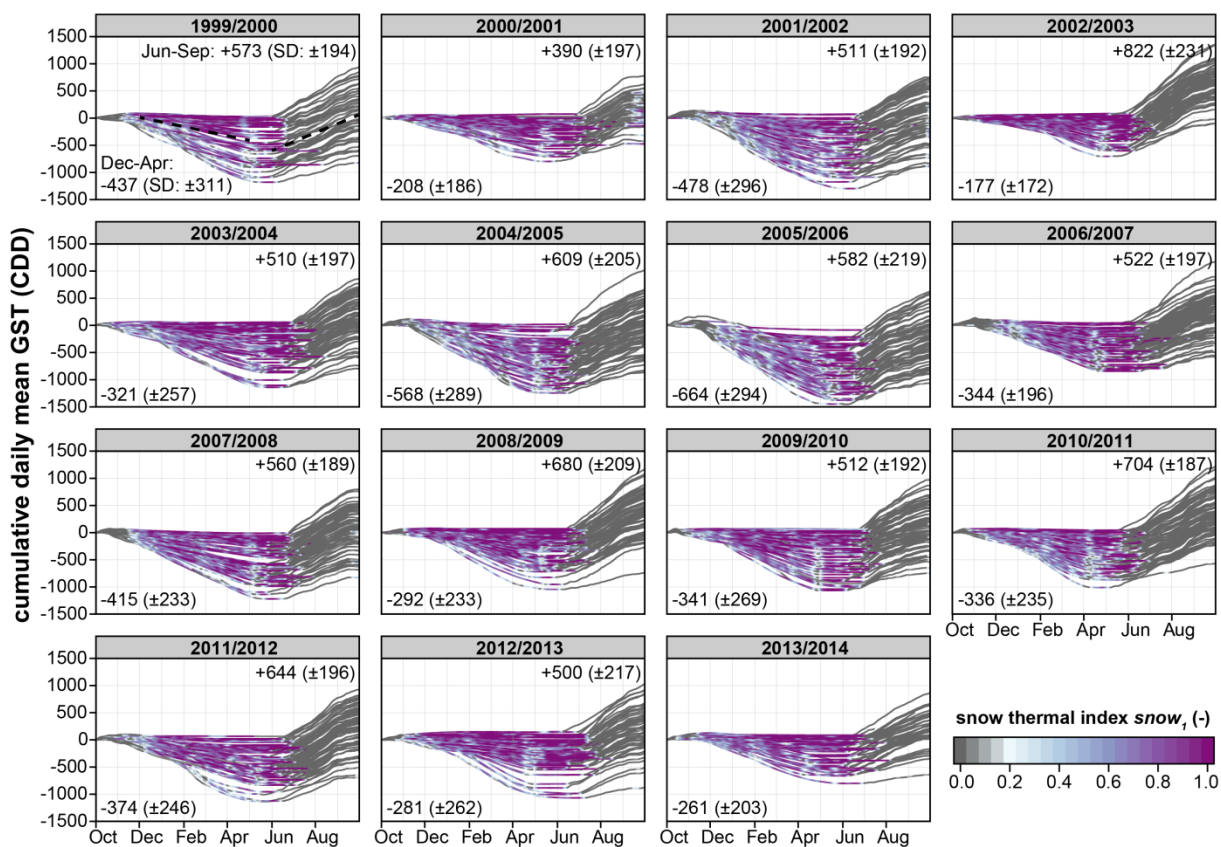


Fig. 7.8: Cumulative GST degree days (CDD) for the same selection of loggers as shown in Fig. 7.2 and separated by hydrological year, starting on October 1st. The colour gradient illustrates the thermal insulation by snow, derived from the GST data based on the index $snow_1$ (Staub and Delaloye, 2016). The numbers in the lower left corner show the mean FDD between December 1 and April 30 with standard deviations in brackets, whereas the numbers in the upper right corner indicate the TDD between June 1 and September 30. Because of data gaps, no TDD values are given for 2014.

The observed GT evolution showed that **after winters of intense ground surface cooling GT can cool efficiently to great depths**. This behaviour is documented for very ice-rich and cold permafrost (e.g. borehole COR_0287 from rock glacier Murtèl-Corvatsch) as well as for the Schilthorn, where the permafrost is close to 0 °C and the subsurface ice content is comparatively low (Fig. 6.5).

The kinematic response of rock glaciers in relation to GT variations and other influencing factors is analysed in the following section.

7.3 Kinematic response

The kinematic activity of rock glaciers can be used as a proxy for the permafrost response to climate change (Sorg et al., 2015). Conversely, GT or GST variations can explain varying surface displacement rates over short-term. Section 7.3.1 illustrates the thermal relationship with examples from several rock glaciers. In section 7.3.2 the relative importance of GT variations and other influencing factors on rock glacier kinematics, such as the infiltration of melt water, is discussed.

7.3.1 Inter-annual variations of rock glacier velocities in reaction to GT variations

The patterns of measured GT variations (Fig. 6.5) and inter-annual rock glacier creep velocities (Fig. 6.7) were very similar. By analogies to the flow of glaciers and the data on the internal deformation of selected rock glaciers (Arenson et al., 2002; Duval et al., 2010; Wagner, 1992), **permafrost creep velocities can be assumed to increase exponentially with warming GT**. Yet, this thermo-mechanical relationship was not provable with standard permafrost monitoring data. Because borehole data does not exist for the rock glaciers of interest, GT variations needed to be approximated first by means of the method described in Sect. 5.5.

The examples illustrated in Fig. 5.7d-f using borehole data from rock glaciers Murtèl-Corvatsch and Schafberg showed that **relative changes in GT can be approximated by GST time series (GT_{synt})**. Therefore, this technique was applied to assess the relationship between variations in (horizontal) rock glacier surface displacement rates and GT_{synt} . Instead of measured GT data, surface velocities relative to the reference period (2010-2012) and the exponential function Eq. 5 (Sect. 2.3) which describes the thermo-mechanical relationship were used to calibrate the optimal time lag and filter window according to Eq. 11. In this process, the filter windows were restricted to 0-36 months and the time lags to 0-24 months, respectively. Finally, the optimal solution in which the creep velocities were most accurately reproduced was chosen (minimum RMSE between estimated and observed creep velocities). The results of this analysis are shown below.

As Fig. 7.9 illustrates, the relationship between creep velocities and MAGST anomalies was weak. But with longer filter windows and by adding a time delay of some months for the simulation of GT_{synt} , clear exponential relationships could be found. Overall, a good starting point to approximate GT_{synt} at the position of the shear horizon(s) were **2-year mean GST with a time delay of 6 months**. However, the examples in Fig. 7.9 also demonstrate that the thermo-mechanical relationship may differ among rock glaciers or zones on these rock glaciers. 37 of the 169 points analysed showed an almost perfect exponential relation with $R^2 \geq 0.99$ (~22 % of all GPS points from the sites REC and LAP). Some scatter

remained in the majority of the situations which needs further investigation. Only very few GPS points show a weak thermal response with $R^2 \leq 0.5$ (~1 %). However, one has to keep in mind that exclusively points in the most active central zones of the rock glaciers were used. These central zones on rock glaciers moved more regularly and were less influenced by other effects.

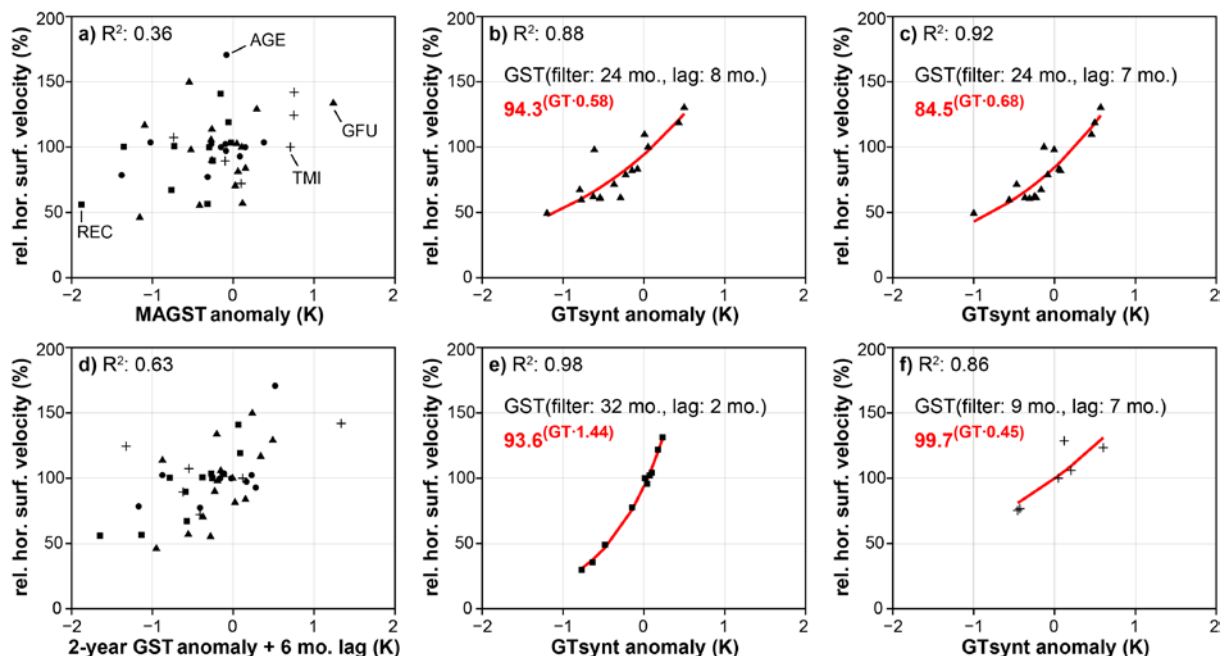


Fig. 7.9: Relationship between GST and GT_{synt} anomalies (K) and changes in the horizontal surface velocity (%) relative to the reference period 2010-2012: a) comparison with MAGST anomalies for the sites AGE (points), GFU (triangles), REC (squares) and TMI (crosses); GPS-point GFU_416 with b) the closest GST thermistor GFU_S004, and c) with another GST thermistor from the rooting zone of the rock glacier; d) same data as in a) but using a 2-year filter window for GST with an additional time lag of 6 months; e) GPS-point REC_346 with the closest GST thermistor REC_S003; f) GPS-point TMI_045 with the closest GST thermistor TMI_S017. Synthetic GT are approximated by GST using the filter windows and time lags indicated in the figures, and the red lines illustrate the corresponding exponential thermo-mechanical relationship.

The obtained **spectra of filter windows and time lags** from which optimal GT_{synt} could be derived are shown in Fig. 7.10. The mean filter window was 23 months and time lags of 5-8 months in most cases matched best with the observed surface displacement rates. Usually, long filter windows were in combination with short time lags and vice versa (Fig. 7.10c-d), which means that in both situations GST anomalies of the prior 1.5-3 years corresponded best with the creep velocity variations. The Becs de Bosson rock glacier at the Réchy site (REC) showed best agreement using filter windows of about 32 months and time lags of 3-6 months. For the rock glaciers at Tsarmine (TMI) and Aget (AGE), which differ a lot from each other in terms of absolute velocity (Fig. 6.7a), much shorter filter windows of only 6-10 months and very distinct time lags of 6-11 months were found.

Theoretically, the filter windows and time lags could provide information on the **position of the shear horizon(s)**, especially for those GPS points which show a very strong covariance between velocity variations and GT_{synt} (e.g. Fig. 7.9e). Of course, the time lags and filter windows are also influenced by the heat transport processes within the subsurface, which are very difficult to assess without borehole or other ground-truthing data (Sect. 5.3 and 5.4). Other factors which influence the movement behaviour in the short term, such as the snow melt, or changes over the long term, such as the movement of the rock glacier into zones of different terrain slope, also have to be considered.

Due to the high covariance (mean R^2 : 0.91) and the small residuals (mean RMSE: 11.4 % of the reference velocities) between estimated and observed velocity variations, **the kinematic activity of rock glaciers seems mainly to depend on the ground thermal regime.** This implies that **GT variations were successfully approximated by GST time series**, although the optimal parameters for Eq. 11 in Sect. 5.5 differ from rock glacier to rock glacier.

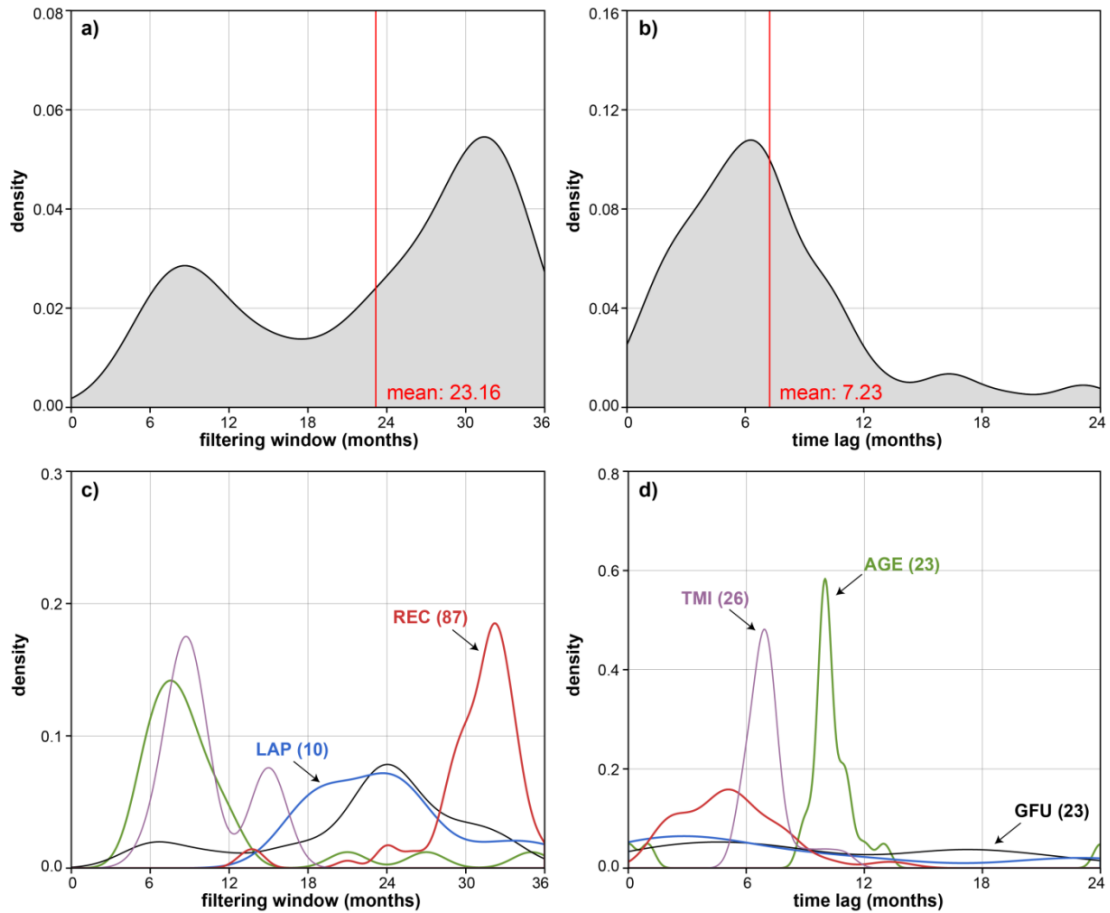


Fig. 7.10: Density distribution of filter windows and time lags of GT_{synt} for five rock glaciers. Only the optimal solutions are shown, in which GT_{synt} correlated best with the creep velocity variations: a) and b) display the results for all rock glaciers and c) and d) show the density distributions for each rock glacier separately. In brackets, the number of GPS points used for the calculation is indicated.

Regarding the obtained parameters for Eq. 5 (Sect. 2.3), a homogeneous pattern can be observed for the factor a , the base of the exponential function. Since relative changes in surface velocities were used, these values are centred closely to 100 %, which corresponds to the respective mean horizontal velocity during the reference period 2010-2012. The exponent b , which is multiplied by GT_{synt} , shows a larger spectrum and differs from site to site. This finding indicates a differing kinematic response to variations in GT_{synt} . The optimal values for the parameters a and b of all GPS points are illustrated in Fig. 7.11.

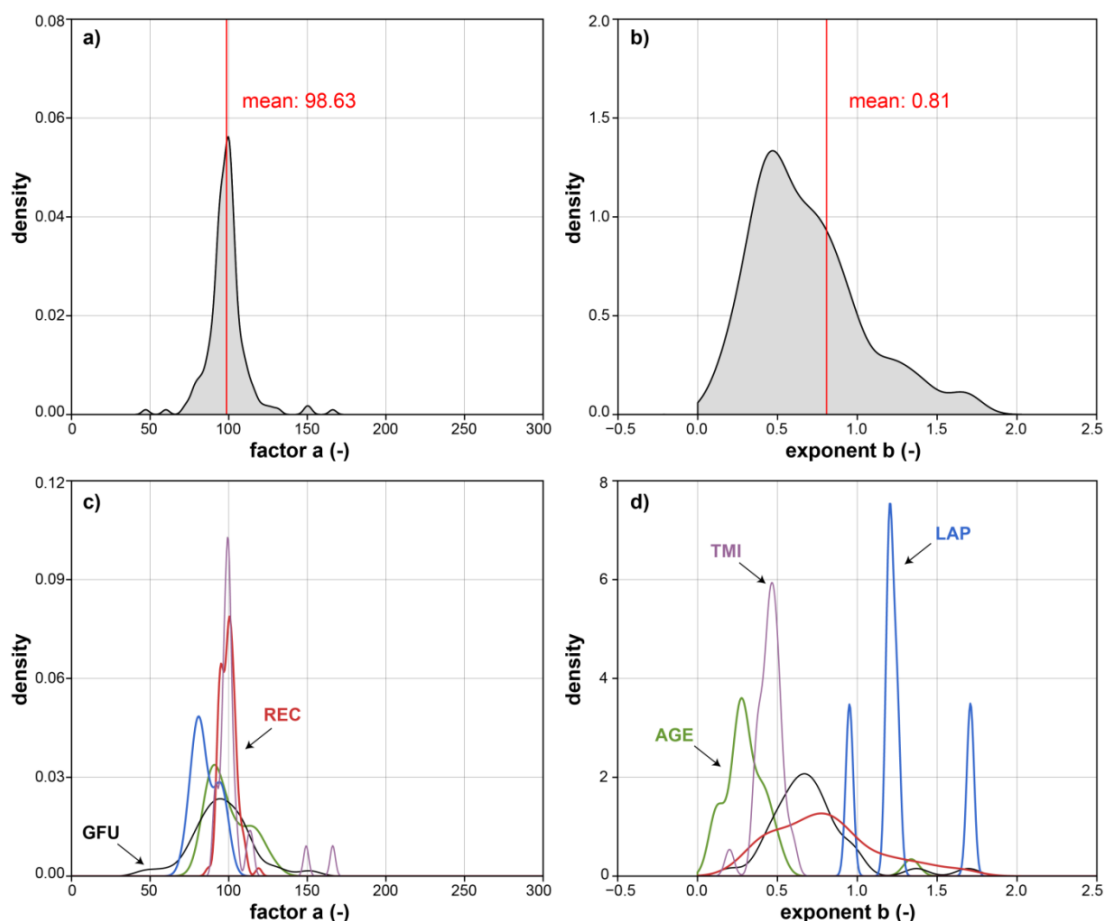


Fig. 7.11: Parameters obtained for the exponential function $v = a \cdot e^{b \cdot GT_{syn}}$ describing the thermo-mechanical movement behaviour of rock glaciers. In a) and c), the base parameter a is shown (density), in b) and d) the results of the temperature-dependant exponent b are plotted.

Generally, **high values for b indicate a stronger kinematic reactivity to temperature changes**. The GPS points from the LAP site were particularly reactive to temperature changes, especially for short time lags and filter windows. Also the rock glaciers at GFU and REC tended to high values for b. As illustrated with lines of similar slope in Fig. 7.12, the **obtained temperature-velocity relationships were very similar among the different GPS points, but differed among the rock glaciers**. The few GPS points for which the slope strongly differed from the site-mean value were located in particular zones on the longitudinal profile. For example, the black lines in Fig. 7.12 with the steepest slope correspond to the GPS points on the Gemmi rock glacier close to the rooting zone. The rooting zone of this rock glacier reacted with a particularly pronounced velocity increase to the recent ground warming, possibly because of a dilatation towards the very rapid zone downslope.

The kinematic reaction of rock glaciers to GT variations seems not to depend on absolute velocities. Hence, currently moderately-moving rock glaciers may react as strongly to future ground warming as fast-moving rock glaciers. The analysis of the influence of infiltrating water, which could influence the creep behaviour as well, is the topic of the following section.

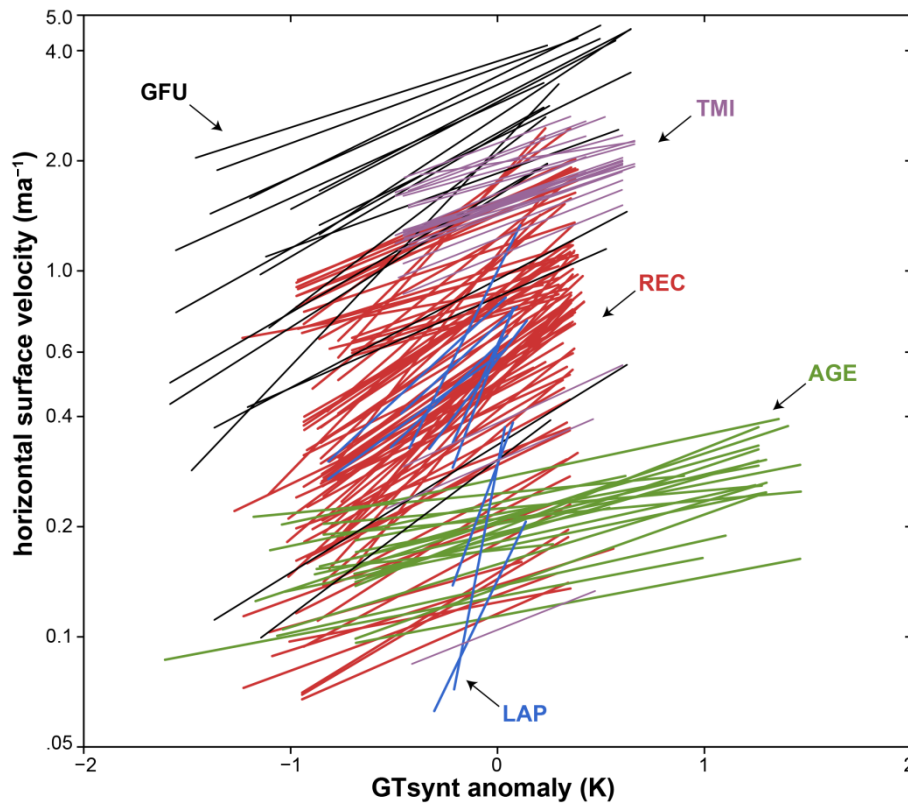


Fig. 7.12: Comparison of the temperature-velocity relationship between GT_{synt} anomalies (relative to the reference period 2010-2012) and estimated horizontal surface velocities (ma^{-1}) for all GPS points of the 5 rock glaciers investigated. Each line shows the best exponential fit of Eq. 5 (Sect. 2.3). For better readability, the y-scale is logarithmic.

7.3.2 Relative importance of ground temperature and melt water infiltration

To assess the relative importance of GT variations and a potential accelerating effect due to snow melt, the residuals between observed velocity changes and the fitted exponential curve were analysed. The standard deviation (SD) of these residuals was in the order of $\pm 10\text{-}15\%$, about 3-4 times lower than the SD of the creep velocity variations over time ($\sim 40\%$). In other words, **the remaining, unexplained variations were small.**

The inter-annual pattern of the velocity residuals on different rock glaciers is shown in Fig. 7.13a. The pattern was compared with inter-annual variations of the snow melt, i.e. the SWE sum approximated by the melt-index described in Staub and Delaloye (2016). No general trends are apparent for the velocity residuals of the entire rock glaciers. However, for some specific landforms or zones, an increasing or decreasing trend was found. Long-term trends at the decadal scale could possibly be due to changes in the rock glacier geometry, or they are the reaction to specific events, such as surcharge by the accumulation of rockslide deposits in the rooting zone of the rock glacier, which occurred several years or decades earlier (Delaloye et al., 2013).

The **infiltration of melt water could cause an acceleration of rock glacier creep velocities** by a hydro-thermal and a hydro-mechanical effect. The **hydro-thermal effect** on rock glacier movement was illustrated with GT and ERT data (Fig. 7.4). As a **hydro-mechanical effect** of infiltrating melt water could decrease the shear strength in layers which contain fine material (Sect. 2.3). Positive pore water pressure due to accumulating water in pockets or at impermeable layers could

temporarily contribute to the driving forces of the downslope permafrost creep. However, the occurrence of positive pore water pressure and potential floating of entire lobes is highly spectacular.

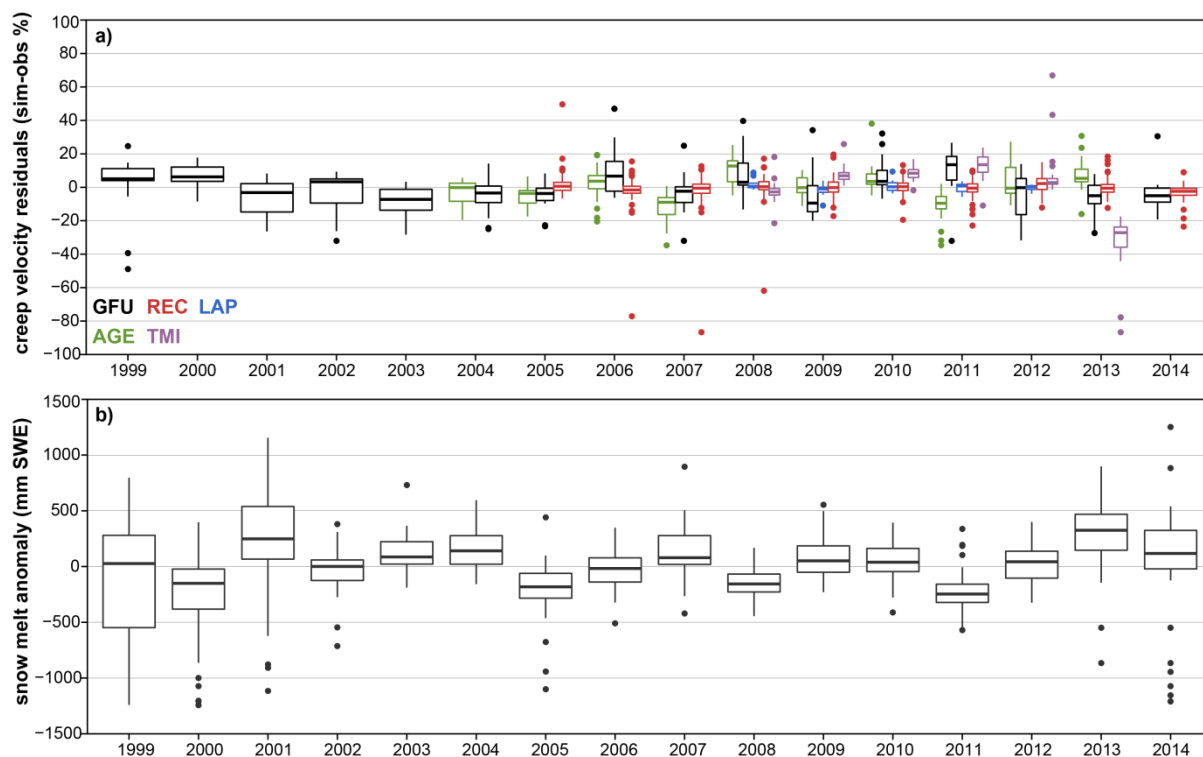


Fig. 7.13: Inter-annual variations of a) the rock glacier creep velocity residuals (exponential thermal model – observations) and b) snow melt anomalies (mm SWE relative to the period 2003-2012) of five rock glaciers. In a), values below 0 mean that the observed creep velocities were faster than the simulated velocities by a thermal model (Sect. 7.3.1).

The **creep velocity residuals** and the **snow melt anomalies** in Fig. 7.13 show an inverse pattern through time. In years with negative velocity residuals (faster observed creep velocities than the simulation by GT_{synt}) the snow melt anomalies were generally higher than on average, e.g. in 2001, 2003, 2004, 2007 and 2013. In other words, the snow melt could have contributed to faster displacement rates. However, the differences among the rock glaciers were large and the variations of the short kinematic time series of Tsarmine (TMI) and Lapires (LAP) should not be overemphasised. More information is required to judge whether the negative creep velocity residuals for TMI in 2013 were caused by the accelerating effects of melt water infiltration. The high-frequency time series from permanent GPS devices as well as the unique bi-monthly kinematic data from the REC site were used to gain a more detailed picture on the question of a potential influence of melt water infiltration on rock glacier kinematics.

A distinct seasonal pattern of the creep velocities was observed at the Becs de Bosson rock glacier at the REC monitoring site with minimum velocities before the snow melt started (Fig. 7.14). Moreover, **a rapid velocity increase in early summer** took place during the snow melt period. The annual velocity peaks occurred in the second half of the year, most likely because of the time delay of GT variations at depth (Fig. 7.5). Data from permanent GPS devices show acceleration during snow melt

in the course of some weeks (Fig. 7.14). This first seasonal velocity peak was usually followed by a phase of deceleration until a second peak followed around October.

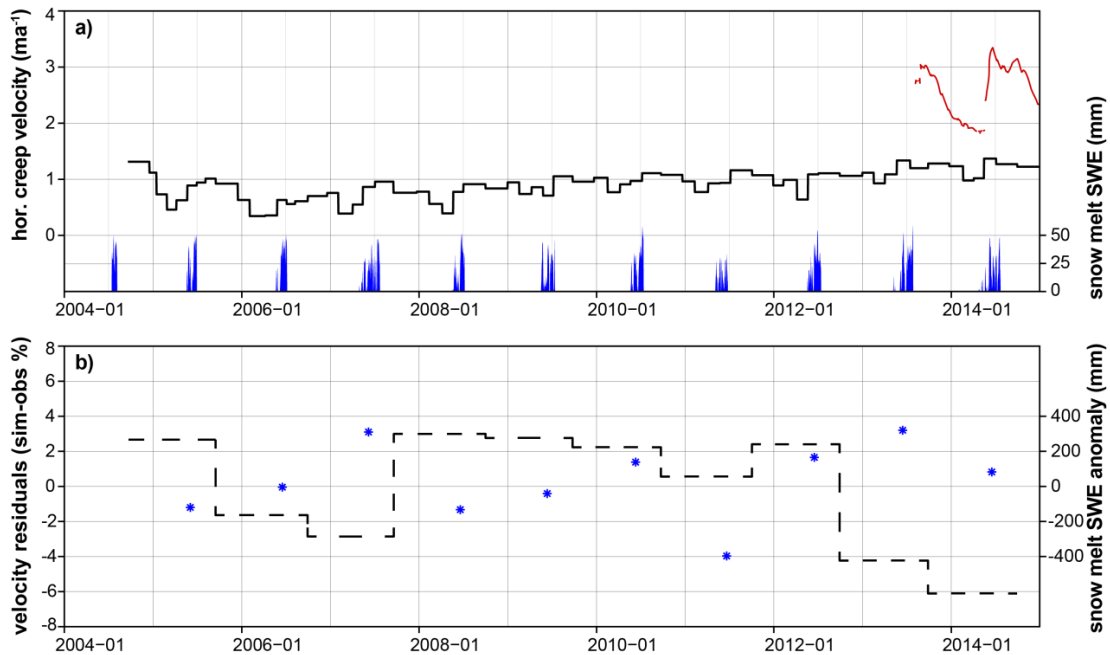


Fig. 7.14: Seasonal variations of rock glacier creep velocities compared with snow melt rates: a) bi-monthly variations of the horizontal surface velocities on the rock glacier Becs de Bosson (REC, 5 GPS points symbolised as a black step-plot), snow melt rates (blue area) approximated by nearby recorded GST time series, and creep velocities recorded by a permanent GPS on a more active zone on the same landform; b) compares annual velocity residuals (simulation-observation, dotted black line) with mean annual snow melt anomalies (stars, deviations from the series mean in mm SWE).

Although a **connection between the snow melt and the timing of the rock glacier activity** appears to exist based on the here discussed examples, the question whether thermo-mechanical or hydro-mechanical processes are more important for rock glacier kinematics could not be fully resolved. Since a relative ground warming coincided with an increase in the relative fraction of ground water (Sect. 6.4), the strong kinematic relation to GT variations could also be a hydro-mechanical effect. However, because of the time delay between the thermal signal at the ground surface and the shear horizon, GST time series could be used to roughly estimate the evolution of rock glacier creep velocities within the following 3-6 months.

7.4 Concluding remarks

During the past 15 years, several meteorological events and superposition of events occurred which greatly influenced the surface energy balance and the GST evolution. Most of these events were at least partly related to the snow cover. Strong thermal reactions at the ground surface as well as at depth were documented. The kinematic reaction of rock glaciers to meteorological events was tentatively explained by GT variations. The concept of exponential velocity increase with ground warming was illustrated by the observational data. In addition, the infiltration of melt water seemed to accelerate rock glaciers. However, no general conclusions on relative importance of snow melt for rock glacier activity can be drawn at this time.

PART IV: SYNTHESIS

8 General discussion

In this chapter, the evolution of mountain permafrost in the Swiss Alps over the past 15 years and the methodological achievements of this PhD thesis are discussed. It is structured following the four main objectives A-D (Sect. 1.4). A major part of this thesis, which also led to the publications Staub and Delaloye (2016) and Staub et al. (subm.), was the development of methods for the homogenization and integrative analysis of permafrost monitoring data. The value and use of these techniques is discussed in section 8.1. Section 8.2 addresses the influence of meteorological events and snow conditions on the ground thermal regime. Moreover, the capability of ground thermal models to reproduce GST variations during the observation period is discussed on the basis of the outcomes of Staub et al. (2015a). Based on the results shown in sections 6.3 and 7.3, the kinematic behaviour of rock glaciers and relevant thermo-mechanical processes are described. In the last section, the current permafrost monitoring strategy is evaluated and recommendations for the future permafrost monitoring in Switzerland are formulated.

8.1 Techniques for data homogenization, gap filling and integrative analysis

Homogenized and gap-filled data are a pre-requisite for the integrative analysis of a multitude of different time series. Major **achievements towards standardized data processing schemes** were made within this PhD thesis in close collaboration with the Swiss permafrost monitoring community. The most significant contribution was the development and application of gap filling techniques for GST data, by which continuous and comparable GST time series were generated at daily resolution for a vast range of different monitoring sites and landforms. Moreover, empirical studies contributed to the documentation of point-specific information about the thermal insulation effect of snow, the approximation of snow melt rates, and estimating GT variations at the depth of the ZAA based on GST time series.

8.1.1 Gap filling of thermal, meteorological and kinematic data

The GST gap filling approach presented in Staub et al. (subm.) is based on linear interpolation as well as on the quantile mapping technique (Gudmundsson et al., 2012; Themessl et al., 2011). The latter proved to be suitable for the spatial transfer of meteorological data to the PERMOS sites where observations are sparse (Rajczak et al., 2015). Since each GST gap was treated separately, the optimal regressor logger and the best gap filling technique could be used based on the availability of complete time series and the topo-climatic and snow conditions (Sect. 4.2). **The spatially very variable snow conditions were the main source of uncertainty.** Uncertainties of the gap-filled GST values were quantified separately for each day of the year, taking into account the inter-annual variability of the common observations. During snow-covered periods, the uncertainties were assumed to be systematic, hence could not be compensated by increasing sample size. Uncertainty estimates within the presumed snow free period were stochastic and can be partly compensated over time. By means of daily uncertainty estimates and by following the error propagation laws, it was possible to estimate uncertainties not only for the derived daily GST values, but for GST aggregates and indices (Fig. 5.1).

The GST gap filling routine was validated by means of ~18'000 artificial data gaps of variable length. It showed that for GST gaps shorter than 4-5 days, linear interpolation works as well as the more complex quantile mapping technique. The validation revealed that **data gaps of up to two months duration can be filled with maximum uncertainties $\leq \pm 0.25$ °C on MAGST**. For gaps of one year duration, the maximum uncertainties for MAGST were usually $\leq \pm 0.5$ °C. Linear interpolation could probably be used to fill gaps in GT time series, especially at great depth where the short-term variations are small. However, the limited number of other GT time series and the complexity of ground thermal processes would make the application of statistical transformation using GT regressor time series demanding.

By applying the GST gap filling routines to the entire PERMOS data set (GST data and uppermost borehole thermistors), the number of hydrological years with **complete data was increased by 70 %**, without exceeding estimated uncertainty maxima of ± 0.25 °C for the respective annual mean values. By aggregating several time series, e.g. to visualize the representative MAGST evolution for a multitude of monitoring sites as shown in Fig. 6.2a, the respective uncertainties became several times smaller than the temporal variations of the single values.

Besides the completion of the GST time series, the application of the gap filling routine revealed **similarities among different GST time series, almost regardless of distance**. Concerning this matter, the example shown in Fig. 4.7 is surprising. The most suitable regressor to reconstruct missing data at REC_S143, a GST-thermistor situated in coarse-blocky terrain on a gently inclined slope (~10 °) with a north-west aspect at 2650 m asl, was a thermistor situated at ~30 km distance at ~2915 m asl on a south-east exposed slope of at least 30 ° (AGE_S006). Although AGE_S006 was significantly colder in winter than REC_S143, the timing of the snow onset and melt were very similar at both locations. In addition to GST data, AirT time series were put into the pool of potential regressors as an alternative for GST at snow-free locations. AirT time series represented the optimal regressor for several data gaps in time series measured in steep rock walls. These examples underline the **high relevance of snow for the ground thermal regime**. For data homogenization purposes, this emphasizes the enormous advantage of having access to a large quantity of long time series which cover diverse topo-climatic conditions.

Kinematic and meteorological data acquired in the frame of PERMOS are also affected by missing or erroneous values. **Annual kinematic time series were successfully gap-filled by means of linear regression** based on the most similar regressor point (usually from the surroundings). In addition, the GPS points in the most active zone in the centre of the rock glaciers were selected and relative values were used to compare velocity changes in respect to a common reference period. This allowed the inter-comparison of representative sets of points from several rock glaciers over time (Fig. 6.7).

To put the ground thermal variations in the context of climate change, **AirT time series were downscaled based on gridded data** (Frei, 2014) for all GST and GT locations. Validation using AirT observations from PERMOS as well as the IMIS snow stations revealed good performance for daily mean AirT values with high covariance ($R^2 \gg 0.9$) and reasonable residuals (RMSE: 1-2 K). The largest residuals ($\gg 3$ K) were due to obvious measurement errors in the station data, e.g. caused by snow

or ice on the thermistors. However, site-specific effects such as surface temperature inversion or local shading effects could not be considered with gridded data.

In addition to AirT, **global radiation was approximated specifically for all GST and GT monitoring locations**. This was done by means of spatially accurate simulations of the potential incoming shortwave radiation (PISR) and the temporally accurate gridded data on the relative sunshine duration as explained in Sect. 4.2.4. Although the ISR estimates (Fig. 4.11) were more uncertain than the AirT estimates, validation with station data was able to realistically reproduce variations at the weekly to monthly scales. Since relative deviations and changes over time were the main goals of the analysis, the accuracies of the absolute AirT and ISR values were of secondary importance.

8.1.2 Indices describing the snow thermal insulation and snow melt rate

Snow information is sparse in the high-alpine domain and very variable at small spatial scales (Sect. 2.1.2). Moreover, the thermal insulation effect of the snow on the ground depends on the thickness, density and structure of the snow cover as well as the terrain roughness. Since the presence of snow diminishes the short-term temperature variations at the ground surface, empirical formulas have been developed to approximate the thermal insulation effect of snow based on GST time series and explicitly for the location of the GST loggers (Staub and Delaloye, 2016). The presence of snow has been previously derived from GST data (Apaloo et al., 2012; Delaloye, 2004; Gubler et al., 2011; Hipp, 2012; Lewkowicz, 2008; Schmid et al., 2012). However, to our knowledge this is the first **approximation of the thermal insulation effect** and the first delineation of the period of high thermal insulation based on GST time series. As described in Staub and Delaloye (2016), topo-climatic and device-specific properties were considered by using flexible thresholds. This flexibility was crucial for the successful application of the method to the large PERMOS GST data set.

Snow indices were validated using data from IMIS snow stations. The comparison of snow indices with snow depths underlined the **great influence of terrain characteristics on the thermal insulation effect of the snow cover**. The minimum snow depth required for effective thermal insulation of the ground (snow-indices > 0.5) ranged between 50 and 100 cm depending on the IMIS station and the season. This range is consistent with previous findings (Haeberli, 1973; Hanson and Hoelzle, 2005; Isaksen et al., 2002; Keller and Gubler, 1993; Luetsch et al., 2008; Zhang, 2005). However, it implies that fixed snow depth thresholds (commonly 80 cm) may be inaccurate for delineating the high-thermal insulation period. Refining the relationship between snow depth and thermal insulation for differing ground surface characteristics could be a promising approach for future research and could lead to an improved calibration of the upper boundary parameters in ground thermal models. In turn, this would permit more robust permafrost simulations to be developed for future climate scenarios (Ekici et al., 2015; Marmy et al., 2015; Staub et al., 2015a).

In addition to the snow thermal indices, a degree-day approach originally developed by Zingg (1951) was used to **estimate daily snow melt rates (mm SWE) at the position of the GST loggers** by means of AirT. The major advantage of coupling the degree-day approach with GST time series was that the melting period could be defined for the specific positions of the GST loggers. For the conversion of

AirT into SWE the factor A of 4.5 proposed by Zingg (1951) was used. The melt-index was validated with IMIS station data and a bulk snow density of 400 kgm^{-3} was applied to convert snow depths into SWE (mm/day). This snow density value is an approximation for the melting period between April and July based on a representative data set presented in Jonas et al. (2009). By comparing the estimated snow melt rates with the measured snow depth differences during the melting period, the optimal melt-rate factor A was computed. In most cases, the optimal value for A ranged between 3.5 and 5, hence close to the proposition made by Zingg (1951).

The melt-index does not take into account processes such as sublimation and the refreezing of melt water in the snowpack. However, it is a simple and reliable estimate to quantify seasonal and inter-annual variations as well as spatial differences in snow melt rates. The maximum snow depths before the start of the melting period can also be approximated by the sum of the annual melt-rate. A modified version of the melt-index including ISR time series revealed no significant improvement (Sect. 5.2.3). **The melt-index was successfully applied to study the thermal and kinematic response to melt water infiltration** (Fig. 7.4 and Sect. 7.3.2). It may also be useful for other applications in combination with geophysical data (i.e. time-lapse ERT and self-potential) and soil moisture data (Hauck, 2013; Hilbich et al., 2011; Scapozza et al., 2008; Scherler et al., 2010) in order to investigate melt water infiltration in permafrost.

8.1.3 Temperature time lags between the surface and different depths

The time lag of GST variations to reach a particular depth was quantified by cross-correlating between temperature time series measured at different depths in boreholes. The results revealed that for many boreholes, **the time delay of the surface signal increases almost linearly with increasing depth** (Fig. 7.5). This finding is in line with the visual analysis of thermal orbits (Fig. 5.6) and the general assumption that conduction is the dominant heat transport mechanism within the subsurface (e.g. Williams and Smith, 1989).

Deviations from the linear pattern can be explained e.g. by phase changes, differing thermal conductivity of ground layers as well as by advective or convective heat fluxes. Due to the superposition of heat conduction with convective or advective heat transport, the time delays were shorter in some cases. For example, the reversal of the time lag around 20 m depth at borehole GEM_0106 can be explained by the three-dimensional temperature field of the Gemsstock mountain peak through which the borehole is drilled at 90° inclination and the influence of the south side. At the Lapires boreholes (LAP_0198, LAP_1108 and LAP_1208), lower R^2 values were obtained within the very warm but ice-rich permafrost layer and the time lags decreased at the permafrost base, possibly because of the previously described internal air circulation effects (Delaloye and Lambiel, 2005). A similar situation was documented by Phillips et al. (2009) for the Flüela talus slope, where rapid degradation of ground ice at the permafrost base occurred. Moreover, the ground thermal regime has a thermal memory. **Current GST variations are superimposed on the ground thermal reaction at depth to long-term climate change** (Harris et al., 2003; Noetzli and Gruber, 2009).

However, the smaller the signal-to-noise ratio between seasonal and inter-annual variations and the thermal resolution (accuracy + precision) of the sensors, the less reliable were the results from the time lag analysis.

Lag times between the surface and 5 m depth depended on the exact depth difference between the thermistors and the subsurface properties and were in the order of two months. These results are comparable to the findings from Zenklusen Mutter and Phillips (2012), who applied a similar technique to quantify time delays but focussed on the snow free period and the active layer instead of the uppermost 15-25 m. To quantify time lags at greater depths, the cross-correlations were calculated step-wise, starting from the surface and then using other thermistors as a upper reference (Sect. 5.3). By means of this method, it was possible to reach depths between 15-20 m with $R^2 \geq 0.5$ (Fig. 7.5). **Typical time delays were 4-5 months to reach 10 m depth and 10-11 months at 20 m**, respectively. Variations in rock glacier creep velocities were found to have similar time delays relative to GST variations (sections 7.3 and 8.3).

8.1.4 Approximation of temperature variations at depth based on GST time series

The knowledge gained from the analysing thermal orbits (Fig. 5.6) and the time difference of GST and GT time series was used to **approximate GT variations at depth based on GST data**. An empirical formula was developed (Eq. 11 in Sect. 5.5) in order to analyse temperature variations at the approximate depth of the shear horizon in rock glaciers. The approach, which consisted of a simple averaging filter and a time lag, proved capable of reproducing GT variations. This is remarkable and emphasizes the relevance of the thermal regime at the ground surface for long-term temperature change at depth, although only the general pattern and not the absolute GT values could be reproduced. The possibility of deriving relative changes in GT in addition to a large variety of temperature and snow indices revealed the **great potential of GST measurements as a simple and cost-efficient monitoring technique**. On moving landforms, such as rock glaciers, the calibration of Eq. 11 can be done by means of variations in surface deformation rates assuming the kinematic response of rock glaciers being based on a thermo-mechanical process (Sect. 7.3). Because of the time delay of GT variations at depth, GST could even be used to predict GT variations in the following 1-2 years.

8.2 Influence of meteorological events and snow conditions on ground temperatures

Several meteorological events in the Swiss Alps caused large GST deviations within the period of observational permafrost monitoring (2000-2014). Meteorological events were defined as weather conditions which had a marked impact on the surface energy balance at the permafrost monitoring sites, such as seasonal or inter-annual variations in AirT, precipitation (mainly in the form of snow) and global radiation (Fig. 7.1). **The ground thermal impact of these meteorological events was qualitatively and quantitatively analysed** by means of GST indices (Sect. 5.1), GST-derived snow information (Sect. 5.2), apparent electrical resistivities (Sect. 6.4) as well as GT variations measured at depth. In the foreground of the analysis were the strength, the reaction time and the reversibility of the thermal response and implications for permafrost creep.

The strongest ground thermal response occurred for events which also involved anomalies of the snow cover duration (Sect. 7.1). Ground warming and ground cooling events were equally affected by early or late snow onset or disappearance, respectively. Regarding the thermal insulation effect of the snow, it was shown that **the direct effect of AirT on inter-annual GST variations is smaller than that of the snow cover**. This finding can be explained by the briefer influence of AirT on the surface energy balance during the snow-free period of 3-5 months between June and October. Hence, variations in MAGST cannot be explained by variations in MAAT (Fig. 7.1). In other words, trends in AirT do not necessarily correlate with those of GST and GT at a temporal scale of years to decades at locations that are influenced by snow. Thus it can be assumed that without a late snow onset in 2006/07, the exceptionally warm AirT between June 2006 and May 2007 would have warmed the ground surface much more. In contrast, for oversteepened rock walls or particularly wind-exposed locations, the surface temperatures are known to be highly correlated with AirT due to the continuous absence of snow, especially in shady areas of limited shortwave radiation (Gruber et al., 2004; Lewkowicz, 2001).

Although winter precipitation is most relevant for the evolution of the snow cover, AirT has a strong indirect influence on the snow disappearance and is the key factor deciding whether precipitation falls in the form of snow or rain. The relationship between anomalies of SDD and TDD proved to be as strong as that between AirT and TDD anomalies during the snow-free period (Fig. 7.7). SDD is influenced by the snow falls in late winter and the AirT evolution between April and July. Therefore, at time scales of several decades **an additional increase in AirT would probably cause a more rapid snow melt**, and depending on the amounts of snow to be melted, lead to an earlier snow disappearance. This hypothesis is consistent with several other studies (Bavay et al., 2009; Gobiet et al., 2014; Marmy et al., 2013; Morán-Tejeda et al., 2013; Schmucki et al., 2014).

Although variations of SDD and TDD have a direct effect on ground thawing and the evolution of MAGST, it was shown that **the spatial and the temporal variability of the ground freezing period are great** (Sect. 6.2). For example, the early snow disappearance in 2003 and 2011 (Fig. 7.1) caused above-average TDD sums (Fig. 6.2d). Nevertheless, the GST maxima at the end of the hydrological year 2002/03 were mainly attributable to limited ground cooling. The latter was due to an exceptionally early start of the high insulating period, which can be recognized in the high FDD values (Fig. 6.2d) and the remarkably homogeneous evolution of cumulative degree days in winter 2002/03 (Fig. 7.8). These results underline findings from Schneider (2014) and others, who showed the high diversity of winter cooling caused by surface and subsurface properties. **The differences among landforms or monitoring sites appear to be less important for the ground thermal regime than local topo-climatic and snow conditions**. However, if the amount of ground ice diminishes in zones of active layer thickening, this implies the loss of a heat sink and will probably cause a stronger seasonal and inter-annual ground warming. For analysing the snow effects on the ground thermal regime using observational data, the snow-indices proved to be a great advantage.

Our results regarding the importance of snow for the ground cooling as well as the start of the thawing season suggest that the **evolution of (solid) precipitation in winter will become crucial for**

the future permafrost evolution. Because precipitation scenarios are still uncertain (CH2011, 2011; Gobiet et al., 2014; Rajczak et al., 2013), estimating the future evolution of SDD in the high-alpine domain remains a challenge. Trends suggest snow will disappear earlier. As illustrated with Fig. 7.8 changes in ground thawing might affect different terrain in a similar way in terms of summer thawing. Assuming an ongoing atmospheric warming, increasing thermal offsets between the permafrost and the ground surface will lead to increased conductive heat transport during the snow-free period as long as the position of the permafrost table does not lower significantly. However, an increase of AirT in autumn could lead to a later snow onset and cause more negative FDD. Whether this later snow onset compensates the increasing TDD will probably depend on the local ground properties, which were shown to be relevant for efficiency of the ground freezeback (Fig. 7.8). **Where efficient winter cooling is favoured by convection such as in coarse-blocky terrain, permafrost has the best chances of persisting in a warming climate.**

The detailed comparison of simulated and observed GST and GT time series was used to assess the ability of the **1D subsurface model COUP** (Jansson and Karlberg, 2004; Jansson, 2012) to reproduce seasonal and inter-annual temperature variations at the Lapires talus slope (Staub et al., 2015a). The study focussed on the upper boundary conditions at the ground surface and specifically on GST variations in response to meteorological events. The model was calibrated for all seasons and for the observation period as a whole. This is the usual procedure in mountain permafrost modelling because of sparse observational data (Marmy et al., 2015). An inaccurate representation of one season potentially leads to a systematic bias in the representation of other seasons. **Systematic biases due to limitations in the model representation of the snow cover were the main problem for an accurate GST simulation.** Although the majority of GST time series showed a good covariance between simulations and observations (R^2 between 0.88 and 0.95), inter-annual GST variations exhibited considerable biases and systematic errors. No clear dependency of the biases on meteorological events could be identified. The largest deviations between simulated and measured GT was observed for the winter season, due to limited ground cooling in the model. Missing convective heat fluxes may have been cause of these biases, which in turn also led to underestimated ground warming in summer. Moreover, the poor signal-to-noise ratio of the GT observations (Sect. 4.1.1) made the model calibration a demanding task. To some degree, the deviations between simulated and observed GST and GT could be attributed to intra-talus air circulation as well as to the re-distribution of the snow by avalanches. **Our study demonstrated the need for detailed model validation regarding meteorological events** and physical processes in order to better define the model's reliability under changing environmental conditions. To further assess the performance of the COUP model related to specific meteorological conditions, a follow-up study would be required which validates the model in separate validation windows and for additional sites.

Based on data analysed in the present PhD project, temperature variations at the ground surface seem to dominate the evolution of GT at depth at time scales of months to several years. From this perspective, **GST variations are the key to understanding permafrost evolution at depth**, and long-term changes of the thermal regime at the ground surface can explain variations in permafrost creep, as will be discussed in the following section.

8.3 Permafrost creep in response to ground temperature variations

The photogrammetric analysis of the three rock glaciers from the Gemmi area illustrated in Fig. 6.6 showed a clear **increase of the kinematic activity during the past 25 years compared to the period between 1960 and 1990** (Staub et al., 2015b). In recent years these rock glaciers moved up to 200-600 % faster than between 1990 and 1995. However, absolute displacement rates differed greatly. Similar decadal creep velocity variations as described here were found by others for several rock glaciers in the European Alps (Bodin et al., 2009; Käab et al., 2007; Kellerer-Pirklbauer and Kaufmann, 2012; Lugon and Stoffel, 2010). The common pattern in permafrost creep variations suggests that a direct or indirect impact of the continuously warm climate during the past three decades is the main driving factor for the overall acceleration of rock glacier activity. Data from the Doesen rock glacier in Austria points to an intermediate velocity decrease between 1954 and 1993 (Kaufmann, 1998), which could be a delayed kinematic response to the short period of positive AirT anomalies around 1950 and the subsequent cold period until the beginning of the 1980^{ies} (Fig. 1.1).

The **hypothesis of climate impacting permafrost creep** was formulated years ago and was mainly supported by photogrammetry studies with data at decadal or pluri-annual resolution (Haeberli, 1985; Käab et al., 2007; Kaufmann and Ladstädter, 2003). Mostly AirT was used as a proxy for the climate impact on the ground due to the lack of local long-term ground temperature records. Nowadays, the improved data situation allows for testing the thermo-mechanical relationship with data at annual resolution (Sect. 7.3.1). **A distinct pattern of inter-annual variations of rock glacier surface displacement rates is documented** in geodetic data from PERMOS (Fig. 6.7) and was reported also by others (Delaloye et al., 2008, 2010; Käab et al., 2003; Kaufmann et al., 2007).

The correlation of GT and AirT variations was poor at the inter-annual scale. But the inter-annual pattern of rock glacier creep velocities (Fig. 6.7) was similar to the GT variations observed at depths between 10 and 30 m (Fig. 6.5). Therefore, the filter described in Sect. 5.5 was used to approximate synthetic GT variations at the presumed depth of the shear horizon based on GST time series. These synthetic GT time series were applied in combination with the exponential function Eq. 5 (Sect. 2.3) proposed by Arenson et al. (2002), which describes the creep velocity dependency on temperature. As illustrated in Sect. 7.3.1, **the observed creep velocity changes closely followed the exponential function of this synthetized GT**. The temperature dependency of rock glacier activity was the subject of several previous studies (Arenson, 2002; Davies et al., 2001; Käab et al., 2007), but this is the first time it has been investigated using long-term observational data.

The coefficients of determination obtained between the exponential thermo-mechanical relationships and the observed velocity variations were surprisingly high for such a complex subsurface phenomenon with many potential influencing factors (Fig. 7.9). The high covariance of the kinematic activity and GT variations implies a strong thermo-mechanical response of creeping mountain permafrost to meteorological events. The ground warming periods before 2004 and since 2008 (Fig. 6.5), and the interim ground cooling period after the cold winters between 2004 and 2007 all caused an extraordinarily rapid and strong kinematic response. **It appears that temperature variations explain the largest part of the creep velocity variations**, at least at the inter-annual scale.

The optimal parameters for the base factor a and the exponent b by which Eq. 5 was solved were similar for each rock glacier. Only few differences were found for a , and for the exponent b the most frequent values were between 0.3 and 1.0 (Fig. 7.11). The higher the exponent b , the more sensitive is the rock glacier to temperature change. As Fig. 7.12 illustrates, **most GPS points showed similar thermo-mechanical relationships for one landform**, although the absolute displacement rates varied strongly. However, to draw conclusions about the response of these landforms to meteorological events, groups of points in functional zones have to be analysed rather than single GPS points, as done for the absolute and relative velocity changes in Fig. 6.7.

The time delay of the kinematic response of rock glaciers to GST variations can be assumed to be approximately equal to that of the GT at the position of the main shear horizon. Observations from Arenson et al. (2002) as well as theoretical considerations from Kannan and Rajagopal (2013) support this hypothesis, because up to 90 % of the movement occurs in thin layer(s) of low viscosity. Therefore, the optimal parameter combinations obtained for Eq. 11 (Sect. 5.5) is expected to provide **information about the depth at which the main shear horizon is located**, without considering borehole data. The results showed the longest filtering time windows for the GPS points located on the Becs de Bosson rock glacier (Fig. 7.10), the largest of all those selected. Because of the delayed ground thermal and kinematic response to GST variations, real-time GST measurements could be used to estimate future variations in GT as well as rock glacier creep velocities.

The exceptionally high annual deformation rates measured on rock glaciers in recent years as well as indications of rock glacier destabilization raise questions regarding **velocity definitions and the transition between active and destabilized rock glaciers**. The differentiation between inactive, active and destabilized rock glaciers is ambiguous, and smooth transitions instead of exact values have been proposed (Appendix A2). An increasing number of rock glaciers monitored in the Valais Alps would nowadays technically belong to the category of destabilized rock glaciers (Delaloye et al., 2013; PERMOS, 2013; Roer et al., 2008). Also the rock glaciers at GFU and TMI, which were discussed in Sect. 7.3, showed rapid deformation (Kummert and Delaloye, 2015; Staub et al., 2015b). For the Gemmi rock glacier, shear zones between the accelerating central zone and a side lobe were detected (Fig. 5.8a). In particular the front of the Gemmi rock glacier appears to have started to slide and collapse after its first velocity maximum in 2003/04 and its morphology no longer corresponds to the typical shape of an active rock glacier. Such morphological change indicates ruptures and structural changes down to several meters depth, possibly accompanied by rapidly changing preferential flow paths of the infiltrating melt water. In this context, it is particularly interesting to analyse deviations from the velocities predicted by the empirical, thermo-mechanical relationship. For the Tsarmine rock glacier, the start of a destabilization process probably explains the velocity residuals in 2013 (Fig. 7.13), especially since the respective velocities increased even more between 2013 and 2014 (Fig. 6.7).

A seasonal acceleration of the Becs de Bosson rock glacier at the start of the snow melt was documented with bi-monthly DGPS surveys and high-frequency GPS measurements (Fig. 7.14). There, the **seasonal maxima occurred in autumn or in early winter** and the minima were observed in late winter before snow melt started (Delaloye et al., 2010; Perruchoud and Delaloye, 2007). Similar seasonal patterns have been reported for other rock glaciers (Kääb et al., 2007; Kölbing, 2001; Wirz et al., 2015). The velocity maxima in early winter can be explained by seasonal temperature variations within the active layer (Fig. 6.4) or by indirect effects of increased GT such as temporally higher hydrostatic pressure at the shear horizon. The hydro-thermo-mechanical processes related to the melt water infiltration are the subject of an ongoing scientific debate (Delaloye et al., 2010; Ikeda et al., 2008; Wirz et al., 2013, 2015). Water infiltration may lead to acceleration due to rapid advection of latent heat from the surface into the ground and/or because of a temporally increase in pore water pressure.

The rock glacier data analysed in Sect. 7.3 provided some limited support that snow melt influences the kinematic activity at the inter-annual scale. In 2013, which was characterised by late and intense snow melt (Sect. 7.1), the rock glaciers Tsarmine (TMI) and Gemmi (GFU) moved faster than the thermal relationship is able to explain (Fig. 7.13), whereas the movement was slower in 2011 when snow melt quantities were below average. There is evidence that the **snow melt has an accelerating effect on the mechanics of rock glaciers**, especially regarding the seasonal creep velocity pattern (Fig. 7.14). However, other causes for the exceptional acceleration of rock glaciers, e.g. the one at TMI in 2013, cannot be excluded. More data at high temporal resolution is required for a variety of different rock glaciers to investigate the phenomena of rock glacier creep in detail.

Other factors such as the geometry or the structure of the rock glacier influence kinematic behaviour. Ice contents, as a structural characteristic, were estimated based on ERT and RST tomograms (Hauck et al., 2015) and by means of the so-called 4-Phase Model 4PM (Hauck et al., 2008, 2011) for the rock glaciers Murtèl, Muragl, Réchy, Dirru, Grabengufer and Lac des Vaux in the frame of the TEMPS project. **No general relation between the ice content and the creep velocity was found.** Still, the hypothesis that variations in the ice content along the longitudinal profile influence the kinematic response to ground temperature changes cannot be rejected entirely. For example at the Gemmi rock glacier (lobe A in Appendix A3), the relative velocity increase between 1995 and 2014 was highest in the rooting zone, where geophysical investigations revealed the highest ice contents (Staub et al., 2015b). However, many other factors, such as differing ground thermal conditions, the inclination of the bedrock, the thickness of the active layer, the depth of the shear horizon or the material supply from the headwall may influence the creep velocity.

8.4 Evaluation of the permafrost monitoring strategy of PERMOS

This PhD thesis demonstrated the broad possibilities for research based on the permafrost monitoring data from PERMOS and the PERMOS partner institutions. Although the focus was on the GST data because of its unique quantity and quality, the availability of other thermal, kinematic, meteorological as well as geophysical variables proved to be highly advantageous. Moreover, this thesis illustrated how complementary data sets can be used to efficiently generate meteorological, snow-specific as well as ground-thermal time series for integrative analysis beyond the level of a single case study. Therefore snow data from the IMIS stations, the gridded data from MeteoSwiss as well as the DEM Alti3D from Swisstopo were linked with permafrost monitoring data.

Not necessarily all parameters are required to be measured at all monitoring sites, but **long time series of high temporal resolution and high quality were shown to be valuable** for assessing changes at the time scale of 10-15 years, and the value of these time series will increase with each additional year. Regarding an extension of monitoring sites, it would be preferable to fill the gaps in the northern Bernese Alps and the northern and Central Grisons. On the one hand, the continuity of well-established and standardized monitoring techniques built the basis for the comparison of temporal and spatial variations over this long period. On the other hand, new methods or unique time series, e.g. the bi-monthly kinematic data of rock glacier Becs de Bosson (REC) or the ERT-M time series measured at the Schilthorn, may permit detailed insights, which could not have been gained by numerous time series at a coarser temporal resolution. In this context, it will be crucial for the future permafrost monitoring strategy to use a **combination of well-established as well as innovative techniques**.

9 Conclusions and perspectives

This PhD thesis provides new knowledge about temporal and spatial variations of mountain permafrost regarding thermal, kinematic and geophysical variables and their interactions based on a large set of observational data from the Swiss Alps. New sophisticated data processing techniques were elaborated to homogenize time series and to maximize the scientific value of the data regarding permafrost-relevant effects such as the thermal insulation of the snow cover. The conclusions which can be drawn from the findings about the evolution of Alpine permafrost and its response to meteorological events are presented in the key messages below. Recommendations are also made to improve the Swiss permafrost monitoring strategy and data processing workflows.

9.1 Main findings

9.1.1 Procedures for data homogenization and integrative data analysis

The data processing routines for the homogenization and gap filling of thermal and kinematic data applied in the present project proved to be suitable for the ambitious task of a joint analysis of different time series of several parameters from many monitoring sites. Gap filling routines were successfully developed and applied to all GST time series and the uppermost borehole thermistors (Sect. 4.2.3). As a result, the number of hydrological years with complete GST data increased by ~70 %, with maximum uncertainties in the order of ± 0.25 °C on annual means (Staub et al., *subm.*). By the differentiation of systematic and stochastic uncertainties and the consistent application of the error propagation laws, uncertainties related to the gap filling procedure were also quantified for aggregates and indices (Fig. 5.1). A similar gap filling approach was successfully applied for surface displacement rates measured on rock glaciers (Fig. 4.12).

Based on GST and AirT time series, point-specific snow information was derived, namely the thermal insulation effect, the occurrence of phase changes (zero curtains) and the snow melt rate (mm SWE) during spring zero curtains (Staub and Delaloye, 2016). The snow-indices, which characterise the thermal insulation effect, proved to be highly beneficial for studying the importance of the snow on the surface energy balance (Fig. 7.1 and Sect. 7.2). For example, these snow-indices can be used to assess the validity of the popular GST-indices BTS and WEqT, which assume a thermal equilibrium within the active layer after a long period of effective thermal insulation by the snow cover. Since such a thermal equilibrium is often not reached, the new term Late Winter Surface Temperature (LWST) is proposed as an alternative to WEqT (Fig. 5.1).

The approach for analysing observational data was based on three main principles: first, the use of anomaly values to put differing time series on a comparable basis; second the comparison of spatially consistent data sets; and third, the consideration of complementary data to study complex phenomena and process interactions. Several examples in this thesis illustrate the power of anomaly values in order to detect changes over time and to improve understanding of processes (chapters 1 and 1). Anomaly values relative to a common reference allow for assessing changes in various data sets. Moreover, anomaly values reduce potential inaccuracies of absolute values, e.g. due to

Conclusions and perspectives

measurement errors or spatial transfer. The use of identical data configuration (e.g. measurement locations) for each time step within a time series turned out to be fundamental for the comparison of aggregates and indices. For analysing temporal variations in rock glacier surface deformation rates, in particular, an identical selection of points needs to be compared within functional zones to ensure unbiased trend analysis. Complementary meteorological and geophysical monitoring data were shown to be very useful for deriving additional information on snow characteristics or structural changes in the subsurface.

The quantification of temporal and spatial variations represented an essential step to put the evolution of thermal, kinematic and geophysical variables in the context of climate change. Consequently, the ability of ground thermal models to reproduce the thermal characteristics measured at the ground surface was analysed (Staub et al., 2015a). GST and GT simulated by the 1D subsurface model COUP (Jansson and Karlberg, 2004; Jansson, 2012) were compared with observations and the respective differences were analysed at the process level. It turned out that despite a reasonable overall covariance of simulated and measured GST, considerable bias resulted in inter-annual GST and GT simulations due to inaccurate representation of the snow cover and the limitation of the model to conductive heat transport. Effects of rapid ground cooling in winter, in particular, were not reproduced correctly by the model.

Permafrost response to meteorological events (Sect. 7.1) was examined by assessing the heat transport from the surface into the ground and the relative importance of AirT and snow on the surface energy balance (Sect. 7.2). Insights gained on the response time and persistence of GT to GST variations were used to simulate GT anomalies at the approximate depth of the shear horizon in rock glaciers using GST time series (Sect. 5.5). With these methods, it was possible to characterise the thermal dependency of rock glacier creep (Fig. 7.9) and to estimate the relative influence of snow melt (Fig. 7.13).

9.1.2 The evolution of mountain permafrost in Switzerland since 2000

The thermal imbalance of the permafrost in the Swiss Alps under the currently warm climatic conditions can be seen in thermal, structural and kinematic changes documented during the past decades. GT measurements showed warming at the majority of the monitoring sites (Fig. 6.5). This GT increase was most distinct at locations with relatively cold temperatures < -1 °C and least pronounced at locations with temperatures close to the melting point due to phase changes. When overlaid with transient and three-dimensional effects which were analysed in other studies, the energy balance at the ground surface dominated over variations in the thermal regime at depth. The time delay the thermal signal needs to reach 10 or 20 m depth from the surface was about 4 and 10 months, respectively (Fig. 7.5). Similar time delays have been found for inter-annual variations of rock glacier velocities relative to GST anomalies (Fig. 7.10).

Because of persistent warm conditions at the ground surface since 2009, the current temperature increase at depth is stronger than on average during the past two decades (Fig. 6.5). The observed ground warming is in line with an increasing fraction of water relative to the ground ice content

(Fig. 6.8) as well as an acceleration of rock glacier creep (Sect. 6.3). Despite site-specific effects relating to the shape of the bedrock, the depth of the shear horizon, the initial thermo-hydro-mechanical conditions and the spatial flow field, the observations indicate that rock glacier activity is mainly a response to temperature variations at the depth of the shear horizon (Fig. 7.9). For the first time, variations in GT were successfully approximated by GST anomalies (Sect. 5.5). Bi-monthly and high-frequency GPS measurements as illustrated in Fig. 7.14 showed that the velocity maxima occur in early winter (Delaloye et al., 2010; Perruchoud and Delaloye, 2007). Additionally, there is evidence that melt water infiltration can temporarily increase the surface deformation for a few weeks to months. However, this effect is so far only documented for selected rock glaciers and the mechanical influence of water on rock glacier activity is not yet fully understood.

GST time series offer a unique data basis to approximate the heat and energy exchange at the ground surface for a multitude of monitoring sites. GST time series allowed for assessing the ground thermal reaction to meteorological events (sections 7.1 and 7.2). The influence of AirT on GST was most direct during the snow melt and the snow-free period. Snow disappearance, which is influenced by the amount and period of winter precipitation, had a significant effect on ground thawing (Fig. 7.7). Overall, snow proved to be more important than AirT regarding inter-annual GST variations at the decadal scale, particularly at the start of the high-insulating period (Fig. 7.8). Especially coarse-blocky terrains required more snow to reach an effective thermal insulation towards the atmosphere compared with smooth ground surfaces (Staub and Delaloye, 2016). Therefore, ground freezing is particularly efficient on rock glaciers and talus slopes with large boulders at the surface. Due to the very heterogeneous terrain and snow conditions, the spatial variability of GST and snow indices was almost as large at the site scale as at the regional scale (Fig. 6.3). However, many GST time series showed similar relative changes over time, especially those with comparable snow conditions (Sect. 6.2). Consequently, the optimal regressor loggers for filling long gaps in GST data were usually characterised by similar timing of the snow onset, melt and disappearance and were not necessarily from the same monitoring site (Fig. 4.7).

Given the currently warm ground thermal conditions, and with the summer heat wave of 2015, an early snow onset in 2015 would have a much greater impact than that in the warm hydrological year 2002/03 and would likely lead to an even stronger increase in ground temperature. Over the long-term, future atmospheric warming will probably cause increasing thawing degree days, accompanied by increasing active layer depths. However, the observations showed that one or two winters of particularly efficient ground cooling due to late or limited thermal insulation by snow, can reverse the net heat exchange at the ground surface and lead to interim phases of ground cooling (Fig. 6.5 and Fig. 7.8). Therefore, ground cooling in winter may become important to the preservation of permafrost in a warming climate. During the observation period considered in the present project, AirT in autumn and early winter did not have an influence on the timing of the snow onset (Sect. 7.2.2). However, precipitation between autumn and spring may become an important factor for future permafrost evolution, and at locations not influenced by snow, the GST evolution will probably be similar to that of AirT.

9.1.3 Recommendations for the mountain permafrost monitoring in the Swiss Alps

The strengths of the current monitoring strategy of PERMOS lie in the diversity of field sites and monitoring methods as well as in the high number of high-quality time series of considerable duration. Continuing measurements for several decades under unchanged conditions is demanding and may, e.g. due to safety issues, not be possible everywhere. However, guaranteeing the continuity of the measurements over the long term is the most important recommendation for mountain permafrost monitoring in Switzerland.

This PhD thesis illustrated the value of GST monitoring time series. It is therefore proposed to continue measuring GST data by covering as many different snow and subsurface conditions at each site as possible (10-15 loggers). If GST and GT were to be measured at higher thermal resolution and in shorter sampling intervals (≤ 1 hour) this would increase information about short-term variations and provide more possibilities for data correction (Sect. 4.1.1). A re-evaluation of the PERMOS monitoring sites and installations is recommended in the near future. GST and meteorological data measured on rapidly moving landforms or in very dynamic terrain are interesting for research but might not be suitable for long-term monitoring due to changing topo-climatic conditions. Since most GT measurements showed a very similar evolution, there is no urgent need for additional boreholes for PERMOS. However, some regions around the Bernese Alps and the Surselva in the Central Grisons (Appendix A1) are currently underrepresented. GST and ERT measurements, in particular, in these regions, would be beneficial in terms of covering a more representative set of different snow conditions as well as surface and subsurface properties.

The automatic ERT time series from the Schilthorn demonstrated the value of this variable regarding its sensitivity to liquid water on a site with particularly warm permafrost. As soon as this technique is fully operational in completely remote areas, it will offer great opportunities for extending and complementing the current monitoring setup. Since power consumption will likely remain an issue in harsh conditions, innovative techniques could be used to trigger other measurement devices in periods of particular interest. For example, accelerometers or permanently installed GPS devices could be used to increase the sampling rate of entire monitoring networks in periods of high kinematic activity, e.g. of thermal and geophysical sensors or automatic cameras. Similarly, the self-potential method, which is sensitive to flowing water, could be used to investigate the thermal and kinematic response of permafrost to melt water infiltration in detail (Hauck, 2013; Scapozza et al., 2008).

Regarding the documentation of rock glacier creep, the annual surveys made in the frame of PERMOS, the unique bi-monthly DGPS time series for the the Becs-de-Bosson rock glacier as well as permanently installed GPS devices cover a wide spectrum of spatio-temporal information. A combination of different techniques appears to be the best way to obtain the required kinematic information, namely the continuation of geodetic surveys (e.g. once or twice a year) with ~ 2 -3 high-frequency GPS sensors per rock glacier and regular aerial images (and/or laser scans). Aerial images may also be useful at shorter time intervals, particularly for fast-moving landforms, where the time interval should be defined as a function of displacement rates and the spatial resolution of the

method. Creep velocities ≥ 0.5 m can be detected and quantified by high-resolution aerial images (Staub et al., 2015b). Having more than one permanent GPS per landform would allow differentiation between movements that happen at depth and movements of the boulder on which the GPS is mounted.

More effort is required in terms of data processing and quality control towards a real-time analysis of the acquired data.

9.2 Perspectives and future research needs

This PhD thesis revealed the high relevance of snow for the evolution of permafrost in different contexts. In a next step, the snow-indices described in Staub and Delaloye (2016) should be tested with GST data from other mountainous regions. Additionally, the thermal insulation effect of snow on different terrains requires further investigation, e.g. by comparing the snow indices with measured snow depths or by measuring the thermal resistance in a vertical snow profile. The approximation of the snow melt rates using AirT also needs to be refined using snow density samples and melt water runoff measurements. Since the thermal insulation by the snow pack proved to be the most problematic point for simulating GST with the COUP model, the snow indices should be tested as additional calibration or validation criteria. In the future, observational permafrost research will make significant contributions to a better representation of short-term variations and the related physical processes of ground thermal models. For example, the time lag analysis presented in this thesis based on GT measurements could be extended to quantify thermal diffusivity for different materials, depths and time periods. Concerning the simulation of future permafrost scenarios, precipitation in autumn and winter will play a key role for the ground freezing and the preservation of permafrost over the long-term. Therefore, improved precipitation predictions are required. The onset of the insulating winter snow cover within the high-alpine domain of Switzerland has to be further investigated, into the future as well as into the past.

The gap filling procedure developed for GST time series, which introduces a new practical application of the quantile mapping technique for a potentially broad research field, needs to be tested in another region and to be optimized for filling gaps in GT data as well. Moreover, the comparison of the empirical-statistical gap filling procedure with reanalysis-runs of a ground thermal model would be of high interest in order to improve understanding of processes, the gap-filling routine and possibly also model calibration. For the exchange between gridded data sets and station data, other variables than meteorological and thermal could be spatially transferred or scaled by means of the quantile mapping technique. When the spatial resolution of remotely sensed data is at scales of a few meters, e.g. on snow coverage, kinematic activity, albedo or thermal radiation, it will increase in importance for permafrost research in mountainous regions like the Swiss Alps. However, observational data will remain the most important source of information for mountain permafrost research.

References

- Anisimov, O. A.: Potential feedback of thawing permafrost to the global climate system through methane emission, *Environmental Research Letters*, 2(4), 045016, doi:10.1088/1748-9326/2/4/045016, 2007.
- Anthony, K. M. W., Anthony, P., Grosse, G. and Chanton, J.: Geologic methane seeps along boundaries of Arctic permafrost thaw and melting glaciers, *Nature Geoscience*, 5(6), 419–426, doi:10.1038/ngeo1480, 2012.
- Apaloo, J., Brenning, A. and Bodin, X.: Interactions between Seasonal Snow Cover, Ground Surface Temperature and Topography (Andes of Santiago, Chile, 33.5°S), *Permafrost and Periglacial Processes*, 23(4), 277–291, doi:10.1002/ppp.1753, 2012.
- Arenson, L.: Unstable alpine permafrost: a potentially important natural hazard-variations of geotechnical behaviour with time and temperature, PhD Thesis, ETH Zürich., 2002.
- Arenson, L., Hoelzle, M. and Springman, S.: Borehole deformation measurements and internal structure of some rock glaciers in Switzerland, *Permafrost and Periglacial Processes*, 13(2), 117–135, doi:10.1002/ppp.414, 2002.
- Auer, I., Boehm, R., Jurkovic, A., Lipa, W., Orlik, A., Potzmann, R., Schoener, W., Ungersböck, M., Matulla, C., Briffa, K., Jones, P., Efthymiadis, D., Brunetti, M., Nanni, T., Maugeri, M., Mercalli, L., Mestre, O., Moisselin, J.-M., Begert, M., Mueller-Westermeier, G., Kveton, V., Bochnicek, O., Stastny, P., Lapin, M., Szalai, S., Szentimrey, T., Cegnar, T., Dolinar, M., Gajic-Capka, M., Zaninovic, K., Majstorovic, Z. and Nieplová, E.: HISTALP—historical instrumental climatological surface time series of the Greater Alpine Region, *International Journal of Climatology*, 27(1), 17–46, doi:10.1002/joc.1377, 2007.
- Barboux, C.: Detection, mapping and monitoring of slope movements in the Alpine environment using DInSAR, PhD Thesis, Department of Geosciences, University of Fribourg, 2014.
- Barsch, D.: Nature and importance of mass-wasting by rock glaciers in alpine permafrost environments, *Earth Surface Processes*, 2(2-3), 231–245, doi:10.1002/esp.3290020213, 1977.
- Barsch, D.: *Rockglaciers. Indicators for the present and former geocology in high mountain environments*, Springer, Berlin., 1996.
- Bavay, M., Lehning, M., Jonas, T. and Löwe, H.: Simulations of future snow cover and discharge in Alpine headwater catchments, *Hydrological Processes*, 23(1), 95–108, doi:10.1002/hyp.7195, 2009.
- Begert, M., Schlegel, T. and Kirchhofer, W.: Homogeneous temperature and precipitation series of Switzerland from 1864 to 2000, *International Journal of Climatology*, 25(1), 65–80, doi:10.1002/joc.1118, 2005.
- Beltrami, H.: Active layer distortion of annual air/soil thermal orbits, *Permafrost and Periglacial Processes*, 7(March), 101–110, 1996.
- Berthling, I.: Beyond confusion: Rock glaciers as cryo-conditioned landforms, *Geomorphology*, 131(3-4), 98–106, 2011.
- Bodin, X., Thibert, E., Fabre, D., Ribolini, A., Schoeneich, P., Francou, B., Reynaud, L. and Fort, M.: Two decades of responses (1986–2006) to climate by the Laurichard rock glacier, French Alps, *Permafrost and Periglacial Processes*, 344(4), 331–344, doi:10.1002/ppp, 2009.
- Boeckli, L., Brenning, A., Gruber, A. and Noetzli, J.: Alpine permafrost index map, Supplement to: Boeckli, Lorenz; Brenning, A; Gruber, A; Noetzli, J (2012): Permafrost distribution in the European Alps: calculation and evaluation of an index map and summary statistics. *The Cryosphere*, 6, 807-820, doi:10.5194/tc-6-807-2012, doi:10.1594/PANGAEA.784450, 2012a.

References

- Boeckli, L., Brenning, A., Gruber, S. and Noetzli, J.: A statistical approach to modelling permafrost distribution in the European Alps or similar mountain ranges, *The Cryosphere*, 6(1), 125–140, doi:10.5194/tc-6-125-2012, 2012b.
- Boeckli, L., Brenning, A., Gruber, S. and Noetzli, J.: Permafrost distribution in the European Alps: calculation and evaluation of an index map and summary statistics, *The Cryosphere*, 6(4), 807–820, doi:10.5194/tc-6-807-2012, 2012c.
- Bollmann, E., Girstmair, A., Mitterer, S., Krainer, K., Sailer, R. and Stötter, J.: A Rock Glacier Activity Index Based on Rock Glacier Thickness Changes and Displacement Rates Derived From Airborne Laser Scanning, *Permafrost and Periglacial Processes*, n/a–n/a, doi:10.1002/ppp.1852, 2015.
- Bommer, C., Phillips, M. and Arenson, L. U.: Practical recommendations for planning, constructing and maintaining infrastructure in mountain permafrost, *Permafrost and Periglacial Processes*, 21(1), 97–104, doi:10.1002/ppp.679, 2010.
- Bonnaventure, P. P. and Lewkowicz, A. G.: Mountain permafrost probability mapping using the BTS method in two climatically dissimilar locations, northwest Canada, *Canadian Journal of Earth Sciences*, 45(4), 443–455, doi:10.1139/E08-013, 2008.
- Brenning, A.: Geomorphological, hydrological and climatic significance of rock glaciers in the Andes of Central Chile (33–35°S), *Permafrost and Periglacial Processes*, 16(3), 231–240, doi:10.1002/ppp.528, 2005.
- Caduff, R., Schlunegger, F., Kos, A. and Wiesmann, A.: A review of terrestrial radar interferometry for measuring surface change in the geosciences, *Earth Surface Processes and Landforms*, 40(2), 208–228, doi:10.1002/esp.3656, 2015.
- CH2011: Swiss Climate Change Scenarios CH2011, C2SM, MeteoSwiss, ETH, NCCR Climate, and OcCC, Zurich, Switzerland., 2011.
- Cremonese, E., Gruber, S., Phillips, M., Pogliotti, P., Boeckli, L., Noetzli, J., Suter, C., Bodin, X., Crepez, a., Kellerer-Pirklbauer, a., Lang, K., Letey, S., Mair, V., Morra Di Cella, U., Ravel, L., Scapozza, C., Seppi, R. and Zischg, a.: Brief communication: 'An inventory of permafrost evidence for the European Alps', *Cryosphere*, 5(3), 651–657, doi:10.5194/tc-5-651-2011, 2011.
- Davies, M. C. R., Hamza, O. and Harris, C.: The effect of rise in mean annual temperature on the stability of rock slopes containing ice-filled discontinuities, *Permafrost and Periglacial Processes*, 12(1), 137–144, doi:10.1002/ppp.378, 2001.
- Delaloye, R.: Contribution à l'étude du pergélisol de montagne en zone marginale, PhD Thesis, Department of Geosciences, University of Fribourg, GeoFocus No. 10, 2004.
- Delaloye, R. and Lambiel, C.: Evidence of winter ascending air circulation throughout talus slopes and rock glaciers situated in the lower belt of alpine discontinuous permafrost (Swiss Alps), *Norsk Geografisk Tidsskrift - Norwegian Journal of Geography*, 59(2), 194–203, doi:10.1080/00291950510020673, 2005.
- Delaloye, R. and Lambiel, C.: Typology of vertical electrical soundings for permafrost/ground ice investigation in the forefields of small alpine glaciers, in *Applied Geophysics in Periglacial Environments*, edited by C. Kneisel and C. Hauck, pp. 101–108, Cambridge University Press, Cambridge., 2008.
- Delaloye, R., Lambiel, C. and Gärtner-Roer, I.: Overview of rock glacier kinematics research in the Swiss Alps, *Geographica Helvetica*, 65(2), 135–145, doi:10.5194/gh-65-135-2010, 2010.
- Delaloye, R., Lambiel, C., Lugon, R., Raetzo, H. and Strozzi, T.: Surging rock glaciers : observations in the Valais Alps, in *2nd Swiss Geoscience Meeting, Lausanne. Abstract.*, 2005.
- Delaloye, R., Morard, S., Barboux, C., Abbet, D., Gruber, V., Riedo, M. and Gachet, S.: Rapidly moving rock glaciers in Mattertal, in *Jahrestagung der Schweizerischen Geomorphologischen Gesellschaft 2011, St. Niklaus*, pp. 21–31., 2013.

Delaloye, R., Perruchoud, E., Avian, M., Kaufmann, V., Bodin, X., Hausmann, H., Ikeda, A., Kääh, A., Kellerer-Pirklbauer, A., Krainer, K., Lambiel, C., Mihajlovic, D., Staub, B., Roer, I. and Thibert, E.: Recent Interannual variations of rockglaciers creep in the European Alps, in *Proceedings of the 9th International Conference on Permafrost*, Fairbanks, Alaska, pp. 343–348., 2008.

Delaloye, R., Reynard, E. and Lambiel, C.: Pergélisol et construction de remontées mécaniques: l'exemple des Lapires (Mont-Gelé, Valais), *Le gel en géotechnique*. Publications de la Société Suisse de Mécanique des Sols et des Roches, 141, 103–113, 2001.

Delaloye, R., Reynard, E., Lambiel, C., Marescot, L. and Monnet, R.: Thermal anomaly in a cold scree slope, Creux du Van, Switzerland, in *Proceedings of the 8th International Conference on Permafrost*, 21-25 July 2003, Zurich, Switzerland, pp. 175–180., 2003.

Deline, P., Gruber, S., Delaloye, R., Fischer, L., Geertsema, M., Giardino, M., Hasler, A., Kirkbride, M., Krautblatter, M., Magnin, F., McColl, S., Ravel, L. and Schoeneich, P.: Ice Loss and Slope Stability in High-Mountain Regions, in *Snow and Ice-Related Hazards, Risks and Disasters*, edited by J. Shroder, W. Haerberli, and C. Whiteman, pp. 521–561, Elsevier., 2015.

Duval, P., Montagnat, M., Grennerat, F., Weiss, J., Meyssonier, J. and Philip, A.: Creep and plasticity of glacier ice: A material science perspective, *Journal of Glaciology*, 56(200), 1059–1068, doi:10.3189/002214311796406185, 2010.

Ekici, A., Chadburn, S., Chaudhary, N., Hajdu, L. H., Marmy, A., Peng, S., Boike, J., Burke, E., Friend, a. D., Hauck, C., Krinner, G., Langer, M., Miller, P. a. and Beer, C.: Site-level model intercomparison of high latitude and high altitude soil thermal dynamics in tundra and barren landscapes, *The Cryosphere*, 9(4), 1343–1361, doi:10.5194/tc-9-1343-2015, 2015.

Endrizzi, S. and Gruber, S.: Investigating the Effects of Lateral Water Flow on the Spatial Patterns of Thaw Depth, in *Tenth International Conference on Permafrost*, Salekhard, Yamal-Nenets Autonomous District, Russia, 25 June 2012 - 29 June 2012, pp. 91–96., 2012.

Falge, E., Baldocchi, D., Olson, R., Anthoni, P., Aubinet, M., Bernhofer, C., Burba, G., Ceulemans, R., Clement, R., Dolman, H., Granier, A., Gross, P., Grünwald, T., Hollinger, D., Jensen, N. O., Katul, G., Keronen, P., Kowalski, A., Lai, C. T., Law, B. E., Meyers, T., Moncrieff, J., Moors, E., Munger, J. W., Pilegaard, K., Rannik, Ü., Rebmann, C., Suyker, A., Tenhunen, J., Tu, K., Verma, S., Vesala, T., Wilson, K. and Wofsy, S.: Gap filling strategies for defensible annual sums of net ecosystem exchange, *Agricultural and Forest Meteorology*, 107(1), 43–69, doi:10.1016/S0168-1923(00)00225-2, 2001.

Fey, C., Rutzinger, M., Wichmann, V., Prager, C., Bremer, M. and Zangerl, C.: Deriving 3D displacement vectors from multi-temporal airborne laser scanning data for landslide activity analyses, *GIScience & Remote Sensing*, 1–25, doi:10.1080/15481603.2015.1045278, 2015.

Fischer, L. and Huggel, C.: Methodical design for stability assessments of permafrost-affected high-mountain rock walls, *Proc. 9th Int. Conf. on Permafrost*, University of Alaska, (July), 439–444, 2008.

Frei, C.: Interpolation of temperature in a mountainous region using nonlinear profiles and non-Euclidean distances, *International Journal of Climatology*, 34(5), 1585–1605, doi:10.1002/joc.3786, 2014.

Freifeld, B. M., Finsterle, S., Onstott, T. C., Toole, P. and Pratt, L. M.: Ground surface temperature reconstructions: Using in situ estimates for thermal conductivity acquired with a fiber-optic distributed thermal perturbation sensor, *Geophysical Research Letters*, 35(14), 3–7, doi:10.1029/2008GL034762, 2008.

Gądek, B. and Leszkiewicz, J.: Influence of snow cover on ground surface temperature in the zone of sporadic permafrost, Tatra Mountains, Poland and Slovakia, *Cold Regions Science and Technology*, 60(3), 205–211, doi:10.1016/j.coldregions.2009.10.004, 2010.

Gao, L., Bernhardt, M. and Schulz, K.: Elevation correction of ERA-Interim temperature data in complex terrain, *Hydrology and Earth System Sciences*, 16(12), 4661–4673, doi:10.5194/hess-16-4661-2012, 2012.

References

- Gärtner-Roer, I.: Sediment transfer rates of two active rockglaciers in the Swiss Alps, *Geomorphology*, 167-168, 45–50, doi:10.1016/j.geomorph.2012.04.013, 2012.
- Gisnås, K., Westermann, S., Schuler, T. V., Litherland, T., Isaksen, K., Boike, J. and Etzelmüller, B.: A statistical approach to represent small-scale variability of permafrost temperatures due to snow cover, *The Cryosphere*, 8(6), 2063–2074, doi:10.5194/tc-8-2063-2014, 2014.
- Glen, J. W.: The Creep of Polycrystalline Ice, *Proceedings of the Royal Society A: Mathematical, Physical and Engineering Sciences*, 228(1175), 519–538, doi:10.1098/rspa.1955.0066, 1955.
- Gobiet, A., Kotlarski, S., Beniston, M., Heinrich, G., Rajczak, J. and Stoffel, M.: 21st century climate change in the European Alps-A review, *Science of the Total Environment*, 493, 1138–1151, doi:10.1016/j.scitotenv.2013.07.050, 2014.
- Goodrich, L. E.: The influence of snow cover on the ground thermal regime, *Canadian Geotechnical Journal*, 19(4), 421–432, doi:10.1139/t82-047, 1982.
- Gruber, S.: Permafrost thaw and destabilization of Alpine rock walls in the hot summer of 2003, *Geophysical Research Letters*, 31(13), 1–4, doi:10.1029/2004GL020051, 2004.
- Gruber, S. and Haeberli, W.: Permafrost in steep bedrock slopes and its temperature-related destabilization following climate change, *Journal of Geophysical Research*, 112(F2), 10, doi:10.1029/2006JF000547, 2007.
- Gruber, S. and Haeberli, W.: Mountain Permafrost, in *Permafrost Soils*, vol. 16, edited by R. Margesin, pp. 33–44, Springer Berlin Heidelberg, Berlin, Heidelberg., 2009.
- Gruber, S. and Hoelzle, M.: The cooling effect of coarse blocks revisited: a modeling study of a purely conductive mechanism, in *Proceedings of the 9th International Conference on Permafrost*, Fairbanks, Alaska, pp. 557–561., 2008.
- Gruber, S., Hoelzle, M. and Haeberli, W.: Rock-wall temperatures in the Alps: Modelling their topographic distribution and regional differences, *Permafrost and Periglacial Processes*, 15(January), 299–307, doi:10.1002/ppp.501, 2004.
- Gubler, S., Fiddes, J., Keller, M. and Gruber, S.: Scale-dependent measurement and analysis of ground surface temperature variability in alpine terrain, *The Cryosphere*, 5(2), 431–443, doi:10.5194/tc-5-431-2011, 2011.
- Gudmundsson, L., Bremnes, J. B., Haugen, J. E. and Engen-Skaugen, T.: Technical Note: Downscaling RCM precipitation to the station scale using statistical transformations - a comparison of methods, *Hydrology and Earth System Sciences*, 16(9), 3383–3390, doi:10.5194/hess-16-3383-2012, 2012.
- Haberkorn, A., Phillips, M., Kenner, R., Rhyner, H., Bavay, M., Galos, S. P. and Hoelzle, M.: Thermal Regime of Rock and Its Relation To Snow Cover in Steep Alpine Rock Walls: Gemsstock, Central Swiss Alps, *Geografiska Annaler: Series A, Physical Geography*, 1–19, doi:10.1111/geoa.12101, 2015.
- Haeberli, W.: Die Basis-Temperatur der winterlichen Schneedecke als möglicher Indikator für die Verbreitung von Permafrost in den Alpen, *Zeitschrift für Gletscherkunde und Glazialgeologie*, 9, 221–227, 1973.
- Haeberli, W.: Untersuchungen zur Verbreitung von Permafrost zwischen Flüelapass und Piz Grialetsch (Graubünden), *Mitteilungen der Versuchsanstalt für Wasserbau, Hydrologie und Glaziologie ETH Zürich*, 17, 228pp., 1975.
- Haeberli, W.: Creep of mountain permafrost: Internal structure and flow of alpine rock glaciers, *Mitteilungen der Versuchsanstalt für Wasserbau, Hydrologie und Glaziologie ETH Zürich*, 77, 142, 1985.
- Haeberli, W., Hallet, B., Arenson, L., Elconin, R., Humlum, O., Ka, A., Käab, A., Kaufmann, V., Ladanyi, B., Matsuoka, N., Springman, S. and Vonder Mühll, D.: Permafrost creep and rock glacier dynamics, *Permafrost and Periglacial Processes*, 214(3), 189–214, doi:10.1002/ppp, 2006.

Haeberli, W., Huder, J., Keusen, H., Pika, J. and Röthlisberger, H.: Core drilling through rock glacier permafrost: V. International Conference on Permafrost, Proceedings, in Proceedings of the 5th International Conference on Permafrost, Trondheim, Norway, pp. 937–942, Versuchsanst. f{ü}r Wasserbau, Hydrologie u. Glaziologie an d. Eidg. Techn. Hochsch., 1988.

Hanson, S. and Hoelzle, M.: Installation of a shallow borehole network and monitoring of the ground thermal regime of a high alpine discontinuous permafrost environment, Eastern Swiss Alps, Norsk Geografisk Tidsskrift - Norwegian Journal of Geography, 59(2), 84–93, doi:10.1080/00291950510020664, 2005.

Harris, C., Arenson, L. U., Christiansen, H. H., Etzelmüller, B., Frauenfelder, R., Gruber, S., Haeberli, W., Hauck, C., Hoelzle, M., Humlum, O., Isaksen, K., Kääb, A., Kern-Lütschg, M. A., Lehning, M., Matsuoka, N., Murton, J. B., Noetzli, J., Phillips, M., Ross, N., Seppälä, M., Springman, S. M. and Vonder Mühll, D.: Permafrost and climate in Europe: Monitoring and modelling thermal, geomorphological and geotechnical responses, Earth-Science Reviews, 92(3-4), 117–171, doi:10.1016/j.earscirev.2008.12.002, 2009.

Harris, C. and Davies, M.: The assessment of potential geotechnical hazards associated with mountain permafrost in a warming global climate, Permafrost and Periglacial, 156(October 2000), 145–156, doi:10.1002/ppp, 2001.

Harris, C. and Murton, J. B.: Interactions between glaciers and permafrost: an introduction, Geological Society, London, Special Publications, 242(1), 1–9, doi:10.1144/GSL.SP.2005.242.01.01, 2005.

Harris, C., Vonder Mühll, D., Isaksen, K., Haeberli, W., Sollid, J. L., King, L., Holmlund, P., Dramis, F., Guglielmin, M. and Palacios, D.: Warming permafrost in European mountains, Global and Planetary Change, 39(3-4), 215–225, doi:10.1016/j.gloplacha.2003.04.001, 2003.

Harris, S. A. and Pedersen, D. E.: Thermal regimes beneath coarse blocky materials, Permafrost and Periglacial Processes, 9(2), 107–120, doi:10.1002/(SICI)1099-1530(199804/06)9:2<107::AID-PPP277>3.0.CO;2-G, 1998.

Hasler, A.: Thermal conditions and kinematics of steep bedrock permafrost, PhD Thesis, Department of Geography, University of Zurich., 2011.

Hasler, A., Gruber, S. and Haeberli, W.: Temperature variability and offset in steep alpine rock and ice faces, The Cryosphere, 5(November), 977–988, 2011.

Hauck, C.: Frozen ground monitoring using DC resistivity tomography, Geophysical Research Letters, 29(21), 10–13, doi:10.1029/2002GL014995, 2002.

Hauck, C.: New Concepts in Geophysical Surveying and Data Interpretation for Permafrost Terrain, Permafrost and Periglacial Processes, doi:10.1002/ppp.1774, 2013.

Hauck, C., Bach, M. and Hilbich, C.: A four-phase model to quantify subsurface ice and water content in permafrost regions based on geophysical data sets, in Proceedings of the 9th International Conference on Permafrost, edited by D. L. Kane and K. M. Hinkel, pp. 675–680., 2008.

Hauck, C., Böttcher, M. and Maurer, H.: A new model for estimating subsurface ice content based on combined electrical and seismic data sets, The Cryosphere, 5(2), 453–468, doi:10.5194/tc-5-453-2011, 2011.

Hauck, C., Delaloye, R., Gärtner-Roer, I., Hasler, A., Hilbich, C., Hoelzle, M., Kenner, R., Kotlarski, S., Lambiel, C., Lüthi, R., Marmy, A., Müller, J., Noetzli, J., Phillips, M., Rajczak, J., Salzmann, N., Schaepman, M., Schär, C., Staub, B. and Völksch, I.: The Evolution of Mountain Permafrost in Switzerland (TEMPS): Final Scientific Report., 2015.

Hauck, C. and Kneisel, C.: Applied Geophysics in Periglacial Environments, Cambridge University Press., 2008.

References

- Hecht, S.: Fallbeispiele zur Anwendung refraktionsseismischer Methoden bei der Erkundung des oberflächennahen Untergrundes, *Zeitschrift für Geomorphologie, Supplement*, 123, 111–123, 2000.
- Hilbich, C.: Geophysical monitoring systems to assess and quantify ground ice evolution in mountain permafrost, PhD Thesis, Department of Geography, University of Jena., 2009.
- Hilbich, C.: Time-lapse refraction seismic tomography for the detection of ground ice degradation, *The Cryosphere*, 4(3), 243–259, doi:10.5194/tc-4-243-2010, 2010.
- Hilbich, C., Fuss, C. and Hauck, C.: Automated Time-lapse ERT for Improved Process Analysis and Monitoring of Frozen Ground, *Permafrost and Periglacial Processes*, 22(4), 306–319, doi:10.1002/ppp.732, 2011.
- Hilbich, C., Marescot, L., Hauck, C., Loke, M. H. and Mäusbacher, R.: Applicability of electrical resistivity tomography monitoring to coarse blocky and ice-rich permafrost landforms, *Permafrost and Periglacial Processes*, 20(3), 269–284, doi:10.1002/ppp.652, 2009.
- Hipp, T.: Mountain Permafrost in Southern Norway: Distribution, Spatial Variability and Impacts of Climate Change, PhD Thesis, Faculty of Mathematics and Natural Science, University of Oslo., 2012.
- Hoelzle, M., Haeberli, W. and Keller, F.: Application of BTS-measurements for modelling mountain permafrost distribution, in *Proceedings of the 6th International Conference on Permafrost*, Beijing, China, pp. 272–277, South China University of Technology Press., 1993.
- Hoelzle, M., Mittaz, C., Etzelmüller, B. and Haeberli, W.: Surface energy fluxes and distribution models of permafrost in European mountain areas: an overview of current developments, *Permafrost and Periglacial Processes*, 12(1), 53–68, doi:10.1002/ppp.385, 2001.
- Hoelzle, M., Wegmann, M. and Krummenacher, B.: Miniature temperature dataloggers for mapping and monitoring of permafrost in high mountain areas: first experience from the Swiss Alps, *Permafrost and Periglacial Processes*, 10(2), 113–124, doi:10.1002/(SICI)1099-1530(199904/06)10:2<113::AID-PPP317>3.0.CO;2-A, 1999.
- Hüsler, F., Jonas, T., Riffler, M., Musial, J. P. and Wunderle, S.: A satellite-based snow cover climatology (1985–2011) for the European Alps derived from AVHRR data, *The Cryosphere*, 8(1), 73–90, doi:10.5194/tc-8-73-2014, 2014.
- Huss, M.: Extrapolating glacier mass balance to the mountain-range scale: The European Alps 1900–2100, *Cryosphere*, 6(2005), 713–727, doi:10.5194/tc-6-713-2012, 2012.
- Ikeda, A., Matsuoka, N. and Käab, A.: Fast deformation of perennially frozen debris in a warm rock glacier in the Swiss Alps: An effect of liquid water, *Journal of Geophysical Research*, 113(F1021), 1–12, doi:10.1029/2007JF000859, 2008.
- IPCC: *Climate Change 2013: Working Group I Contribution to the Fifth Assessment Report of the Intergovernmental Panel on Climate Change*, WMO / UNEP, Cambridge University Press, Geneva., 2013.
- Isaksen, K., Hauck, C., Gudevang, E., Ødegård, R. S. and Sollid, J. L.: Mountain permafrost distribution in Dovrefjell and Jotunheimen, southern Norway, based on BTS and DC resistivity tomography data, *Norsk Geografisk Tidsskrift - Norwegian Journal of Geography*, 56(2), 122–136, doi:10.1080/002919502760056459, 2002.
- Isaksen, K., Ødegård, R. S., Etzelmüller, B., Hilbich, C., Hauck, C., Farbrot, H., Eiken, T., Hygen, H. O. and Hipp, T. F.: Degrading Mountain Permafrost in Southern Norway: Spatial and Temporal Variability of Mean Ground Temperatures, 1999–2009, *Permafrost and Periglacial Processes*, 22(4), 361–377, doi:10.1002/ppp.728, 2011.
- Ishikawa, M.: Thermal regimes at the snow–ground interface and their implications for permafrost investigation, *Geomorphology*, 52(1-2), 105–120, doi:10.1016/S0169-555X(02)00251-9, 2003.
- Jansson, P. E.: CoupModel: Model Use, Calibration, and Validation, *Transactions of the ASABE*, 55(4), 1337–1346, doi:10.13031/2013.42245, 2012.

- Jansson, P. E. and Karlberg, L.: Coupled heat and mass transfer model for soil-plant-atmosphere systems, , 364, 2004.
- Jonas, T., Marty, C. and Magnusson, J.: Estimating the snow water equivalent from snow depth measurements in the Swiss Alps, *Journal of Hydrology*, 378(1-2), 161–167, doi:10.1016/j.jhydrol.2009.09.021, 2009.
- Kääb, A., Frauenfelder, R. and Roer, I.: On the response of rockglacier creep to surface temperature increase, *Global and Planetary Change*, 56(1-2), 172–187, doi:10.1016/j.gloplacha.2006.07.005, 2007.
- Kääb, A., Haeberli, W. and Gudmundsson, G. H.: Analysing the creep of mountain permafrost using high precision aerial photogrammetry: 25 years of monitoring Gruben rock glacier, Swiss Alps, *Permafrost and Periglacial Processes*, 8(October), 409–426, 1997.
- Kääb, A., Kaufmann, V., Ladstädter, R. and Eiken, T.: Rock glacier dynamics: implications from high-resolution measurements of surface velocity fields, in *Proceedings of the 8th International Conference on Permafrost*, 21-25 July 2003, Zurich, Switzerland, vol. 1, pp. 501–506., 2003.
- Kääb, A., Reynolds, J. and Haeberli, W.: Glacier and permafrost hazards in high mountains, *Global Change and Mountain Regions*, 225–234, 2005.
- Kannan, K. and Rajagopal, K. R.: A model for the flow of rock glaciers, *International Journal of Non-Linear Mechanics*, 48, 59–64, doi:10.1016/j.ijnonlinmec.2012.06.002, 2013.
- Kaufmann, V.: Deformation analysis of the Doesen rock glacier (Austria), in *Proceedings of the 7th International Conference on Permafrost*, pp. 551–556, Collection Nordicana 55, Yellowknife, Canada., 1998.
- Kaufmann, V.: Detection and quantification of rock glacier creep using high-resolution orthoimages of virtual globes, *International Archives of the Photogrammetry, Remote Sensing and Spatial Information Sciences*, XXII ISPRS Congress, 25 August – 01 September 2012, Melbourne, Australia., XXXIX(B5), 517–522, 2012.
- Kaufmann, V. and Ladstädter, R.: Quantitative analysis of rock glacier creep by means of digital photogrammetry using multi-temporal aerial photographs: two case studies in the Austrian Alps, in *8th International Conference on Permafrost*, Zurich, Switzerland, pp. 525–530., 2003.
- Kaufmann, V., Ladstädter, R. and Kienast, G.: 10 years of monitoring of the Doesen rock glacier (Ankogel Group, Austria) - A review of the research activities for the time period 1995-2005, Petrovic D. (Ed.): *Proceedings 5th Mountain Cartography Workshop*, 29 March - 1 April 2006, Bohinj, Slovenia, 129–144, 2007.
- Keller, F.: *Interaktionen zwischen Schnee und Permafrost. Eine Grundlagenstudie im Oberengadin. Mitteilungen der VAW-ETH Zürich*, Zürich., 1994.
- Keller, F., Frauenfelder, R., Gardaz, J.-M., Hoelzle, M., Kneisel, C., Lugon, R., Phillips, M., Reynard, E. and Wenker, L.: Permafrost map of Switzerland, in *Proceedings of the 7th International Conference on Permafrost*, Yellowknife (Canada), pp. 557–562., 1998.
- Keller, F. and Gubler, H.: Interaction between snow cover and high mountain permafrost, Murtèl-Corvatsch, Swiss Alps, in *Proceedings of the 6th International Conference on Permafrost*, Beijing, China, vol. 1, edited by J. Brown, H. M. French, N. A. Grave, C. Guodong, L. King, E. A. Koster, and T. L. Pève, pp. 332–337, South China University of Technology Press, Wushan Guangzhou China., 1993.
- Kellerer-Pirklbauer, A. and Kaufmann, V.: About the relationship between rock glacier velocity and climate parameters in central Austria, *Austrian Journal of Earth Sciences*, 105(2), 94–112, 2012.
- Kenner, R., Bühler, Y., Delaloye, R., Ginzler, C. and Phillips, M.: Monitoring of high alpine mass movements combining laser scanning with digital airborne photogrammetry, *Geomorphology*, 206, 492–504, doi:10.1016/j.geomorph.2013.10.020, 2014.
- Kölbing, D.: *Saisonale Bewegungen des Blockgletschers im Furggentälte*, Gemmi/VS, Diploma thesis, Department of Geography, University of Berne., 2001.

References

- Kotlarski, S., Luethi, D. and Schaer, C.: The elevation dependency of 21st century European climate change: an RCM ensemble perspective, *International Journal of Climatology*, n/a–n/a, doi:10.1002/joc.4254, 2015.
- Kraus, K.: *Photogrammetry: Geometry from Images and Laser Scans*, Second Edi., De Gruyter, Goettingen, Germany., 2007.
- Krautblatter, M., Funk, D. and Günzel, F. K.: Why permafrost rocks become unstable: A rock-ice-mechanical model in time and space, *Earth Surface Processes and Landforms*, 38, 876–887, doi:10.1002/esp.3374, 2013.
- Krautblatter, M., Huggel, C., Deline, P. and Hasler, A.: Research Perspectives on Unstable High-alpine Bedrock Permafrost: Measurement, Modelling and Process Understanding, *Permafrost and Periglacial Processes*, 23(1), 80–88, doi:10.1002/ppp.740, 2012.
- Krummenacher, B., Budmiger, K., Mihajlovic, D. and Blank, B.: *Periglaziale Prozesse und Formen im Furggentälti, Gemmipass*, Mitteilungen SLF, 56, 245 pp., 1998.
- Krummenacher, B., Mihajlovic, D., Nussbaum, A. and Staub, B.: *20 Jahre Furggentälti - Permafrostuntersuchungen auf der Gemmi*, G80 ed., Geographica Bernensia, Bern., 2008.
- Kummert, M. and Delaloye, R.: Quantifying sediment transfer between the front of an active alpine rock glacier and a torrential gully, in *Geomorphometry for Geosciences*, edited by J. Jasiewicz, Z. Zwolinski, H. Mitasova, and T. Hengl, pp. 193–196, Adam Mickiewicz University in Poznan - Institute of Geoecology and Geoinformation, International Society for Geomorphometry, Poznan., 2015.
- Lambiel, C.: *Inventaire des glaciers rocheux entre le Val de Bagnes et le Val d'Heremence (Valais)*, Université de Lausanne., 1999.
- Lambiel, C.: *Le pergélisol dans les terrains sédimentaires à forte déclivité: distribution, régime thermique et instabilités*, Travaux et recherches Vol 33., 2006.
- Lambiel, C. and Delaloye, R.: Contribution of real-time kinematic GPS in the study of creeping mountain permafrost: examples from the Western Swiss Alps, *Permafrost and Periglacial Processes*, 15(3), 229–241, doi:10.1002/ppp.496, 2004.
- Lawrence, D. M. and Slater, A. G.: A projection of severe near-surface permafrost degradation during the 21st century, *Geophysical Research Letters*, 32(24), 1–5, doi:10.1029/2005GL025080, 2005.
- Lehning, M., Völksch, I., Gustafsson, D., Nguyen, T. A., Stähli, M. and Zappa, M.: ALPINE3D: a detailed model of mountain surface processes and its application to snow hydrology, *Hydrological Processes*, 20(10), 2111–2128, doi:10.1002/hyp.6204, 2006.
- Lewkowicz, A. G.: Temperature regime of a small sandstone tor, latitude 80 °N, Ellesmere Island, Nunavut, Canada, *Permafrost and Periglacial Processes*, 12(4), 351–366, doi:10.1002/ppp.396, 2001.
- Lewkowicz, A. G.: Evaluation of miniature temperature-loggers to monitor snowpack evolution at mountain permafrost sites, northwestern Canada, *Permafrost and Periglacial Processes*, 19(3), 323–331, doi:10.1002/ppp.625, 2008.
- Loke, M. H. and Barker, R. D.: Rapid least-squares inversion of apparent resistivity pseudosections by a quasi-Newton method, *Geophysical Prospecting*, 44(1), 131–152, doi:10.1111/j.1365-2478.1996.tb00142.x, 1996.
- Luetsch, M., Lehning, M. and Haeberli, W.: A sensitivity study of factors influencing warm/thin permafrost in the Swiss Alps, *Journal of Glaciology*, 54(187), 696–704, doi:10.3189/002214308786570881, 2008.
- Lugon, R., Delaloye, R., Serrano, E., Reynard, E., Lambiel, C. and González-Trueba, J. J.: Permafrost and Little Ice Age glacier relationships, Posets Massif, Central Pyrenees, Spain, *Permafrost and Periglacial Processes*, 15(3), 207–220, doi:10.1002/ppp.494, 2004.

- Lugon, R. and Stoffel, M.: Rock-glacier dynamics and magnitude-frequency relations of debris flows in a high-elevation watershed: Ritigraben, Swiss Alps, *Global and Planetary Change*, 73(3-4), 202–210, 2010.
- Magnin, F., Deline, P., Ravel, L., Noetzli, J. and Pogliotti, P.: Thermal characteristics of permafrost in the steep alpine rock walls of the Aiguille du Midi (Mont Blanc Massif, 3842 m a.s.l), *The Cryosphere*, 9(1), 109–121, doi:10.5194/tc-9-109-2015, 2015.
- Marmy, A., Rajczak, J., Delaloye, R., Hilbich, C., Hoelzle, M., Kotlarski, S., Lambiel, C., Noetzli, J., Phillips, M., Salzmann, N., Staub, B. and Hauck, C.: Semi-automated calibration method for modelling of mountain permafrost evolution in Switzerland, *The Cryosphere Discussions*, 9(5), 4787–4843, doi:10.5194/tcd-9-4787-2015, 2015.
- Marmy, A., Salzmann, N., Scherler, M. and Hauck, C.: Permafrost model sensitivity to seasonal climatic changes and extreme events in mountainous regions, *Environmental Research Letters*, 8(3), 035048, doi:10.1088/1748-9326/8/3/035048, 2013.
- Marty, C.: Regime shift of snow days in Switzerland, *Geophysical Research Letters*, 35(12), 1–5, doi:10.1029/2008GL033998, 2008.
- Medici, F. and Rybach, L.: Geothermal map of Switzerland, *Géophysique*, 30, 1995.
- MeteoSwiss: Klimareport 2013, Bundesamt für Meteorologie und Klimatologie MeteoSchweiz, Zürich., 2014.
- Mihajlovic, D., Kölbinger, D., Kunz, I., Schab, S., Kienholz, H., Budmiger, M. and Imhof, M.: Developing new methods for monitoring periglacial phenomena, *Proceedings of the 8th International Conference on Permafrost*, 21-25 July 2003, Zurich, Switzerland, 765–770, 2003.
- Milsom, J. and Eriksen, A.: *Field Geophysics*, John Wiley & Sons, Ltd, Chichester, UK., 2011.
- Mittaz, C., Hoelzle, M. and Haeberli, W.: First results and interpretation of energy-flux measurements over Alpine permafrost, *Annals of Glaciology*, 31(1), 275–280, doi:10.3189/172756400781820363, 2000.
- Moffat, A. M., Papale, D., Reichstein, M., Hollinger, D. Y., Richardson, A. D., Barr, A. G., Beckstein, C., Braswell, B. H., Churkina, G., Desai, A. R., Falge, E., Gove, J. H., Heimann, M., Hui, D., Jarvis, A. J., Kattge, J., Noormets, A. and Stauch, V. J.: Comprehensive comparison of gap-filling techniques for eddy covariance net carbon fluxes, *Agricultural and Forest Meteorology*, 147(3-4), 209–232, doi:10.1016/j.agrformet.2007.08.011, 2007.
- Morán-Tejeda, E., López-Moreno, J. I. and Beniston, M.: The changing roles of temperature and precipitation on snowpack variability in Switzerland as a function of altitude, *Geophysical Research Letters*, 40(10), 2131–2136, doi:10.1002/grl.50463, 2013.
- Morard, S., Delaloye, R. and Dorthe, J.: Seasonal thermal regime of a mid-latitude ventilated debris accumulation, in *Proceedings of the 9th International Conference on Permafrost*, Fairbanks, Alaska, pp. 1233–1238., 2008.
- Müller, J., Gärtner-Roer, I., Kenner, R., Thee, P. and Morche, D.: Sediment storage and transfer on a periglacial mountain slope (Corvatsch, Switzerland), *Geomorphology*, 218, 35–44, doi:10.1016/j.geomorph.2013.12.002, 2014a.
- Müller, J., Gärtner-Roer, I., Thee, P. and Ginzler, C.: Accuracy assessment of airborne photogrammetrically derived high-resolution digital elevation models in a high mountain environment, *ISPRS Journal of Photogrammetry and Remote Sensing*, 98, 58–69, doi:10.1016/j.isprsjprs.2014.09.015, 2014b.
- Noetzli, J. and Gruber, S.: *Alpiner Permafrost - ein Überblick*, Lintzmeyer, K. (Ed.), Jahrbuch des Vereins zum Schutz der Bergwelt, Selbstverlag, München, 70, 111–121, 2005.
- Noetzli, J. and Gruber, S.: Transient thermal effects in Alpine permafrost, *The Cryosphere*, 3(1), 85–99, doi:10.5194/tc-3-85-2009, 2009.

References

- Noetzli, J., Gruber, S., Kohl, T., Salzmann, N. and Haeberli, W.: Three-dimensional distribution and evolution of permafrost temperatures in idealized high-mountain topography, *Journal of Geophysical Research*, 112(F02S13), 1–14, doi:10.1029/2006JF000545, 2007.
- Oke, T. R.: *Boundary Layer Climates*, Second Edi., Cambridge University Press, Cambridge., 1987.
- Olaya, V.: Basic Land-Surface Parameters, in *Geomorphometry - Concepts, Software, Applications*, vol. 33, pp. 141–169, Elsevier., 2009.
- Osterkamp, T. E. and Osterkamp, T. E.: Response of Alaskan Permafrost to climate, in *Proceedings of the IV. International Conference on Permafrost*, Fairbanks, Alaska, USA, pp. 145–152., 1983.
- Outcalt, S. I., Nelson, F. E. and Hinkel, K. M.: The zero-curtain effect: Heat and mass transfer across an isothermal region in freezing soil, *Water Resources Research*, 26(7), 1509–1516, doi:10.1029/WR026i007p01509, 1990.
- Paine, D. P. and Kiser, J. D.: *Aerial Photography and Image Interpretation*, John Wiley & Sons, Inc., Hoboken, NJ, USA., 2012.
- PERMOS: Permafrost in Switzerland 2004/2005 and 2005/2006. Noetzli, J., Naegeli, B., and Vonder Muehll, D. (eds.), *Glaciological Report Permafrost No. 6/7 of the Cryospheric Commission of the Swiss Academy of Sciences.*, 2009.
- PERMOS: Permafrost in Switzerland 2006/2007 and 2007/2008. Noetzli, J. and Vonder Muehll, D. (eds.), *Glaciological Report Permafrost No. 8/9 of the Cryospheric Commission of the Swiss Academy of Sciences.*, 2010.
- PERMOS: Permafrost in Switzerland 2008/2009 and 2009/2010. Noetzli, J. (ed.), *Glaciological Report Permafrost No. 10/11 of the Cryospheric Commission of the Swiss Academy of Sciences*, Zurich, Switzerland., 2013.
- PERMOS 2016: PERMOS Database. Swiss Permafrost Monitoring Network, Fribourg, Switzerland. DOI:10.13093/permos-2016-01.
- Perruchoud, E. and Delaloye, R.: Short-Term Changes in Surface Velocities on the Becs-de-Bosson Rock Glacier (Western Swiss Alps), *Grazer Schriften der Geographie*, 43(September), 131–136, 2007.
- Phillips, M., Mutter, E. Z., Kern-Luetschg, M. and Lehning, M.: Rapid degradation of ground ice in a ventilated talus slope: Flüela Pass, Swiss Alps, *Permafrost and Periglacial Processes*, 20(1), 1–14, doi:10.1002/ppp.638, 2009.
- Pomeroy, J. W. and Brun, E.: Physical properties of snow, in *Snow ecology: an interdisciplinary examination of snow-covered ecosystems*, vol. 7, edited by H. G. Jones, J. W. Pomeroy, D. A. Walker, and R. W. Hoham, pp. 45–118, Cambridge University Press, Cambridge, UK., 2001.
- Rajczak, J., Kotlarski, S., Salzmann, N. and Schär, C.: Robust climate scenarios for sites with sparse observations: a two-step bias correction approach, *International Journal of Climatology*, n/a–n/a, doi:10.1002/joc.4417, 2015.
- Rajczak, J., Pall, P. and Schaer, C.: Projections of extreme precipitation events in regional climate simulations for Europe and the Alpine Region, *Journal of Geophysical Research: Atmospheres*, 118(9), 3610–3626, doi:10.1002/jgrd.50297, 2013.
- Rangecroft, S., Harrison, S., Anderson, K., Magrath, J., Castel, A. P. and Pacheco, P.: Climate change and water resources in arid mountains: An example from the bolivian andes, *Ambio*, 42(7), 852–863, doi:10.1007/s13280-013-0430-6, 2013.
- Ravello, L., Allignol, F., Deline, P., Gruber, S. and Ravello, M.: Rock falls in the Mont Blanc Massif in 2007 and 2008, *Landslides*, 7(4), 493–501, doi:10.1007/s10346-010-0206-z, 2010.
- Rist, A. and Phillips, M.: First results of investigations on hydrothermal processes within the active layer above alpine permafrost in steep terrain, *Norsk Geografisk Tidsskrift - Norwegian Journal of Geography*, 59(2), 177–183, doi:10.1080/00291950510020574, 2005.

- Rist, A., Phillips, M. and Springman, S. M.: Inclinable Shear Box Simulations of Deepening Active Layers on Perennially Frozen Scree Slopes, *Permafrost and Periglacial Processes*, 23(1), 26–38, doi:10.1002/ppp.1730, 2012.
- Roer, I., Haeberli, W., Avian, M., Kaufmann, V., Delaloye, R., Lambiel, C. and Kääh, A.: Observations and considerations on destabilizing active rock glaciers in the European Alps, in *Proceedings of the 9th International Conference on Permafrost*, Fairbanks, Alaska, pp. 1505–1510., 2008.
- Roer, I., Kääh, A. and Dikau, R.: Rockglacier acceleration in the Turtmann valley (Swiss Alps): Probable controls, *Norsk Geografisk Tidsskrift - Norwegian Journal of Geography*, 59(2), 157–163, doi:10.1080/00291950510020655, 2005.
- Rolland, C.: Spatial and Seasonal Variations of Air Temperature Lapse Rates in Alpine Regions, *Journal of Climate*, 16(7), 1032–1046, doi:10.1175/1520-0442(2003)016<1032:SASVOA>2.0.CO;2, 2003.
- Scapozza, C.: Stratigraphie, morphodynamique, paléoenvironnements des terrains sédimentaires meubles à forte déclivité du domaine périglaciaire alpin (Géovisions n°40)., 2013.
- Scapozza, C., Gex, P., Lambiel, C. and Reynard, E.: Contribution of self-potential (SP) measurements in the study of alpine periglacial hydrology: examples from the southern Swiss Alps, in *Proceedings of the 9th International Conference on Permafrost*, Fairbanks, Alaska, edited by D. Kane and K. Hinkel, pp. 1583–1588, Institute of Northern Engineering, University of Alaska Fairbanks, Fairbanks, Alaska., 2008.
- Scapozza, C., Lambiel, C., Abbet, D., Delaloye, R. and Hilbich, C.: Internal structure and permafrost characteristics of the Lapires talus slope (Nendaz, Valais). 8th Swiss Geoscience Meeting 2010, Fribourg, Switzerland, 19–20 November 2010. Extended Abstract 7.16, , 166–167, 2010.
- Schaer, C. and Jendritzky, G.: Climate change: hot news from summer 2003., *Nature*, 432(7017), 559–60, doi:10.1038/432559a, 2004.
- Scherler, M., Hauck, C., Hoelzle, M. and Salzmann, N.: Modeled sensitivity of two alpine permafrost sites to RCM-based climate scenarios, *Journal of Geophysical Research: Earth Surface*, 118(2), 780–794, doi:10.1002/jgrf.20069, 2013.
- Scherler, M., Hauck, C., Hoelzle, M., Stähli, M. and Völksch, I.: Meltwater infiltration into the frozen active layer at an alpine permafrost site, *Permafrost and Periglacial Processes*, 21(4), 325–334, doi:10.1002/ppp.694, 2010.
- Scherler, M., Schneider, S., Hoelzle, M. and Hauck, C.: A two-sided approach to estimate heat transfer processes within the active layer of the Murtèl–Corvatsch rock glacier, *Earth Surface Dynamics*, 2(1), 141–154, doi:10.5194/esurf-2-141-2014, 2014.
- Schmid, M.-O., Gubler, S., Fiddes, J. and Gruber, S.: Inferring snowpack ripening and melt-out from distributed measurements of near-surface ground temperatures, *The Cryosphere*, 6(5), 1127–1139, doi:10.5194/tc-6-1127-2012, 2012.
- Schmucki, E., Marty, C., Fierz, C. and Lehning, M.: Simulations of 21st century snow response to climate change in Switzerland from a set of RCMs, *International Journal of Climatology*, n/a–n/a, doi:10.1002/joc.4205, 2014.
- Schneider, S.: The heterogeneity of mountain permafrost - A field-based analysis of different periglacial materials, PhD Thesis, Department of Geosciences, University of Fribourg., 2014.
- Schneider, S., Hoelzle, M. and Hauck, C.: Influence of surface and subsurface heterogeneity on observed borehole temperatures at a mountain permafrost site in the Upper Engadine, Swiss Alps, *The Cryosphere*, 6(2), 517–531, doi:10.5194/tc-6-517-2012, 2012.
- Schrott, L. and Hoffmann, T.: Refraction seismics, in *Applied Geophysics in Periglacial Environments*, edited by C. Hauck and C. Kneisel, pp. 57–80, Cambridge University Press, Cambridge., 2008.
- Schuur, E. A. G., Bockheim, J., Canadell, J. G., Euskirchen, E., Field, C. B., Goryachkin, S. V., Hagemann, S., Kuhry, P., Lafleur, P. M., Lee, H., Mazhitova, G., Nelson, F. E., Rinke, A., Romanovsky, V. E.,

References

- Shiklomanov, N., Tarnocai, C., Venevsky, S., Vogel, J. G. and Zimov, S. A.: Vulnerability of Permafrost Carbon to Climate Change: Implications for the Global Carbon Cycle, *BioScience*, 58(8), 701, doi:10.1641/B580807, 2008.
- Selby, M. J.: *Hillslope Materials and Processes*, second edi., Oxford University Press., 1993.
- Smerdon, J. E., Beltrami, H., Creelman, C. and Stevens, M. B.: Characterizing land surface processes: A quantitative analysis using air-ground thermal orbits, *Journal of Geophysical Research*, 114(D15), D15102, doi:10.1029/2009JD011768, 2009.
- Sorg, A., Kääh, A., Roesch, A., Bigler, C. and Stoffel, M.: Contrasting responses of Central Asian rock glaciers to global warming, *Scientific Reports*, 5, 8228, doi:10.1038/srep08228, 2015.
- Staub, B. and Delaloye, R.: Using Near-Surface Ground Temperature Data to Derive Snow Insulation and Melt Indices for Mountain Permafrost Applications, *Permafrost and Periglacial Processes*, doi:10.1002/ppp.1890, 2016.
- Staub, B., Hasler, A., Noetzli, J. and Delaloye, R.: Gap filling algorithm for ground surface temperature data, Submitted to *Permafrost and Periglacial Processes*.
- Staub, B., Marmy, A., Hauck, C., Hilbich, C. and Delaloye, R.: Ground temperature variations in a talus slope influenced by permafrost: a comparison of field observations and model simulations, *Geographica Helvetica*, 70, 45–62, doi:10.5194/gh-70-45-2015, 2015a.
- Staub, B., Vogel, D., Budmiger, K., Krummenacher, B., Delaloye, R. and Kienholz, H.: Einsatz der Photogrammetrie und Bildanalyse zur Quantifizierung von Blockgletscherbewegungen, *Geomatik Schweiz*, 113(9), 356–361, 2015b.
- Steger, C., Kotlarski, S., Jonas, T. and Schaer, C.: Alpine snow cover in a changing climate: a regional climate model perspective, *Climate Dynamics*, 41(3-4), 735–754, doi:10.1007/s00382-012-1545-3, 2012.
- Stocker-Mittaz, C.: *Permafrost distribution modeling based on energy balance data*, PhD Thesis, University of Zurich., 2002.
- Stocker-Mittaz, C., Hoelzle, M. and Haeberli, W.: Modelling alpine permafrost distribution based on energy-balance data: a first step, *Permafrost and Periglacial Processes*, 13(4), 271–282, doi:10.1002/ppp.426, 2002.
- Tardivo, G. and Berti, A.: A Dynamic Method for Gap Filling in Daily Temperature Datasets, *Journal of Applied Meteorology and Climatology*, 51(6), 1079–1086, doi:10.1175/JAMC-D-11-0117.1, 2012.
- Tardivo, G. and Berti, A.: The selection of predictors in a regression-based method for gap filling in daily temperature datasets, *International Journal of Climatology*, 34(4), 1311–1317, doi:10.1002/joc.3766, 2014.
- Themessl, M. J., Gobiet, A. and Leuprecht, A.: Empirical-statistical downscaling and error correction of daily precipitation from regional climate models, *International Journal of Climatology*, 31(10), 1530–1544, doi:10.1002/joc.2168, 2011.
- Vonder Mühll, D., Delaloye, R., Haeberli, W., Hoelzle, M. and Krummenacher, B.: *Permafrost Monitoring Switzerland PERMOS - 1. Jahresbericht 1999/2000*, Glaciological Report (Permafrost) No. 1 of the Glaciological Commission of the Swiss Academy of Sciences., 2001a.
- Vonder Mühll, D., Hauck, C. and Gubler, H.: Mapping of mountain permafrost using geophysical methods, *Progress in Physical Geography*, 26(4), 643–660, doi:10.1191/0309133302pp356ra, 2002.
- Vonder Mühll, D., Hauck, C., Gubler, H., McDonald, R. and Russill, N.: New geophysical methods of investigating the nature and distribution of mountain permafrost with special reference to radiometry techniques, *Permafrost and Periglacial Processes*, 12(1), 27–38, doi:10.1002/ppp.382, 2001b.

- Vonder Mühll, D., Noetzli, J., Makowski, K. and Delaloye, R.: Permafrost in Switzerland 2000/2001 and 2001/2002, Glaciological Report (Permafrost) No. 2/3 of the Glaciological Commission of the Swiss Academy of Sciences, Zurich, Switzerland., 2004.
- Vonder Mühll, D., Noetzli, J., Roer, I., Makowski, K. and Delaloye, R.: Permafrost in Switzerland 2002/2003 and 2003/2004, Glaciological Report (Permafrost) No. 4/5 of the Cryospheric Commission of the Swiss Academy of Sciences, Zurich, Switzerland., 2007.
- Wagner, S.: Creep of alpine permafrost, investigated on the murtel rock glacier, *Permafrost and Periglacial Processes*, 3(2), 157–162, doi:10.1002/ppp.3430030214, 1992.
- Wakonigg, H.: Unterkühlte Schutthalden, Beiträge zur Permafrostkartierung in Österreich. Arbeiten aus dem Inst. f. Geogr. Karl-Franzens-Universität Graz, 209–223, 1996.
- Westermann, S., Boike, J., Langer, M., Schuler, T. V. and Etzelmüller, B.: Modeling the impact of wintertime rain events on the thermal regime of permafrost, *The Cryosphere*, 5(4), 945–959, doi:10.5194/tc-5-945-2011, 2011.
- Westermann, S., Schuler, T. V., Gislås, K. and Etzelmüller, B.: Transient thermal modeling of permafrost conditions in Southern Norway, *The Cryosphere*, 7(2), 719–739, doi:10.5194/tc-7-719-2013, 2013.
- Wever, N., Jonas, T., Fierz, C. and Lehning, M.: Model simulations of the modulating effect of the snow cover in a rain-on-snow event, *Hydrology and Earth System Sciences*, 18(11), 4657–4669, doi:10.5194/hess-18-4657-2014, 2014.
- Williams, P. J. and Smith, M. W.: *The Frozen Earth: Fundamentals of Geocryology*, Cambridge University Press, Cambridge., 1989.
- Wirz, V., Beutel, J., Buchli, B., Gruber, S. and Limpach, P.: Temporal Characteristics of Different Cryosphere-Related Slope Movements in High Mountains, in *Landslide Science and Practice*, pp. 383–390, Springer Berlin Heidelberg, Berlin, Heidelberg., 2013.
- Wirz, V., Beutel, J., Gruber, S., Gubler, S. and Purves, R. S.: Estimating velocity from noisy GPS data for investigating the temporal variability of slope movements, *Natural Hazards and Earth System Science*, 14(9), 2503–2520, doi:10.5194/nhess-14-2503-2014, 2014.
- Wirz, V., Gruber, S., Purves, R. S., Beutel, J., Gärtner-Roer, I., Gubler, S. and Vieli, A.: Short-term velocity variations of three rock glaciers and their relationship with meteorological conditions, *Earth Surface Dynamics Discussions*, 3(2), 459–514, doi:10.5194/esurfd-3-459-2015, 2015.
- Wirz, V., Schirmer, M., Gruber, S. and Lehning, M.: Spatio-temporal measurements and analysis of snow depth in a rock face, *The Cryosphere*, 5(4), 893–905, doi:10.5194/tc-5-893-2011, 2011.
- Zenklusen Mutter, E. and Phillips, M.: Active Layer Characteristics At Ten Borehole Sites In Alpine Permafrost Terrain, Switzerland, *Permafrost and Periglacial Processes*, 23(2), 138–151, doi:10.1002/ppp.1738, 2012.
- Zhang, T.: Influence of the seasonal snow cover on the ground thermal regime: An overview, *Reviews of Geophysics*, 43(4), RG4002, doi:10.1029/2004RG000157, 2005.
- Zingg, T.: Beziehung zwischen Temperatur und Schmelzwasser und ihre Bedeutung für Niederschlags- und Abflussfragen, IUGG General Assembly of Bruxelles, IAHS Publ. no. 32, 266–269, 1951.

PART V: JOURNAL PUBLICATIONS

Publication I

Using near-surface ground temperature data to derive snow insulation and melt indices for mountain permafrost applications

Citation: Staub, B. & Delaloye, R.: Using near-surface ground temperature data to derive snow insulation and melt indices for mountain permafrost applications. *Permafrost and Periglacial Processes*, 2016. DOI: [10.1002/ppp.1890](https://doi.org/10.1002/ppp.1890).

Abstract: The timing and duration of snow cover in areas of mountain permafrost affect the ground thermal regime by thermally insulating the ground from the atmosphere and modifying the radiation balance at the surface. Snow depth records, however, are sparse in high-mountain terrains. Here we present data processing techniques to approximate the thermal insulation effect of snow cover. We propose some simple “snow thermal insulation indices” using daily and weekly variations in ground surface temperatures (GST), as well as a “snow melt index” that approximates the snow melt rate using a degree-day approach with air temperature during the zero curtain period. The indices consider point-specific characteristics and allow reconstruction of past snow thermal conditions and snow melt rates using long GST time series. The application of these indices to GST monitoring data from the Swiss Alps revealed large spatial and temporal variability in the start and duration of the high-insulation period by snow and in the snow melt rate.

Keywords: Mountain permafrost, ground surface temperature, thermal insulation, snow onset, snow water equivalent, snow melt rate

1 Introduction

Mountain permafrost environments higher than ~2500 m above sea level (asl) in the Swiss Alps (Noetzli and Gruber, 2005) are characterized by rough topography, highly variable micro-topoclimates and long-lasting seasonal snow cover. Snow accumulation, redistribution and melt strongly influence the energy balance at the ground surface and thus the ground thermal regime (e.g. Goodrich, 1982; Hoelzle et al., 2001; Stocker-Mittaz et al., 2002). Accumulation of an insulating snow cover in autumn plays a key role on inter-annual ground temperature variations, because of its long-lasting effect throughout winter (Delaloye, 2004; Marmy et al., 2013). The total quantity of snow melt and the melting rate per day are significant to the analysis of thawing processes in the active layer and the quantification of the influence of melt water infiltration on rock glacier kinematics. The development of the snow cover is regionally dependent on precipitation patterns and locally influenced by wind, avalanches and radiation, factors that make its development highly variable in space and time (Gisnås et al., 2014; Laternser and Schneebeli, 2003). But snow data are measured only at a few points. However, as ground surface temperatures (GST) are influenced by the local snow characteristics, GST data recorded with common miniature temperature loggers (Hoelzle et al., 1999) can be used to extract snow information directly at the points of interest for mountain permafrost research.

This paper uses GST time series to estimate the thermal insulation effect of the snow, from which periods of high insulation and snow melt can be delineated. It also approximates the snow melt rate during zero curtain periods using a degree-day approach with air temperature (AirT). The applicability of these methods is demonstrated with selected GST monitoring time series from the Swiss Alps.

2 Background

2.1 Relevance of the seasonal snow cover for the ground thermal regime

The thermal conductivity of snow ranges from 0.1 (fresh snow with a large fraction of air) to 0.5 (old snow with higher density) $\text{Wm}^{-1}\text{K}^{-1}$ and is 5-20 times lower than that of mineral soils (Zhang, 2005). Therefore, snow can thermally decouple the ground from the atmosphere with increasing snow depth. According to the literature, snow depth thresholds for effective thermal insulation range between 60 and 100 cm (Haeberli, 1973; Hanson and Hoelzle, 2005; Isaksen et al., 2002; Keller and Gubler, 1993; Luetschg et al., 2008; Zhang, 2005), but strongly depend on the density and structure of the snow as well as the roughness of the terrain (Apaloo et al., 2012; Delaloye, 2004; Hoelzle et al., 1999). Snow also changes the radiation balance through increased albedo and high emissivity (Ishikawa, 2003; Luetschg et al., 2008; Pomeroy and Brun, 2001; Zhang, 2005). This alteration of the surface energy balance may cause very efficient ground cooling, particularly for thin snow covers and clear sky conditions (“autumn snow effect”, see Keller and Gubler, 1993). The thermal insulation effect produces the largest changes at snow depths on the order of centimetres to decimetres (Isaksen et al., 2011). However, data on the depth and the thermal resistance of the snowpack are required to quantify thresholds for different snow densities and terrains.

2.2 Spatial variability of the snow cover and available snow data

Snow depth data are sparse in the high-alpine domain and remote sensing products are not yet available at high spatial (metre scale) and temporal (daily) resolution (Hüsler et al., 2014). Moreover, point measurements are limited representations due to the spatial heterogeneity of the snow cover. As illustrated in Figure 1a, continuously measured snow depth at one point may not be representative of snow thickness over an entire landform. Deviations of up to several metres in thickness have been observed in the vicinity. For the specific case of a typical mountain permafrost monitoring site illustrated in Figure 1, repeated measurements of snow depth showed that its spatial pattern may significantly differ from year to year (standard deviation SD : ± 65 cm), even if the respective mean values are almost identical (Figure 1b). Hence, places receiving more snow in one year may have substantially less snow in another year. For understanding the surface energy balance and the ground thermal regime over permafrost, the spatial and temporal variability of the snow cover needs to be considered, and point-specific snow information is required.

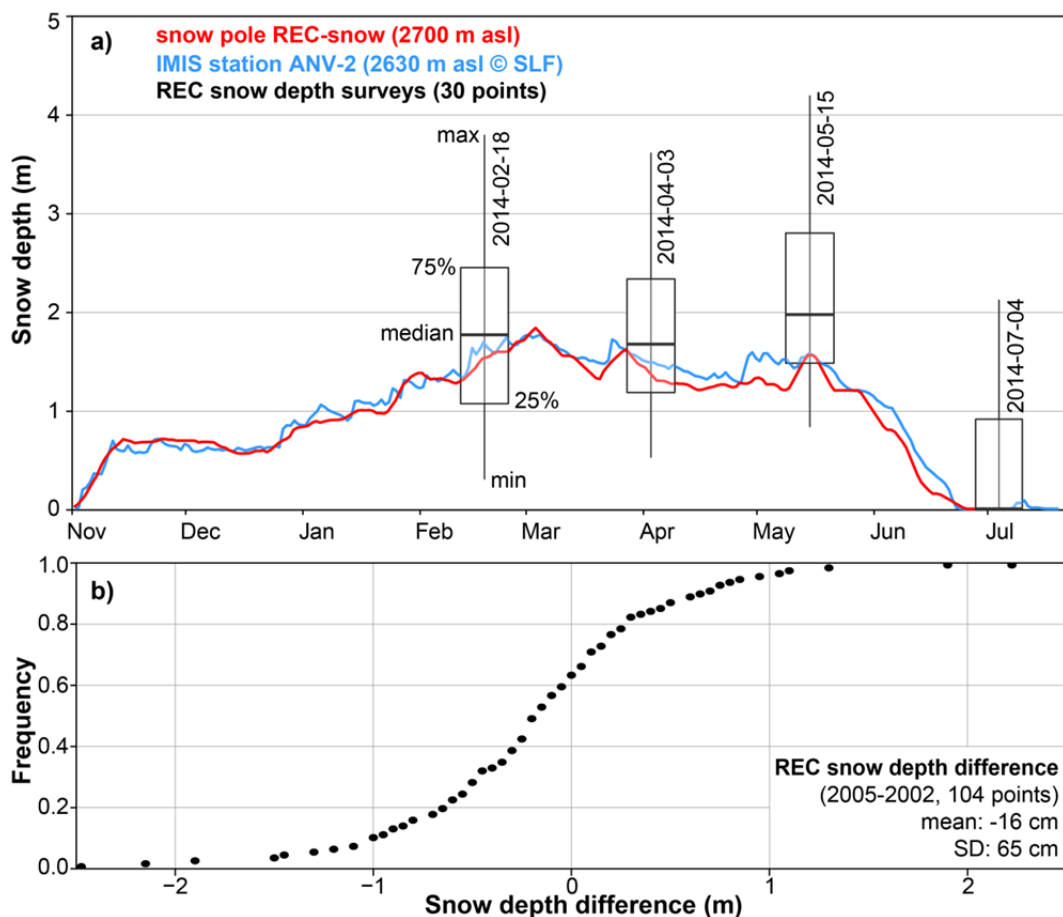


Figure 1: Time series and spatial variability of snow depth at the Becs de Bosson rock glacier at the Réchy site (REC in Figure 2): a) the coloured lines represent 7-day running means of continuously measured snow depths during winter 2013-2014, in red data from a snow pole on the same landform, in blue from IMIS station ANV-2 at ~ 3 km distance (source: SLF). Although the snow depth evolution at these two stations is similar in that particular year, the spatial variability is very large even within short distances. This is illustrated with the boxplots representing the range of snow depth values for 30 monitoring points near to the REC snow pole (~ 0.15 km²) of similar altitude, slope and aspect at four specific dates. In b) snow depths measured on the same landform in March 2002 and 2005 at 104 points reveal that the spatial snow distribution may greatly differ from year to year (large SD in snow depth difference of ± 65 cm and local deviations of up to ± 2 m).

Using near-surface ground temperature data to derive snow insulation and melt indices for mountain permafrost applications

2.3 GST-derived snow information in mountain permafrost research

GSTs are usually measured about 5-20 cm below the ground surface, at a depth where daily and seasonal temperature variations may be large. GSTs are sensitive to fluctuations in the energy balance at the ground surface, and are therefore useful for analysing some snow thermal insulation effects at the point scale by means of thermal sensors (Hipp, 2012; Schmid et al., 2012). The presence or absence of snow, as well as the start and end of the melting period in spring, have been successfully derived from GST time series (Apaloo et al., 2012; Delaloye, 2004; Hoelzle et al., 1999; Schmid et al., 2012). The thermal insulation effect and snow melt rates, however, have yet to be derived from them.

2.4 Terms and abbreviations

The following terms and abbreviations are used for GST-derived snow information. Periods of phase change are identified as zero curtains (Outcalt et al., 1990). The start of the spring zero curtain is abbreviated as *RD*, the basal ripening date according to Schmid et al. (2012), and the first day with positive GST following the spring zero curtain is considered as the snow disappearance date (*SDD*). The first day of the winter period with snow is defined as the snow onset date (*SOD*), and the beginning of periods of high thermal insulation, which last at least two weeks, as *HTI_{start}*. The abbreviation *SMR* refers to the snow melt rate, which is the ratio between a given snow water equivalent (SWE in mm) and a time interval.

3 Data description and pre-processing

For this study, we have used GST and snow depth data from the Swiss Permafrost Monitoring Network PERMOS and the WSL Institute for Snow and Avalanche Research SLF for a total of 60 sites in the Swiss Alps (cf. Figure 2) as well as gridded AirT data from the Federal Office for Meteorology and Climatology MeteoSwiss. The different data sets and pre-processing steps are described in the following sections.

3.1 GST and snow data from PERMOS

Most PERMOS field sites (PERMOS 2013) contain ~5-20 GST loggers (27 sites in total), which measure temperatures over an area of ~1 km². Snow depth, however, is recorded at only one point at a few sites (at an automatic weather station or with a snow stake equipped with thermal sensors). GST time series are available for more than 200 locations, many of which are 10-15 years long. Most GST data have been recorded by Universal Temperature Loggers UTL (Geotest, Switzerland), but other devices such as ThermoChron iButtons® (Dallas Semiconductor Corporation, USA) have also been used. All GST data were first corrected for offsets to 0 °C during zero curtain periods. Second, the raw data (30 minutes to 3 hours) were linearly resampled to two-hour intervals (*GST_{2h}*) to address potential heterogeneity related to the thermal resolution of the sensors and the sampling rate. On this basis, daily mean temperatures (*GST_{day}*), as well as daily (*GST_{SDDay}*) and weekly (*GST_{SDweek}*) standard deviations (*SD*) were calculated.

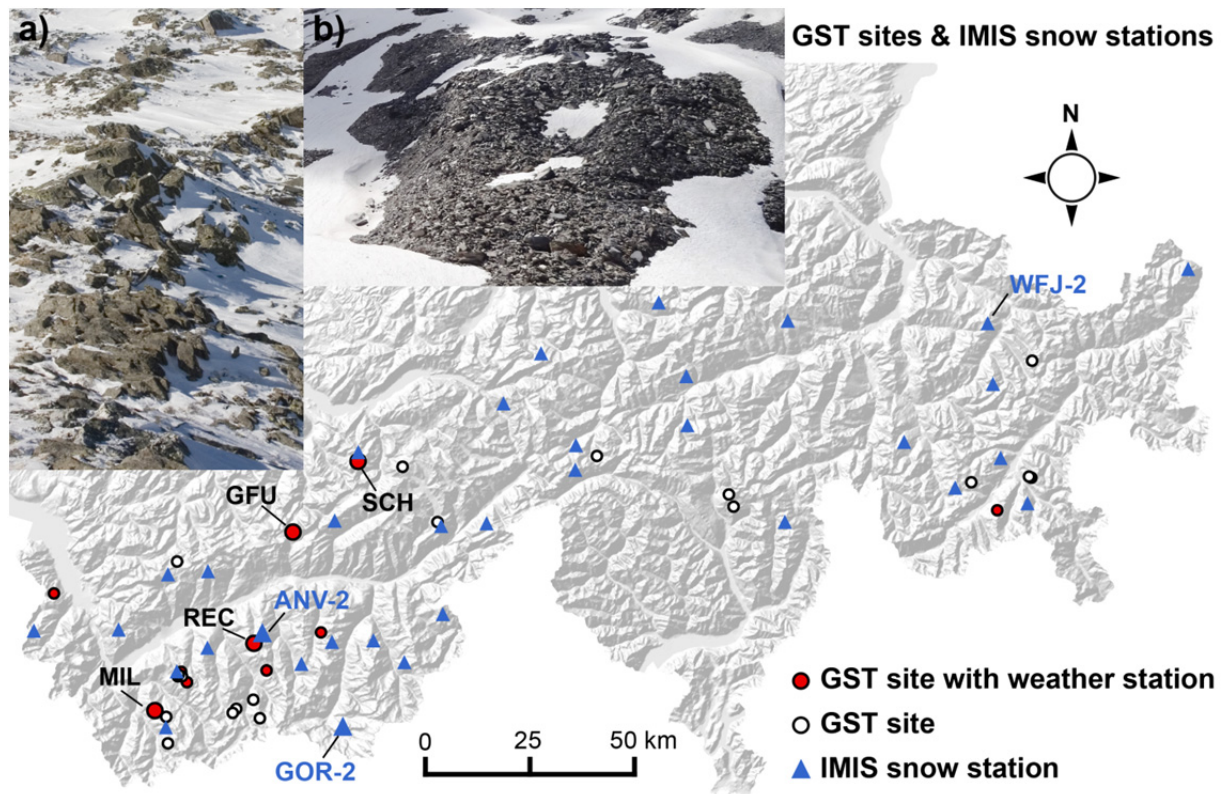


Figure 2: GST sites (circles) and IMIS snow stations (blue triangles) in the Swiss Alps. The photographs show typical, spatially heterogeneous snow conditions a) along a wind-exposed mountain ridge in early winter and b) in early summer. Source background map: Federal Office of Topography.

3.2 GST, snow depth and air temperature data recorded at IMIS stations

To assess the relationship between the thermal insulation effect of the snow and GST, both parameters need to be measured at exactly the same point. Therefore, data from the Intercantonal Measurement and Information System (IMIS, maintained by SLF) were used for validation for the period between 1994 and 2015. IMIS stations record meteorological parameters such as snow depth and GST (at the ground surface) between 2000 and 3000 m asl in the Swiss Alps, but many of these stations are not located on permafrost (Table S1). The snow depth data from the IMIS stations are measured indirectly by ultrasonic sensors, and raw data were used for this study. IMIS GST time series were pre-processed similar to those from PERMOS and the same aggregates were calculated.

3.3 Gridded air temperature data from MeteoSwiss

Because AirT is not measured at all PERMOS sites but is required to approximate snow melt rates, the gridded data product TabsD (2 km resolution based on ~90 stations in Switzerland) from MeteoSwiss has been used for daily mean AirT (Frei, 2014). Using this data and assuming a constant lapse rate of 0.55 °C/100m, daily mean AirT time series were reconstructed for each of the GST loggers. The lapse rate was used to correct for the remaining elevation difference between the closest grid cells (the overlapping cell and 8 surrounding cells were used) and the point of interest. Validation with on-site AirT records from IMIS stations revealed a good agreement (R^2 : 0.98, RMSE: 1.56 °C, p-value < 0.01, n: ~180,000 days) regarding daily mean values.

Using near-surface ground temperature data to derive snow insulation and melt indices for mountain permafrost applications

4 Methods

The following procedures have been empirically developed on a large set of GST data in order to provide a robust and flexible toolset applicable to different situations concerning data availability, quality and temporal resolution. The full documentation of the data processing can be found as supplementary material including R code and a small sample data set.

4.1 Relationship between GST variability and snow thermal insulation

In mountainous areas such as the Swiss Alps, the daily SD of AirT ranges between 0.5 and 5 °C with little seasonal differences. As long as the ground is not thermally insulated and remains dry, the daily SD of GST (GST_{SDday}) is on the same order; values are slightly higher if recorded at (“skin surface temperature”) or very close to the ground surface, and slightly lower if measured 10-20 cm below the surface. As Figure 3 illustrates, the presence of an insulating snow cover reduces GST_{SDday} by a factor of at least 5-10. Hence, semi-quantitative information on the thermal insulation effect of the snow cover and periods of phase change can be derived from short-term GST variations.

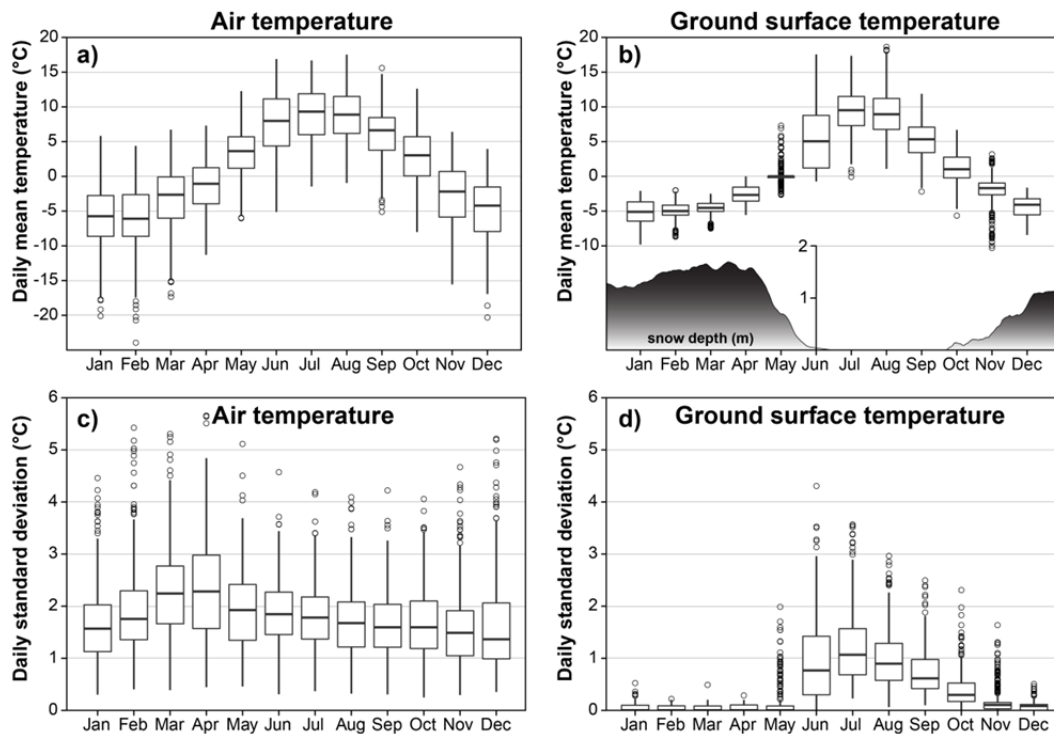


Figure 3: Seasonal patterns of air temperature (~2 m above ground surface) and ground surface temperature (GST, ~20 cm below the surface) at the rock glacier “Alpage de Mille” (2400 m asl, MIL in Figure 2) over the period 1997-2014: a) and b) visualize daily mean temperatures as well average snow depth measured at a nearby snow pole, c) and d) illustrate the high influence of the snow on the daily GST standard deviation.

4.2 Detection of zero curtains, basal ripening and snow disappearance

During snow melt, GST should, theoretically, remain constantly at 0 °C with short-term variations very close to ~0 °C, because phase changes have the largest influence on the GST signal. To account for the rather coarse thermal resolution of some miniature temperature loggers (e.g. UTL-1 with ± 0.23 - 0.27 °C), a threshold th_{zc} is set to 0.25 °C. During periods of phase change, absolute GST values

will likely not surpass th_{ZC} . Even if GST values fluctuate between two values due to the limited thermal resolution of the sensors, GST_{SDday} would still remain below half of th_{ZC} . Based on GST_{2h} , we calculated GST_{SDday} in running windows of 24-hours aligned at the beginning (GST_{SDday_prior}) and end (GST_{SDday_after}) of this period. Similarly, weekly SD (GST_{SDweek_prior} , GST_{SDweek_after}) can be calculated from daily means. Accordingly, the zero curtain period (ZC) can be delineated as:

$$ZC = \begin{cases} 1 & \text{if } |GST_{2h}| \leq th_{ZC} \wedge \left(GST_{SDday_prior} \leq \frac{th_{ZC}}{2} \vee GST_{SDday_after} \leq \frac{th_{ZC}}{2} \right) \\ 0 & \text{if } |GST_{2h}| > th_{ZC} \vee GST_{SDday_prior} > \frac{th_{ZC}}{2} \vee GST_{SDday_after} > \frac{th_{ZC}}{2} \end{cases} \quad (1)$$

Or, if only daily mean GST are available, as:

$$ZC = \begin{cases} 1 & \text{if } |GST_{day}| \leq th_{ZC} \wedge \left(GST_{SDweek_prior} \leq \frac{th_{ZC}}{2} \vee GST_{SDweek_after} \leq \frac{th_{ZC}}{2} \right) \\ 0 & \text{if } |GST_{day}| > th_{ZC} \vee GST_{SDweek_prior} > \frac{th_{ZC}}{2} \vee GST_{SDweek_after} > \frac{th_{ZC}}{2} \end{cases} \quad (2)$$

Describing the start of the snow melt, the basal ripening date (*RD*) is arbitrarily defined as the first day which fulfils the criteria in Equations 1 or 2, respectively. Similarly, the snow disappearance date (*SDD*) represents the first day with positive GST following a continuous zero curtain period. The successful detection of *RD* is limited to locations and years displaying negative winter GST. A zero curtain period may occur during (a) the melt of snow when the active layer is frozen (spring zero curtain); (b) the melt of fresh snow on still unfrozen ground (as often occurs in autumn); (c) ground freezing; or (d) after rain-on-snow events when water percolates through the snowpack and refreezes at the bottom (Westermann et al., 2011; Wever et al., 2014).

4.3 Estimation of the thermal insulation effect of the snow and the snow onset

The difference between AirT and GST variations can be used to approximate such snow cover properties as the presence/absence of snow, snow thickness, and timing of the snow melt (Hipp, 2012; Lewkowicz, 2008; Lundquist and Lott, 2008; Schmid et al., 2012; Schmidt et al., 2009; Schneider et al., 2012; Tyler et al., 2008; Apaloo et al., 2012). In contrast to previous work, the snow thermal insulation indices described hereafter classify different levels of thermal insulation and delineate the start of the high-insulation period. In addition to the variability terms GST_{SDday} (when analysing hourly data) and GST_{SDweek} (based on daily means), a GST-change term ΔGST_{week} is used to describe the GST trend over one week. Similar to the zero curtain detection, empirically defined thresholds are used to distinguish between periods of higher and lower thermal insulation: th_1 is defined as the 95 % quantile of GST_{SDday} (or GST_{SDweek} , respectively) during January-March (when an insulating snow cover is most likely in the Swiss Alps) and is constrained to the value range 0.1-0.5. Likewise, the threshold th_2 is derived from the 95 % quantile of ΔGST_{week} and is constrained to the values 0.5-1.5. In other words, these thresholds represent values which are very unlikely to be surpassed if a thermally insulating snow cover is present.

Using near-surface ground temperature data to derive snow insulation and melt indices for mountain permafrost applications

The snow thermal indices $snow_1$ (based on hourly data) and $snow_2$ (based on daily means) consist of a SD and a $\Delta change$ term and are defined as follows:

$$snow_1[0, \dots, 1] = \frac{\left(\frac{-GST_{SDday}}{th_1} + 1 \right) + \left(\frac{-\Delta GST_{week}}{th_2} + 1 \right)}{2} \wedge GST_{hour} \leq 1 \quad (3)$$

$$snow_2[0, \dots, 1] = \frac{\left(\frac{-GST_{SDweek}}{th_1} + 1 \right) + \left(\frac{-\Delta GST_{week}}{th_2} + 1 \right)}{2} \wedge GST_{day} \leq 0.5 \quad (4)$$

If $GST_{SDday} > th_1$, $GST_{SDweek} > th_1$ or $\Delta GST_{week} > th_2$, the respective term is set to 0, indicating no thermal insulation. If the respective thresholds are undercut, the indices become positive and may approach the maximum value 1 when the variability and $\Delta change$ term are equal to 0 (complete thermal insulation).

To account for site-specific characteristics, such as the placement depth of the sensors, the exposure to solar radiation and wind, as well as the roughness and porosity of the ground material at the surface, th_1 and th_2 are defined separately for each time series. The values obtained for th_1 were similar to short-term variations in GST representing snow-covered periods reported in other studies (Schmid et al., 2012; Schneider et al., 2012). To achieve comparable results across different sites and years, both thresholds were constrained to a reasonable range of values. ΔGST_{week} was introduced to address the weekly scale and potentially underestimated insulation when the GST values are fluctuating between two values due to limited thermal resolution. The additional filter criteria using absolute GST_{2h} or GST_{day} avoids scatter in summer and autumn, when small snow events may lead to a temporary thermal insulation (Hipp, 2012; Lewkowicz, 2008; Schmid et al., 2012). Capturing such short snow events is, however, not the aim of the indices $snow_1$ and $snow_2$. $snow_2$ may be particularly suitable for time series with changing temporal resolution over time, or if only daily mean GST values are available. To remove spikes, both indices were additionally smoothed with a one-week median filter.

To compare $snow_1$ and $snow_2$, we adapted an algorithm proposed by Hipp (2012), originally developed for the automatic detection of snow depths from snow poles instrumented with iButtons (Lewkowicz, 2008). This approach, here called $snow_3$, estimates the thermal insulation effect of the snow cover based on the temperature variability above (AirT) and below (GST). It was modified by using weekly SD (GST_{SDweek} , $AirT_{SDweek}$) instead of the hourly variance to preserve the units and to make its application possible even if only daily means are available (cf. Equation 5). Like $snow_2$, $snow_3$ was also restricted to $GST_{day} \leq 0.5$ °C and smoothed with a weekly median filter.

$$snow_3[0, \dots, 1] = \frac{(AirT_{SDweek} - GST_{SDweek})}{(AirT_{SDweek} + GST_{SDweek})} \wedge GST_{day} \leq 0.5 \quad (5)$$

All three indices may be used to delineate periods of differing thermal insulation, such as the first day of positive snow indices in winter (snow onset date, *SOD*), or the first day of a subsequent period of high thermal insulation of at least two weeks with mean snow indices ≥ 0.5 (HTI_{start}).

4.4 Approximation of snow melt rates and maximal snow depths

Snow melt is primarily controlled by air temperature (*AirT*) and the radiation balance at the surface (Ohmura, 2001). Melting is further influenced by the refreezing of melt water within the snowpack and the percolation of rain and surface runoff into the snow (Pomeroy and Brun, 2001; Senese et al., 2014). Because point-specific data on radiation, precipitation, snow density and albedo are usually lacking, only very simple models are suitable to quantify the snow melt in high-alpine terrains. *AirT* is the proxy of choice since it partly integrates many components of the energy balance and may be extrapolated over distances of 10-100 km with reasonable uncertainty (Tardivo and Berti, 2012; Lang and Braun, 1990). Degree-day and energy balance approaches approximating snow melt have been developed and successfully applied in hydrological modelling (Hock, 2003; Lehning et al., 2006; Martinec, 1960) and glacier mass balance studies (Braithwaite and Zhang, 2000; Pellicciotti et al., 2005; Senese et al., 2014). However, the absolute accuracy of such a degree-day model is limited due to simplifications (e.g., unknown snow density, neglected spatial patterns) and scale issues (Lang and Braun, 1990).

Reasonable values for the snow density ρ are required. Jonas et al. (2009) found, from snow probings in the Swiss Alps, that ρ typically ranges between 300 and 500 kgm^{-3} between April and June. This is the period when snow melt occurs at PERMOS sites. SWE records obtained by Schmid et al. (2012) around “Piz Corvatsch” (eastern Switzerland) in March and April 2010 were on the same order ($\sim 360 \text{ kgm}^{-3}$ some weeks before the snow melt started at high-altitude). Therefore, a bulk snow density of $\sim 400 \text{ kgm}^{-3}$ is assumed for permafrost areas in the Swiss Alps during the snow melt period, similar to values for old and wet snow (Judson and Doesken, 2000; Meløysund et al., 2007).

By coupling the point-specific information on the timing of the melting period (zero curtain, cf. Equations 1 and 2) with positive daily *AirT* data (*AirT*⁺), the SWE of the maximal snow depth at the basal-ripening date (*RD*) and daily snow melt rates can be approximated, specifically for the points where GST is measured. The melt index (Equation 6) is a linear degree-day model based on *AirT*⁺ using the factor *A* for calibration. *A* was chosen according to a study from Zingg (1951) on the Weissfluhjoch (WFJ-2 in Figure 2), which revealed strong agreement between *AirT*⁺ and melt water runoff measurements with *A* = 4.5. For example, an average melting day in early summer with *AirT*⁺ of +10 °C would melt ~ 45 mm SWE or ~ 11 cm of snow, respectively.

$$\text{melt index } [SWE, mm] \cong \frac{\Delta h_s \cdot \rho}{\Delta t} \cong \frac{A \cdot \sum_{t=RD}^{SDD} \text{AirT}^+}{\Delta t_{(SDD-RD)}} \quad (6)$$

The approach is based on the assumption that the total amount of snow converted into water during a given time window is mainly related to the sum of *AirT*⁺ within the same period.

5 Validation

5.1 Validation of the snow thermal indices

Because the snow indices characterise the thermal decoupling of the ground surface from variations in AirT but do not indicate snow depth, their validation can only be done qualitatively or by comparing snow insulation classes and snow depth for specific periods. For a first visual comparison, all three snow indices (Equations 3-5) have been overlain with the GST and snow depth records from IMIS stations. As Figure 4 shows for station GOR-2, there are large seasonal and inter-annual variations in the timing and thickness of the snow cover.

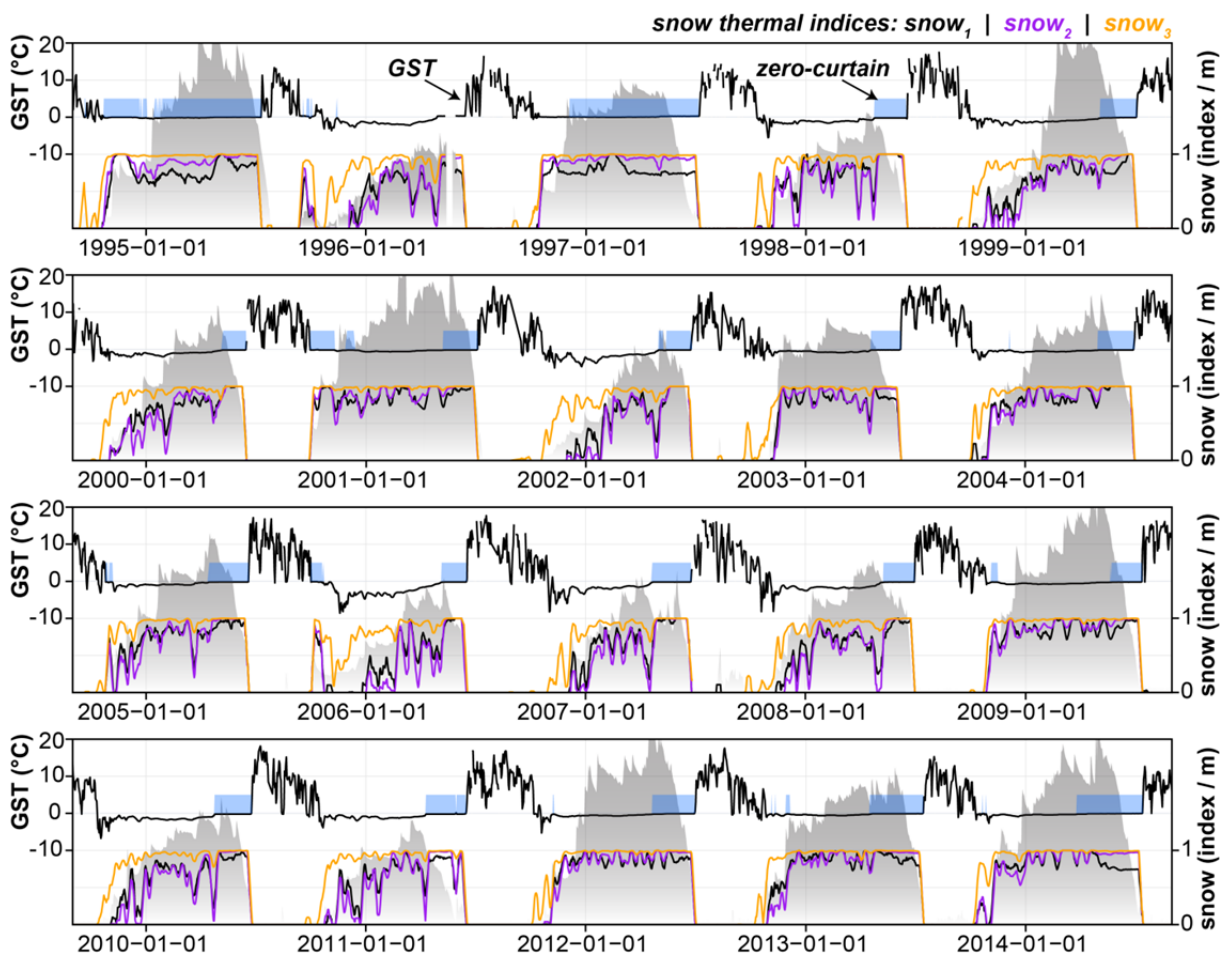


Figure 4: Visual comparison of GST and the derived snow indices at the IMIS station GOR-2 for the past 20 years. The blue areas on top of the GST curves represent periods with zero curtains (Equation 1), and the grey-shaded area at the bottom show the measured snow depth (m). The coloured lines are the GST-derived snow indices (Equations 3-5) indicated at the top of the figure. Snow and GST data © SLF.

The snow indices seem capable of representing this behaviour, and the timing of the high-insulation period can be detected. Moreover, these examples show some typical problems: for the detection of the melting period (zero curtain, *RD* and *SDD*) well-calibrated GST input data are required. This explains why in 1996 the zero curtain period could not be automatically detected for GOR-2, because there was a small yet systematic GST offset. In 1995 and 1997, phase changes dominated the GST signal throughout winter. If GST warms very rapidly before the zero curtain, the snow indices may spontaneously drop. The snow indices peak during the melting period.

Monthly mean snow depths and snow indices are compared in Figures 5a-c for a second validation. Variations between snow-rich and snow-poor periods seem to be distinguishable with all snow indices. However, $snow_3$ appears to be much more sensitive to shallow snow depths < 50 cm, compared to $snow_1$ and $snow_2$. The large scatter can be explained by site-specific and temporal differences in the terrain and snow characteristics. However, intermediate snow indices do not show a clear relation to respective snow depths (e.g. 20-50 cm) because very smooth surfaces may require up to 30-50 cm less snow than rough, coarse-blocky terrains to reach the same thermal insulation effect. Raw data for the IMIS stations were checked for plausible values but were not corrected. Overall, the snow indices indicate the general snow thermal characteristics of different years or locations.

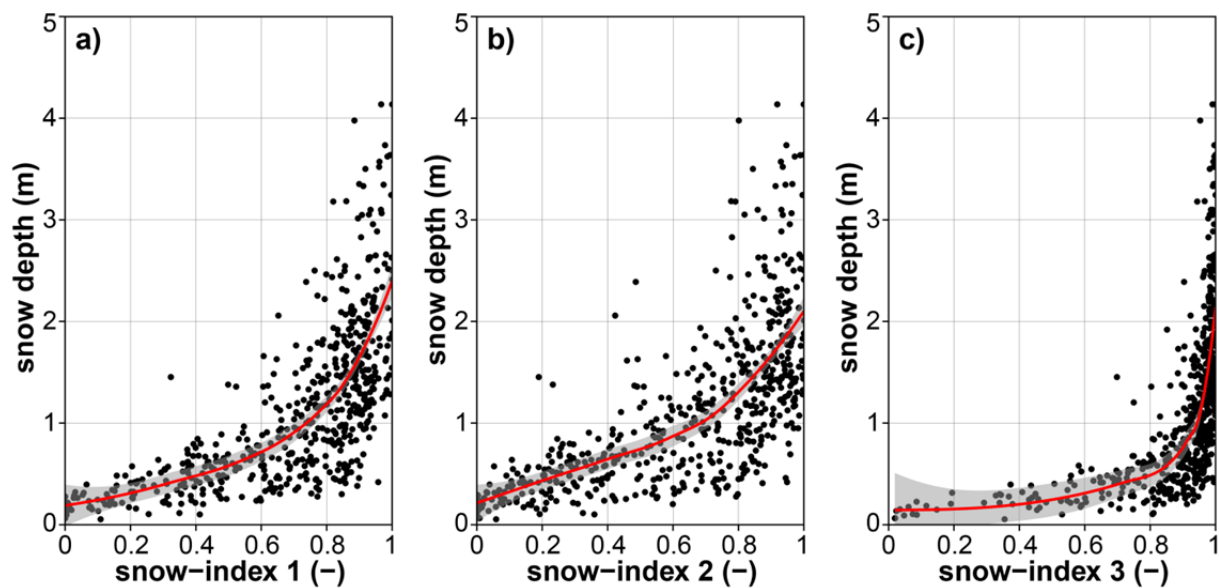


Figure 5: Comparison of snow indices derived from GST data and snow depth observations recorded at 33 IMIS stations. Each point corresponds to the mean value of one month ($n=528$, restricted to monthly mean GST ≤ -0.3). The red lines represent local polynomial regressions fitted through the data with the corresponding 95 % confidence interval in grey. Snow and GST data © SLF.

5.2 Validation of the snow melt index

The melt index (Equation 6) has been validated using IMIS data for ~ 500 melting periods. Cumulative SMR and cumulative snow depth loss (converted into SWE using a bulk density of 400 kgm^{-3}) have been compared. As Figure 6 shows, this relationship is strong ($R^2: \sim 0.88$) and nearly linear. However, the compaction of the snow cover with time, spatio-temporal variance in global radiation, precipitation events during the melting period and the refreezing of melt water are not taken into account. Regarding the data obtained, the optimal value for A ranges between 3.5 and 5 depending on the station, but the average regression slope (~ 4.1) is close to the value of 4.5 as proposed by Zingg (1951).

Using near-surface ground temperature data to derive snow insulation and melt indices for mountain permafrost applications

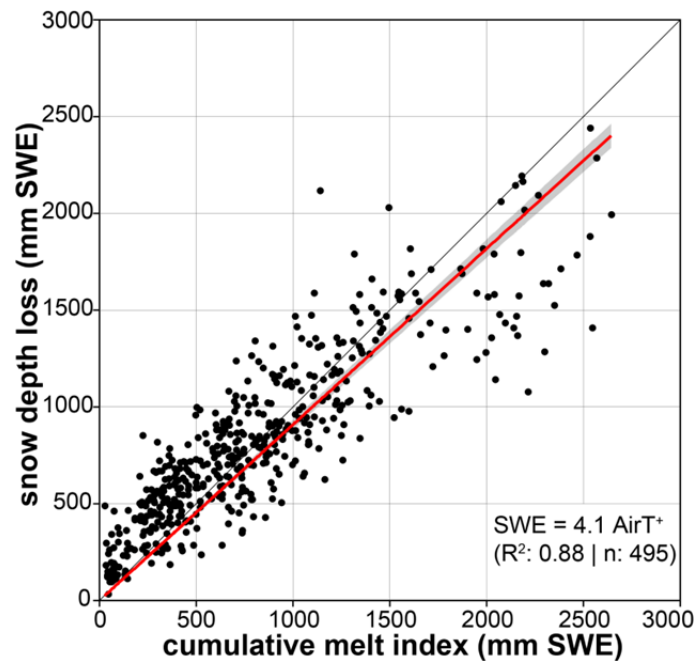


Figure 6: Validation of the melt index using the degree-day factor A of 4.5 (x-axis) with the respective cumulative snow depth loss (y-axis). Each data point represents the mean of one melting period ($n=495$). With the red line, the best linear fit is shown (slope of 4.1); the grey area represents the 95 % regression confidence interval. Snow water equivalents (SWE mm) have been approximated using a bulk snow density of 400 kg m^{-3} . Snow data © SLF.

Because the variance of AirT is the only proxy for all the processes influencing snow melt, absolute SMR values require cautious interpretation. The largest uncertainty of this degree-day model relates to the snow density, which may vary up to $\pm 20\%$, as well as the disregarded variance in global radiation. As long as relative values (e.g. differences between years) are compared, reliable results are expected, due to large inter-annual differences.

6 Application of the snow and melt indices on GST monitoring data

The snow and melt indices have been applied to GST monitoring time series from the Swiss Alps, and selected results are shown subsequently in order to illustrate the potential use in mountain permafrost research.

6.1 Snow onset and thermal insulation

The thermal insulation of the snowpack and the timing of the snow onset are important to the ground thermal regime of mountain permafrost, because they control the intensity of ground cooling over a long period of the year. As Figure 7 shows, the differences in the thermal insulation by the snow cover can be very large even for adjacent loggers: while logger GFU_S002 is situated on a ridge and exposed to wind, GFU_S003 is situated ~ 20 m away on the same landform but in a gully prone to snow accumulation. In consequence, at GFU_S002 the thermal insulation is clearly lower and the high thermal insulation period (HTI_{start}) starts later in the season, which results in more negative GST values during winter. The example from the Schilthorn (SCH_S007 in Figure 7) further shows that fine-grained subsurface materials are prone to zero curtain periods in autumn and spring, due to the increased moisture content (latent heat) and heat capacity of the (upper) ground layers.

In such situations, HTI_{start} cannot be determined and the informative value of the snow indices regarding the thermal insulation effect is limited. The spatial variability between the different loggers is largest in years with early HTI_{start} , while winter cooling peaks in years with late HTI_{start} .

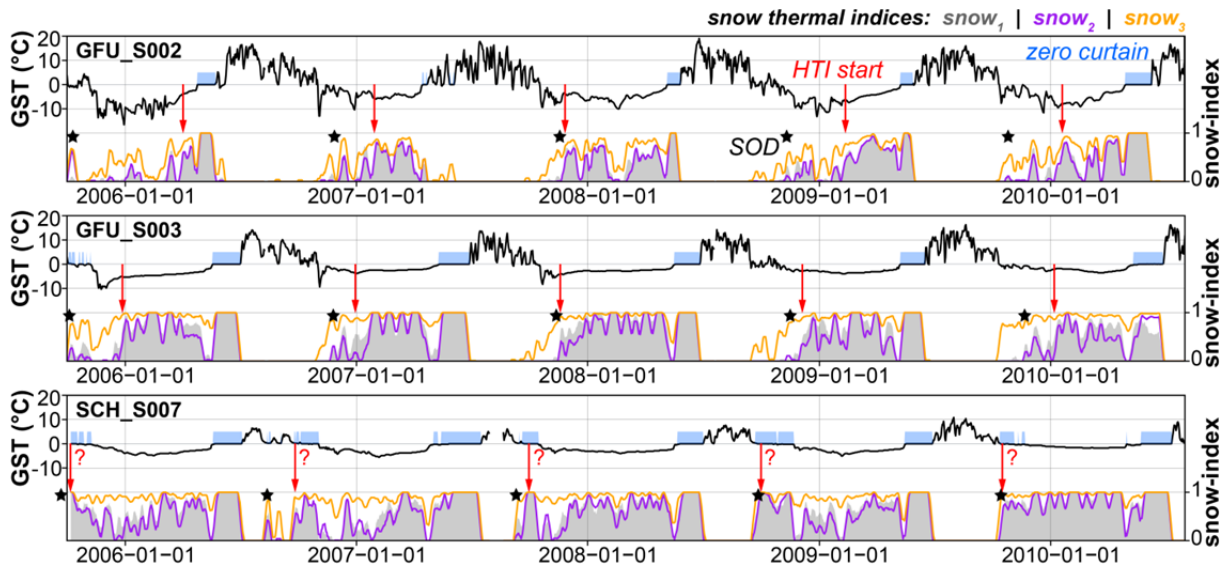


Figure 7: Comparison of GST and snow indices for selected GST time series from the sites Gemmi (GFU) and Schilthorn (SCH). Black line: daily mean GST; blue areas: periods with phase change (zero curtains); grey areas: snow index $snow_1$; purple line: $snow_2$; orange line: $snow_3$; black stars: snow onset date (SOD) based on $snow_1$; red arrows: start of the high-insulation winter period (HTI_{start}) based on $snow_1$. HTI_{start} may occur at the same time as SOD or much later in the season.

6.2 Timing and duration of the melting period

The timing of the snow melt (particularly SDD) greatly influences the surface energy balance in early summer, resulting in up to 5-10 °C difference between snow-free and the snow-covered locations, equalling an impact on the annual mean of 0.01-0.02 °C per day. Regarding the temporal evolution of SDD , no clear trend has been observed during the past 15 years, although the inter-annual variations are considerable (SD : ± 20 days). The spatial variability of SDD is even larger than the temporal variations, and some locations experiencing an early melt-out may be snow-free up to two months before the snow nearby is completely gone (Figure 2b, 4 and 7). The mean zero curtain duration ($SDD-RD$) for more than 1500 clearly identifiable melting periods is 48 days (SD : ± 20 days). Such long zero curtains as well as the high spatial and temporal variability illustrate the influence of snow on the local surface energy balance in early summer.

6.3 Estimated snow water equivalents and snow melt rates

The application of the melt index using GST time series from the PERMOS network revealed large spatial and temporal variability concerning daily snow melt rates (SMR). Figure 8 illustrates the temporal evolution of SMR for one example, and summarizes 74 complete GST time series from 11 sites for the period 2002-2013. Similarly to the snow indices, considerable inter-annual differences also appear regarding SMR . The total sum of SMR melted during the zero curtain ranges from nearly 0 to about 2500 mm (SWE). The average value of the 840 melting periods analysed is 890 mm (SWE), equalling a thickness of ~ 2.2 m of snow at a density of 400 kgm^{-3} .

Using near-surface ground temperature data to derive snow insulation and melt indices for mountain permafrost applications

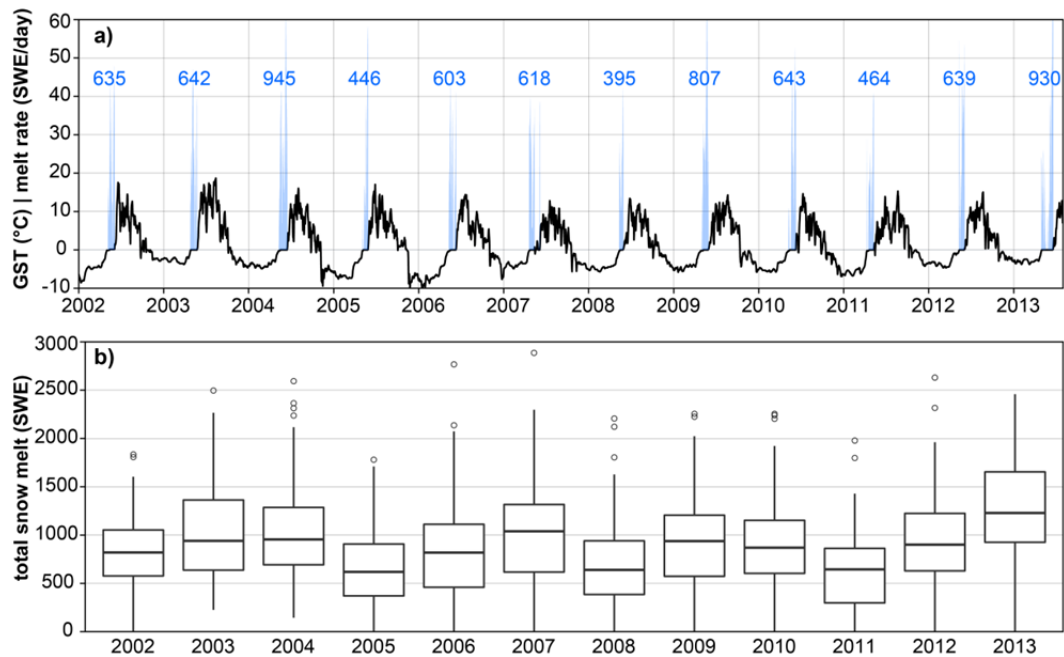


Figure 8: Snow melt rates (*SMR*) for GST locations derived from Equation 6: a) daily mean GST (black) and *SMR* for logger MIL_S005 (MIL on Figure 2). The numbers in blue indicate the total SWE (mm) melted during the zero curtain. In b) inter-annual variations of the total SWE melted during the zero curtain are shown for 12 years based on 74 loggers with complete data from 11 different study sites. On average total SWE is about 890 mm, what equals ~ 2.2 m of snow assuming a bulk snow density of 400 kg m^{-3} .

This simple approach seems capable of reproducing seasonal and inter-annual variations of *SMR* that are close to natural variations. It achieves this in spite of the high uncertainty related to the assumption of the constant snow density, by neglecting the distinction between melt and sublimation (Strasser et al., 2008) and disregarding the effects of radiation and the refreezing of water in the snowpack. One major benefit is its ability to extract *SMR* time series (or the cumulated snow melt), which is highly irregular at short time scales of days to weeks. While *SMR* increases in June due to increased AirT (and high radiation), it dips below 1 mm SWE per day almost every third day.

7 Discussion

Our snow indices contain semi-quantitative information on the thermal insulation effect of the snow, information which could not be directly extracted from snow depth records because the thermal resistance of the snow layer depends on its density and structure as well as terrain characteristics. The indices can also help reconstruct past snow thermal conditions using long-term GST monitoring data. To our knowledge, the snow indices are a unique approach to describe the snow onset and the start of the high-insulation period in a systematic and standardized way. They also elucidate the spatio-temporal variability of snow characteristics in remote areas by using miniature temperature loggers, which are well established in the permafrost community.

The validation of the snow indices, however, is demanding, and interpretation of the results requires expert knowledge of the local terrain and microclimate. In situations with early snow fall, the start of the high-insulation period (HTI_{start}) and the snow ripening date (*RD*) can be difficult to delineate,

particularly at locations with relatively warm or humid conditions because variations in the surface energy balance in the GST data may be masked by phase changes (Figures 4 and 7). Moreover, the density and structure of the snow as well as the amount of snow required for a given thermal insulation effect change throughout the season, as the density increases 100-300 % from fresh snow to old and wet snow (Jonas et al., 2009). The threshold definitions might require adaptation in order to apply the method to other climatic situations or using a different measurement setup for the GST data. The application using GST monitoring time series from the Swiss Alps showed that an insulating snow cover is present in the majority of cases, at least for some weeks each winter. However, the timing and duration of these high-insulation periods may vary greatly for different locations, sites and years. The potential absence or temporal shift of the high-insulation period implies that theoretical values which depend on the concept of thermal insulation in late winter, such as the base temperature of the winter snow cover (Haeberli, 1973) or the winter equilibrium temperature WEqT (Delaloye, 2004), may not be determined in all situations.

The melt index (which describes the snow melt rate) agrees well with snow data from the IMIS stations using the degree-day factor $A = 4.5$ as proposed by Zingg (1951). Its application on GST monitoring data revealed promising new insights on the spatial and temporal variability of the melt water released from the snowpack at the position of the GST loggers. The use of daily means seems appropriate because A was also calibrated using daily means (Zingg, 1951), and the downscaling of point-specific air temperature values from gridded data or remote stations is supposed to be quite robust for daily means. For the Swiss Alps, the gridded daily mean AirT from MeteoSwiss agree closely with observations from the IMIS stations. These gridded data facilitate the processing of the melt index for numerous sites when on-site AirT observations are lacking. The key use of the melt index will probably be in the analysis of rock glacier kinematics, where clear relationships between annual displacement rates and GST variations have been found (Delaloye et al., 2010), but the role of the melt water infiltration is still not sufficiently understood. To make the melt index physically more consistent, the bulk snow density function applied by Jonas et al. (2009) could be integrated, or an explicit radiation component could be introduced if such data are available.

8 Conclusions and Outlook

Our new data processing techniques quantify the thermal insulation effect of the snow cover on the ground and delineate periods of high thermal insulation and snow melt, as well as the snow melt rate during zero curtain periods in spring. The algorithms are designed for permafrost conditions using GST data and were validated with field data from snow stations in the Swiss Alps.

Potential applications of the indices may characterise the snow thermal insulation and snow melt rate for different locations and years. However, the threshold definitions and the degree-day factor should be adapted before applying the indices to other regions with differing climate, snow and ground properties. The snow indices might be used as an additional validation parameter to assess the representation of upper boundary conditions in permafrost models (Gisnås et al., 2014; Staub et al., 2015).

Using near-surface ground temperature data to derive snow insulation and melt indices for mountain permafrost applications

Acknowledgements

We highly acknowledge the Swiss National Science Foundation for the funding of the Sinergia TEMPS project (project no. CRSII2 136279) as well as PERMOS and our colleagues within TEMPS for providing observational data. Special thanks go to Dragan Vogel for his valuable advice on the signal processing of GST time series, and to Brianna Rick for proofreading the English. Moreover we would like to thank to the editor Julian Murton as well as to two anonymous referees for their detailed and helpful comments and suggestions. IMIS snow station data was kindly provided by the WSL Institute for Snow and Avalanche Research SLF, and gridded air temperature data by the Federal Office for Meteorology and Climatology MeteoSwiss.

References

- Apaloo J, Brenning A, Bodin X. 2012. Interactions between Seasonal Snow Cover, Ground Surface Temperature and Topography (Andes of Santiago, Chile, 33.5°S). *Permafrost and Periglacial Processes* 23: 277–291. DOI: 10.1002/ppp.1753
- Braithwaite RJ, Zhang Y. 2000. Sensitivity of mass balance of five Swiss glaciers to temperature changes assessed by tuning a degree-day model. *Journal of Glaciology* 46: 7–14. DOI: 10.3189/172756500781833511
- Delaloye R. 2004. Contribution à l'étude du pergélisol de montagne en zone marginale. PhD Thesis, Department of Geosciences, University of Fribourg, GeoFocus No. 10.
- Delaloye R, Lambiel C, Gärtner-Roer I. 2010. Overview of rock glacier kinematics research in the Swiss Alps. *Geographica Helvetica* 65: 135–145. DOI: 10.5194/gh-65-135-2010
- Frei C. 2014. Interpolation of temperature in a mountainous region using nonlinear profiles and non-Euclidean distances. *International Journal of Climatology* 34: 1585–1605. DOI: 10.1002/joc.3786
- Gisnås K, Westermann S, Schuler TV, Litherland T, Isaksen K, Boike J, Etzelmüller B. 2014. A statistical approach to represent small-scale variability of permafrost temperatures due to snow cover. *The Cryosphere* 8: 2063–2074. DOI: 10.5194/tc-8-2063-2014
- Goodrich LE. 1982. The influence of snow cover on the ground thermal regime. *Canadian Geotechnical Journal* 19: 421–432. DOI: 10.1139/t82-047
- Haeberli W. 1973. Die Basis-Temperatur der winterlichen Schneedecke als möglicher Indikator für die Verbreitung von Permafrost in den Alpen. *Zeitschrift für Gletscherkunde und Glazialgeologie* 9: 221–227.
- Hanson S, and Hoelzle M. 2005. Installation of a shallow borehole network and monitoring of the ground thermal regime of a high alpine discontinuous permafrost environment, Eastern Swiss Alps. *Norsk Geografisk Tidsskrift - Norwegian Journal of Geography* 59: 84–93. DOI: 10.1080/00291950510020664
- Hipp T. 2012. Mountain Permafrost in Southern Norway: Distribution, Spatial Variability and Impacts of Climate Change. PhD Thesis, Faculty of Mathematics and Natural Science, University of Oslo.
- Hock R. 2003. Temperature index melt modelling in mountain areas. *Journal of Hydrology* 282: 104–115. DOI: 10.1016/S0022-1694(03)00257-9
- Hoelzle M, Mittaz C, Etzelmüller B, Haeberli W. 2001. Surface energy fluxes and distribution models of permafrost in European mountain areas: an overview of current developments. *Permafrost and Periglacial Processes* 12: 53–68. DOI: 10.1002/ppp.385
- Hoelzle M, Wegmann M, Krummenacher B. 1999. Miniature temperature dataloggers for mapping and monitoring of permafrost in high mountain areas: first experience from the Swiss Alps. *Permafrost and Periglacial Processes* 10: 113–124. DOI: 10.1002/(SICI)1099-1530(199904/06)10:2<113::AID-PPP317>3.0.CO;2-A
- Hüsler F, Jonas T, Riffler M, Musial JP, Wunderle S. 2014. A satellite-based snow cover climatology (1985–2011) for the European Alps derived from AVHRR data. *The Cryosphere* 8: 73–90. DOI: 10.5194/tc-8-73-2014

Publication I

- Isaksen K, Hauck C, Gudevang E, Ødegård RS, Sollid JL. 2002. Mountain permafrost distribution in Dovrefjell and Jotunheimen, southern Norway, based on BTS and DC resistivity tomography data. *Norsk Geografisk Tidsskrift - Norwegian Journal of Geography* 56: 122–136. DOI: 10.1080/002919502760056459
- Isaksen K, Ødegård RS, Eitzelmüller B, Hilbich C, Hauck C, Farbroth H, Eiken T, Hygen HO, Hipp TF 2011. Degrading Mountain Permafrost in Southern Norway: Spatial and Temporal Variability of Mean Ground Temperatures, 1999-2009. *Permafrost and Periglacial Processes* 22: 361–377. DOI: 10.1002/ppp.728
- Ishikawa M. 2003. Thermal regimes at the snow-ground interface and their implications for permafrost investigation. *Geomorphology* 52: 105–120. DOI: 10.1016/S0169-555X(02)00251-9
- Jonas T, Marty C, Magnusson J. 2009. Estimating the snow water equivalent from snow depth measurements in the Swiss Alps. *Journal of Hydrology* 378: 161–167. DOI: 10.1016/j.jhydrol.2009.09.021
- Judson A, Doesken N. 2000. Density of Freshly Fallen Snow in the Central Rocky Mountains. *Bulletin of the American Meteorological Society* 81: 1577–1587. DOI: 10.1175/1520-0477(2000)081<1577:DOFFSI>2.3.CO;2
- Keller F, Gubler H. 1993. Interaction between snow cover and high mountain permafrost, Murtèl-Corvatsch, Swiss Alps. In *Proceedings of the 6th International Conference on Permafrost, Beijing, China*. South China University of Technology Press, pp. 332–337.
- Lang H, Braun L. 1990. On the information content of air temperature in the context of snow melt estimation. *IAHS* 190: 347–354.
- Latenser M, Schneebeli M. 2003. Long-term snow climate trends of the Swiss Alps (1931-99). *International Journal of Climatology* 23: 733–750. DOI: 10.1002/joc.912
- Lehning M, Völksch I, Gustafsson D, Nguyen TA, Stähli M, Zappa M. 2006. ALPINE3D: a detailed model of mountain surface processes and its application to snow hydrology. *Hydrological Processes* 20: 2111–2128. DOI: 10.1002/hyp.6204
- Lewkowicz AG. 2008. Evaluation of Miniature Temperature-loggers to Monitor Snowpack Evolution at Mountain Permafrost Sites, Northwestern Canada. *Permafrost and Periglacial Processes* 19: 323–331. DOI: 10.1002/ppp.625
- Luetschg M, Lehning M, Haeberli W. 2008. A sensitivity study of factors influencing warm/thin permafrost in the Swiss Alps. *Journal of Glaciology* 54: 696–704. DOI: 10.3189/002214308786570881
- Lundquist JD, Lott F. 2008. Using inexpensive temperature sensors to monitor the duration and heterogeneity of snow-covered areas. *Water Resources Research* 44: 1–6. DOI: 10.1029/2008WR007035
- Marmy A, Salzmann N, Scherler M, Hauck C. 2013. Permafrost model sensitivity to seasonal climatic changes and extreme events in mountainous regions. *Environmental Research Letters* 8: 035048. DOI: 10.1088/1748-9326/8/3/035048
- Martinez J. 1960. The degree-day factor for snowmelt-runoff forecasting. *IAHS-AISH P.* 468–477.
- Meløysund V, Leira B, Høiseth KV, Lisø KR. 2007. Predicting snow density using meteorological data. *Meteorological Applications* 14: 413–423. DOI: 10.1002/met.40
- Noetzli J, Gruber S. 2005. *Alpiner Permafrost - ein Überblick*. Lintzmeyer K (ed.). *Jahrbuch des Vereins zum Schutz der Bergwelt*, Selbstverlag, München 70: 111–121.
- Ohmura A. 2001. Physical Basis for the Temperature-Based Melt-Index Method. *Journal of Applied Meteorology* 40: 753–761. DOI: 10.1175/1520-0450(2001)040<0753:PBFTTB>2.0.CO;2
- Outcalt SI, Nelson FE, Hinkel KM. 1990. The zero-curtain effect: Heat and mass transfer across an isothermal region in freezing soil. *Water Resources Research* 26: 1509–1516. DOI: 10.1029/WR026i007p01509
- Pellicciotti F, Brock B, Strasser U, Burlando P, Funk M, Corripio J. 2005. An enhanced temperature-index glacier melt model including the shortwave radiation balance: development and testing for Haut Glacier d’Arolla, Switzerland. *Journal of Glaciology* 51: 573–587. DOI: 10.3189/172756505781829124
- PERMOS 2013. *Permafrost in Switzerland 2008/2009 and 2009/2010*. Noetzli, J. (ed.), *Glaciological Report Permafrost No. 10/11 of the Cryospheric Commission of the Swiss Academy of Sciences, Zurich, Switzerland*.

Using near-surface ground temperature data to derive snow insulation and melt indices for mountain permafrost applications

Pomeroy JW, Brun E. 2001. Physical properties of snow. In *Snow ecology: an interdisciplinary examination of snow-covered ecosystems*. Jones HG, Pomeroy JW, Walker DA, Hoham RW (eds). Cambridge, UK: Cambridge University Press, pp. 45–118.

Schmid MO, Gubler S, Fiddes J, Gruber S. 2012. Inferring snowpack ripening and melt-out from distributed measurements of near-surface ground temperatures. *The Cryosphere* 6: 1127–1139. DOI: 10.5194/tc-6-1127-2012

Schmidt S, Weber B, Winiger M. 2009. Analyses of seasonal snow disappearance in an alpine valley from micro- to meso-scale (Loetschental, Switzerland). *Hydrological Processes* 23: 1041–1051. DOI: 10.1002/hyp.7205

Schneider S, Hoelzle M, Hauck C. 2012. Influence of surface and subsurface heterogeneity on observed borehole temperatures at a mountain permafrost site in the Upper Engadine, Swiss Alps. *The Cryosphere* 6: 517–531. DOI: 10.5194/tc-6-517-2012

Senese A, Maugeri M, Vuillermoz E, Smiraglia C, Diolaiuti G. 2014. Using daily air temperature thresholds to evaluate snow melting occurrence and amount on Alpine glaciers by T-index models: the case study of the Forni Glacier (Italy). *The Cryosphere* 8: 1921–1933. DOI: 10.5194/tc-8-1921-2014

Staub B, Marmy A, Hauck C, Hilbich C, Delaloye R. 2015. Ground temperature variations in a talus slope influenced by permafrost: a comparison of field observations and model simulations. *Geographica Helvetica* 70: 45–62. DOI: 10.5194/gh-70-45-2015

Stocker-Mittaz C, Hoelzle M, Haeberli W. 2002. Modelling alpine permafrost distribution based on energy-balance data: a first step. *Permafrost and Periglacial Processes* 13: 271–282. DOI: 10.1002/ppp.426

Strasser U, Bernhardt M, Weber M, Liston GE, Mauser W. 2008. Is snow sublimation important in the alpine water balance? *The Cryosphere* 2: 53–66. DOI: 10.5194/tc-2-53-2008

Tardivo G, Berti A. 2012. A Dynamic Method for Gap Filling in Daily Temperature Datasets. *Journal of Applied Meteorology and Climatology* 51: 1079–1086. DOI: 10.1175/JAMC-D-11-0117.1

Tyler SW, Burak SA, McNamara JP, Lamontagne A, Selker JS, Dozier J. 2008. Spatially distributed temperatures at the base of two mountain snowpacks measured with fiber-optic sensors. *Journal of Glaciology* 54: 673–679. DOI: 10.3189/002214308786570827

Westermann S, Boike J, Langer M, Schuler TV, Etzelmüller B. 2011. Modeling the impact of wintertime rain events on the thermal regime of permafrost. *The Cryosphere* 5: 945–959. DOI: 10.5194/tc-5-945-2011

Wever N, Jonas T, Fierz C, Lehning M. 2014. Model simulations of the modulating effect of the snow cover in a rain-on-snow event. *Hydrology and Earth System Sciences* 18: 4657–4669. DOI: 10.5194/hess-18-4657-2014

Zhang T. 2005. Influence of the seasonal snow cover on the ground thermal regime: An overview. *Reviews of Geophysics* 43: RG4002. DOI: 10.1029/2004RG000157

Zingg T. 1951. Beziehung zwischen Temperatur und Schmelzwasser und ihre Bedeutung für Niederschlags- und Abflussfragen. *IAHS Publ. no. 32*: 266–269.

Table S1 - Meta-data and characteristics of selected IMIS snow stations:

The values for MAT (mean air temperature), MGST (mean GST), MGSTDJF (mean GST for Dec-Feb) and snow depth (mean Dec-Feb) are calculated based on the available data in the hydrological years 2004-2013 (aggregates with more than 5 % missing data are indicated with *).

ID	Name	Since	Elevation (m asl)	MAT (°C)	MGST (°C)	MGST_{DJF} (°C)	Snow_{DJF} (cm)
ANV-2	Anniviers - Orzival	1997	2630	-0.34	2.04	-0.69	128
ANV-3	Anniviers - Tracuit	1997	2590	0.1	3.68	-0.39	77
ATT-2	Les Attelas	1993	2545	-0.59	3.36	-0.24	121
BED-2	Bedretto - Cavanna	1996	2450	-0.03	2.1	-0.1	200
BER-3	Bernina - Puoz Bass	2000	2620	-0.42	3.14	-0.63	64
BEV-2	Bever - Valetta	1997	2510	-0.26	3.69	0.43*	98
BOV-2	Boveire - Pointe de Toules	2001	2700	-0.58	2.45	-1.1	86
CMA-2	Crap Masegn	1993	2330	0.31	3.22	-0.18	127
DAV-2	Davos - Baerentaelli	1998	2560	-0.48	2.79	0.23	105
DIA-2	Les Diablerets	1992	2575	-1.44	2.38	-0.86	184
EGH-2	Eggishorn	1993	2495	-0.5	2.91	-0.24*	116
FUL-2	Fully - Grand Cor	1999	2610	-0.85	1.84	-0.13	185
GAN-2	Gandegg	1996	2717	-1.05	1.8	-0.48	204
GOM-2	Goms - Ernergalen	1999	2450	0.01	3.05	-0.15	111
GOR-2	Gornergrat	1993	2950	-2.3	1.81	-1.34	116
GUT-2	Guttannen - Homad	1999	2110	2.19	3.85	-0.11	88
ILI-2	Val d'Illiez - Les Collines	2000	2020	3.26	4.3	-0.21	79
JUL-2	Julier - Vairana	1998	2430	-0.16	2.85	0.12	98
MES-2	Mesocco - Pian Grand	2002	2380	0.37	2.66	-0.65	113
NEN-2	Nendaz - Essertse	1999	2325	1.68	3.97	-0.43	61
PMA-2	Piz Martegnas	1993	2430	0.22	4.23	0.88	79
PUZ-2	Puzzetta	1996	2195	0.78	3.71	-0.08	76
SAA-2	Saas - Seetal	1997	2480	0.57	3.55	-1.27	52
SAA-3	Saas - Schwarz mies	1997	2810	-1.24	-0.13	-8.53	37
SCA-3	Schaechtal - Alpler Tor	1999	2330	0.64	2.26	-0.19	185
SCH-2	Schilthorn	1996	2360	1.57	2.6	0	154
SPN-2	Simplon - Alpjer	1996	2620	-0.5	1.25	-4.09	42
STN-2	St. Niklaus – Ob. Stelligletscher	1998	2910	-1.79	1.01	-1.24	82
TIT-2	Titlis	1993	2140	2.18	3	-0.7	135
URS-2	Urseren - Giltnasen	1997	2170	1.42	3.58	-0.08	75
VDS-2	Val. de la Sionne - Donin du Jour	1998	2390	1.02	2.66	-0.18	174
VIN-2	Vinadi - Alpetta	1998	2730	-1.97	-0.25	-4.5	84
WFJ-2	Weissfluhjoch	1992	2540	-0.71	2.54	-0.42	129

Table S1 and other supplementary material including R code and a small sample data set can be downloaded at: <http://onlinelibrary.wiley.com/doi/10.1002/ppp.1890/suppinfo>.

Publication II

Gap filling algorithm for ground surface temperature data measured in permafrost and periglacial environments

Citation: Staub, B., Hasler, A., Noetzli, J. & Delaloye, R.: Gap filling algorithm for ground surface temperature data measured in permafrost and periglacial environments. Submitted to *Permafrost and Periglacial Processes*.

Abstract: Ground surface temperatures (GST) are widely measured in mountain permafrost areas and can be interrupted by gaps of different timing and duration, e.g. due to limited access or broken loggers due to rough meteorological conditions. Gaps complicate the calculation of aggregates and indices required for the analysis of temporal and spatial variability between loggers and sites. This article presents an algorithm for the estimation of daily mean GST and the resulting uncertainty. It is designed for the automatic filling of data gaps in a large data base of several tens to hundreds of time series such as for example the Swiss Permafrost Monitoring Network PERMOS. Using a large number of randomly generated artificial gaps, the performance of the gap filling routine was validated regarding the bias resulting on annual means and thawing and freezing degree days and the accuracy of the uncertainty estimation. Quantile mapping has shown to be the most reliable gap filling approach. But up to gap durations of 3-5 days, linear interpolation between neighbouring values performed as good. Finding the most similar regressors is crucial and also the main source of errors, particularly because of the large spatial and temporal variability of ground and snow properties in high mountain terrains. Applying the gap filling technique presented to the PERMOS GST data, the total amount of complete hydrological years available for analysis could be increased by 70 % (>450 filled gaps), likely without exceeding a maximal uncertainty of ± 0.25 °C in calculated annual mean values.

Keywords: Mountain permafrost, ground surface temperature GST, long-term monitoring, gap filling, uncertainty estimation, Swiss Alps

1 Introduction

Ground surface temperatures (GST) are widely measured to investigate the spatial variability of the thermal conditions in potential permafrost areas (Bonnaventure and Lewkowicz, 2008; Etzelmüller et al., 2007, Guglielmin, 2006; Hoelzle et al., 1999; Wu et al., 2013). Especially in mountainous terrains with highly variable topo-climatic and snow characteristics, indices like mean annual ground surface temperatures (MAGST) and thawing and freezing degree-days (TDD, FDD) are frequently used to compare between sites and to reveal inter-annual changes (Gubler et al., 2011; Isaksen et al., 2011; Luetschg et al., 2008). For a reasonable calculation of such aggregates or indices, uninterrupted time series are required. Although within the Swiss Permafrost Monitoring Network PERMOS many GST time series cover now 10-15 years (PERMOS, 2013), the majority of the data series are affected by gaps of different duration (hours to years). To increase the amount of complete time series, the data need to be resampled to a common time interval (e.g. daily means) and gaps to be filled. Ideally, estimated values of the missing data would come together with a statistical estimate of their uncertainties to finally consider the propagation of these uncertainties for the calculation of aggregates and indices.

This paper presents a fully-automatic algorithm to treat gaps in large sets of GST data by considering typical terrain- and snow characteristics of high-mountain areas as well as differences related to the thermistors in use and their placement in the field. To ensure a consistent calculation, the algorithms use daily means as for input and output. Although the gap-filled, synthesized output data intend to be representative for the mean thermal state during a specific gap and at best considering local characteristics, it should only be used for aggregates and not at the daily scale e.g. to derive additional information such as snow characteristics (Schmid et al., 2012; Staub and Delaloye, in press). The reanalysis of past GST variations as well as the use of physically-based models are not intended, and in principle, simple techniques are preferred. The applicability of the approach is validated by means of artificial gaps in the PERMOS GST data.

2 Data description

2.1 Characteristics of GST time series in permafrost

The seasonal pattern and inter-annual variations of GST are dominated by the snow characteristics (Delaloye, 2004; Gislén et al., 2014; Park et al., 2014; Staub and Delaloye, in press; Zhang, 2005). In the snow-covered state, GST usually remain close to 0 °C at locations without permafrost and/or rather fine-grained and humid substrates. But especially at locations with intense ground cooling (e.g. on ridges less influenced by snow or in coarse-blocky and porous ground material favouring convection) GST may be subject to large inter-annual variations in FDD or MAGST (Gislén et al., 2014; Gubler et al., 2011; Hasler et al., 2015). During the snow-free period air temperature is the dominating factor and the differences among various GST time series are much smaller (Guglielmin et al., 2012). The remaining spatial variability is mainly a result of radiation and shading effects, the placement depth of the sensor, as well as terrain and subsurface properties (roughness, humidity, porosity and thermal conductivity etc.). Very characteristic for a specific measurement location is

also the melting period in spring, when phase changes keep GST at 0 °C (so called zero curtain, cf. Outcalt et al. (1990)). This zero curtain effect can occasionally be observed in autumn if snow falls on still warm ground and basal melting occurs. Steep bedrock or windblown locations show no (or very short) zero curtains and generally follow much more the variations of air temperature. All these characteristics imply that the similarity of different GST time series rather depends on topography and snow characteristics than spatial proximity. Therefore, gap filling approaches are particularly promising when being applied to large data sets, where similar characteristics for several time series become more likely.

2.2 Accuracy and pre-processing

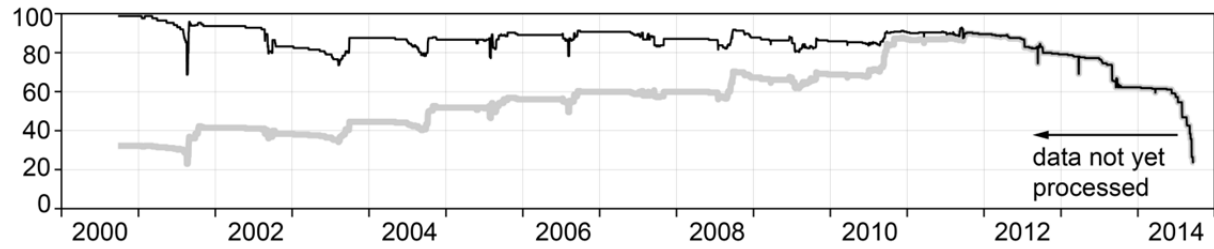
GST are usually recorded with low-cost miniature temperature loggers (Hoelzle et al., 1999; Lewkowitz, 2008). Wherever zero curtains occur, offsets to 0 °C are minimized to calibrate the sensors. Potential inhomogeneities, both in a time series or between time series, can be related to the sampling resolution (ranging between 30 min and 6 hours), the precision of the sensors (0.23-0.27 °C for UTL-1 (75 % of PERMOS GST data), <0.1 °C for UTL-3 (8 %), 0.5 °C for iButton® DS1922L (6 %), 0.1 °C for Geoprecision M-Logs (11 %)), the placement of the loggers in the field as well as changes of the terrain morphology (e.g. on fast moving rock glaciers). While the last points cannot be improved during post-processing, different measurement intervals can at least partly be homogenized. Here, we linearly interpolated the data on regular time intervals (e.g. 2h) in a first step and aggregated them to daily means in a second step. Days with missing raw data or a sampling resolution of less than 4h were not included. However, any other systematic data preparation procedure could be used to achieve a consistent and comparable data basis. Time series of at least five years with measurements have been used for validation (Section 4). Working with daily means allows an accurate calculation of MAGST or degree-day indices.

2.3 Gap characteristics and completeness of PERMOS GST data

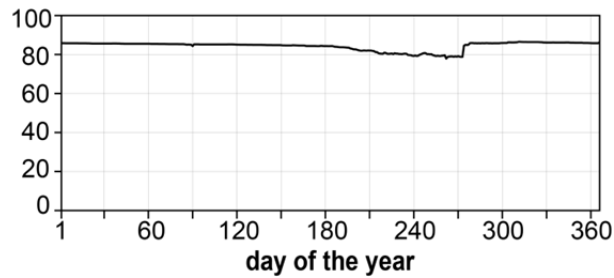
GST time series as obtained within the PERMOS network start between 1994 and 2011 and have gaps ranging from some days to more than a year. For the 278 loggers and the hydrological years 2000/01-2013/14 shown in Figure 1a, the 150 longest GST time series are interrupted by about 300 gaps with a mean duration of 145 days. But about 50 % of these gaps are shorter than one month and 30 % are no longer than 5 days (Figure 1c). Most gaps occurred in the summer season, probably because maintenance was sometimes not done in the field directly but later in the lab (Figure 1b). Because in the snow-free period GST are influenced by common, atmospheric signals, covariance between different time series is high and empirical-statistical algorithms (Section 3) are expected to perform most reliable for filling data gaps.

Gap filling algorithm for ground surface temperature data measured in permafrost and periglacial environments

a) GST data completeness: temporal evolution (%)



b) GST data completeness: seasonal (%)



a) GST gap duration (%)

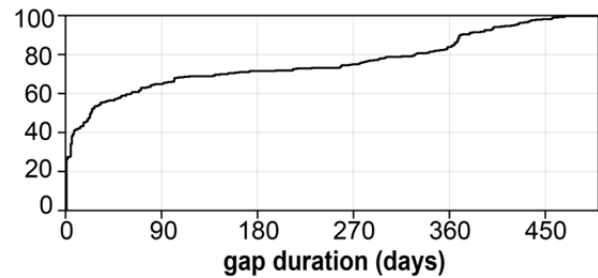


Figure 1: Data completeness and gap characteristics of the PERMOS GST data for the hydrological years 2000/01-2013/14 (gaps after 2012 are mainly because the data were not yet processed): a) data completeness relative to the total number of GST series already started (black line) and relative to the maximal number of GST loggers (in %, 278 in 2011/12, grey line); b) seasonal pattern of data completeness with most data gaps in summer; c) empirical cumulative density function of the gap duration for gaps < 500 days.

3 Gap filling algorithm

3.1 Approaches

Dealing with missing data is a major problem of many different research disciplines and the need for standardization has been identified (Falge et al., 2001; Gudmundsson et al., 2012). The list of potential approaches ranges from process-based models to empirical-statistical transformations, notably with very different requirements regarding input data, time windows and intervals, the applicability to reproduce the mean conditions and/or to retain the short-term variability, their ease of implementation and performance (e.g. Moffat et al., 2007). However, no studies are available comparing gap filling methods explicitly for ground temperature data measured in permafrost and periglacial environments. Gisnås et al. (2014) used air temperature to fill short gaps of only some days during the snow-free period. Hasler et al. (2015) replaced missing data with mean GST values and mean uncertainties for the comparison of annual means. Magnin et al. (2015) filled gaps < 5 days by linear interpolation between the nearest available data points. Gaps up to 1.5 months they filled with the average value of 30 days on each side of the gap, as already done by Hasler et al. (2011). Within PERMOS, gaps in reference GST time series used for reporting were filled by linear regression on the basis of monthly means or monthly degree-day sums to calculate the indices MAGST, TDD and FDD (PERMOS, 2013). For a more flexible use of the measured and synthesized data, daily means with daily uncertainty estimates are required.

Process-based models (Ekici et al., 2015; Lehning et al., 2006; Westermann et al., 2013) are not feasible for larger quantities of GST time series because of the high requirements on input variables (meteorological data and calibration parameters) and the high computational effort. Empirical

statistical methods (Gudmundsson et al., 2012; Themessl et al., 2011) are more appropriate. Statistical transformations are the most commonly used for the bias correction and the spatial transfer of meteorological parameters (Gudmundsson et al., 2012; Rajczak et al., 2015; Tardivo and Berti, 2014).

In the following, we describe the different techniques used for this study: **Linear interpolation LI** (Section 3.2) from GST values prior and after the gap of the same logger is independent from other data and is mainly applicable to fill very short gaps of a few days. For gaps longer than the persistence of synoptic weather patterns, a more sophisticated method is required based on similar regressor time series and using techniques for the spatial transfer and bias correction, which adjust for the shape of the distribution (Gudmundsson et al., 2012; Rajczak et al., 2015; Themessl et al., 2011). The **quantile mapping** method (**QM**, nonparametric statistical transformation) was used for the filling of long GST gaps of up to several months. With the **QM** technique, which is widely used to adjust simulation results (e.g. coarse-gridded RCM output) to local station observations, gaps in meteorological data have been successfully filled for several PERMOS sites (Rajczak et al., 2015). **QM** uses the empirical distribution of the data and is therefore not depending on a pre-defined distribution. Yet, **QM** is based on the assumption that the differences between the regressor and target logger are stationary, which is a simplification regarding inter-annual variations and long-term trends. We however consider that **QM** could account for the high temporal and spatial variability of high-mountain GST quite realistically as long as the regressor and target logger are influenced by the same processes. Therefore, the **QM** approach has been selected for the filling of long GST gaps as described in Section 3.3.

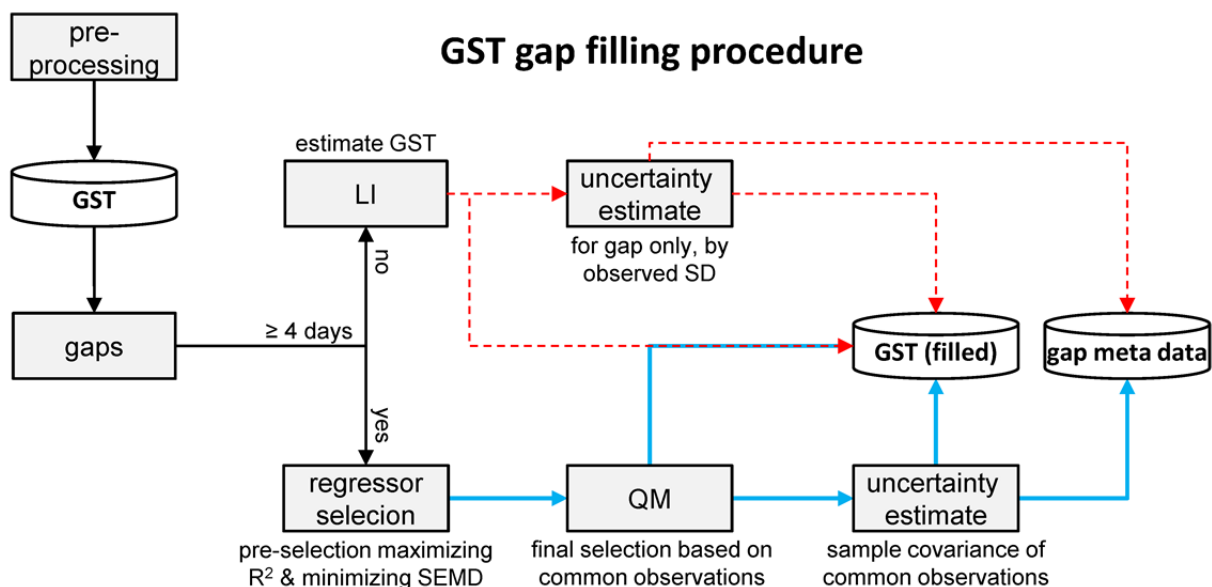


Figure 2: Flow chart describing the general approach for the GST gap filling: Depending on the duration of the gaps, either linear interpolation (LI, for gaps durations < 4 days) or quantile mapping (QM) were used to estimate missing GST data. Besides of the GST estimates (daily means), we suggest to store the resulting uncertainties as well as meta-information (regressor logger, residuals etc.). The figure illustrates how the gap filling routine could be implemented into a monitoring data base structure.

Gap filling algorithm for ground surface temperature data measured in permafrost and periglacial environments

As illustrated in Figure 2, the general work flow first checks the gap characteristics, selects the appropriate gap filling approach and (only for *QM*) the most suitable regressor logger. In a second step, GST values as well as the resulting uncertainties are estimated for the target logger. The operational programming routine written in R (R Core Team, 2015) and a small demo data set are available as supplementary information.

3.2 Linear interpolation of values in short gaps

Calculation of expected GST value

Based on GST average values before (GST_{prior}) and after the gap (GST_{after}), missing data (GST_{synt}) at date i in the gap of length n can be filled by linear interpolation (*LI*, Equation 1) as examples in Figure 3 show.

$$GST_{synt,i} = GST_{prior} + \left(\frac{GST_{after} - GST_{prior}}{n + 1} \right) i, \text{ with } i = \{1, 2, \dots, n\} \quad (1)$$

While gaps of only one day are ideally interpolated just between the two nearest neighbours (Figure 3c), longer gaps require longer aggregation windows before and after the gap to calculate representative values for GST_{prior} and GST_{after} (Figure 3d). Therefore, the length m of the aggregation windows is defined as:

$$m = \left\lceil \frac{n}{2} \right\rceil \in \mathbb{N} \quad (2)$$

Because GST data are highly autocorrelated during the snow-covered periods when the ground is thermally insulated from air temperature variations, *LI* would technically be suitable also to fill gaps of up to several weeks during this time of the year. Such gaps were, however, not observed in the PERMOS data because they usually persist until the next maintenance takes place in summer (no remote-control and no access to replace the logger during winter). The analysis of artificial gaps (Section 4.1) showed that on average, the *QM* approach (Section 3.3) is more reliable for gaps longer than 3 days regarding the estimated GST values.

Calculation of uncertainty

For short gaps filled by linear interpolation (Equation 1), the mean uncertainty σ (°C, cf. Equation 3) can be estimated with the standard deviation (SD) calculated over all days in GST_{prior} and GST_{after} . This method accounts for differences in the short-term GST variability, resulting in greater uncertainties if this variability is larger (Figure 3a and b). These uncertainties are supposed to be stochastic and partly self-compensating, which is why the mean uncertainty of a GST aggregate can be divided by the square root of observations (Section 3.4).

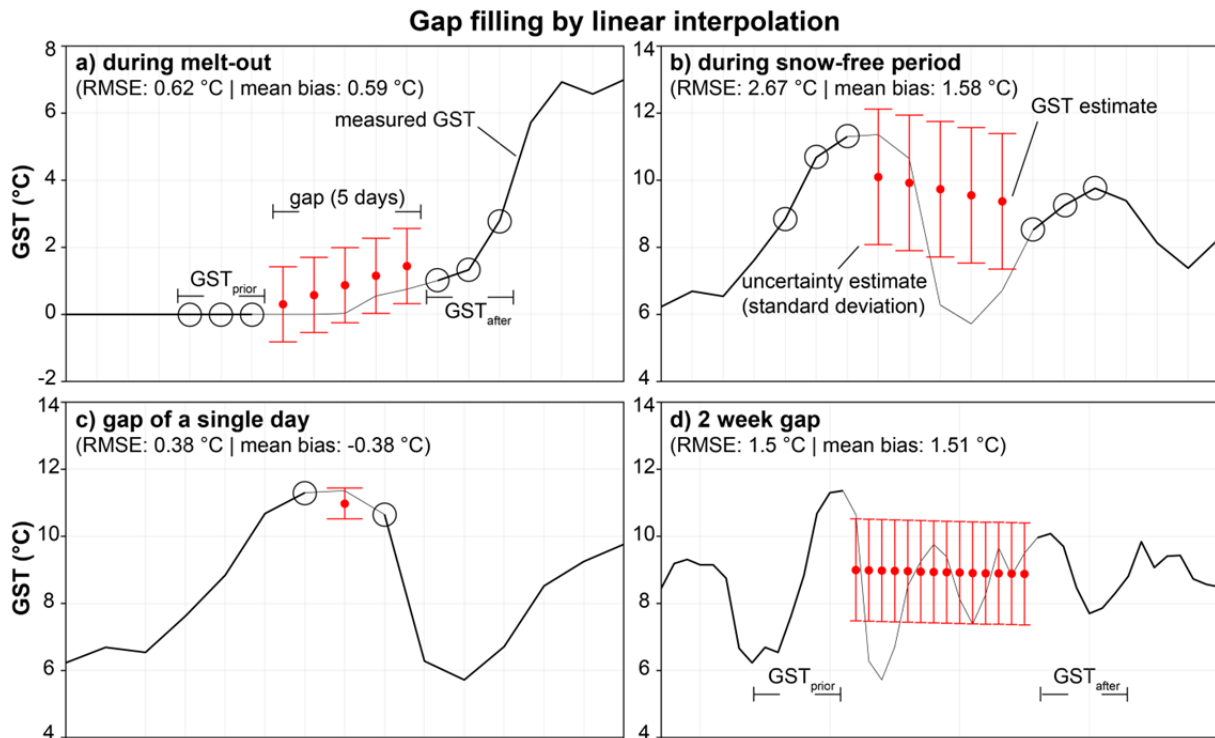


Figure 3: Examples for artificial gaps filled using linear interpolation: a) at the end of the snow melt period in early summer; b) when the ground is snow-free; c) for a gap of a single day; and d) a gap of two weeks. The red dots represent the interpolated GST values, the mean uncertainty (error bars) was approximated based on the SD of GST_{prior}/GST_{after} . The RMSE values and mean bias is calculated between the interpolated, synthetic GST in comparison to the real values (black lines).

3.3 Quantile mapping using best regressor for long gaps

Selection of the best regressor logger

The selection of the best regressor logger (cf. Figure 2) is the crucial task for filling gaps using the *QM* approach, particularly in mountainous terrain with its extreme spatial heterogeneity. The robustness of the transformation further increases with the number of common observations. The regressor logger is hence selected in the following steps:

- 1) Completeness of measurement data during the entire gap is required.
- 2) The season of the gap needs to be covered by the target and regressor logger in common in at least 5 years. Gaps shorter than 30 days are extended to a minimum length of 30 days for the assessment of similarities with other loggers.
- 3) Calculation of the maximum of the Pearson product-moment and Spearman's rank correlation coefficients as well as the minimum of the standard error of the mean differences (SEMD, see below for further details) for the remaining common observations (Figure 4b). The best 5 % of potential regressors for these three criteria are selected for step 4.
- 4) Application of the *QM* method to the selected regressor loggers and calculation of residuals between fitted values and observations. The logger with the minimal standard error of these residuals is selected as final regressor logger (Figure 4a-b).

Gap filling algorithm for ground surface temperature data measured in permafrost and periglacial environments

By maximizing the Pearson correlation in step 3, the regressors of best covariance with the target logger can be selected. This is particularly important for *QM* because the statistical transformation corrects for errors in the mean and the percentiles, but not the daily correspondence between the regressor and the target logger (Rajczak et al., 2015). The Spearman's rank correlation is added to additionally identify potential regressors, which data show a strong but non-linear relationship to the data of the target logger. Since correlation is only defined for finite $SD > 0$, which is not necessarily given e.g. during periods of snow melt, SEMD is used in addition. It is computationally efficient and accounts for the number of observations. For this study, the top 5 % of all statistical measures have been pre-selected in step 3. This pre-selection of regressor loggers mainly reduces computation time for large data sets because the statistical transformation (Figure 4c-d) is only evaluated for a subset of the potentially most suitable regressor loggers. To account for seasonally differing snow and meteorological conditions, only the days of the year where the gap occurs were used to fit the *QM* model. Within step 2, the minimal gap duration of short gaps is therefore set to 30 days to gain a representative sample of values for fitting the *QM* model.

Calculation of expected GST value

The relatively homogeneous evolution of GST at different sites (PERMOS, 2013) allows the use of *QM* even for filling long gaps of several months (Figure 4). Most challenging are the highly variable snow conditions influenced by precipitation, wind, radiation and avalanches, which may substantially differ even in short spatial distances. Therefore, each season of the gap period should be equally represented in the calibration data (Figure 4a). The robustness to fit means and extremes is the great advantage of the *QM* approach (Themessl et al., 2011). See Gudmundsson et al. (2012) for a more detailed description of the *QM* technique and Gudmundsson (2014) for the implementation and use in R.

Calculation of uncertainty

The uncertainty could be estimated for the entire gap, e.g. as a standard error of the mean as done by Hasler et al. (2015), or separately for each day. To gain accuracy regarding the seasonal pattern and to be more flexible for the quantification of mean uncertainties of aggregates and indices (Section 3.4), we suggest daily uncertainty estimates. Based on the residuals ε between the observations and the fitted values during the calibration period, uncertainty estimates (σ) can be approximated for each day of the year. To account for the length of the calibration period, the corrected sample standard deviation is used with n_{year} being the number of years with common observations (Equation 3).

$$\sigma = \pm \sqrt{\frac{1}{n_{year} - 1} \cdot \sum \varepsilon^2} \quad (3)$$

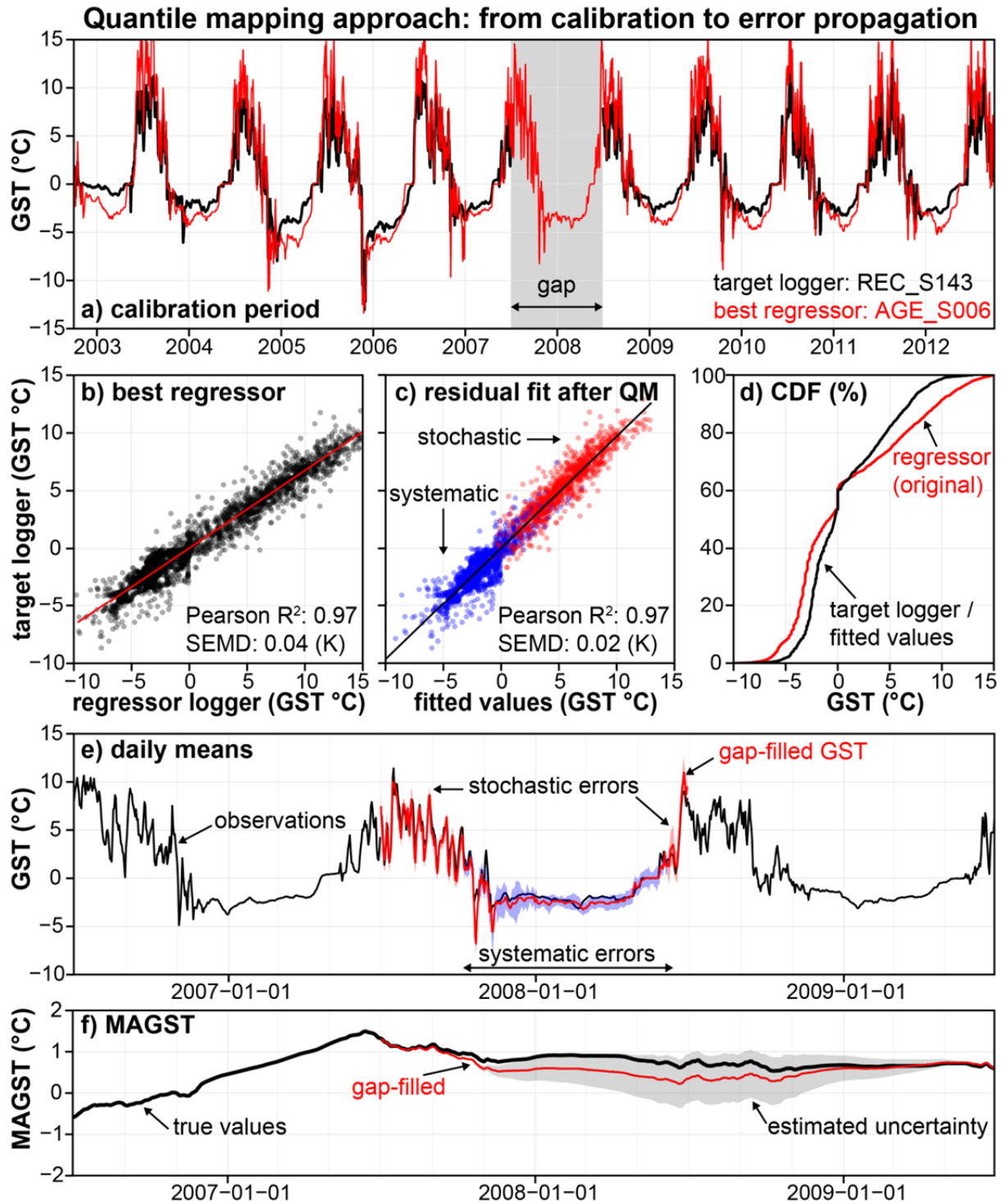


Figure 4: Illustration of the quantile mapping (QM) approach to fill data gaps at the example of an artificial 365-day gap: a) and b) compare the target logger and the best regressor for the entire calibration period (SEMD: standard error of the mean differences); c) comparison of the fitted values after the QM transformation, based on the remaining residuals, stochastic and systematic uncertainties are quantified; d) illustration of the cumulative density function (CDF) of the regressor and the target logger; the results of the gap filling are illustrated as daily means in e) and as running MAGST in f) in comparison with observations (black).

Assuming that the calibration period (common observations in the respective season, cf. Figure 4a) covers different meteorological and snow conditions, the inter-annual variability is to some extent included in this estimate. Especially at the beginning and the end of the melting period, but also

Gap filling algorithm for ground surface temperature data measured in permafrost and periglacial environments

during winter when the ground is snow-covered, the uncertainty estimates are larger because of larger inter-annual variability (Figure 4c and e). As a general tendency, the residuals are more likely to be systematic (and not self-compensating) when snow insulates the ground thermally. Therefore, we suggest using a simplified snow-detection filter similar to those suggested by Schmid et al. (2012) and Staub and Delaloye (in press). Here, days were considered as snow-covered when the weekly SD of daily mean GST were ≤ 0.25 °C to identify days of the year where either the target or the regressor logger are likely to be snow-covered. Based on this snow-information, stochastic and systematic errors can be separated (Section 3.4).

3.4 Uncertainty propagation for indices

According to the error propagation laws, the uncertainties resulting from gap filling can be calculated also for aggregates and indices. Theoretically, stochastic errors (σ_{sto}) are supposed to be close to normal distribution and self-compensating with increasing sample size n_{sto} (Figure 4e-f). Therefore, the mean error for a given period $i=\{1,2,\dots,n_{sto}\}$ can be divided by the square root of the total number of observations or rather gap length (Equation 4). Systematic errors (σ_{sys}) are additive and need to be averaged over all samples j in n_{sys} to calculate the mean uncertainty of the gap (σ_{gap}). The stochastic errors are basically restricted to the snow-free period and identified as described in Section 3.3.

$$\sigma_{gap} = \pm \sqrt{\left(\frac{\sigma_{sto}}{\sqrt{n_{sto}}}\right)^2 + \sigma_{sys}^2} = \pm \sqrt{\left(\frac{1}{n_{sto}} \sum_{i=1}^{n_{sto}} \sigma_{sto,i}\right)^2 + \left(\frac{1}{n_{sys}} \sum_{j=1}^{n_{sys}} \sigma_{sys,j}\right)^2} \quad (4)$$

An example of uncertainty estimates for running annual means (MAGST) is illustrated in Figure 4f. Measurement errors due to the limited accuracy of the sensors and the precision of the loggers (cf. Section 2.2) could be included analogously.

4 Validation with artificial gaps

4.1 Overview and comparison of the *LI* and *QM* approach for short gaps

We validated the gap filling routine with artificial gaps using complete GST observations from 18 different field sites and 173 different loggers over 10 hydrological years (2002/03-2011/12). The large majority of these time series were measured on gently inclined terrain and only some originated from steep bedrock. Hence, the difficulties related to the temporally and spatially variable snow conditions mentioned in Section 2.1 made the application and validation of the gap filling very challenging. The starting dates (day of the year), loggers and gap durations were randomly selected but forced to match the characteristics of the existing gaps in the PERMOS data (Figure 1). In a first simulation, the performance of the linear interpolation (*LI*, Section 3.2) and the *QM* approach (Section 3.3) was compared for short gaps of up to 30 days between June and October ($n: \sim 24'000$ gaps). This first simulation aimed at defining the threshold for the maximal gap duration, until which *LI* could be chosen as an alternative for *QM* (cf. Figure 2). The validation showed that the *QM* method performed significantly better regarding the GST estimates than *LI* for gaps of 4 days or more.

Based on this threshold, the second validation run applied the final gap filling routine for gap durations between 1-500 days (n: ~18'000 gaps, ~2.5 Mio. days with missing values). For temperature data with less short-term variability (e.g. ground temperatures at depth or GST during winter), $L1$ would be a reasonable choice for longer gaps as well.

4.2 Validation of gap filling algorithm

Calculation of expected GST value

The synthetic (simulated/gap-filled) GST data showed a good overall agreement compared to observations. The time series of the simulated daily mean GST was close to the observations with an R^2 of 0.93 (RMSE ~1.6 °C), although the reconstruction of the correct daily values was not the primary aim. More relevant was the performance for aggregates and indices. Because errors partly compensate, the RMSE of simulated and observed GST mean values for the entire gap (MGST) was even better (Figure 5a). Also the degree-day sums FDD and TDD calculated on the basis of gap-filled and observed data showed a very high covariance and reasonable RMSE values (Figure 5b). For comparison: The temporal variation (SD) of TDD values was about ± 140 and ± 180 for FDD, respectively. The spatial variations were even larger, with SD around ± 230 for TDD and ± 255 for FDD. The largest outliers occurred during the transition period between the snow melt to the snow-free summer season (cf. scatters along the 0 °C-lines on Figure 5a). With larger gap sizes, the resulting bias on annual means tended to increase (Figure 5c). In 95 % of the situations, the maximal bias on MAGST (if running MAGST would be computed based on the gap-filled data) remained below 0.5 °C even for gaps of 6-8 months duration. In the best 50 % of instances, the maximal MAGST bias did not exceed 0.25 °C. Inter-annual MAGST variations observed in the PERMOS data ranged between an amplitude of 2-3 °C and the respective SD was in the order of ~0.5 °C (cf. PERMOS, 2013). Applied to the real gaps in the PERMOS GST data (Figure 1), more than 450 gaps could be filled, very likely without exceeding a maximal MAGST bias of ± 0.25 °C. This equals an increase of complete hydrological years by ca. 70 % with uncertainties in the order of the precision of the most popularly used miniature logger UTL-1. Since GST measured on steep bedrock are less influenced by snow and closely follow the variations of air temperature, these data sets can theoretically be filled with smaller uncertainties as long as a suitable regressor time series is available. This was, however, not observed due to the limited amount of time series used representing steep bedrock.

Calculation of uncertainty

At the daily scale, the differences between estimated uncertainties and the observed absolute bias (synthetic-observed GST values) were smallest during the winter season and largest at the end of the spring zero curtain because of the spatially and temporally very variable snow disappearance (Figure 6a). The median difference remained very close to 0 °C all year long, which means that uncertainty was not systematically over or underestimated. The remaining scatter visible in Figure 6a was also due to the limited significance of the uncertainty estimation at daily scale (Section 3.4). Regarding the aggregation level of entire gaps, the estimated uncertainties were slightly larger than the observed absolute bias, +0.045 °C on average. For ~60 % of all gaps (~70 % of all reconstructed daily mean values), the observed absolute errors were smaller than the estimated uncertainty and

Gap filling algorithm for ground surface temperature data measured in permafrost and periglacial environments

the differences were generally small (RMSE: 0.21 °C) and normally distributed (Figure 6b-c). However, the correlation between the estimated uncertainties and the observed absolute bias was not very clear (R^2 : 0.37).

Validation of the expected GST value

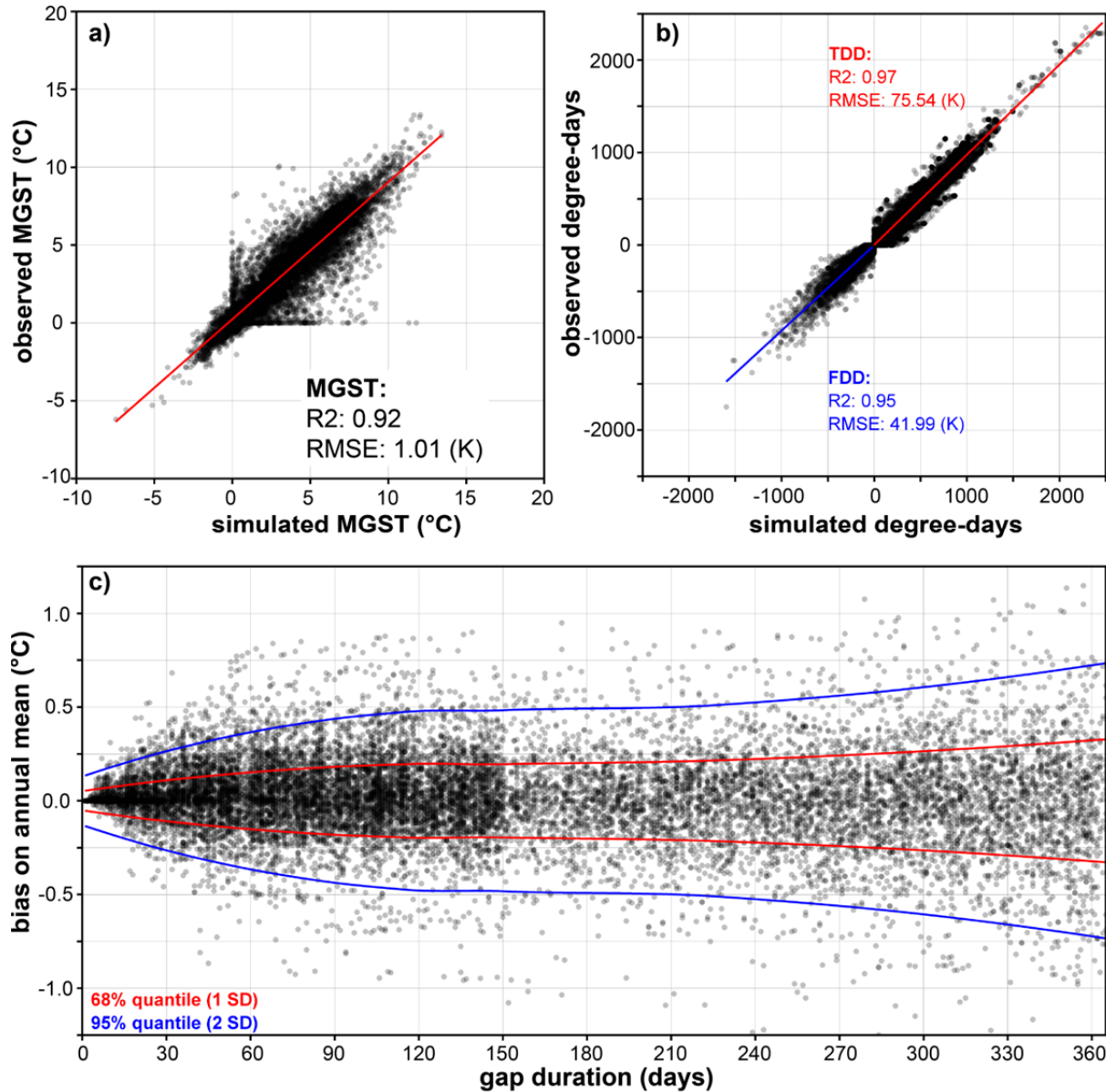


Figure 5: Comparison of simulated (synthetic/gap-filled) and observed GST for ~18'000 gaps (~2.5 Mio daily mean values): a) scatterplot based on mean GST (MGST) for entire gaps; b) scatterplot comparing simulated and observed thawing (TDD) and freezing degree days (FDD); c) maximal bias resulting on MAGST in function of the gap duration: each point corresponds to one artificial gap, the red lines show the limits of 1 SD (68 % quantile) and the blue lines for 2 SD (95 % quantile) of the absolute annual bias.

The uncertainty estimation for the shortest gaps of up to 3 days, for which the mean uncertainty was estimated based on the short-term variability before and after the gap according to the *LI* approach (Section 3.2), has shown to be very accurate with R^2 of 0.86 and RMSE of 0.27 °C. The high autocorrelation of the GST time series at very short temporal scales was the most probable cause for this high covariance between estimated uncertainty and observed bias.

But also the first validation run which compared the *LI* and *QM* approach for gap durations between 1 and 30 days revealed that in ~60 % of the situations the uncertainty estimation of the *LI* method performed better than that of *QM*. However, to fill gaps in GST time series, we recommend the *QM* method for gap durations in the order of weeks because it estimates the GST values clearly more accurately. But especially for data of lower daily and seasonal variation such as ground temperatures measured at depth or GST during the snow-covered period, the *LI* method could be very promising also regarding the uncertainty estimation.

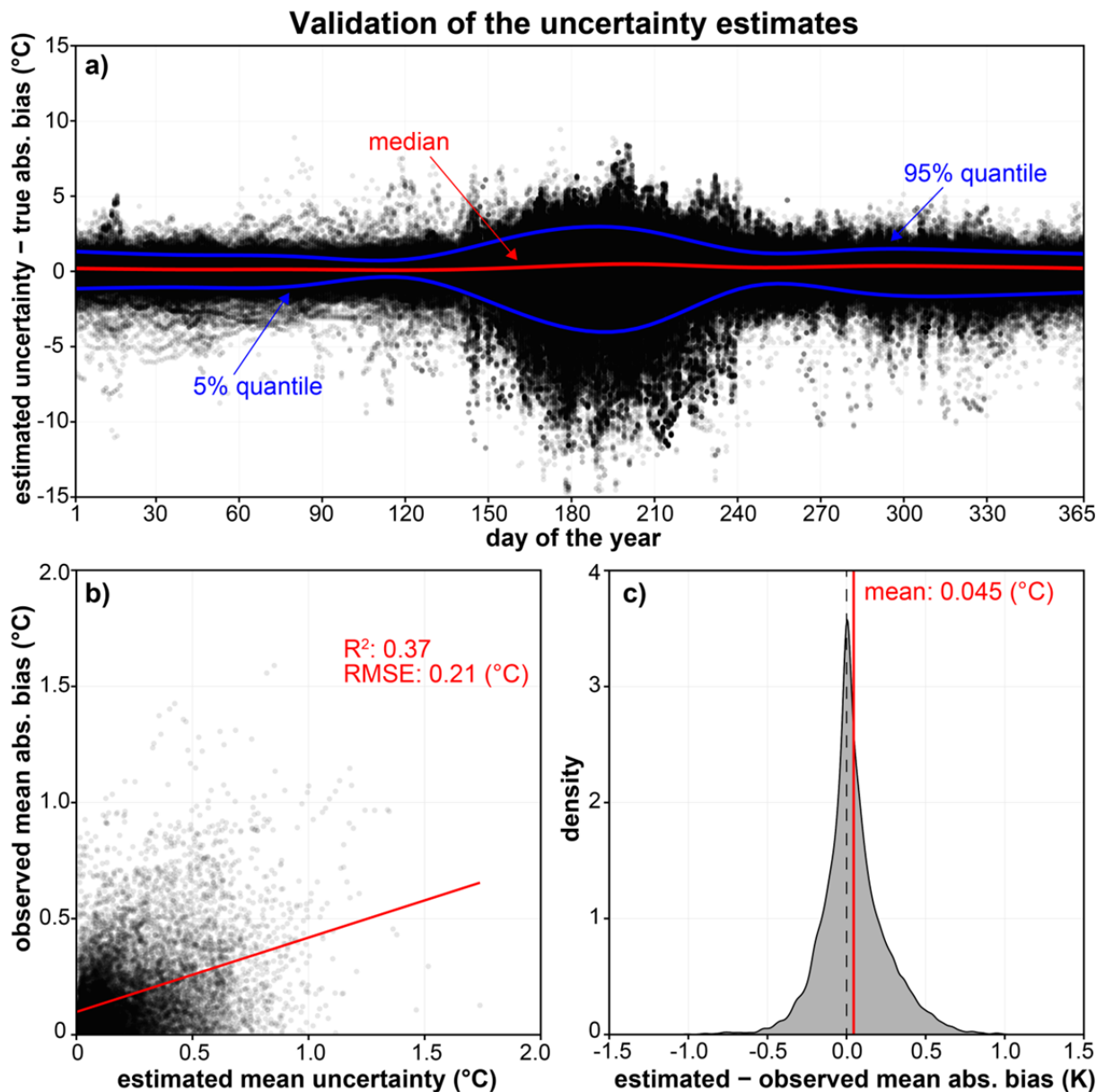


Figure 6: Comparison of estimated uncertainties and the true absolute bias: a) seasonal pattern based on daily mean values (the red line indicates the median, the blue lines illustrate the 5 % and 95 % quantiles); b) scatterplot comparing the estimated mean uncertainties and the mean absolute bias for entire gaps; c) density distribution of the same data as shown in b.

Gap filling algorithm for ground surface temperature data measured in permafrost and periglacial environments

To improve the uncertainty estimation for the *QM* approach, the inter-annual variability could be assessed in more detail by means of separated validation data, e.g. by means of cross-validation techniques. Thereby, each year of the common observation period could be validated separately by excluding it from calibration. This would, however, only make sense for long time series of at least ~10 years. Alternatively, expected GST values could be calculated for a multitude of regressor loggers and the daily uncertainty values be estimated from the resulting differences. The latter approach would probably be more adequate for the usually short GST time series and take the spatial variability into account.

The validation using artificial data gaps gave also insights on similarities of the different GST time series. For almost 50 % of the gaps where *QM* was applied, the selected regressor logger was from the same study site (usually in 50-500 m distance). For gaps during the winter period, this proportion was slightly higher. Especially for short gaps during summer, only ~35 % of the regressor loggers originated from the same site. This means that in the majority of situations, the most similar GST time series were potentially several tens or even hundreds of kilometres away. Moreover, each target logger used 7 different regressor loggers on average (4 % of all available loggers). Among these preferred regressor loggers, the most frequently used filled 57 % of all gaps of the corresponding target logger. These observations demonstrate how a large set of distributed time series can be of use to fill data gaps, especially in highly heterogeneous mountain terrain. Furthermore, they illustrate the relevance of snow and the point-specific, topo-climatic conditions in high-mountain terrains for the evolution of GST at various time scales. In this regard, the diversity of the potential regressor time series is more important than their quantity, especially for filling gaps during the winter season. It could be interesting to assess in more detail the minimal number of time series required to apply the gap filling approach e.g. for the entire Swiss Alps. Possibly, 30-50 continuous time series measured in very diverse ground and snow properties and characterising the precipitation effects of 3-5 main regions could be sufficient to fill the majority of data gaps in the PERMOS GST data set. The more time series are available, the higher the chances are to find appropriate regressors.

Conclusions

This paper introduces an automatic procedure to fill gaps in GST data sets on the basis of daily mean values. The approach is optimized to consider spatial and temporal variations which result from the heterogeneous terrain and snow characteristics of high-mountain regions. A validation was done using artificial gaps and GST data from the PERMOS network. The main conclusions on the use and limitations of the presented approach are:

- Linear interpolation (*LI*) works well to fill gaps shorter than one week. The analysis with artificial gaps showed that *LI* performed as good or better as the more complex quantile mapping (*QM*) approach for gaps up to three days duration. The uncertainty estimation of the *LI* method was slightly more robust than that of the *QM* approach for gap durations of up to one month.

- Since *QM* corrects well for mean biases, even gaps of several months duration may be filled with reasonable bias on MAGST in the order of the precision of the common UTL-1 data logger. Maximal MAGST bias resulting from one-year gaps did mostly not overpass ± 0.5 °C, what corresponds to the standard deviation of inter-annual MAGST variations. Probably, a high number of potential regressors as well as long periods with common observations make the approximation of GST values and the quantification of uncertainties more reliable.
- The validation with artificial gaps showed that the resulting mean error was usually smaller compared to the estimated uncertainty. Although the uncertainty estimation and error propagation approach is rather conservative regarding the effects of snow, the results are not yet fully satisfying, particularly during snow disappearance. Potentially, the uncertainties of the GST estimates could be quantified more reliably based on an ensemble of several simulations using a multitude of regressor loggers.
- The selection of the regressor logger is the most crucial point for an accurate representation of the specific ground thermal conditions with the *QM* approach. Moreover, inter-annual variations in the snow and meteorological conditions need to be captured, e.g. with long observations. The *QM* technique performed well also for GST measured on steep bedrock and the uppermost thermistors of boreholes. To increase the quantity of potential regressors, also air temperatures and ground temperatures measured in reasonable proximity to the surface can be included, even from distant locations. In the Swiss Alps, several GST time series showed high covariance up to distances of several hundred kilometres, especially during the snow free period.
- The application of the gap filling approach on the PERMOS GST data illustrated the high relevance of point-specific terrain, snow and micro-meteorological characteristics for the evolution of GST at time scales of days to several months.

The processing routine (R code) as well as a small sample GST data set are available as supplementary information.

Acknowledgements

We highly acknowledge the Swiss National Science Foundation for the funding of the Sinergia TEMPS project (project no. CRSII2 136279). The data time series have been provided by the Swiss Permafrost Monitoring Network PERMOS and the TEMPS project. We thank all the individual researchers from the partner institutions for their work in the field and the pre-processing as well as the two projects for the data preparation and access. The constructive and useful comments of two anonymous referees as well as the editor are highly acknowledged.

Gap filling algorithm for ground surface temperature data measured in permafrost and periglacial environments

References

- Bonnaventure PP, and Lewkowicz AG. 2008. Mountain permafrost probability mapping using the BTS method in two climatically dissimilar locations, northwest Canada. *Canadian Journal of Earth Sciences* 45 : 443–455. DOI: 10.1139/E08-013.
- Delaloye R. 2004. Contribution à l'étude du pergélisol de montagne en zone marginale. PhD Thesis. PhD Thesis, Department of Geosciences, University of Fribourg, GeoFocus No. 10.
- Ekici A, Chadburn S, Chaudhary N, Hajdu LH, Marmy A, Peng S, Boike J, Burke E, Friend AD, Hauck C, Krinner G, Langer M, Miller PA, Beer C. 2015. Site-level model intercomparison of high latitude and high altitude soil thermal dynamics in tundra and barren landscapes. *The Cryosphere* 9 : 1343–1361. DOI: 10.5194/tc-9-1343-2015.
- Etzelmüller B, Farbrót H, Guðmundsson Á, Humlum O, Tveito OE, Björnsson H. 2007. The regional distribution of mountain permafrost in Iceland. *Permafrost and Periglacial Processes* 18 : 185–199. DOI: 10.1002/ppp.583.
- Falge E, Baldocchi D, Olson R, Anthoni P, Aubinet M, Bernhofer C, Burba G, Ceulemans R, Clement R, Dolman H, Granier A, Gross P, Grünwald T, Hollinger D, Jensen NO, Katul G, Keronen P, Kowalski A, Lai CT, Law BE, Meyers T, Moncrieff J, Moors E, Munger JW, Pilegaard K, Rannik Ü, Rebmann C, Suyker A, Tenhunen J, Tu K, Verma S, Vesala T, Wilson K, Wofsy S. 2001. Gap filling strategies for defensible annual sums of net ecosystem exchange. *Agricultural and Forest Meteorology* 107 : 43–69. DOI: 10.1016/S0168-1923(00)00225-2.
- Gisnås K, Westermann S, Schuler TV, Litherland T, Isaksen K, Boike J, Etzelmüller B. 2014. A statistical approach to represent small-scale variability of permafrost temperatures due to snow cover. *The Cryosphere* 8 : 2063–2074. DOI: 10.5194/tc-8-2063-2014.
- Gubler S, Fiddes J, Keller M, Gruber S. 2011. Scale-dependent measurement and analysis of ground surface temperature variability in alpine terrain. *The Cryosphere* 5 : 431–443. DOI: 10.5194/tc-5-431-2011.
- Guðmundsson L. 2014. qmap. Statistical transformations for post-processing climate model output. R package qmap version 1.0-3.
- Guðmundsson L, Bremnes JB, Haugen JE, Engen-Skaugen T. 2012. Technical Note: Downscaling RCM precipitation to the station scale using statistical transformations - a comparison of methods. *Hydrology and Earth System Sciences* 16 : 3383–3390. DOI: 10.5194/hess-16-3383-2012.
- Guglielmin M. 2006. Ground surface temperature (GST), active layer and permafrost monitoring in continental Antarctica. *Permafrost and Periglacial Processes* 17 : 133–143. DOI: 10.1002/ppp.553.
- Guglielmin M, Worland MR, Cannone N. 2012. Spatial and temporal variability of ground surface temperature and active layer thickness at the margin of maritime Antarctica, Signy Island. *Geomorphology* 155-156 : 20–33. DOI: 10.1016/j.geomorph.2011.12.016.
- Hasler A, Geertsema M, Foord V, Gruber S, Noetzli J. 2015. The influence of surface characteristics, topography and continentality on mountain permafrost in British Columbia. *The Cryosphere* 9 : 1025–1038. DOI: 10.5194/tc-9-1025-2015.
- Hasler A, Gruber S, Haeberli W. 2011. Temperature variability and offset in steep alpine rock and ice faces. *The Cryosphere* 5 : 977–988.
- Hoelzle M, Wegmann M, Krummenacher B. 1999. Miniature temperature dataloggers for mapping and monitoring of permafrost in high mountain areas: first experience from the Swiss Alps. *Permafrost and Periglacial Processes* 10 : 113–124. DOI: 10.1002/(SICI)1099-1530(199904/06)10:2<113::AID-PPP317>3.0.CO;2-A.
- Isaksen K, Ødegård RS, Etzelmüller B, Hilbich C, Hauck C, Farbrót H, Eiken T, Hygen HO, Hipp TF. 2011. Degrading Mountain Permafrost in Southern Norway: Spatial and Temporal Variability of Mean Ground Temperatures, 1999–2009. *Permafrost and Periglacial Processes* 22 : 361–377. DOI: 10.1002/ppp.728.
- Lehning M, Völksch I, Gustafsson D, Nguyen TA, Stähli M, Zappa M. 2006. ALPINE3D: a detailed model of mountain surface processes and its application to snow hydrology. *Hydrological Processes* 20 : 2111–2128. DOI: 10.1002/hyp.6204.

- Lewkowicz AG. 2008. Evaluation of miniature temperature-loggers to monitor snowpack evolution at mountain permafrost sites, northwestern Canada. *Permafrost and Periglacial Processes* 19 : 323–331. DOI: 10.1002/ppp.625.
- Luetschg M, Lehning M, Haeberli W. 2008. A sensitivity study of factors influencing warm/thin permafrost in the Swiss Alps. *Journal of Glaciology* 54 : 696–704. DOI: 10.3189/002214308786570881.
- Magnin F, Deline P, Ravanel L, Noetzli J, Pogliotti P. 2015. Thermal characteristics of permafrost in the steep alpine rock walls of the Aiguille du Midi (Mont Blanc Massif, 3842 m a.s.l.). *The Cryosphere* 9 : 109–121. DOI: 10.5194/tc-9-109-2015.
- Moffat AM, Papale D, Reichstein M, Hollinger DY, Richardson AD, Barr AG, Beckstein C, Braswell BH, Churkina G, Desai AR, Falge E, Gove JH, Heimann M, Hui D, Jarvis AJ, Kattge J, Noormets A, Stauch VJ. 2007. Comprehensive comparison of gap-filling techniques for eddy covariance net carbon fluxes. *Agricultural and Forest Meteorology* 147 : 209–232. DOI: 10.1016/j.agrformet.2007.08.011.
- Outcalt SI, Nelson FE, Hinkel KM. 1990. The zero-curtain effect: Heat and mass transfer across an isothermal region in freezing soil. *Water Resources Research* 26 : 1509–1516. DOI: 10.1029/WR026i007p01509.
- Park H, Sherstiukov AB, Fedorov AN, Polyakov IV, Walsh JE. 2014. An observation-based assessment of the influences of air temperature and snow depth on soil temperature in Russia. *Environmental Research Letters* 9 : 7pp. DOI: 10.1088/1748-9326/9/6/064026.
- PERMOS. 2013. Permafrost in Switzerland 2008/2009 and 2009/2010. Noetzli, J. (ed.), Glaciological Report Permafrost No. 10/11 of the Cryospheric Commission of the Swiss Academy of Sciences, Zurich, Switzerland.
- R Core Team. 2015. R: A Language and Environment for Statistical Computing, Vienna, Austria: R Foundation for Statistical Computing.
- Rajczak J, Kotlarski S, Salzmann N, Schär C. 2015. Robust climate scenarios for sites with sparse observations: a two-step bias correction approach. *International Journal of Climatology* 36: 1226–1243. DOI: 10.1002/joc.4417.
- Schmid MO, Gubler S, Fiddes J, Gruber S. 2012. Inferring snowpack ripening and melt-out from distributed measurements of near-surface ground temperatures. *The Cryosphere* 6 : 1127–1139. DOI: 10.5194/tc-6-1127-2012.
- Staub B, Delaloye R. In press. Snow-indices for mountain permafrost applications derived from near-surface ground temperature data. *Permafrost and Periglacial Processes*. DOI: 10.1002/ppp.1890
- Tardivo G, Berti A. 2014. The selection of predictors in a regression-based method for gap filling in daily temperature datasets. *International Journal of Climatology* 34 : 1311–1317. DOI: 10.1002/joc.3766.
- Themessl MJ, Gobiet A, Leuprecht A. 2011. Empirical-statistical downscaling and error correction of daily precipitation from regional climate models. *International Journal of Climatology* 31 : 1530–1544. DOI: 10.1002/joc.2168.
- Westermann S, Schuler TV, Gislén K, Etzelmüller B. 2013. Transient thermal modeling of permafrost conditions in Southern Norway. *The Cryosphere* 7 : 719–739. DOI: 10.5194/tc-7-719-2013.
- Wu T, Zhao L, Li R, Wang Q, Xie C, Pang Q. 2013. Recent ground surface warming and its effects on permafrost on the central Qinghai-Tibet Plateau. *International Journal of Climatology* 33 : 920–930. DOI: 10.1002/joc.3479.
- Zhang T. 2005. Influence of the seasonal snow cover on the ground thermal regime: An overview. *Reviews of Geophysics* 43 : RG4002. DOI: 10.1029/2004RG000157.

Publication III

Ground temperature variations in a talus slope influenced by permafrost: A comparison of field observations and model simulations

Citation: Staub, B., Marmy, A., Hauck, C., Hilbich, C., & Delaloye, R.: Ground temperature variations in a talus slope influenced by permafrost: a comparison of field observations and model simulations. *Geographica Helvetica*, 70, 45–62, 2015. DOI: [10.5194/gh-70-45-2015](https://doi.org/10.5194/gh-70-45-2015).

Abstract: Variations in surface and near-surface ground temperatures (GST) dominate the evolution of the ground thermal regime over time and represent the upper boundary condition for the subsurface. Focusing on the Lapires talus slope in the south-western part of the Swiss Alps, which partly contains massive ground ice, and using a joint observational and modelling approach, this study compares and combines observed and simulated GST in the proximity of a borehole. The aim was to determine the applicability of the physically-based subsurface model COUP to accurately reproduce spatially heterogeneous GST data and to enhance its reliability for long-term simulations. The reconstruction of GST variations revealed very promising results, even though two-dimensional processes like the convection within the coarse-blocky sediments close to the surface or ascending air circulation throughout the landform (“chimney effect”) are not included in the model. For most simulations, the model bias revealed a distinct seasonal pattern mainly related to the simulation of the snowpack. The study shows that by means of a detailed comparison of GST simulations with ground truth data, the calibration of the upper boundary conditions – which are crucial for modelling the subsurface – could be enhanced.

Keywords: Mountain permafrost, ground temperature variations, meteorological events, talus slope, COUP model, upper boundary conditions



Ground temperature variations in a talus slope influenced by permafrost: a comparison of field observations and model simulations

B. Staub¹, A. Marmy¹, C. Hauck¹, C. Hilbich^{1,2}, and R. Delaloye¹

¹University of Fribourg, Department of Geosciences, Geography, Chemin du Musée 4, 1700 Fribourg, Switzerland

²University of Zurich, Department of Geography, Glaciology and Geomorphodynamics Group, Winterthurerstr. 190, Zurich, Switzerland

Correspondence to: B. Staub (benno.staub@unifr.ch)

Received: 3 June 2014 – Revised: 7 November 2014 – Accepted: 28 November 2014 – Published: 23 February 2015

Abstract. Variations in surface and near-surface ground temperatures (GST) dominate the evolution of the ground thermal regime over time and represent the upper boundary condition for the subsurface. Focusing on the Lapires talus slope in the south-western part of the Swiss Alps, which partly contains massive ground ice, and using a joint observational and modelling approach, this study compares and combines observed and simulated GST in the proximity of a borehole. The aim was to determine the applicability of the physically based subsurface model COUP to accurately reproduce spatially heterogeneous GST data and to enhance its reliability for long-term simulations. The reconstruction of GST variations revealed very promising results, even though two-dimensional processes like the convection within the coarse-blocky sediments close to the surface or ascending air circulation throughout the landform (“chimney effect”) are not included in the model. For most simulations, the model bias revealed a distinct seasonal pattern mainly related to the simulation of the snow cover. The study shows that, by means of a detailed comparison of GST simulations with ground truth data, the calibration of the upper boundary conditions – which are crucial for modelling the subsurface – could be enhanced.

1 Introduction

Permafrost, defined as ground material remaining at temperatures below or at 0°C for two or more consecutive years (Williams and Smith, 1989), is a widespread phenomenon in the Alps covering approximately 5% (Boeckli et al., 2012) of the surface area of Switzerland. It typically occurs in locations with a cold microclimate at elevations above 2500 m a.s.l. not covered by thick glaciers (Gruber and Haeberli, 2009; Noetzi and Gruber, 2005). Except for some characteristic landforms like rock glaciers or push moraines, mountain permafrost is basically invisible from the surface and direct (and especially non-invasive) observation is therefore difficult. However, with regard to ongoing and future climatic changes, a comprehensive understanding of the processes influencing these potentially very fragile environments is essential to explain causes for recent variations and

to analyse its possible future evolution (Harris et al., 2009). Therefore this study investigates the response of mountain permafrost to selected meteorological and snow cover conditions using a combined observational and modelling approach with focus on surface and near-surface ground temperatures (GST).

1.1 Permafrost characteristics in high-alpine terrain

Typical permafrost landscapes in the Swiss Alps are characterised by a rough topography; often heterogeneous composition of the (sub)surface regarding the structure of the sediment; the porosity and the repartition of water, air and ice within the voids (Gruber and Haeberli, 2007; Schneider et al., 2012, 2013); and a short but spatio-temporally highly variable snow-free period. As permafrost is defined thermally, its spatial distribution (cf. Boeckli et al., 2012) is largely

influenced by all factors controlling the energy balance at the ground surface (Hoelzle et al., 2001; Stocker-Mittaz et al., 2002) and additionally by lateral and hydrothermal effects (Endrizzi and Gruber, 2012; Noetzli and Gruber, 2009; Scherler et al., 2010). In addition to topo-climatic parameters like altitude, exposition, slope angle or albedo influencing the temperature and humidity at the surface, spatio-temporal dynamics of the snow cover are also of particular importance for seasonal and inter-annual variations of GST (usually measured 5–20 cm below the ground surface) and ground temperatures (GT, e.g. measured at greater depths in boreholes) (Delaloye, 2004; Gubler et al., 2011; Zhang, 2005). A snow layer of more than ~ 80 cm thickness (depending on the roughness of the terrain and the inner structure of the snow cover) is able to thermally decouple the ground from the atmosphere (Goodrich, 1982; Ishikawa, 2003; Luetsch et al., 2008; Zhang, 2005). On the other hand, a thin discontinuous snow cover of less than ~ 5 –20 cm (again highly depending on the terrain roughness) may intensify ground cooling (“autumn snow effect”) on a coarse-grained surface compared to snow-free conditions due to the increased albedo and the absence of the thermal insulation (Hoelzle et al., 1999; Keller and Gubler, 1993). For almost two decades, the relative influence of the timing of the onset and melt-out of the snow cover and the corresponding efficiency of ground cooling and ground warming on mean annual ground temperatures (MAGT) have been topics of discussion (Apaloo et al., 2012; Delaloye, 2004; Zhang, 2005). Results from Schneider (2014) and others indicate that ground cooling in late autumn might be more important (for inter-annual temperature variations) due to its long-lasting effect (Delaloye, 2004; Vonder Mühll et al., 1998) over the whole winter season. But regarding the long-term permafrost evolution, increasing air temperatures in summer and in the annual mean (MAAT) might play the key role (Etzelmüller et al., 2011; IPCC, 2014; Isaksen et al., 2011; Marmy et al., 2013; Scherler et al., 2013).

Initial conditions and spatio-temporal variations in the composition of the substrate (Arenson et al., 2002; Kneisel et al., 2008), especially of the ground ice and water content (Hanson and Hoelzle, 2005; Hilbich et al., 2011; Schneider et al., 2013), are important for the response of ground temperatures to warmer atmospheric conditions (Engelhardt et al., 2010; Scherler et al., 2013). Ice-rich landforms with a thick, coarse-blocky active layer showed a slower GT increase during a simulation with warming surface conditions (Scherler et al., 2013), whereas sites with small amounts of ground ice and water may react faster to ground-heating events in terms of GT increase (Hilbich et al., 2011; Luetsch et al., 2008; Zenklusen Mutter and Phillips, 2012). Therefore general conclusions about the current state and future evolution of Alpine permafrost require comprehensive data sets, sophisticated data analysis and modelling techniques, and careful interpretation of both observations and model simulations.

1.2 Ground temperature modelling in the Alpine domain

The heterogeneity of the surface and subsurface material as well as the complex topography complicate long-term modelling in mountainous terrain (Engelhardt et al., 2010). In addition, many permafrost model applications are faced with disparities in scale between coarse-gridded input data (e.g. from regional climate models) and observational calibration and validation time series (Fiddes and Gruber, 2014). The high cumulated uncertainty from scenarios, downscaling issues and the complexity of real-world processes are major disadvantages of models compared to direct observations (Hawkins and Sutton, 2009). Recent studies (Ekici et al., 2014; Marmy et al., 2013; Scherler et al., 2013) applied the 1-D subsurface model COUP (see Sect. 2.4) for the field sites Schilthorn (mountain peak in the northern Swiss Alps) and Murtèl (Scherler et al., 2013) in the Upper Engadine, which are part of the Swiss permafrost monitoring network, PERMOS. The experience from the very coarse-blocky and ice-rich Murtèl rock glacier showed that many processes which were not or only partially included in the model such as convection, the lateral flow of (melt) water or the thermal radiation between blocks play an important role in reality, making subsurface modelling very challenging (Scherler et al., 2010, 2014). Against this background, further experience should be gained by applying COUP to other PERMOS study sites with different landforms, topo-climatic characteristics, and surface and subsurface properties.

Marmy et al. (2013) showed with simulations for the Schilthorn that the thermal regime of the active layer may react very sensitively to systematically increasing air temperatures, especially in autumn, when repartitioning of precipitation into rain or snow is a function of air temperature, and least during the winter months, when the presence of a snow cover is independent of air temperature. Changes in mean annual precipitation showed no clear effect on GST, but the precipitation distribution among the seasons and in general the timing and duration of the snow cover does matter (Marmy et al., 2013). However, questions still remain with regard to if and how much the stability and reliability of model simulations depend on the meteorological conditions during the calibration period. This gap in research is of particular importance because the permafrost monitoring data indicate large inter-annual variations in GST, mainly related to snow cover dynamics (Delaloye, 2004; PERMOS, 2013). Moreover, GST represents the most important upper boundary calibration parameter because any systematic bias may cumulate in the simulations. Therefore COUP should also be applied for a set of GST loggers, focusing on the performance of upper boundary conditions compared to observations.

1.3 Research questions and aims of this article

In this study, we apply the COUP model to simulate several GST time series in the surroundings of a borehole on a talus slope characterised by rather coarse debris. The aim is to evaluate the performance of the COUP model for the reconstruction of GST time series focusing on inter-annual and seasonal patterns, and also to improve the calibration of the upper boundary conditions for the simulation of subsurface temperatures. In particular we address the following research questions:

1. How well can the one-dimensional subsurface model COUP (see Sect. 2.4) reproduce observed ground and ground surface temperature variations over spatially heterogeneous mountain permafrost?
2. How similar are observed and modelled reactions of the ground thermal regime to selected meteorological and snow cover conditions?
3. Which processes are under- or overestimated, or even missing, in the COUP model, and how can the calibration of the upper boundary parameters be validated and improved?

2 Data and methods

2.1 Study area: the Lapires talus slope

The study comprises the analysis of observed and simulated GST and GT from the Lapires site, a large north-facing talus slope at an altitude range of 2400–2700 m a.s.l. (Valais Alps, between Verbier and Nendaz; see Fig. 1). The site has been selected because so far no talus slope has been simulated using the COUP model and based on the availability of GST and GT time series at least 10 years long (Table 1) and down-scaled reconstructed meteorological data (see Sect. 2.2). The relatively regular topography of the Lapires talus slope further limits the complexity of microclimatic effects.

Four boreholes have been drilled at the Lapires site within a number of different research projects: the drilling of the oldest borehole, LAP_0198, was done as percussion drilling, which prohibited obtaining detailed information about the internal structure and composition. The structure of the sediments around LAP_0198 is illustrated in Fig. 2 and was estimated by compiling data from excavations done for the construction of two cable car pylons in 1998 (Delaloye et al., 2001), the cores that were drilled in 2008 (Scapozza, 2013), the geophysical measurements (Delaloye, 2004; Hilbich, 2010; Lambiel, 2006) and the GT records: the active layer of about 4–5.5 m thickness is situated on top of an ice-rich permafrost layer of ~ 15 m thickness with temperatures very close to the melting point. The porosity within the permafrost layer ranges from 30 to 60 % and is mostly sealed by ice (Scapozza, 2013). The bedrock (gneiss) was never

reached while drilling any of the boreholes and hence must be at least at 40 m depth (Scapozza, 2013). The occurrence of permafrost within the Lapires talus slope is of discontinuous nature (see Fig. 1; Delaloye 2004; Lambiel, 2006; Scapozza, 2013) and linked to a complex system of internal air circulation (Delaloye and Lambiel, 2005). The latter is also called the “chimney effect” and most effective when the temperature (and density) gradient between the air and the voids in the porous substrate is large and may be responsible for a rapid ground cooling within a short amount of time (days/hours), in particular at the bottom of the talus slope, where cold air is aspirated in winter (Gądek, 2012; Phillips et al., 2009; Wakonigg, 1996). In contrast to scree slopes at lower altitudes, where the chimney effect is dominant for the presence or absence of permafrost (Delaloye et al., 2003; Morard et al., 2008; Wakonigg, 1996), it likely plays an important but secondary role (Delaloye and Lambiel, 2005) for the permafrost evolution at the Lapires site (cf. Table 1 for a qualitative estimate of this effect). But the thermally driven convection of interstitial air in the porous, coarse-blocky substrate during winter may be of major influence, causing very effective cooling of the uppermost ground layers (Gruber and Hoelzle, 2008; Harris and Pedersen, 1998).

2.2 Data sets

From the available data, eight GST loggers and one borehole have been selected (Table 1, Fig. 1). The GST time series used for this study were measured every 2 h with miniature temperature loggers (type UTL-1), which are characterised by an absolute measurement error of ± 0.1 K and a dynamics resolution of 0.27 K (8 bit). The loggers are placed 10–20 cm below the ground surface. During the snow melt period in spring and early summer, GSTs are close to 0 °C (“zero curtain”) due to the consumption and release of latent heat. This period is used to calibrate the sensors. GST measurements are usually representative of one specific point only or a small area and may spatially vary up to 2.5–3 °C over distances of 10–100 m (Gubler et al., 2011; Isaksen et al., 2011) because of the heterogeneity of the ground properties, snow conditions and topoclimatic effects. The samples used for this study are more homogeneous and have a mean standard deviation of 1.2 K over a spatial range of ~ 500 m (based on daily mean values from all loggers and a common period of 1717 days).

For the calibration of the COUP model runs (see Sect. 2.4), the GST time series were used at 2 h resolution. The analysis of the GST time series and the comparison with the COUP simulations are based on daily means centred at mid-day (12:00 UTC+1).

GT measurements show permafrost conditions for borehole LAP_0198, as well as LAP_1108 and LAP_1208 (Scapozza, 2013). The fourth borehole, LAP_1308, higher up on the talus slope, is permafrost-free, which confirms a local warming effect of internal air circulation (Delaloye

Table 1. Characteristics of the selected GST loggers and the uppermost thermistor* of borehole LAP_0198. The topographic parameters altitude, slope, aspect and potential incoming shortwave radiation (PISR) have been computed using SAGA GIS (Olaya, 2009). All other values are based on daily mean GST recorded during the hydrological years 2006/07, 2009/10 and 2010/11, where complete observations were available for all loggers. SD: standard deviation among all available daily mean GSTs; BTS: bottom temperature of the winter snow cover (mean GST during March); FDD: freezing degree days (sum of negative temperatures per hydrological year); TDD: thawing degree days. Chimney effect: “yes” for points with evidence of internal air circulation according to the GST records and field observations.

	LAP_S015	LAP_S019	LAP_S026	LAP_S028	LAP_S029	LAP_S036	LAP_S037	LAP_S038	LAP_0198
Sensor depth (m)	0.2	0.1	0.1	0.2	0.2	0.2	0.1	0.2	0.2*
Installed since (yr)	1999	2000	2000	2000	2000	2000	2001	2003	1999
Altitude (m a.s.l.)	2510	2505	2445	2450	2450	2375	2490	2480	2500
Slope (°)	27	30	26	23	21	15	21	19	24
Aspect (°)	10	7	29	13	56	36	37	39	13
PISR ($\text{kWh m}^{-2} \text{ yr}^{-1}$)	905	834	1018	996	1143	1201	1129	1121	972
GST _{mean} (°C)	0.70	1.12	1.29	1.36	1.33	-0.26	0.33	-0.45	0.55
SD _{mean} (K)	3.70	4.22	3.91	4.17	4.14	5.92	4.29	4.50	4.19
BTS (°C)	-2.34	-2.50	-1.30	-2.29	-2.49	-6.62	-4.03	-4.03	-3.08
FDD ($^{\circ}\text{C d yr}^{-1}$)	-351	-361	-238	-276	-291	-942	-514	-752	-452
TDD ($^{\circ}\text{C d yr}^{-1}$)	606	769	709	773	778	847	633	589	655
Chimney effect	yes	yes	yes	?	?	yes	?	yes	yes
Snow-free date	18 June	26 May	12 June	20 June	11 June	02 June	30 June	17 June	20 June

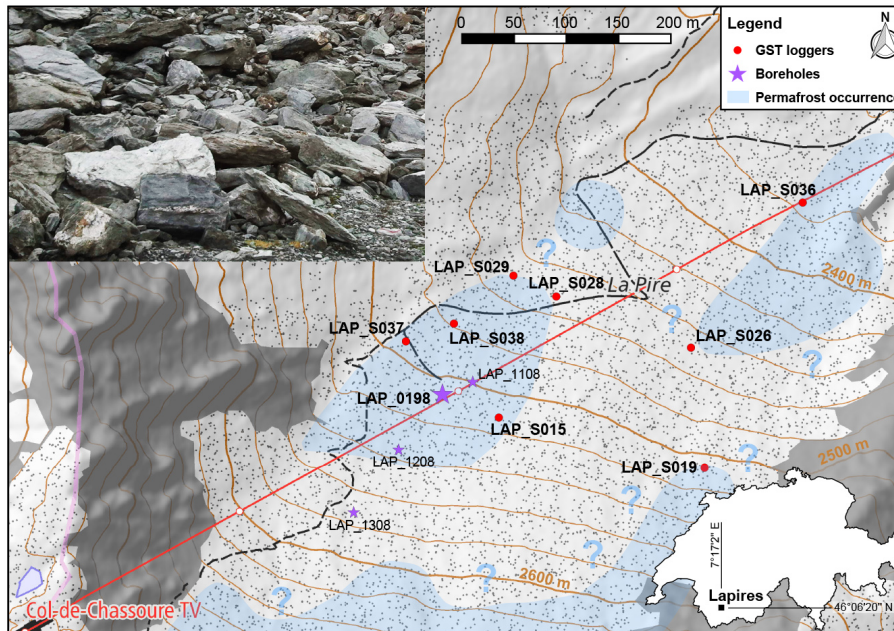


Figure 1. The Lapires study site is located in the Lower Valais in the south-east of Switzerland in the ski area of Nendaz/Verbiers. The map shows the positions of four boreholes (among which LAP_0198 was used for this study) and eight GST loggers, as well as a qualitative indication of the spatial extent of permafrost occurrence according to Delaloye (2004), Lambiel (2006) and Scapozza (2013). The photograph was taken close to borehole LAP_0198 and provides a closer look at the surface characteristics, which mainly consist of coarse blocks but also some finer material. Reproduced with permission of Swissstopo (BA14056).

and Lambiel, 2005; Scapozza, 2013). As the simulation with COUP requires long calibration time series, we focus on borehole LAP_0198. Because the GT variations recorded within the permafrost layer of LAP_0198 are very small (of the order of the measurement uncertainty of the old thermistor chain in place until 2009; since then, sensors of the type “YSI 44031” have been installed) and close to the melting

point, these data needed to be checked for plausibility and have been corrected or removed where necessary.

Meteorological data for this site are available through a local weather station at borehole LAP_0198, which has been measuring air temperature and shortwave radiation since 1998, as well as wind and snow depths since 2009 (with interruptions). Precipitation, which is needed as forcing data

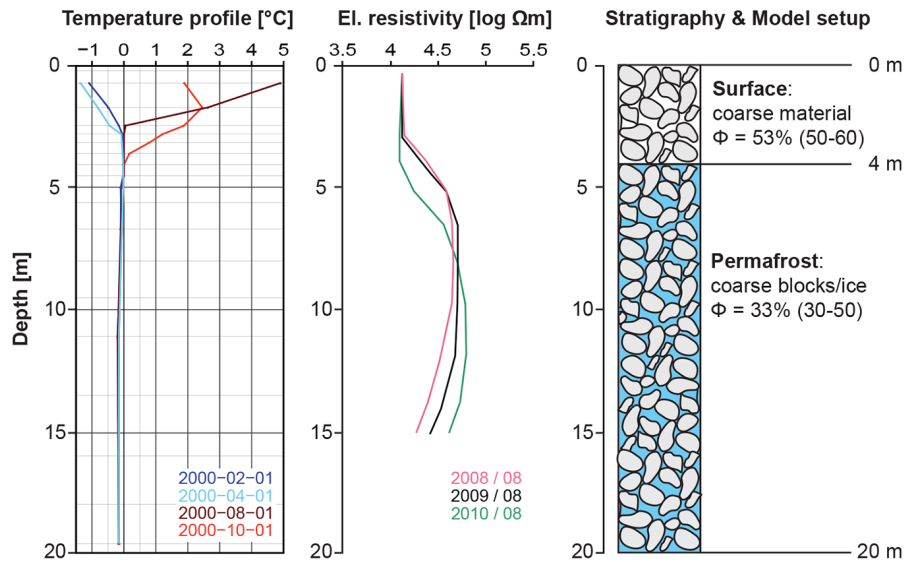


Figure 2. Vertical profile of GT and electrical resistivities according to PERMOS (2013) for borehole LAP_0198 and the stratigraphy (Scapozza, 2013) on which basis the initial model setup for LAP_0109 was created.

for the COUP model, is not measured on-site. In order to have continuous and physically consistent meteorological input data for the COUP model for all the above-mentioned parameters, a reconstruction has been driven in the framework of the ongoing project “The Evolution of Mountain Permafrost in Switzerland” (TEMPS, 2011–2015). Using an empirical–statistical downscaling approach (Rajczak et al., 2015), the bias correction and spatial transfer from RCM output data to the point of interest is done within two steps over a most representative station with long-term measurements (MeteoSwiss station “Grand-St. Bernard” in the case of Lapires). The reconstructed data reproduce the general behaviour of the on-site meteorological parameters well (performance for air temperature based on ~ 3500 days of observations: $R^2 = 0.97$, $RMSE = 1.23$ K), but they may be less accurate when analysing single meteorological events, especially for precipitation. For qualitative comparison with the simulated snow pack, snow depth records were taken from the closest snow station of the IMIS/ENET network (ATT-2, “Les Attelas”; source: SLF), which is at the same elevation level as the GST loggers but ~ 1.5 km to the west of the study site in an almost flat area (usually not influenced by avalanches, below a slope exposed to the north-west).

2.3 GST aggregates and indices

Daily, seasonal and inter-annual temperature variations are most prominent at the ground surface and become buffered and delayed at depth (Goodrich, 1982). Distributed and continuous GST measurements are therefore a good data source to analyse meteorological effects on the site-specific ground thermal regime at various spatial and temporal scales (Delaloye, 2004; Fiddes and Gruber, 2012; Gubler et al., 2011;

Schmid et al., 2012). The comparison between sites and years, as well as between simulated (GST_{sim}) and observed (GST_{obs}) GST, can be simplified by using anomaly values (inter-annual deviations from the mean during a common reference period, further identified with the annex (a)). In addition, aggregates over specific time periods (e.g. monthly and annual means) and time series of the model bias (sim-obs) and running Pearson correlation are used.

To investigate inter-annual temperature variations, we calculated running annual means for GST ($rMAGST$, Eq. 1), air temperature ($rMAAT$) and GT ($rMAGT$) on the basis of daily mean values, aligned at the end (date t) of a 365-day period, in the form

$$rMAGST_t [^\circ C] = \frac{GST_t + GST_{t-1} + \dots + GST_{t-364}}{365}. \quad (1)$$

As a proxy for the thermal decoupling and the direction of the heat flux between the ground and the atmosphere, daily (SO , Eq. 2) and annual surface offsets ($rMASO = rMAGST - rMAAT$) were calculated.

$$SO_t [K] = GST_t - AirT_t \quad (2)$$

To compare the cumulative temperature evolution for different years, cumulative degree day sums (CDD) were calculated from daily mean GST for each day (t) and hydrological year (hy, starting on 1 October) as described in Eq. (3):

$$CDD_{hy,t} [DD] = \sum_{t=Oct-01}^{Sep-30} GST_t. \quad (3)$$

CDDs have been computed for GST_{obs} and GST_{sim} , which further allow the calculation of the cumulative model bias ($CMB = CDD_{sim} - CDD_{obs}$).

On the “zero curtain” (Sect. 2.2) the timing of the snow melt in spring can be determined (Schmid et al., 2012), and because of the insulating effect of the snow, the first arrival of a thermally insulating snow cover in early winter can also be approximated. For this study, GST time series have been considered as “snow-covered” as far as the weekly standard deviation undercut the dynamic resolution.

2.4 COUP model calibration and parameterisation

The COUP model is a numerical one-dimensional model coupling the heat and subsurface water transfer processes using the general heat flow equation (Jansson and Karlberg, 2004; Jansson, 2012) together with several empirical equations to model various subsurface and snow parameters. The model has already been used for a variety of subsurface conditions, and has also been applied in Alpine permafrost studies (e.g. Ekici et al., 2014; Marmy et al., 2013; Scherler et al., 2010).

The COUP model settings for this study consist of 50 vertical layers to a depth of 20 m with increasing thickness of model layers with depth. For the analysis of the GST, only the first layer was considered (thickness = 20 cm), but the whole profile was simulated to take into account the influence from subsurface processes. The upper boundary conditions are calculated by a complete energy balance calculation at the ground surface (cf. Scherler et al., 2014) and are drastically influenced by the snow conditions that temporarily decouple the ground from the atmosphere. The lower boundary conditions are calculated from the analytical solution of the sine variation at the ground surface and a mean value for the damping of the temperature signal for the whole profile of the subsurface. The geothermal heat flux is negligible as only surface processes are being analysed and the timescales considered are short. The subsurface has been divided into two main horizons (see Fig. 2). The data available from the temperature measurements, geophysics and the cores that were drilled in the surroundings in 2008 (PERMOS, 2013; Scapozza, 2013) provide indications about the porosity, although their values all include a large uncertainty. Therefore we defined ranges of plausible porosities for both horizons (50–60 % for the surface and 30–50 % at depth) according to available information (Sect. 2.1) and let the model choose the most suitable values with the GLUE method (see below). As shown in Fig. 2, the resulting profile is (a) from the surface to 4 m depth with a porosity of 53 %, representing the coarse blocky material, and (b) from 4 m to the bottom (20 m) with a lower porosity (33 %).

The model is run with the reconstructed meteorological data set at daily resolution (available for 1981–2013; see Sect. 2.2), with a spin-up of 3 years for the GST simulations and a longer spin-up of 20 years for borehole LAP_0198. This spin-up procedure is sufficient to have the model in equilibrium because the initial conditions are estimated by the model.

In addition to the meteorological forcing data set and the setup of the vertical profile of the subsurface, the COUP model simulations depend on a large number of parameter settings, which are usually not known exactly for a specific site, and are partly determined by calibration (Jansson, 2012). In our study, the calibration has been driven by inverse modelling using the general likelihood uncertainty estimation (GLUE) method (Beven and Binley, 1992). The GLUE method tests different sets of parameter values chosen stochastically among a physically reasonable range. The analysis of the equivalence between model results and observations enables the set of parameter values giving the best fit with the observed system to be selected. In this study, a setup of 20 000 (for LAP_0198) and 10 000 (for the GST) different parameter combinations has been tested and the performance has been analysed statistically using the coefficient of determination and the mean model bias in temperature to reach the best fit with the observations. The parameters used for the calibration are summarised in Table 2. This approach may lead to the equifinality problem creating a substantial uncertainty if the model is used for prediction (Beven and Freer, 2001) when the simulation period is longer than the calibration period. For the present study, the optimal parameter combination has been selected.

The snow parameters are hereby crucial for both the GST and the borehole calibration as they influence the upper boundary conditions. Among them, CritSnowCoverDepth specifies the snow thickness at which the surface is considered fully covered by snow. Below this threshold value, the ground surface is considered only as partly snow-covered and the surface temperature and the surface albedo are then calculated as a ratio between the values for bare ground and snow-covered ground (Jansson and Karlberg, 2004). The density of the snow is dynamic and COUP simulates the snow density using the density of new snow (DensityNewSnow) and a compaction rate depending on the depth of the total snow cover. The density also influences the thermal conductivity of snow. The melting of the snow is influenced by the global radiation (MeltCoefGlobalRad), the air temperature (MeltCoefAirTemp) and the heat flow from the ground.

In addition to the snow parameters, the parameters influencing the albedo have also been used for calibration. The albedo of snow is a function of snow surface age and can be tuned by setting a differential minimal albedo value for old snow (AlbSnowMin). The albedo of the bare ground is a function of pressure head (i.e. water content) and limited by a maximum (AlbedoDry) and a minimum (AlbedoWet) value.

For the subsurface the following parameters were determined by inverse modelling: the porosity (Porosity) and the hydraulic conductivity parameter (MatrixConductivity and TotalConductivity). The parameters not used in the GLUE calibration procedure were set to literature values (Jansson and Karlberg, 2004).

Table 2. List of calibration parameters and their values obtained by inverse modelling. Concerning the hydraulic conductivity parameters (set for borehole LAP_0198): (a) value assigned to the upper 4 m of the vertical profile and (b) value assigned from 4 m depth to the bottom of the vertical profile.

	LAP_S015	LAP_S019	LAP_S026	LAP_S028	LAP_S029	LAP_S036	LAP_S037	LAP_S038	LAP_0198
Snow parameters									
CritSnowCoverDepth (m)	0.15	0.17	0.21	0.28	0.13	0.21	0.25	0.30	0.30
DensityNewSnow (kg m ⁻³)	145.59	144.79	175.52	105.07	121.52	175.77	185.12	176.90	133.90
MeltCoefGlobalRad	6.5×10^{-9}	2.5×10^{-8}	1.6×10^{-7}	1.9×10^{-7}	1.2×10^{-7}	2.1×10^{-6}	1.9×10^{-6}	1.6×10^{-6}	7.2×10^{-8}
MeltCoefAirTemp	1.68	2.84	1.48	0.64	1.37	0.90	2.64	1.22	0.90
Albedo parameters									
AlbSnowMin (%)	20.89	55.89	24.83	42.52	45.32	49.88	55.09	43.88	26.92
AlbDry (%)	68.63	71.93	75.46	45.23	61.00	79.42	77.73	77.32	55.92
AlbWet (%)	18.29	13.24	23.29	18.04	11.23	7.89	12.17	7.35	17.61
Hydraulic conductivity parameters									
Porosity (%)									53 ^a /33 ^b
MatrixConductivity (mm day ⁻¹)									13 225 ^a /98 412 ^b
TotalConductivity (mm day ⁻¹)									13 225 ^a /98 412 ^b

3 Results

3.1 Meteorological events and their influence on GST

We define “meteorological events” as meteorological conditions that show distinct effects on rMAGST. We propose to use the first derivative of rMAGST as a non-universal attempt at numerical detection. Rapid changes in rMAGST clearly exceeding the standard deviation of the whole time series in a moving time window of 90 days indicate specific meteorological and/or snow cover conditions. Such events can occur within the time frame of a few days (e.g. snow or rain events), weeks (e.g. summer heatwave or dry fall conditions) or even several months (e.g. air temperature anomalies, perennial snow patches from avalanche deposits), but their effect on the ground thermal regime might be of very different intensity and persistence. Meteorological events are part of the natural variability of the system with a high recurrence, but because of analogies to possible future climate scenarios, they are often discussed within the same scientific context (e.g. Marmy et al., 2013; Schär et al., 2004). One should be aware that changes in running means depend on the averaging time window and are less sensitive to consecutive anomalies of the same algebraic sign (causing, for example, the intensive ground cooling in winter 2005/06 to be masked by the precedent cold rMAGST period; see Fig. 3b).

Figure 3a shows inter-annual variations in rMAGSTa, rMAATa and running annual surface offset (rMASO; see Sect. 2.3) for the period 2000–2012 at the Lapires field site, as well as snow depth records from the nearby snow station ATT-2 (see Sect. 2.2). Although Fig. 3 shows the results for one location and the temporal evolution of the snow cover can be spatially heterogeneous, the temporal behaviour of rMAGSTa is very similar in many parts of the Swiss Alps (PERMOS, 2013).

The observed inter-annual rMAGSTa variations are in the same range as those of rMAATa, but with a significantly different pattern of alternating warmer and colder periods (Fig. 3a). The surface offset rMASOa (rMAGSTa–rMAATa, cf. Eq. 2) can be explained in large part by inter-annual variations in snow conditions (Fig. 3c). Positive rMASOa indicates a net warming influence of the snow cover (usually due to early and/or much snow in the first half of the winter, or early melt-out in spring). Negative rMASOa typically occur in years with late and/or limited snow fall or delayed snow-melt. Figure 3 also shows that meteorological and mainly snow cover conditions in autumn and early winter are of particular importance for the variations in rMAGSTa (which explains, for example, the earlier increase of rMAGSTa compared to rMAATa in event E3, cf. Table 3), because these effects may cumulate during the whole winter (Delaloye, 2004). Eleven events covering a wide range of considerably different meteorological and snow cover conditions are highlighted in Fig. 3b and further described in Table 3. The performance of the GST simulations will be analysed in the following sections regarding these events, in particular regarding potential relations between good/bad model performance and the various types of meteorological events.

For all events listed in Table 3 (except for E7 and E9), the timing of the snow cover played a major role: in the case of E1, E3, E8 and E10, early snow fall in autumn limited ground cooling, whereas the events E2, E4 and E6 tended to be cooler due to a late onset of an insulating snow cover. The date of the melt-out in summer was also partially responsible for the warmer (E3, E5, E10) and colder (E2, E4, E11) periods. Air temperature has a likewise high impact on the ground thermal regime, as it (1) influences the melt rate of the snow cover in spring, (2) directly heats (or cools) the ground during the snow-free season and (3) modifies the thermal gradient between the ground and the snow surface (E3, E6–E10).

Table 3. Selected meteorological events during the observation period with significant influence on GST.

Event	Type	Start	End	Meteorological and snow conditions
E1	warming	2000-09	2001-06	Early snow fall in September 2000 and heavy precipitation event in October 2000 lead to limited ground cooling during winter 2000/01
E2	cooling	2001-07	2002-06	Late snow melt in 2001 and late snow fall in 2001/02 (dry November and December 2001)
E3	warming	2002-08	2003-08	Short snow event in mid-summer 2002, early snow in 2002/03, early melt-out and heatwave in summer 2003
E4	cooling	2004-06	2005-05	Late snow melt in summer 2004 and late snow fall in winter 2004/05, relatively cold winter air temperatures
E5	warming	2005-05	2005-08	Early snow melt in June 2005
E6	warming	2006-06	2007-06	Record-breaking warm air temperatures between June 2006 and June 2007, but late snow in 2006/07
E7	cooling	2007-07	2007-12	Cold period between July and December 2007
E8	warming	2008-09	2009-09	Early snow in October 2008 limited ground cooling, but moderate snow depths in January 2009 coinciding with cold air temperatures, very hot spring and warm late summer 2009
E9	cooling	2010-09	2010-12	Cold air temperatures and little precipitation in September and October 2010
E10	warming	2011-06	2011-11	Early snow melt already by end of May 2011 and warm September and November 2011
E11	cooling	2012-05	2012-09	Large snow falls in late winter 2011/12 and delayed melt-out in 2012

3.2 Comparison of observed and simulated inter-annual GST variations

For a first comparison, GST_{sim} values have been plotted against GST_{obs} for the uppermost thermistor of borehole LAP_0198 and eight GST loggers, and completed with summary statistics (Fig. 4). Even though the results look fairly good at a first glance (mean $R^2 \sim 0.9$), there are some prominent simulation errors, in particular during the snow melt phase (scatters along 0°C). The causes for these errors can either be related to (1) the microclimate (differing from the reconstructed meteorological data that has been adjusted to match meteorological conditions at LAP_0198), (2) particularities regarding the dynamics of the snow cover (e.g. modification by wind, avalanches, skiers) or (3) other local characteristics related to the before-mentioned ventilation effects or subsurface properties.

As shown in Fig. 5a for logger LAP_S015, GST_{sim} and $snow_{sim}$ closely follow the observations during the whole period between 1999 and 2013. At first glance, the model seems capable of reproducing strong GST variations over short timescales. Warming events (e.g. E5, E6 or E10), as well as some cooling events (e.g. E2, E4 or E11), are also well represented. Regarding running annual means (Fig. 5b),

most observed and simulated inter-annual variations are very similar, despite a slightly larger bias during the events E3 and E7. The logger LAP_S015 shown in Figs. 5a and b was mainly selected because it is not interrupted by gaps and situated close to borehole LAP_0198. In Figs. 5c and d, the model bias of LAP_S015 is compared with the other loggers regarding the temporal evolution of the mean 365-day model bias and the Pearson correlation coefficient (running 365-day R^2 between GST_{sim} and GST_{obs}). For all GST loggers the mean model bias ranges between -1 and $+2$ K. The temporal behaviour is similar for many loggers, but over the years no systematic trend can be observed. Pearson correlation is generally high (mean: 0.92), but weaker between summer 2001 and 2003 (several years with delayed melt-out in a row), 2007 and 2009 (bias in the melt-out day and weak model performance in February–May 2009), and 2012 and 2013 (delayed melt-out in 2012; see Fig. 5d). However, the similarity between different loggers may be related to (1) the meteorological input data (mainly precipitation), (2) the model parameterisation or (3) effects which cannot be simulated by the model at all (such as snow redistribution).

Because the spatio-temporal variability of the snow cover is a key parameter for both the seasonal and inter-annual GST variations and has been identified as the source of se-

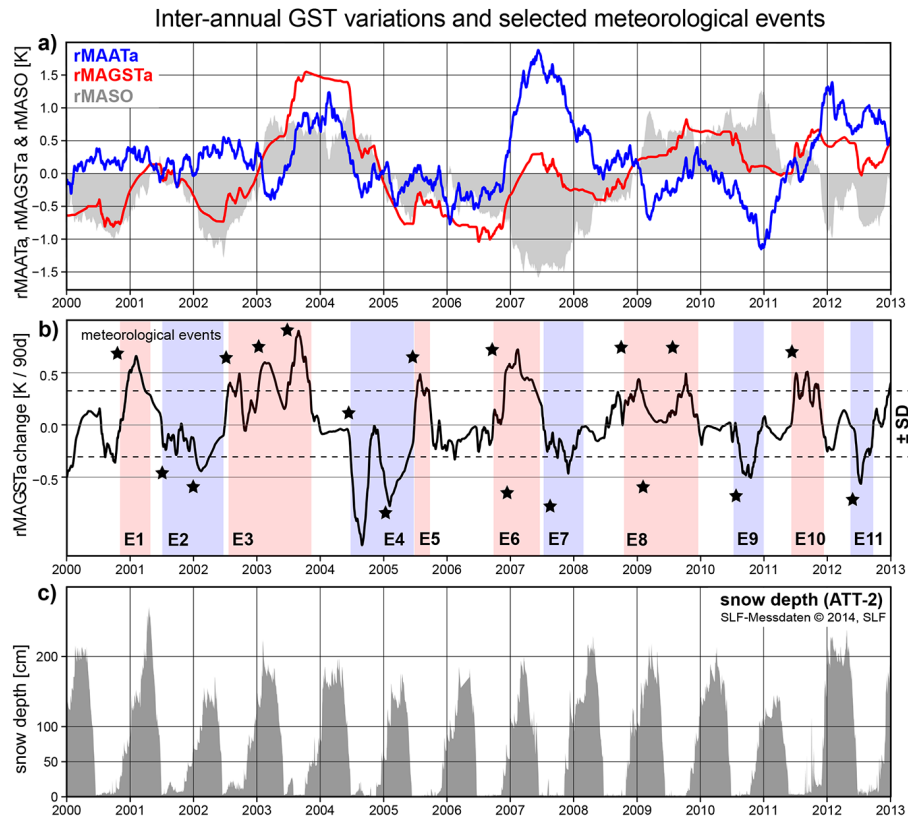


Figure 3. The evolution of air temperature, GST and snow cover at Lapieres: **(a)** rMAGST (mean of the two longest GST series LAP_S015 and LAP_S028) and rMAAT (based on the reconstructed air temperature) anomalies and their difference (rMASO) over time. **(b)** Meteorological events (stars E1–E11) identified by the change in rMAGSTa (running 90-day difference) are indicated by red (warming effect) and blue (cooling effect) bars and are further described in Table 3. **(c)** Temporal evolution of the snow cover at the nearby snow station ATT-2 (“Les Attelas”; source: SLF). Running means are aggregated at the end of the period; the date scales indicate 1 January.

vere model biases in other modelling studies (e.g. Ekici et al., 2014), special attention is devoted to (1) the timing of the onset and melt-out of the snow cover and (2) its thermal insulation effect, which mainly depends on the thickness, density and structure of the snow layer but also on the roughness of the terrain. Simulated snow depths correlate well with the observed snow depths at Les Attelas (for LAP_S015: $R^2 = 0.88\text{--}0.97$). But because the snow depths are recorded in a place with different topography and microclimate, this comparison is of limited validity. More reliable is information about the timing and insulation effect of the snow cover directly derived from the GST time series: Table 4 compares the timing and duration of the snow-covered period (cf. Sect. 2.3) and the snow melt in spring. While for some loggers the timing of the simulated snow melt period is very close to the observations (e.g. for LAP_0198, LAP_S015, LAP_S029), for others the simulated melting period ends several weeks too early (mainly for LAP_S036, LAP_S037, LAP_S038). This may lead to substantially wrong GST_{sim} in spring and early summer, which also explains the large variations in model bias and R^2 (see Figs. 4, 5c and d). The causes can be related to the redistribution of snow by wind or

avalanches affecting the observations as well as the parameterisation of the model. Because the GST difference between the snow-covered state and the first days after melt-out is of the order of 5–10 K, a delayed melt-out of as little as 5 days in the simulation can cause a model bias of approximately +0.1 K with respect to the annual mean. Early and late starting of the snow melt has less effect on the annual model bias, as the mean error is usually smaller than 2–3 K each day. The duration of the snow melt period tends to be overestimated by the model (mean: +5 days), which can either be due to model parameterisation (e.g. melt coefficients, snow albedo or suboptimal model layer structure), or processes of snow redistribution and compaction (avalanches, wind, skiers) not simulated in the model. The onset of the winter snow cover is generally better reproduced by the model than the melt-out. Regarding snow depths and the amount of days with a given snow depth (Table 4), the simulations look plausible for LAP_S015, LAP_S019, LAP_S026, LAP_S028 and LAP_S029. But for the other loggers as well as for the borehole, the simulated snow depths seem rather too shallow.

In summary, the model bias is neither constant nor increasing over time but highly depends on the simulation of the

Table 4. Timing and duration of the observed and simulated snow cover (obs|sim) for the three hydrological years with complete data: 2006/07, 2009/10 and 2010/11 (average values representing the day of the year starting on 1 January and the duration in days, respectively). Since no direct observations exist for the GST loggers, only simulated snow depths (average between November and May and the standard deviation) are indicated.

Snow cover characteristics	LAP_S015	LAP_S019	LAP_S026	LAP_S028	LAP_S029	LAP_S036	LAP_S037	LAP_S038	LAP_0198
Start snow melt	118 104	113 114	109 103	114 102	109 103	114 112	116 115	114 118	113 106
End snow melt	170 171	147 151	164 154	172 170	163 161	154 132	182 137	169 137	172 173
Snow melt duration (days)	53 68	35 38	56 52	59 69	55 59	41 21	67 23	56 20	60 68
Onset winter snow cover	320 317	320 326	328 326	317 325	319 318	339 326	325 318	323 325	336 318
Snow _{Nov–May} depth (cm)	64 ± 31	56 ± 34	57 ± 32	68 ± 33	65 ± 33	27 ± 26	27 ± 26	29 ± 26	28 ± 14
Days with snow depth ≥ 30 cm	196	164	171	197	187	91	93	95	145

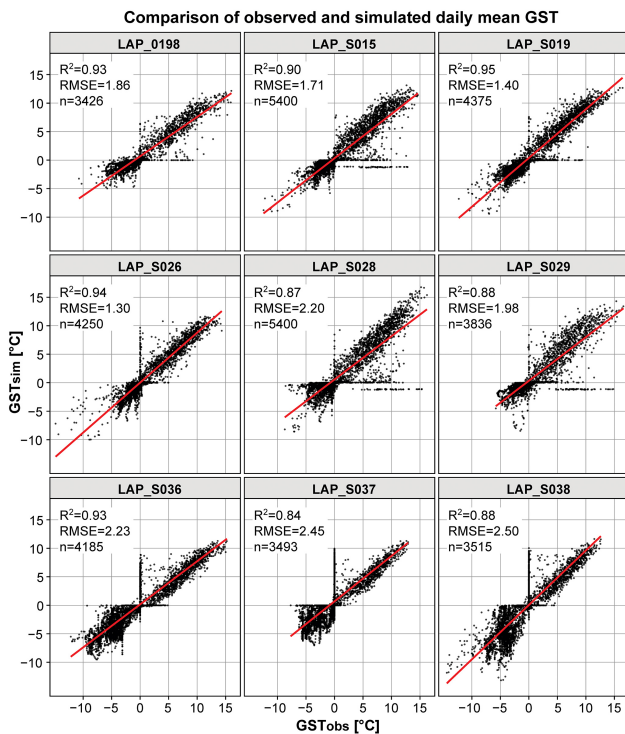


Figure 4. Comparison of GST_{sim} and GST_{obs} based on daily mean values for the uppermost thermistor at LAP_0198 (20 cm) and eight GST loggers (cf. Table 1).

snow cover. The inter-annual pattern of the model bias is similar for most loggers but does not seem to be directly linked to specific meteorological conditions.

3.3 Comparison of observed and simulated seasonal GST variations

Figure 6 illustrates the seasonal variability of the model bias, and it shows that the strongest deviations occur (1) during the second part of the winter and (2) after the snow melt period. Even though the variability between different (cold/warm) years is low from February to April, the model bias remains positive between +0.5 and +2 K, whereas during the snow-free period the variability is much larger, but with a

smaller mean model bias. Loggers LAP_S036, LAP_S037 and LAP_S038 show different behaviour, mainly because the timing and duration of the snow melt is not well captured by the model (see Sect. 3.2) and the snow depths seem to be underestimated (short-time variations are unrealistically large). These loggers are situated in areas of higher potential incoming radiation (cf. Table 1), which might be a first explanation for the different seasonal patterns (Fig. 6) and the larger RMSE (Fig. 4). In addition, LAP_S036 is situated at the bottom of the talus slope in a zone of probably intense internal air circulation (Delaloye and Lambiel, 2005).

In summary, GST_{sim} values are systematically too warm between February and May, changes in the model bias are largest before and after the snow melt, and for most loggers the model bias increases between July and November. The observed seasonality of the model bias requires further investigation (see Sect. 4.2), especially regarding (a) the responsible processes and (b) a potential cumulative effect over time. The latter can be analysed in terms of the cumulative GST model bias (CMB; see Fig. 7). For most years and loggers the model bias cumulates to positive values for individual hydrological years (which equates to an overestimation of the simulated temperatures), with maxima around 500 degree days (DD) between April and July. The mostly negative model bias in summer is partly able to compensate for the positive bias during the rest of the year. For the two time series LAP_S015 and LAP_S028, negative CMB occurred in 2002/03 (event E3) and 2010/11, mainly due to underestimated GST during the snow-free period. A possible explanation would be overestimated subsurface water content, because the ground was very dry in summer 2003. The most positive CMB occurred in 2011, due to a strong overestimation of the winter GST and a much too early start of the snow melt (2–3 weeks).

3.4 Comparison of observed and simulated ground temperatures at depth

To further investigate the processes that might be responsible for the model bias observed so far in GST_{sim} , GT_{sim} values were also compared with those of GT_{obs} for all thermistors from borehole LAP_0198 (Table 1). In addition to

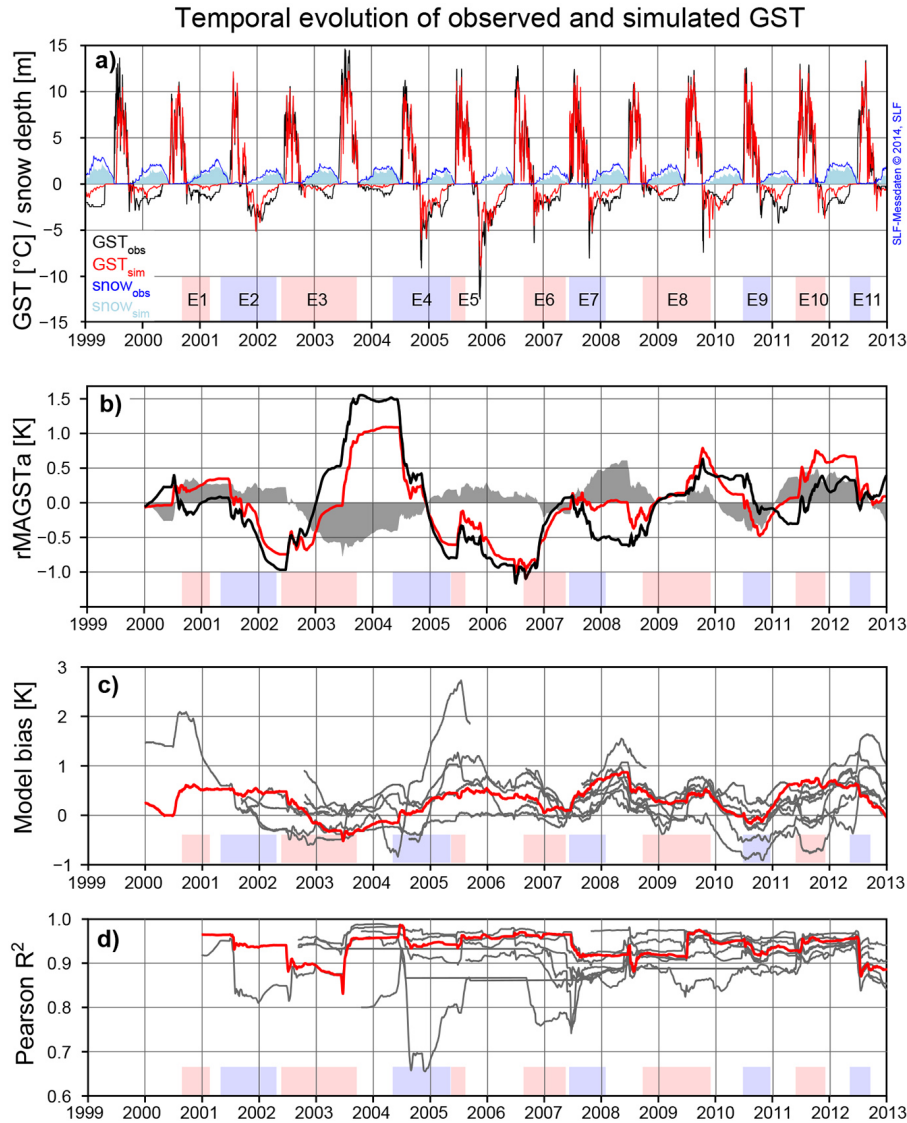


Figure 5. (a) Comparison of GST_{sim} (red) and GST_{obs} (black) for logger LAP_S015; the blue area and blue line denote simulated and measured (station ATT-2, source: SLF) snow depth, respectively. (b) rMAGST_{sim} (red) and rMAGST_{obs} (black) anomalies for LAP_S015; the shaded area represents the running 365-day model bias. (c) Running 365-day model bias for all loggers (LAP_S015 in red). (d) Pearson correlation coefficients (R^2) in a moving 365-day time window, based on R^2 between GST_{sim} and GST_{obs} (LAP_S015 in red). The colour bars at the bottom indicate the meteorological events described in Fig. 3 and Table 3.

the upper boundary conditions, the model for LAP_0198 was also calibrated to fit the temperatures at depth (lower boundary condition) and the parameters listed in Table 2. Figure 8 shows that, similar to the GST simulations (Fig. 7), the winter cooling tends to be underestimated (GT_{sim} values are too warm during winter) and in general the seasonal amplitudes of GT_{sim} are smaller compared to GT_{obs}. This is interesting because the simulated snow depths seem rather shallow (Table 4), which should lead to a pronounced cooling of the ground during winter, but of course the cooling by convection between coarse blocks is not included in the model.

As Fig. 8 shows, the general pattern of different meteorological events (e.g. E3, E4 or E9) is well captured by the model, even though the freezing processes are not as fast or effective as in reality, which may be due to the missing convective and radiative heat transport through the coarse blocky layer in the model (Gruber and Hoelzle, 2008; Scherler et al., 2014). The lowering of the active layer thickness observed in the GT records and geophysical monitoring data (cf. Fig. 2) after E3 (2002/03) and E8 (2009) is also reproduced by the COUP model.

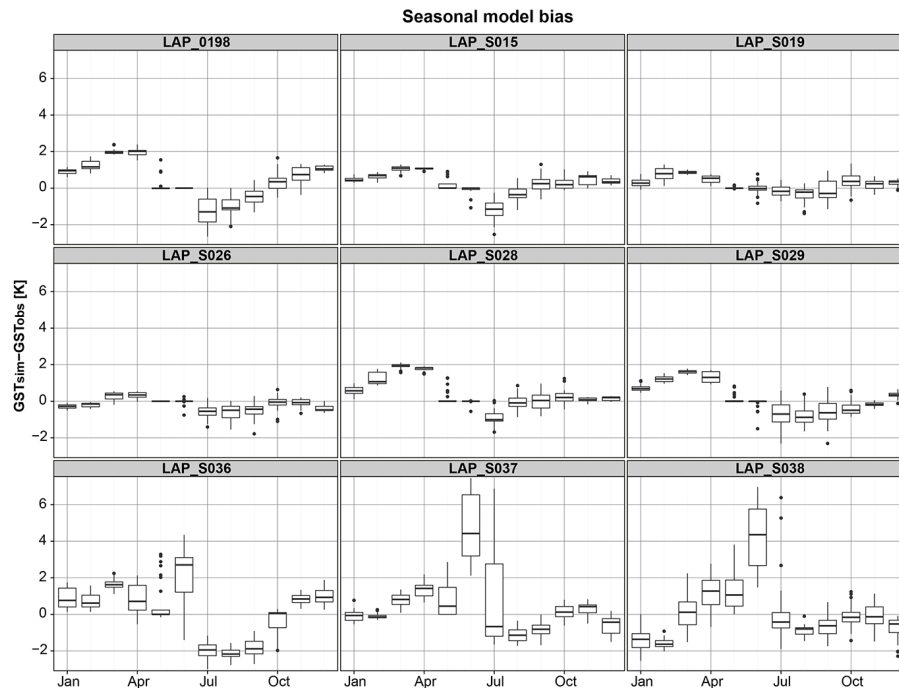


Figure 6. The seasonal evolution of the model bias ($GST_{sim} - GST_{obs}$), aggregated for each month for the uppermost thermistor of borehole LAP_0198 and all eight GST loggers. Dots at the end of the boxplots represent outliers (whiskers with maximum 1.5 IQR).

4 Discussion

4.1 Inter-annual variations and reaction to recent meteorological events

In general, the simulated variations in rMAGST closely follow the observed variations. Periods with the highest and lowest Pearson correlation between GST_{sim} and GST_{obs} were very different regarding the dominant meteorological and snow cover conditions (cf. Figs. 2 and 3), but usually coincide with large deviations of the melt-out day and the zero-curtain duration. No clear over- or underestimation of specific meteorological and/or snow cover conditions was found, and the relationship between the 365-day model bias and observed rMAGSTa is very weak (see Fig. 9a). The relationship gets even weaker for running 365-day Pearson correlation (Fig. 9b), indicating that the similarity between GST_{sim} and GST_{obs} is not influenced by inter-annual GST variations.

This implies that inter-annual GST variations and “meteorological events” are well enough simulated by the COUP model to cause no additional problems for long-term GST simulations, e.g. by additionally increasing the cumulative model bias. Even though the simulated snow depths agree astonishingly well with the recordings from ATT-2 and are also plausible regarding the variations of GST_{obs} (except for LAP_S036–38), temporarily larger model bias and weaker R^2 are likely related to snow cover dynamics and in particular with the timing of the snow melt. Cold GST_{obs} values with rather large short-time variations during winter (as the case

for LAP_S036–38) were optimised by GLUE (Sect. 2.4) to simulate high densities of the new snow (Table 2) and in consequence shallow snow depths (Table 4). The higher thermal conductivity of the simulated snowpack explains untimely melt-out. Ekici et al. (2014) found that underestimated snow depths always lead to a cold GST model bias, whereas overestimated snow depths may cause positive or negative model bias. While this is clearly the case for some loggers (e.g. LAP_S038 in the hydrological year 2010/11, cf. Fig. 7), in many other situations positive model biases have been found even though the simulated snow depths seemed underestimated. But since the connection between the model bias and the snow cover depends on many factors, such as the quality of the meteorological input data, effects like the redistribution of snow by wind and avalanches as well as the physics and parameterisation of the model remain important fields of current and future research.

4.2 Seasonal patterns and bias accumulation

A distinct seasonal pattern in the GST model bias was observed (Fig. 6). The systematic positive model bias in late winter is likely caused by (1) the ice core at depth missing in the model that acts as a heat sink (Scherler et al., 2014) and/or (2) underestimated (or missing) convective and advective processes that are known to occur in this kind of coarse-blocky substrate (Gruber and Hoelzle, 2008; Harris and Pedersen, 1998). The first effect is most prominent in winters

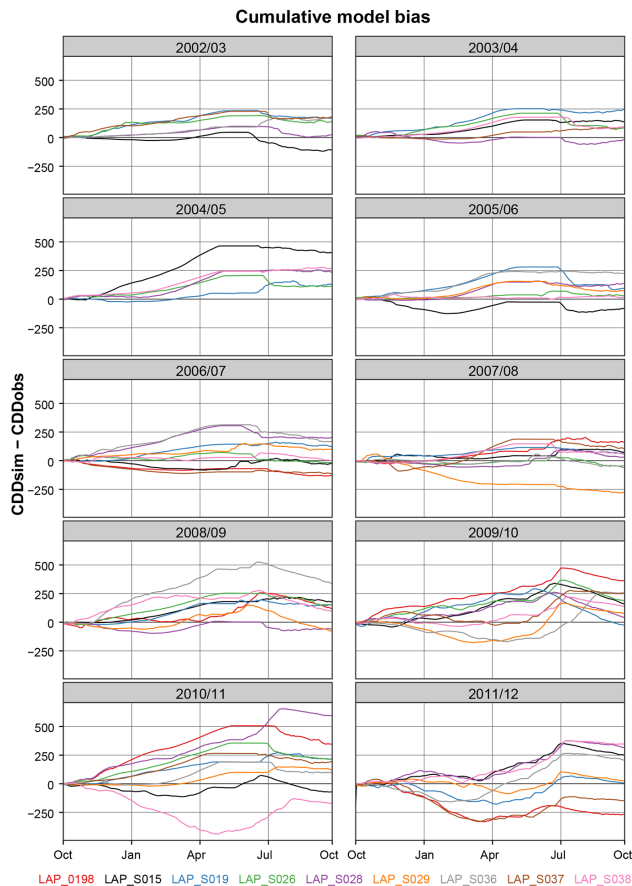


Figure 7. Cumulative GST model bias as degree days (DD) for the hydrological years (2003–2012): only loggers with complete observations are shown (cf. colour legend at the bottom).

with early ground insulation due to the snow (e.g. 2002/03, 2003/04 or 2008/09), when the cooling of the ground is limited.

The best model performance was observed during the snow-free season as well as in winters with very little snow, particularly in the colder period between autumn 2004 and late winter 2006 (event E4, cf. Figs. 3 and 5). By means of the CMB (Fig. 7) it was shown that the cumulative effect of the seasonal biases is positive in most years, although too cold GST_{sim} values in June and July (delayed melt-out, potentially underestimated radiation influence) did partially compensate for the positive bias during winter. The resulting model bias remained more or less constant during the whole observation period (Fig. 5) without clear trends, indicating that the bias of the final simulation year is not larger/worse than in the first year of the simulation. This may be different when the model is applied before or after the observation period and one should be aware of eventually cumulating errors in the near-surface layers. Having an observation period with very diverse conditions could be an advantage, first to analyse the reaction of the model during the calibration period

and second to tune the model to a large variety of possible situations. However the sensitivity of the snow and albedo parameters (Table 2) to extreme years during the calibration period requires further investigation and will give insight into the reliability of the models.

The simulation of GT using borehole LAP_0198 was more difficult than for GST mainly because of the coarse dynamic resolution of the old thermistor chain (data until October 2009). Without a careful correction of the observations, the model would have been forced to several phase changes within the permafrost during the calibration period due to sometimes slightly positive (but erroneous) GT. The availability of geophysical measurements (which clearly showed a massive ice core which likely does not undergo complete melt processes) was very useful for plausibility checks and correcting the GT. The performance of the final simulation is comparable to those from other studies that have applied COUP to other boreholes from the PERMOS network (Marmy et al., 2013; Scherler et al., 2013, 2014). This is a surprisingly good result because multi-dimensional effects such as an up- and downslope air circulation cannot directly be simulated with a one-dimensional model like COUP, which also explains part of the model bias. Scherler et al. (2013, 2014) discussed the particularities of the energy balance within the coarse blocky surface layer of a rock glacier, using both direct observations and simulation results from the COUP model. They found a significant improvement of subsurface temperature simulations by adding a seasonally varying heat source/sink term, which parameterises the cooling effect of the coarse blocky material. Without this artificial heat sink, no permafrost would have been simulated (Scherler et al., 2014). At Lapires, this effect might be less extreme and superimposed by intra-talus ventilation, but it is likely still present. The internal air circulation in talus slopes is complex, and as it depends mainly on the temperature gradient between inside and outside the system (Delaloye and Lambiel, 2005), it likely has the strongest influence in situations with rather extreme cold or warm air temperatures. A parameterisation of these coupled processes was clearly beyond the scope of this paper but remains an open field for future research.

4.3 Possibilities and limitations of COUP for GST and GT reconstruction

We assume that (a) avalanche activity, (b) a spatially varying ice content in the underlying permafrost, (c) site-specific intra-talus air circulation and (d) the disturbance of the snow cover by skiers are particularly difficult to capture with a model only calibrated by GST. Points (a) and (d) can increase or decrease the thermal conductivity of the snow cover by either purging parts of the snow pack apart from or onto the point of interest, modifying the density of the snow pack, or disturbing it. We assume that (d) is less important but leads to a slightly higher density of the snow pack, which might

be less thermally insulating towards the end of the ski season and last a bit longer until its complete melt-out. The reconstruction of the avalanche activity (a) is difficult and beyond the scope of this article, but it could eventually explain the remarkable GST bias in some years (e.g. “avalanche winter” 1999) and for some loggers located in potential deposition zones of avalanches (mainly LAP_S026, LAP_S028, LAP_S029, LAP_S036, LAP_S037 and LAP_S038). The systematic overestimation of the late-winter GST in years with early and intensive thermal insulation by the snow cover indicates that (b) also plays a major role, for example, in the hydrological years 2003 and 2009, when cold temperatures at greater depth (Fig. 5) were responsible for the cooling of the upper active layer before snow melt. Intra-talus ventilation (c) affects at least some of the GST loggers and the observations show that this effect mainly causes secondary temperature variations (Delaloye and Lambiel, 2005). We assume that this process is not dominant for the model bias and less important than other effects of the coarse-blocky material missing in the COUP model. As discussed in Scherler et al. (2013, 2014), convection and thermal radiation may be responsible for the systematic overestimation of the late-winter GST, even though the snow parameters (see Table 2) can partially account for this.

Since COUP is calibrated to a minimal RMSE between GST_{sim} and GST_{obs} , the depth of the sensor below the surface could be estimated in the model setup if no precise values are known. On the other hand, homogeneous monitoring conditions are of course very important for the observations. Long time series of high-quality data for the input and validation variables are essential for a stable calibration and good model performance.

In this study, we used the entire observation period of meteorological and GST observations. It would also be useful to validate the quality of the calibration with complementary data sets (e.g. water content, electrical resistivity as a proxy for the ice content or the local snow depth) if the time series are sufficiently long. In addition, some years or periods of different meteorological conditions could be excluded from the calibration to analyse this effect on the model parameters and performance. Of course, the inverse modelling approach (GLUE) also faces the issue of computing power. In order to test some parameters and to find the optimal fit, a certain number of successive simulations should be done, which is time- and computing-power-consuming.

4.4 Benefits of joint observational and modelling studies

To benefit from joint research, it is important to analyse the strengths and weaknesses of the different methods. The main advantages of direct observations are (1) the comprehensive knowledge about and experience with site-specific conditions (surface characteristics, snow conditions etc.) from field work and various measurements obtained and (2) the observations themselves, which reflect the physical processes in all

their complexity of the real world. On the other hand, model studies are beneficial (1) to improve the understanding of the physical processes, (2) to simulate changes over long time periods and (3) to assess sensitivities while only changing one parameter at a time. The superposition of various influencing factors makes the quantification of physical processes based only on monitoring data very difficult. Model-based approaches, however, are faced with the need for simplification, the negligence of terrain heterogeneities, lateral and 3-D effects (at least for the COUP model used for this study) and a tendency towards over-parameterisation, which may lead to correct results but for the wrong reasons, as the observed seasonality of the model bias has shown. Furthermore, the short observation period (~ 10 – 15 years) and remote study areas complicate both direct time series analysis (not sufficient to analyse trends on a decadal timescale) and scenario-based subsurface modelling (time series are often too short or incomplete regarding meteorological parameters for statistical downscaling of RCM output data and independent model validation).

5 Conclusions and future perspectives

The COUP model has shown to be suitable for the reconstruction of GST time series situated on a talus slope. Not surprisingly, the best performance was found for periods without or with limited snow cover. Although the simulation of GST using only a prescribed upper boundary condition revealed surprisingly good results for the surface (which is not evident in locations with a coarse ground surface underlain by permafrost and prone to intra-talus air circulation; Delaloye and Lambiel, 2005), winters with limited ground cooling (usually after snow events in autumn) were systematically too warm in most of the simulations.

Simulated GST can serve (1) to fill gaps in the observations or to reconstruct GST of the past, (2) to investigate possible reasons for variations in the model bias and also (3) to assess the quality and uncertainty of model results. The key element to minimise the GST model bias is the reconstruction of an accurate snow cover, which is influenced by many factors and processes and particularly depends on precise meteorological input data (foremost precipitation) and a good parameterisation of the model (cf. Table 2). The meteorological input data used for this study (Rajczak et al., 2015) led to plausible results for the majority of the GST loggers and years regarding the snow cover evolution. This is remarkable because no local precipitation measurements were available. The simulation of the snow cover could possibly be further improved by separating the snowpack into several layers (for a more realistic structure with various temperature gradients), or by modelling the snowpack with software such as SNOWPACK (Lehning et al., 1999) or Alpine3D (Lehning et al., 2006).

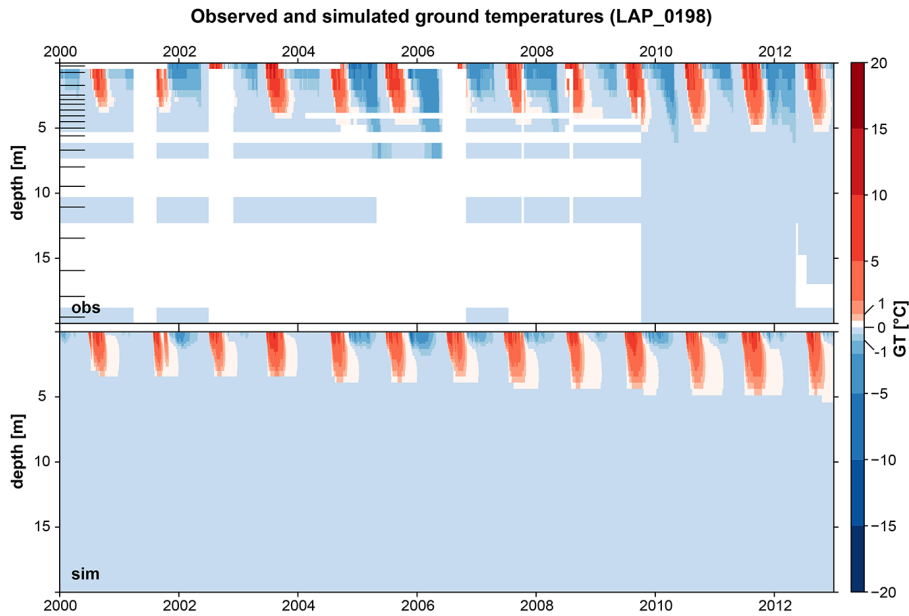


Figure 8. Contour plot showing GT_{obs} (top) and GT_{sim} (bottom) over 20 m depth between 2000 and 2012 for borehole LAP_0198 at the Lapires talus slope. The marks inside of the vertical axis on the observation panel indicate the depth of the thermistors. In white areas, observations are either missing or had to be removed because of bad quality (see Sect. 2.3).

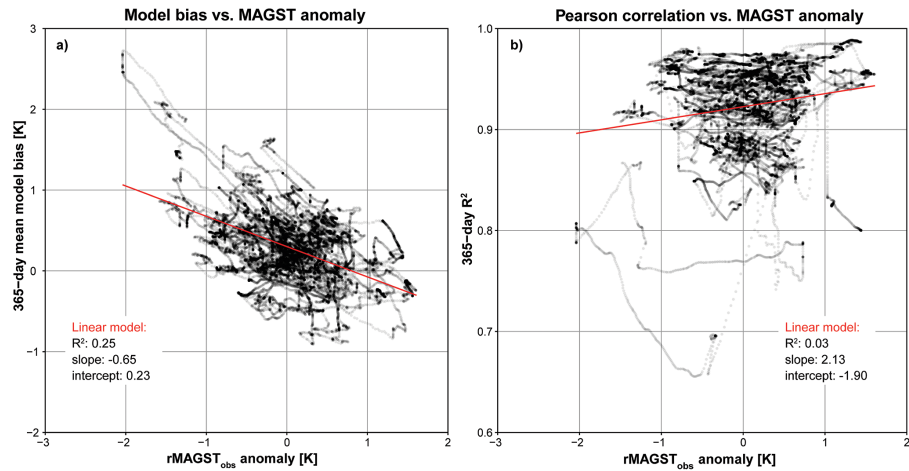


Figure 9. Comparison of rMAGST anomaly for all GST loggers and the entire observation period ($n = 31\,266$) with (a) the model bias ($GT_{sim} - GT_{obs}$) and (b) running 365-day R^2 .

The identification of specific meteorological and snow cover conditions revealed that events of very short duration (days–weeks) can largely affect variations in rMAGST. This is an issue to keep in mind when driving thermal subsurface models with downscaled RCM input data, which cannot reflect unique meteorological events but represent the mean state and seasonality of the climate. Furthermore, the influence of the calibration period should be analysed in detail and with consideration of the effects of meteorological events on the calibration parameters and model performance. At the moment it is not clear whether comparatively extreme years

should be included (to capture this natural variability in the model) or excluded from the calibration (to reduce the model bias during other periods). Further research is needed to fill this research gap. We recommend analysing inter-annual and seasonal patterns of the model bias during the calibration and validation period for every model study to understand how the model might react in different situations. This could be further combined with sensitivity assessments for the effects of single meteorological events on the snow and albedo calibration parameters by separating the validation from the calibration time window.

An important requirement for satisfying model results is having high-quality input data for long observation periods as well as precise information about the structure and composition of the subsurface which is representative of the point scale. These pre-conditions were rather good at our investigated study site, Lapires, in comparison with many other sites of the Swiss permafrost observing network PERMOS. The GST simulation at locations with permafrost evidence could be improved by prescribing a constant temperature of 0 °C at the maximal depth of the active layer (between 5.5 and 6 m for borehole LAP_0198, cf. PERMOS 2013) and/or to improve the structure and material composition of the subsurface in the model (especially porosity, water and ice content) using, for example, the four-phase model approach (Hauck et al., 2011). Finally, more sophisticated downscaling methods of the meteorological input parameters could be applied, for instance, by correcting the influence of topography on the shortwave incoming radiation separately for each point instead of using the same meteorological input data for all GST loggers and the borehole. A detailed analysis and validation of the upper boundary conditions during the observation period clearly improves the reliability of any model for long-term simulations.

Acknowledgements. We greatly acknowledge the Swiss National Science Foundation for the funding of the Sinergia TEMPS project (project no. CRSII2_136279), within which this study was conducted. Special thanks are due to our colleagues within TEMPS and PERMOS for providing the observational and reconstructed meteorological data, namely C. Lambiel from the University of Lausanne and J. Rajczak from ETH Zurich. We gratefully acknowledge the detailed and constructive comments of the two anonymous reviewers.

Edited by: M. Hoelzle

Reviewed by: two anonymous referees

References

- Apaloo, J., Brenning, A., and Bodin, X.: Interactions between Seasonal Snow Cover, Ground Surface Temperature and Topography (Andes of Santiago, Chile, 33.5° S), *Permafrost Periglac.*, 23, 277–291, doi:10.1002/ppp.1753, 2012.
- Arenson, L., Hoelzle, M., and Springman, S.: Borehole deformation measurements and internal structure of some rock glaciers in Switzerland, *Permafrost Periglac.*, 13, 117–135, doi:10.1002/ppp.414, 2002.
- Beven, K. and Binley, A.: The future of distributed models: Model calibration and uncertainty prediction, *Hydrol. Process.*, 6, 279–298, doi:10.1002/hyp.3360060305, 1992.
- Beven, K. and Freer, J.: Equifinality, data assimilation, and uncertainty estimation in mechanistic modelling of complex environmental systems using the GLUE methodology, *J. Hydrol.*, 249, 11–29, doi:10.1016/S0022-1694(01)00421-8, 2001.
- Boeckli, L., Brenning, A., Gruber, S., and Noetzli, J.: Permafrost distribution in the European Alps: calculation and evaluation of an index map and summary statistics, *The Cryosphere*, 6, 807–820, doi:10.5194/tc-6-807-2012, 2012.
- Delaloye, R.: Contribution à l'étude du pergélisol de montagne en zone marginale, PhD Thesis, University of Fribourg, Switzerland, 244 pp., GeoFocus, 2004.
- Delaloye, R. and Lambiel, C.: Evidence of winter ascending air circulation throughout talus slopes and rock glaciers situated in the lower belt of alpine discontinuous permafrost (Swiss Alps), *Norsk Geografisk Tidsskrift – Norwegian Journal of Geography*, 59, 194–203, doi:10.1080/00291950510020673, 2005.
- Delaloye, R., Reynard, E., and Lambiel, C.: Pergélisol et construction de remontées mécaniques: l'exemple des Lapires (Mont-Gelé, Valais), *Le gel en géotechnique*, Publications de la Société Suisse de Mécanique des Sols et des Roches, 141, 103–113, 2001.
- Delaloye, R., Reynard, E., Lambiel, C., Marescot, L., and Monnet, R.: Thermal anomaly in a cold scree slope, Creux du Van, Switzerland, in: *Proceedings of the 8th International Conference on Permafrost*, 21–25 July 2003, Zurich, Switzerland, 175–180, 2003.
- Ekici, A., Chadburn, S., Chaudhary, N., Hajdu, L. H., Marmy, A., Peng, S., Boike, J., Burke, E., Friend, A. D., Hauck, C., Krinner, G., Langer, M., Miller, P. A., and Beer, C.: Site-level model intercomparison of high latitude and high altitude soil thermal dynamics in tundra and barren landscapes, *The Cryosphere Discuss.*, 8, 4959–5013, doi:10.5194/tcd-8-4959-2014, 2014.
- Endrizzi, S. and Gruber, S.: Investigating the Effects of Lateral Water Flow on the Spatial Patterns of Thaw Depth, in: *Tenth International Conference on Permafrost*, Salekhard, Yamal-Nenets Autonomous District, Russia, 25 June 2012–29 June 2012, 91–96, 2012.
- Engelhardt, M., Hauck, C., and Salzmann, N.: Influence of atmospheric forcing parameters on modelled mountain permafrost evolution, *Meteorol. Z.*, 19, 491–500, doi:10.1127/0941-2948/2010/0476, 2010.
- Etzelmüller, B., Schuler, T. V., Isaksen, K., Christiansen, H. H., Farbro, H., and Benestad, R.: Modeling the temperature evolution of Svalbard permafrost during the 20th and 21st century, *The Cryosphere*, 5, 67–79, doi:10.5194/tc-5-67-2011, 2011.
- Fiddes, J. and Gruber, S.: TopoSUB: a tool for efficient large area numerical modelling in complex topography at sub-grid scales, *Geosci. Model Dev.*, 5, 1245–1257, doi:10.5194/gmd-5-1245-2012, 2012.
- Fiddes, J. and Gruber, S.: TopoSCALE v.1.0: downscaling gridded climate data in complex terrain, *Geosci. Model Dev.*, 7, 387–405, doi:10.5194/gmd-7-387-2014, 2014.
- Ğadek, B.: Debris slopes ventilation in the periglacial zone of the Tatra Mountains (Poland and Slovakia): The indicators, *Cold Reg. Sci. Technol.*, 74–75, 1–10, doi:10.1016/j.coldregions.2012.01.007, 2012.
- Goodrich, L. E.: The influence of snow cover on the ground thermal regime, *Can. Geotech. J.*, 19, 421–432, doi:10.1139/t82-047, 1982.
- Gruber, S. and Haeberli, W.: Permafrost in steep bedrock slopes and its temperature-related destabilization following climate change, *J. Geophys. Res.*, 112, F02S18, doi:10.1029/2006JF000547, 2007.

- Gruber, S. and Haeberli, W.: Mountain Permafrost, in *Permafrost Soils*, vol. 16, edited by: Margesin, R., 33–44, Springer Berlin Heidelberg, Berlin, Heidelberg, 2009.
- Gruber, S. and Hoelzle, M.: The cooling effect of coarse blocks revisited: a modeling study of a purely conductive mechanism, in: *Proceedings of the 9th International Conference on Permafrost*, Fairbanks, Alaska, 557–561, 2008.
- Gubler, S., Fiddes, J., Keller, M., and Gruber, S.: Scale-dependent measurement and analysis of ground surface temperature variability in alpine terrain, *The Cryosphere*, 5, 431–443, doi:10.5194/tc-5-431-2011, 2011.
- Hanson, S. and Hoelzle, M.: Installation of a shallow borehole network and monitoring of the ground thermal regime of a high alpine discontinuous permafrost environment, *Eastern Swiss Alps*, *Norsk Geografisk Tidsskrift – Norwegian J. Geogr.*, 59, 84–93, doi:10.1080/00291950510020664, 2005.
- Harris, C., Arenson, L. U., Christiansen, H. H., Etzelmüller, B., Frauenfelder, R., Gruber, S., Haeberli, W., Hauck, C., Hoelzle, M., Humlum, O., Isaksen, K., Kääh, A., Kern-Lütschg, M. A., Lehning, M., Matsuoka, N., Murton, J. B., Noetzli, J., Phillips, M., Ross, N., Seppälä, M., Springman, S. M., and Vonder Mühl, D.: Permafrost and climate in Europe: Monitoring and modelling thermal, geomorphological and geotechnical responses, *Earth-Sci. Rev.*, 92, 117–171, doi:10.1016/j.earscirev.2008.12.002, 2009.
- Harris, S. A. and Pedersen, D. E.: Thermal regimes beneath coarse blocky materials, *Permafrost Periglac.*, 9, 107–120, doi:10.1002/(SICI)1099-1530(199804/06)9:2<107::AID-PPP277>3.0.CO;2-G, 1998.
- Hauck, C., Böttcher, M., and Maurer, H.: A new model for estimating subsurface ice content based on combined electrical and seismic data sets, *The Cryosphere*, 5, 453–468, doi:10.5194/tc-5-453-2011, 2011.
- Hawkins, E. and Sutton, R.: The Potential to Narrow Uncertainty in Regional Climate Predictions, *B. Am. Meteorol. Soc.*, 90, 1095–1107, doi:10.1175/2009BAMS2607.1, 2009.
- Hilbich, C.: Time-lapse refraction seismic tomography for the detection of ground ice degradation, *The Cryosphere*, 4, 243–259, doi:10.5194/tc-4-243-2010, 2010.
- Hilbich, C., Fuss, C., and Hauck, C.: Automated Time-lapse ERT for Improved Process Analysis and Monitoring of Frozen Ground, *Permafrost Periglac.*, 22, 306–319, doi:10.1002/ppp.732, 2011.
- Hoelzle, M., Wegmann, M., and Krummenacher, B.: Miniature temperature dataloggers for mapping and monitoring of permafrost in high mountain areas: first experience from the Swiss Alps, *Permafrost Periglac.*, 10, 113–124, doi:10.1002/(SICI)1099-1530(199904/06)10:2<113::AID-PPP317>3.0.CO;2-A, 1999.
- Hoelzle, M., Mittaz, C., Etzelmüller, B., and Haeberli, W.: Surface energy fluxes and distribution models of permafrost in European mountain areas: an overview of current developments, *Permafrost Periglac.*, 12, 53–68, doi:10.1002/ppp.385, 2001.
- IPCC: *Climate Change 2013: The Physical Science Basis. Contribution of Working Group I to the Fifth Assessment Report of the Intergovernmental Panel on Climate Change*, Cambridge University Press, Cambridge, 2014.
- Isaksen, K., Ødegård, R. S., Etzelmüller, B., Hilbich, C., Hauck, C., Farbrot, H., Eiken, T., Hygen, H. O., and Hipp, T. F.: Degrading Mountain Permafrost in Southern Norway: Spatial and Temporal Variability of Mean Ground Temperatures, 1999–2009, *Permafrost Periglac.*, 22, 361–377, doi:10.1002/ppp.728, 2011.
- Ishikawa, M.: Thermal regimes at the snow–ground interface and their implications for permafrost investigation, *Geomorphology*, 52, 105–120, doi:10.1016/S0169-555X(02)00251-9, 2003.
- Jansson, P. E.: CoupModel: Model Use, Calibration, and Validation, *Transactions of the ASABE*, 55, 1337–1346, doi:10.13031/2013.42245, 2012.
- Jansson, P. E. and Karlberg, L.: Coupled heat and mass transfer model for soil-plant-atmosphere systems, 365 pp., 2004.
- Keller, F. and Gubler, H.: Interaction between snow cover and high mountain permafrost, Murtèl-Corvatsch, Swiss Alps, in: *Proceedings of the 6th International Conference on Permafrost*, Beijing, China, edited by G. Cheng, 332–337, South China University of Technology Press, Guangzhou, 1993.
- Kneisel, C., Hauck, C., Fortier, R., and Moorman, B.: Advances in geophysical methods for permafrost investigations, *Permafrost Periglac.*, 19, 157–178, doi:10.1002/ppp.616, 2008.
- Lambiel, C.: Le pergélisol dans les terrains sédimentaires à forte déclivité: distribution, régime thermique et instabilités, 280 pp., *Travaux et recherches Vol. 33*, 2006.
- Lehning, M., Bartelt, P., Brown, B., Russi, T., Stöckli, U., and Zimmerli, M.: snowpack model calculations for avalanche warning based upon a new network of weather and snow stations, *Cold Reg. Sci. Technol.*, 30, 145–157, doi:10.1016/S0165-232X(99)00022-1, 1999.
- Lehning, M., Völksch, I., Gustafsson, D., Nguyen, T. A., Stähli, M., and Zappa, M.: ALPINE3D: a detailed model of mountain surface processes and its application to snow hydrology, *Hydrol. Process.*, 20, 2111–2128, doi:10.1002/hyp.6204, 2006.
- Luetschg, M., Lehning, M., and Haeberli, W.: A sensitivity study of factors influencing warm/thin permafrost in the Swiss Alps, *J. Glaciol.*, 54, 696–704, doi:10.3189/002214308786570881, 2008.
- Marmy, A., Salzmann, N., Scherler, M., and Hauck, C.: Permafrost model sensitivity to seasonal climatic changes and extreme events in mountainous regions, *Environ. Res. Lett.*, 8, 035048, doi:10.1088/1748-9326/8/3/035048, 2013.
- Morard, S., Delaloye, R., and Dorthe, J.: Seasonal thermal regime of a mid-latitude ventilated debris accumulation, in: *Proceedings of the 9th International Conference on Permafrost*, Fairbanks, Alaska, 1233–1238., 2008.
- Noetzli, J. and Gruber, S.: *Alpiner Permafrost - ein Überblick*, edited by: Lintzmeyer, K., *Jahrbuch des Vereins zum Schutz der Bergwelt*, Selbstverlag, München, 70, 111–121, 2005.
- Noetzli, J. and Gruber, S.: Transient thermal effects in Alpine permafrost, *The Cryosphere*, 3, 85–99, doi:10.5194/tc-3-85-2009, 2009.
- Olaya, V.: *Basic Land-Surface Parameters*, in *Geomorphometry – Concepts, Software, Applications*, vol. 33, 141–169, Elsevier, 2009.
- PERMOS: *Permafrost in Switzerland 2008/2009 and 2009/2010*. Noetzli, J. (ed.), *Glaciological Report (Permafrost) No. 10/11 of the Cryospheric Commission of the Swiss Academy of Sciences (SCNAT)*, Zurich, Switzerland, 2013.
- Phillips, M., Mutter, E. Z., Kern-Luetschg, M., and Lehning, M.: Rapid degradation of ground ice in a ventilated talus slope: Flüela Pass, Swiss Alps, *Permafrost Periglac.*, 20, 1–14, doi:10.1002/ppp.638, 2009.

- Rajczak, J., Kotlarski, S., Salzmann, N., and Schär, C.: Robust climate scenarios for sites with sparse observations: A two-step bias correction approach, *Int. J. Climatol.*, submitted, 2015.
- Scapoza, C.: Stratigraphie, morphodynamique, paléoenvironnements des terrains sédimentaires meubles à forte déclivité du domaine périglaciaire alpin (Géovisions no. 40), PhD Thesis, University of Lausanne, 580 pp., 2013.
- Schär, C., Vidale, P. L., Lüthi, D., Frei, C., Haeberli, C., Liniger, M. A., and Appenzeller, C.: The role of increasing temperature variability in European summer heatwaves, *Nature*, 427, 332–6, doi:10.1038/nature02300, 2004.
- Scherler, M., Hauck, C., Hoelzle, M., Stähli, M., and Völksch, I.: Meltwater infiltration into the frozen active layer at an alpine permafrost site, *Permafrost Periglac.*, 21, 325–334, doi:10.1002/ppp.694, 2010.
- Scherler, M., Hauck, C., Hoelzle, M., and Salzmann, N.: Modeled sensitivity of two alpine permafrost sites to RCM-based climate scenarios, *J. Geophys. Res.: Earth Surface*, 118, 780–794, doi:10.1002/jgrf.20069, 2013.
- Scherler, M., Schneider, S., Hoelzle, M., and Hauck, C.: A two-sided approach to estimate heat transfer processes within the active layer of the Murtèl-Corvatsch rock glacier, *Earth Surf. Dynam.*, 2, 141–154, doi:10.5194/esurf-2-141-2014, 2014.
- Schmid, M.-O., Gubler, S., Fiddes, J., and Gruber, S.: Inferring snowpack ripening and melt-out from distributed measurements of near-surface ground temperatures, *The Cryosphere*, 6, 1127–1139, doi:10.5194/tc-6-1127-2012, 2012.
- Schneider, S.: The heterogeneity of mountain permafrost – A field-based analysis of different periglacial materials, PhD Thesis, University of Fribourg, 176 pp., 2014.
- Schneider, S., Hoelzle, M., and Hauck, C.: Influence of surface and subsurface heterogeneity on observed borehole temperatures at a mountain permafrost site in the Upper Engadine, Swiss Alps, *The Cryosphere*, 6, 517–531, doi:10.5194/tc-6-517-2012, 2012.
- Schneider, S., Daengeli, S., Hauck, C., and Hoelzle, M.: A spatial and temporal analysis of different periglacial materials by using geoelectrical, seismic and borehole temperature data at Murtèl-Corvatsch, Upper Engadin, Swiss Alps, *Geogr. Helv.*, 68, 265–280, doi:10.5194/gh-68-265-2013, 2013.
- Stocker-Mittaz, C., Hoelzle, M., and Haeberli, W.: Modelling alpine permafrost distribution based on energy-balance data: a first step, *Permafrost Periglac.*, 13, 271–282, doi:10.1002/ppp.426, 2002.
- Vonder Mühl, D., Stucki, T., and Haeberli, W.: Borehole temperatures in alpine permafrost: a ten year series, in: Proceedings of the 7th International Conference on Permafrost, Yellowknife (Canada), 1089–1095, Collection Nordicana, 57, 1998.
- Wakonigg, H.: Unterkühlte Schutthalden, Beiträge zur Permafrostkartierung in Österreich, Arbeiten aus dem Inst. f. Geogr. Karl-Franzens-Universität Graz, 209–223, 1996.
- Williams, P. J. and Smith, M. W.: *The Frozen Earth: Fundamentals of Geocryology*, Cambridge University Press, Cambridge, 1989.
- Zenkhusen Mutter, E. and Phillips, M.: Active Layer Characteristics At Ten Borehole Sites In Alpine Permafrost Terrain, Switzerland, *Permafrost Periglac.*, 23, 138–151, doi:10.1002/ppp.1738, 2012.
- Zhang, T.: Influence of the seasonal snow cover on the ground thermal regime: An overview, *Rev. Geophys.*, 43, 23, doi:10.1029/2004RG000157, 2005.

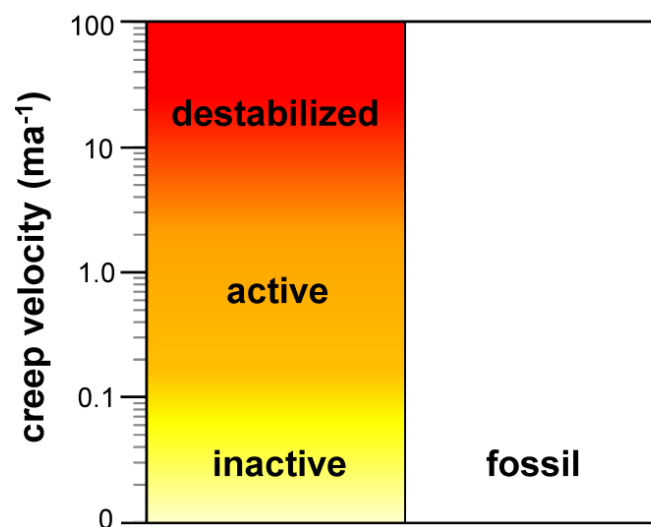
APPENDIX

A1: Region names of the Swiss Alps



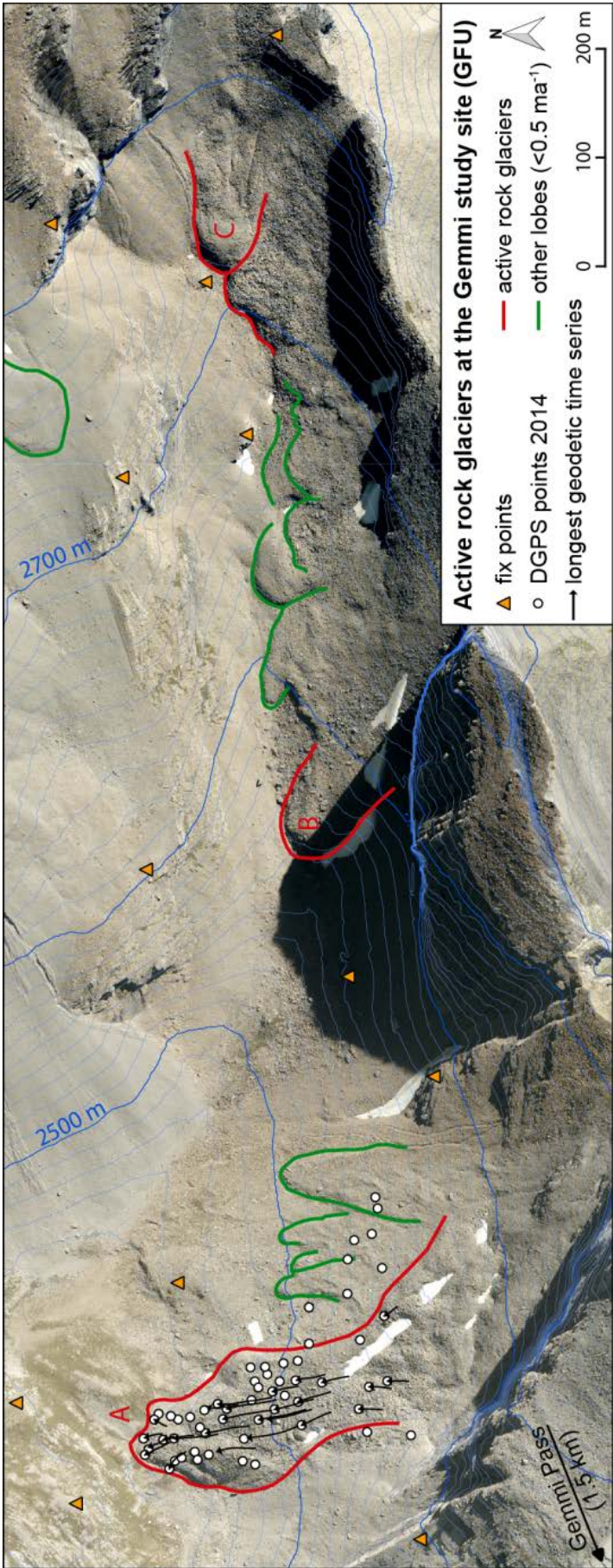
Geographical terminology of region names of the Swiss Alps: the major political regions. Source: WSL Institute for Snow and Avalanche Research SLF (Publisher) 2014: *Avalanche Bulletins and other products. Interpretation Guide*. Edition 2014. 13th revised edition. WSL Institute for Snow and Avalanche Research SLF, 50pp.: page 42.

A2: Categories of rock glacier activity



Categories of rock glacier activity depending on surface displacement rates: Literature values for velocities for active rock glaciers (Barsch, 1977, 1996; Haeblerli, 1985; Haeblerli et al., 2006; Käab et al., 2003) range between 0.1 and 2 (ma^{-1}). Illustration kindly provided by Luc Braillard, University of Fribourg.

A3: Overview map of the Gemmi rock glaciers



Site overview of the three active rock glaciers located at the Gemmi monitoring site (Staub et al., 2015b).

A4: Borehole meta data

Name	Project	Depth	Inclination	East	North	Elevation	Slope	Aspect	Morphology	Surface type	Sensor type	Logging system
ATT_0108	PERMOS	26.0	0	587'196	105'043	2661	25	270	talus slope	debris	YSI 440xx	Campbell CR800
ATT_0208	PERMOS	21.0	0	587'243	105'040	2689	30	270	talus slope	coarse blocks	YSI 440xx	Campbell CR800
COR_0287	PERMOS	62.0	0	783'160	144'720	2670	10	315	rock glacier	coarse blocks	YSI 44006	Campbell CR1000
DRE_0104	PERMOS	15.0	0	557'670	124'805	1580	30	90	talus slope	coarse blocks	MADD	MAAD logger
DRE_0204	TEMPS	4.9	0	557'695	124'805	1567	25	90	talus slope	coarse blocks	UTL-1	UTL-1
FLU_0102	PERMOS	23.0	0	791'375	180'575	2394	26	45	talus slope	debris	YSI 46006	Campbell CR10X
GEM_0106	PERMOS	40.0	90	689'781	161'780	2940	50	315	crest	bedrock	YSI 44008	Campbell CR1000
GEN_0102	PERMOS	20.0	0	589'467	103'586	2888	20	90	moraine	debris	MADD	MADD logger
JFJ_0195	PERMOS	21.0	80	641'000	155'120	3590	55	5	crest	bedrock	YSI 46008	Campbell CR10X
LAP_0198	PERMOS	19.6	0	588'070	106'080	2500	25	45	talus slope	coarse blocks	YSI 44031	Campbell CR1000
LAP_1108	PERMOS	40.0	0	588'099	106'092	2500	25	45	talus slope	coarse blocks	YSI 44031	Campbell CR1000
LAP_1208	PERMOS	35.0	0	588'028	106'027	2535	25	45	talus slope	coarse blocks	YSI 44031	Campbell CR1000
MAT_0205	PERMOS	53.0	0	618'399	92'334	3295	0	-	crest	bedrock	YSI 44008	Campbell CR10X
MBP_0196	PERMOS	18.0	0	791'314	152'493	2946	38	315	talus slope	debris	YSI 44008	Campbell CR10X
MBP_0296	PERMOS	18.0	0	791'339	152'513	2942	38	315	talus slope	debris	YSI 44008	Campbell CR10X
MDO_0196	TEMPS	10.0	0	601'246	97'232	2840	38	80	talus slope	debris	YSI 46008	Campbell CR10X
MUR_0199	PERMOS	70.2	0	791'025	153'726	2536	15	315	rock glacier	coarse blocks	YSI 44006	Campbell CR10X
MUR_0299	PERMOS	64.0	0	790'989	153'687	2539	15	315	rock glacier	coarse blocks	YSI 44006	Campbell CR10X
MUR_0399	PERMOS	72.0	0	791'038	153'679	2558	15	315	rock glacier	coarse blocks	YSI 44006	Campbell CR10X
MUR_0499	PERMOS	71.0	0	791'017	153'688	2549	15	225	rock glacier	coarse blocks	YSI 44006	Campbell CR10X
RIT_0102	PERMOS	30.0	0	631'755	113'775	2690	0	-	rock glacier	coarse blocks	YSI 44006	Campbell CR10X
SBE_0290	PERMOS	60.0	0	790'856	152'745	2732	0	-	rock glacier	coarse blocks	YSI 44006	Campbell CR10X
SCH_5000	PERMOS	101.0	0	630'350	156'410	2910	30	45	crest	debris	YSI 44006	Campbell CR1000
SCH_5198	PERMOS	14.0	0	630'365	156'410	2910	30	45	crest	debris	YSI 44006	Campbell CR1000
SCH_5200	PERMOS	100.0	30	630'350	156'410	2910	30	45	crest	debris	YSI 44006	Campbell CR1000
STO_6000	PERMOS	100.0	0	629'878	92'876	3410	8	180	crest	debris	YSI 44006	Campbell CR1000
STO_6100	PERMOS	31.0	0	629'867	92'850	3410	8	180	crest	debris	YSI 44006	Campbell CR1000
TSA_0104	PERMOS	20.0	0	608'490	106'400	3040	30	270	crest	bedrock	MADD	MADD logger

Meta data overview for selected PERMOS/TEMPS boreholes: The first 3 letters of the borehole names correspond to the site abbreviations in Fig. 3.1 and Table 3.1. Data source: PERMOS/TEMPS data base and PERMOS (2016).

CURRICULUM VITAE

Benno Staub

Born the 17th of January 1984, Berne (CH)

Education

- Mar 2012 – present **University of Fribourg:** PhD candidate at the Institute of Geography
- Nov 2009 – Apr 2010 **ETH Zurich:** Certificate of Advanced Studies in Geographic Information Systems (GIS)
- Sep 2003 – Oct 2008 **University of Berne:** Diploma (MSc) in Geography with focus on physical geography, minors in Earth Sciences and General Ecology
- Aug 1998 – Jul 2002 **Gymnasium K niz:** Swiss Maturity Diploma (major: economics and law)

Work experience

- Mar 2012 – present **University of Fribourg:** PhD student for the SNF Sinergia project „The Evolution of Mountain Permafrost in Switzerland“ (TEMPS 2011-2015)
- Oct 2013 – Jan 2014 **National Platform for Natural Hazards (PLANAT):** Civil service at the Federal Office for the Environment FOEN
- Nov 2011 – Feb 2012 **FHNW Muttenz:** Civil service at the Institute of Geomatics Engineering
- Jan 2010 – Oct 2011 **Emch+Berger AG Berne:** Project engineer for natural hazards, division for environment and security
- Feb 2009 – Aug 2011 **University of Berne:** Research assistant at the Institute of Geography, group of Applied Geomorphology and Natural Hazards (AGNAT)
- Sep – Dec 2010 **ETH Zurich:** Lectureship at the Department of Earth Sciences for the course „Introduction to Natural Hazard Management“
- May 2007 – Apr 2010 **Swiss Agency for Development and Cooperation (SDC):** Consultant for technical support on Disaster Risk Reduction (DRR)
- Jun – Nov 2009 **Swiss Federal Institute for Forest, Snow and Landscape Research WSL:** Civil service for the the long-term forest ecosystem research programme

Jun 2004 – Nov 2008 **University of Berne:** Junior research assistant at the Institute of Geography, group of Applied Geomorphology and Natural Hazards (AGNAT)

Apr – Dec 2006 **Federal Office of Topography swisstopo:** Student assistant in the topography division

Main publications

Staub, B., Marmy, A., Hauck, C., Hilbich, C. & Delaloye, R. (2015): Ground temperature variations in a talus slope influenced by permafrost: a comparison of field observations and model simulations. *Geographica Helvetica* 70: 45–62. DOI: 10.5194/gh-70-45-2015.

Staub, B., Hasler, A., Noetzli, J. & Delaloye, R. (subm.): Gap filling algorithm for ground surface temperature data. *Submitted to Permafrost and Periglacial Processes*, 2015.

Staub, B. & Delaloye, R. (2016): Using near-surface ground temperature data to derive snow insulation and melt indices for mountain permafrost applications. *Permafrost and Periglacial Processes*. DOI: 10.1002/ppp.1890

Staub, B., Vogel, D., Budmiger, K., Krummenacher, B., Delaloye, R., Kienholz, H. (2015): Einsatz der Photogrammetrie und Bildanalyse zur Quantifizierung von Blockgletscher-bewegungen. *Geomatik Schweiz*, vol. 113, no. 9, pp. 356-361, 2015.

Krummenacher, B., Mihajlovic, D., Nussbaum, A. & **Staub, B.** (Hrsg.) 2008: 20 Jahre Furggentälti - Permafrostuntersuchungen auf der Gemmi, *Geographica Bernensia* (G80), Bern.

Other publications

Rogers, S.R. & **Staub, B.** (2013): Standard use of Geographic Information System (GIS) techniques in honey bee research. *Journal of Apicultural Research* 52: 1–48. DOI: 10.3896/IBRA.1.52.4.08.

Delaloye, R., Perruchoud, E., Avian, M., Kaufmann, V., Bodin, X., Hausmann, H., Ikeda, A., Kääb, A., Kellerer-Pirklbauer, A., Krainer, K., Lambiel, C., Mihajlovic, D., **Staub, B.**, Roer, I. & Thibert, E. (2008): Recent Interannual variations of rockglaciers creep in the European Alps. *Proceedings of the 9th International Conference on Permafrost, Fairbanks, Alaska*. pp. 343–348.

Marmy, A., Rajczak, J., Delaloye, R., Hilbich, C., Hoelzle, M., Kotlarski, S., Lambiel, C., Noetzli, J., Phillips, M., Salzmann, N., **Staub, B.** and Hauck, C.: Semi-automated calibration method for modelling of mountain permafrost evolution in Switzerland, *The Cryosphere Discussions*, 9(5), 4787–4843, doi:10.5194/tcd-9-4787-2015, 2015.

Selected conference abstracts

Staub, B. (2015): Key messages from observational mountain permafrost research, Final symposium of the SNSF-Project TEMPS 2015, Sion (presentation)

Staub, B., Hasler, A., Delaloye, R. (2014): Gap filling procedures for ground surface temperature time series of the PERMOS network, Swiss Geoscience Meeting 2014, Fribourg (poster)

Staub, B., Delaloye, R. (2014): Variations in GST over mountain permafrost in Switzerland: the role of landform- and site-specific effects and regional aspects, EUCOP4, Evora (presentation)

Staub, B., Marmy, A., Hauck, C., Hilbich, C., Delaloye, R. (2014): The influence of weather events on the thermal regime over mountain permafrost: A comparison of field observations and model simulations at the Lapires talus slope, EUCOP4, Evora (poster)

Staub, B., Delaloye, R., Lambiel, C. (2013): Joint analysis of rock glacier kinematics and complementary permafrost monitoring elements observed in the Swiss Alps, IAG 2013, Paris (poster)

Staub, B., Delaloye, R., Lambiel, C. (2013): Combining observation- and model-based methods in mountain permafrost research, SGmG-Jahrestagung 2013, Basel (presentation)

Staub, B., Hilbich, C., Noetzli, J., Lambiel, C., Völksch, I., Delaloye, R. (2013): 10-15 years of GST monitoring over mountain permafrost in Switzerland: Indicators for driving forces for permafrost evolution, EGU 2013, Vienna, EGU2013-11214 (poster)

Delaloye, R., Hilbich, C., Lambiel, C., Noetzli, J., **Staub, B.,** Völksch, I. (2012): Towards an integrative analysis of mountain permafrost monitoring elements, Swiss Geoscience Meeting 2012, Bern (poster)

Staub, B., Delaloye, R., Vogel, D., Krummenacher, B. (2012): The evolution of ground surface temperatures and rock glacier dynamics in the Furggentälti Valley (Gemmi, VS), Swiss Geoscience Meeting 2012, Bern (poster)